MULTIPHOTON CORRELATIONS AND EMITTERS

EDUARDO ZUBIZARRETA CASALENGUA MSC

ADVISOR:

PROF. DR. FABRICE P. LAUSSY

A thesis submitted in partial fulfilment of the requirements of the University of Wolverhampton for the degree of Doctor of Philosophy

Wolverhampton, November 2022

Date: 13th November 2022

This Thesis is wholeheartedly dedicated to
my parents, Gerardo and Raquel,
and my sister Begoña

Gracias a los tres

ABSTRACT

The characterisation of the quantum states of light and their subsequent realisation is thought to be an indispensable step to bring in quantum technologies to the real world. The emergence of quantum cryptography, quantum security protocols or quantum computers, among others, demand implicitly or explicitly trustworthy tools and components to carry through the research in its first stages. A deterministic or on-demand single-photon source and, more recently, an N-photon emitter, seem to play a crucial role. Nevertheless, even the correct characterisation of the former is still a source of discussion and there exist several criteria to do so. The identification of the latter is, as expected, a challenging task.

With the emergence of multiphoton physics, the horizon of quantum light sources is wider. The tools to identify and classify multiphoton emission are still in development. We present the methods to study the dynamics and correlations of some candidate systems that have been proposed, focusing on the analytical solutions through perturbative methods, valid, for instance, for weakly driven or weakly coupled systems. In particular, the frequency-resolved correlations can be exactly obtained in this way. We also consider the effect of detection on the correlations. The noisy apparatus and their finite time resolution can modify the photon statistics. Some photons may be left undetected or misplaced (in time), additional counts may be recorded as well.

We revisit the photon counting formula, that was popular in the birth of Quantum Optics, to obtain the counting probabilities in continuously driven (CW) systems and we focus then on the spontaneous emission of N photons. We observe, for probability distributions of CW systems, a clear deviation from Poissonian statistics in both the short and long time regimes. We find how such a behaviour is inherited from the photon correlations. A good starting point to study the *bundler*—the N-photon emitter—is the spontaneous emission of N photons. The counting probabilities are computed without and with spectral filtering, making emphasis on how the kind of filter affects the detection. Then, the full structure of the bundle is completely captured by the probability functions of the emission time of the individual photons. The results are ultimately compared with the actual bundler, showing qualitative and quantitative agreement.

A brief introduction is given to spatial correlation induced by the ensemble statistics. Some clarifying examples reveal how the statistics are manifested depending on the kind of states. On the other hand, a dynamical model introducing a space dependent sensor method is provided for the scattering and how the spatial distribution is modified by the time resolution limitation. Interestingly, the wave packet before and after the scattering get effectively admixed and interfere with itself displaying characteristic fringes.

The main objective of this Thesis is to make an exhaustive characterisation of multiphoton emission, starting with the usual treatment in terms of the luminescence spectrum and the second-order photon correlation function $g^{(2)}$, considering mechanisms that can take place in the detection process such as spectral filtering or contamination of the signal due to time jitter and noise. We develop tools to facilitate and speed up the computation of these quantities, either analytically or numerically, within the range of validity of the Born–Markov approximation and highlighting situations in which perturbation theory is applicable. Finally, we go beyond and take into account other statistical quantities such as the waiting time distribution or higher order correlators and eventually compute counting statistics, which results in a good and promising procedure to characterise and subsequently classify multiphoton emission.

PUBLICATIONS

Some ideas and figures have appeared in the following publications:

[Z1] E. Zubizarreta Casalengua, J. C. López Carreño, E. del Valle, and F. P. Laussy. "Structure of the harmonic oscillator in the space of n-particle Glauber correlators." In: *J Math Phys* 58.062109 (2017). DOI: 10.1063/1.4987023.

[Z2] L. Hanschke, L. Schweickert, J. C. López Carreño, E. Schöll, K. D. Zeuner, T. Lettner, E. Zubizarreta Casalengua, M. Reindl, S. F. Covre da Silva, R. Trotta, et al. "The Origin of Antibunching in Resonance Fluorescence." In: *Phys. Rev. Lett.* 125.170402 (2020). DOI: 10.1103/PhysRevLett.125.170402.

[Z3] G. Díaz Camacho, E. Zubizarreta Casalengua, J. C. López Carreño, S. Khalid, Elena del Valle, C Tejedor, and F. P. Laussy. "Multiphoton emission." In: *arXiv:2109.12049* (2021). URL: https://arxiv.org/abs/2109.12049.

[Z4] E. Zubizarreta Casalengua, G. Díaz Camacho, S. Khalid, J. C. López Carreño, Elena del Valle, and F. P. Laussy. "Effect of filtering on photon detection." Submitted to *Phys. Rev. A*. 2021.

[Z5] F. Sbresny, L. Hanschke, E. Schöll, W. Rauhaus, B. Scaparra, K. Boos, H. Riedl E. Zubizarreta Casalengua and, E. del Valle, J. J. Finley, K. Jöns, et al. "Stimulated Generation of Indistinguishable Single Photons from a Quantum Ladder System." In: *Phys. Rev. Lett.* 128.093603 (2022). DOI: 10.1103/PhysRevLett.128.093603.

[Z6] J. C. López Carreño, E. Zubizarreta Casalengua, B. Silva, E. del Valle, and F. P. Laussy. "Loss of Antibunching." In: *Phys. Rev. A* 105.023724 (2022). DOI: 10.1103/PhysRevA.105.023724.

[Z7] E. Zubizarreta Casalengua, F. P. Laussy, and E. del Valle. "Pertubational approach to time-resolved correlators." In preparation. 2023.

CONTENTS

ACRONYMS

2LS	Two-Level System
EM	Electromagnetic
CW	Continuous Wave
CWSE	Continuous Wave Spontaneous Emission
FWHM	Full Width at Half Maximum
RWA	Rotating Wave Approximation
SE	Spontaneous Emission
WTD	Waiting Time Distribution

Et toutesfois je n'ay point apporté ces exemples,
pour vous faire croire abfolument, que cette Lumiere
eft autre dans les objets que dans nos yeux;
mais feulement afin que vous en doutiez, & que,
vous gardant d'eftre préoccupé du contraire,
vous puiffiez maintenant mieux examiner
avec moy ce qui en eft.

— R. Descartes, *Le monde. Traité de la lumiere*

ACKNOWLEDGMENTS

This work would have been impossible without the support of Fabrice and Elena. The first time I met them, I was still finishing my Physics degree in Madrid. Their passion for Science promptly enchanted me and eventually convinced me to follow their footsteps. I might not acknowledge you enough for all the support that I received from you all these years. In a silent and concealed way, I already did, however: I wanted to dedicate this first paragraph to you. It's the least I can do, you deserve it!

Then, I want to give credit to Camilo and Guillermo, with whom I have been working these years and who played an essential role in my research. Thank you for helping me and answering a *bunch* of my questions. I only have kind words for you.

I have to thank Toni and Lara, my trusted mathematicians who I consulted so many times, Guille, that helped me choosing Descartes' quote and Alonso, the other physicist of our group. You all make my life easier and more enjoyable. *Danke schön, Leute!*

From Universidad Autónoma de Madrid, there are too many people I would like to name. Needless to say, I think of everybody. I make a special mention to Sofía, Gonzalo and Carlos. Our discussions were and are a precious source of inspiration.

And last but not least, my family: my parents, Gerardo and Raquel, and my sister Begoña. Thank you for your infinite support and interest. Also, I could not forget to mention our little cats (Bego would kill me otherwise), Mine and Camille, the main cause of my constant distractions. Still, I could finish the Thesis.

Thank you!

THESIS STRUCTURE

The Electromagnetic field, light, is presented in Chapter 1, starting from the light quanta, *the photons*, describing the quantum states of light and the physical observables and all the statistical quantities which comprise the scaffolding that bear the weight of the original research contained in the Thesis. In particular, Section 1.1 is dedicated to discussing the structure of the Hilbert space of a photonic mode by means of the observables $g^{(n)}$ (Article [Z1]). The next Section describes the statistical treatment of the photon and in Subsection 1.2.1. We introduce and extend the theory of frequency-resolved correlators to include new families of spectral filters (from Article [Z4]) and, later on, an analysis of the noise sources and time detection limitations can be found in Subsection 1.2.2 (Article [Z6]).

The missing ingredient is the matter, that couples to the electromagnetic field to produce interesting states of light (Chapter 2). The most fundamental and simple case is a 2-level system, the single-photon emitter *par excellence*. Even being a long-standing and apparently well-understood system, as of today, we still discover puzzling and astonishing new properties. The quantum theory of light-matter interaction, Quantum Electrodynamics, is presented from the Quantum Optics perspective and, after that, a brief derivation of quantum open systems is done. The lossy and non-Hamiltonian dynamics are required to successfully explain the spontaneous emission, dephasing and other dissipative processes and are described through the markovian Lindblad-like master equation. The next Sections are dedicated to solving the dynamics of the 2-level system under different types of excitation, introducing more methodology followed all along the Thesis and then we derive and further characterise the single-photon emission (Article [Z6]). The last Section includes the theoretical and experimental realisation of a scheme for single-photon generation based on semiconductor Quantum Dots, which goes beyond the 2-level system description (Article [Z5]).

We present a new technique in Chapter 3, a perturbational theory to resolve the dynamics of any light-matter system provided that there is at least one perturbation parameter in the Master Equation (Article [Z7]). The theory is followed by a series of examples to show the versatility of the method. We compute the correlations of light-matter system under weak driving such as the Dicke or Jaynes-Cummings

model. Additionally, the sensor method to compute the frequency-filtered photon statistical quantities is formally justified and then applied to the 2-level system (with either coherent or incoherent excitation), finding analytical expressions for the frequency-resolved correlators (Article [Z6]). For Resonance Fluorescence, we also provide the theory that support the experimental evidences. This also verifies the validity of the theoretical results (Article [Z2]).

In Chapter 4, we derive and discuss more statistical properties of light using the theory of photon detection providing exact and approximated results comparing the dynamics of the 2-level system, a single-photon emitter, and a cavity, potentially a multi-photon generator, in the Continuous Wave regime. Following Sections are focused on characterising the Spontaneous Emission of a N-photon bundle, finding exact expressions for the photon-counting probabilities for the bare and filtered emission (Articles [Z3] and [Z4]), as well as the probability distributions of the k photons forming the bundle. Ultimately the results are compared to the CW full quantum model of the *bundler*.

Finally, we address the spatial correlations in simple light-matter systems induced by the intrinsic collective statistical properties of indistinguishable particles (Chapter 5). We generalise, using the Reduced Density Matrix formalism, the well-known case of 2-body antisymmetric or symmetric wavefunction exhibiting larger or smaller mean distance than the distinguishable case, firstly, to N-particle Fock states and, later on, to multi-particle Gaussian states such as the coherent or thermal states. In the last part of the Chapter, we studied the evolution of a (polariton) wave packet undergoing a scattering process and how its spatial distribution is modified by frequency-filtered measurements and the resulting interference between the past and future contributions of the same packet.

Throughout the text, margin notes are inserted that, in my opinion, summarize some of the most original and important results derived in this text. A broader overview is given in the conclusions and, of course, the eventual extent and value of the results are left to the consideration of the reader.

1

QUANTUM LIGHT

1.1 QUANTUM STATES OF LIGHT AND PHOTON STATISTICS

Since the quantization of light by Glauber [1, 2] (see Appendix A.1 for a brief overview of the key quantities), it is understood that its description is best made in terms of correlators of the type:

$$G^{(n)} = \langle a^{\dagger n} a^n \rangle \,, \tag{1.1}$$

as well as their normalised version

$$g^{(n)} = \frac{\langle a^{\dagger n} a^n \rangle}{\langle a^\dagger a \rangle^n} \,, \tag{1.2}$$

as defined in the Appendix A.1. The full Hilbert space is of course extremely complex, and one typically refers to very particular cases only, such as the coherent, thermal and Fock states. Here, we will take a more general view trying to describe all the states in terms of the Glauber correlators (1.2).

1.1.1 THE TRUNCATED HILBERT SPACE

We precise the connection between the quantum states, their number distribution P_n and the Glauber correlators, both $G^{(n)}$ and $g^{(n)}$, which are the main results of Ref. [Z1]. Conveniently, we will start defining the truncated Hilbert spaces $\mathcal{H}_n$, restricting the number of excitations to at most N. In turn, they are subspaces of the (infinite-dimensional) Hilbert space $\mathcal{H}_\infty$:

$$\mathcal{H}_N = \left\{ \sum_{k=0}^{N} c_k \left| k \right\rangle \;;\; \Big(\alpha_k \in \mathbb{C} \Big) \wedge \Big(\sum_{k=0}^{N} |c_k|^2 = 1 \Big) \right\} . \tag{1.3}$$

This approach is inspired by the work of Pegg and Barnett [3], where they defined a phase operator. Working in a truncated space of maximum particle-number N allows us to get access to physical properties that become pathological in the infinite-dimensional space. In the same manner, we will consider truncated spaces to subsequently take the limiting process, in which case $\mathcal{H}_\infty \equiv \bigcup_{N=0}^{\infty} \mathcal{H}_N$.

The portrayal of the truncated Hilbert space $\mathcal{H}_N$ given by Eq. (1.3), however, hides a convoluted structure which we shall attempt to clarify via its visualization in terms of $g^{(n)}$ observables. The urge for this study is motivated by the recent interest in exciting optical targets with quantum light [4, 5] carried through by the progress in quantum sources engineering [6]. The accessible states when the harmonic oscillator is driven by means of a quantum light source fall outside the fair amount of particular cases mentioned above.

In most cases, the classifications follow from a particular scheme that allows one to engineer the corresponding states. As such, they do not provide a picture of the Hilbert space that is both simple and comprehensive and that would be practical to survey which regions of the Hilbert space have already been covered, are the most easy of access, which are its boundaries, if any, and what areas remain to be explored. This is such a picture that is provided below based on the particles joint-correlation properties.

We split the state

$$\rho = \sum_{k=0}^{N} P_k \left|k\right\rangle \left\langle k\right| + \sum_{\substack{k,l=0 \\ k\neq l}}^{N} \rho_{l,k} \left|k\right\rangle \left\langle l\right| , \tag{1.4}$$

with $\rho_{k,l} \in \mathbb{C}$ in general but $P_k \in \mathbb{R}$ and select only the diagonal part (the first term). From Eqs. (A.3)–(A.5) we can see that any state with fixed diagonal terms P_k and distinct off-diagonal terms $\rho_{l,k}$ (with $l \neq k$) is indistinguishable for $G^{(n)}$ from another one whose choice of $\rho_{k,k'}$ is completely different. That is, all states that share the same photon-number distribution P_k, either pure or mixed states, have the same $G^{(n)}$ and $g^{(n)}$.

For instance, $c_n = \exp\left(-|\alpha|^2\right)\alpha^n/\sqrt{n!}$ can be both the genuine coherent state or a random-phase coherent state [7] (whose off-diagonal elements are all zero). The two versions exist for the thermal distribution $c_n = \sqrt{(1-\theta)\theta^n}$ (for $0 \leq \theta \leq 1$), being either the thermal state, which has zero off-diagonal elements, or the pure state version that is the eigenstate of the Susskind-Glogower phase operator $(aa^\dagger)^{-1/2}a$ [8], in which case it is known as the "coherent phase state" [9] (for its resemblance with the coherent state, eigenstate of a). Thus, our exploration is focused on the diagonal part of the state while the rest, the off-diagonal part, is characterised by the purity or of degree coherence of the state.

More formally, in $\mathcal{H}_N$ where the total number of excitations is truncated, $P_{N+m} = 0$ for $m \geq 1$ in Eq. (1.4), therefore, computing the correlators (A.4) on the states (1.4) yields the linear system:

$$1 = \sum_{n=0}^{N} P_n \,, \tag{1.5a}$$

$$n_0 = \sum_{n=0}^{N} n P_n \,, \tag{1.5b}$$

$$G^{(2)} = \sum_{n=0}^{N} n(n-1) P_n \,, \tag{1.5c}$$

$$\vdots$$

$$G^{(N)} = \sum_{n=0}^{N} n(n-1)\dots(n-N+1) P_n \,. \tag{1.5d}$$

In this case, there is a bijection between the allowed $G^{(n)}$ correlators and the states uniquely defined through the first sum in Eq. (1.4). The system is also represented in matrix form as

$$\vec{G} = \mathbb{M}\vec{P} \tag{1.6}$$

between the vectors of $(N+1)$ elements $\vec{P} = (P_0, \cdots, P_N)^T$ and $\vec{G} = (1, n_0, G^{(2)}, ..., G^{(N)})^T$ with:

$$\mathbb{M} = \begin{pmatrix} 1 & 1 & 1 & \dots & 1 & 1 \\ 0 & 1 & 2 & \dots & N-1 & N \\ 0 & 0 & 2 & \dots & (N-2)(N-1) & N(N-1) \\ \dots & \dots & \dots & \dots & \dots & \dots \\ 0 & 0 & 0 & \dots & 0 & N(N-1)\cdots 1 \end{pmatrix} , \tag{1.7}$$

where, by definition:

$$1 = \sum_{n=0}^{N} P_n \,, \tag{1.8}$$

which, being upper-triangular, allows us to solve Eq. (1.6) by Gaussian elimination:

$$P_{N-k} = \frac{1}{(N-k)_{N-k}} \left\{ G^{(N-k)} - \sum_{k'=N-k+1}^{N} (N-k)_{k'} P_{k'} \right\} , \tag{1.9}$$

where $(n)_k = \prod_{p=0}^{k-1}(n-p)$ is the falling factorial. Expanding all the coefficients explicitly, we find

This useful connection between the probabilities (diagonal elements of the density matrix) and the Glauber correlators is well-known only in its inverse formulation ($G^{(j)}$ as a function of P_i). In fact, we know no mention of it in the literature.

$$P_i = \sum_{j\geq i}^{N} (-1)^{i+j} \frac{G^{(j)}}{i!(j-i)!}, \tag{1.10}$$

for $0 \leq i \leq N$. This is exactly the inverse relation of Eq. (1.5).

This result is always true for any N and does hold when $N \to \infty$. An alternative way to obtain Eq. (1.10) is through the factorial moment generating function [10]. The connection between P_k and $G^{(n)}$ is settled, we shall now proceed to map the space via the $g^{(n)}$ observables. To do so, we consider how a distribution of states from $\mathcal{H}_N$ is mapped into the space charted by $g^{(n)}$. To tell the different descriptions of the space apart will call the latter space $\mathcal{G}_N$. Given the inequalities $0 \leq P_n \leq 1$ for all n together with the normalisation condition, the anticipated correlator space might be full of complex constraints.

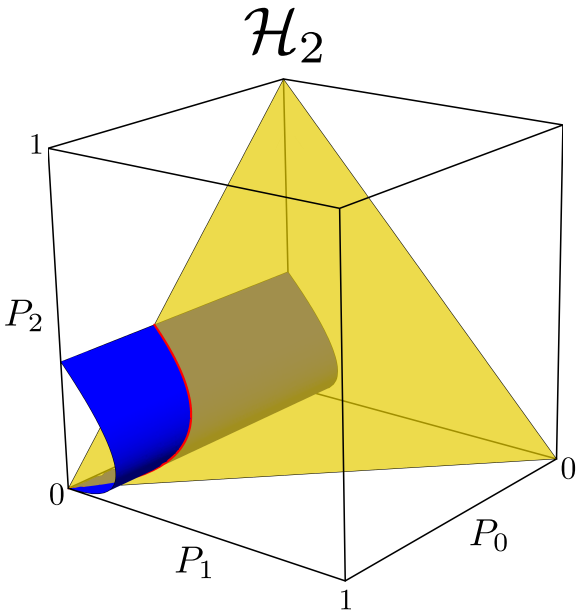

Figure 1.1: The mapping of the two-particle Hilbert space $\mathcal{H}_2$ in terms of P_k, the probabilities for the Fock state $|k\rangle$ corresponds to an equilateral triangle or non-standard 2-simplex (yellow). The blue surface is spanned by all the states of constant $g^{(2)}$ (namely, here $g^{(2)} = 1.3$). The intersection of both surfaces, shown as the red line, captures all the (normalised) quantum states with the corresponding $g^{(2)}$. The total length of the red curve correspond to their density in the space. Reproduced from [Z1], with the permission of AIP Publishing.

Regarding the particular state distribution, we consider as a fair representation of $\mathcal{H}_N$ a distribution where each element of the space $\mathcal{H}_N$ has the same probability to be sampled, this is, the distribution is uniform over the whole space.

As an example, the Hilbert space $\mathcal{H}_2$ is described by a 2D equilateral triangle in the 3D space (P_0, P_1, P_2) (see Fig. 1.1). All the physical quantum states of at most two excitations are represented by the uniform distribution over this geometry. That is, the probability distribution is constant in all the triangle area. Outside this triangular region, the probability turns to zero. The correlator space spanned by $c_0 |0\rangle + c_1 |1\rangle + c_2 |2\rangle$, with the normalisation constraint $P_0 + P_1 + P_2 = 1$, reaches its maximum population $n_0 = 2$ when $P_2 = 1$. $G^{(2)}$ is likewise maximised when the state is $|2\rangle$ (with $G^{(2)} = 2$). The lower bound is obviously zero, the vacuum $|0\rangle$ is the unique state that minimises both the population and the 2-photon Glauber correlator $G^{(2)}$. The limits are therefore $n_0 \geq 0, G^{(2)} \geq 0$. The rest of correlators are zero since $P_{k>2} = 0$. The normalised correlator $g^{(2)}$ is also positive but unbounded. This two-particle extreme superbunching behaviour was already known in the context of bosonic cascades [11].

Given a certain population n_0 or $g^{(2)}$, the normalised states with those correlator fixed are generated by the intersection of the triangle and the plane $P_1 + 2P_2 - n_0 = 0$ or the surface $(P_1 + 2P_2)^2 - 2P_2/g^{(2)} = 0$, respectively. In figure (1.1), the red curve corresponds to states with fixed $g^{(2)}$. The length of this curve is proportional to the number of states with constant observable n_0 or $g^{(2)}$. The density of states is associated to arc length (for 1D), area (for 2D) or, in general, the hypersurface of the subspace. The measure of the surface is independent of the choice of the parametrisation or the metric of the space. In differential geometry, the area element of the surface is described by the First Fundamental Form $\mathbb{F}$, that provides the trajectory in one space that is parametrically defined in the other. It is defined as

$$\mathbb{F}_{k,k'} = \partial_{G^{(k)}} \vec{P} \cdot \partial_{G^{(k')}} \vec{P}\,, \tag{1.11}$$

where $1 \leq k, k' \leq N$ and $\cdot$ is the scalar product between the $\partial \vec{P}$ vectors. Since the transformation Eq. (1.6) is linear, the elements of $\mathbb{F}$ are constant, given by $\mathbb{F}_{k,k'} = \sum_{i \leq k,k'} (-1)^{k+k'} / \left[i!^2 (k-i)!(k'-i)! \right]$. The area element of (hyper)surface in $\mathcal{H}_N$ is related to the corresponding element in $\mathcal{G}_N$ by $\mathcal{P}_G dn_0 \cdots dG^{(N)} = (\sqrt{|\mathbb{F}|}/A_N) dP_0 \cdots dP_N$ with $\mathcal{P}_G$ the density of probability, A_N is the volume of the Hilbert space $\mathcal{H}_N$, that, being a N-simplex (of side $\sqrt{2}$ and dimension $N+1$), reads:

$$A_N = \frac{\sqrt{N+1}}{N!}\,, \tag{1.12}$$

and $|\mathbb{F}|$ the determinant of $\mathbb{F}$ is computed from Eq. (1.11) and expressed in terms of the superfactorial $\mathrm{sf}(N) = \prod_{i=0}^{N} i!$ as:

$$\sqrt{|\mathbb{F}|} = \frac{\sqrt{N+1}}{\mathrm{sf}(N)}\,. \tag{1.13}$$

While the computation is conveniently performed with $\vec{G}$, we are eventually interested in the space of normalized correlators $g^{(n)}$, that we will call $\mathcal{g}_N$. A summary of the spaces involved and the notations to identify them is given in Table (1.1). There is another bijection from $\mathcal{G}_N$ to $\mathcal{g}_N$, that simply dilates or shrinks each coordinate by the powers of n_0 as $(n_0, G^{(2)}, ..., G^{(N)}) = (n_0, n_0^2 g^{(2)}, ..., n_0^N g^{(N)})$. The change of variables and its subsequent transformed hypersurface element is given by the Jacobian

$$\begin{aligned} J = \left|\frac{\partial G^{(i)}}{\partial g^{(j)}}\right| &= \begin{vmatrix} 1 & 0 & 0 & 0 & \dots & 0 \\ 2n_0 g^{(2)} & n_0^2 & 0 & 0 & \dots & 0 \\ 3n_0^2 g^{(3)} & 0 & n_0^3 & 0 & \dots & 0 \\ \dots & \dots & \dots & \dots & \dots & \dots \\ N n_0^{N-1} g^{(N)} & 0 & 0 & 0 & \dots & n_0^N \end{vmatrix} \\ &= \prod_{p=2}^{N} n_0^p = n_0^{(N^2+N-2)/2}\,. \end{aligned} \tag{1.14}$$

The joint density of probability in the space $\mathcal{g}_N$ is then $\mathcal{P}_g\left(n_0, \dots, g^{(N)}\right)$. Particularly, a randomly chosen infinitely small region from $\mathcal{H}_N$ whose corresponding correlators are $n_0, \dots, g^{(N)}$ in the hypervolume element $dn_0 \cdots dg^{(N)}$ has the associated probability $\mathcal{P}_g\, dn_0 \dots dg^{(N)}$. The density of probability is found as

This provides the distribution of quantum states in the Hilbert space charted by the Glauber correlators.

$$\boxed{\mathcal{P}_g\left(n_0, g^{(2)}, \dots, g^{(N)}\right) = \frac{n_0^{(N^2+N-2)/2}}{\mathrm{sf}(N-1)}\Theta(\mathcal{g}_N)\,,} \tag{1.15}$$

where $\Theta(\mathcal{g}_N)$ is the support for the image of $\mathcal{H}_N$ through the successive bijections (from $\mathcal{H}_N$ to $\mathcal{G}_N$ and, after that, to $\mathcal{g}_N$). It is 1 only if exists a state with joint-correlators n_0, $g^{(2)}$, ..., $g^{(n)}$ and is 0 otherwise. We still need to identify the explicit shape of this bijection in the correlator space. It is remarkable that for physical states, $\mathcal{P}_g$ is independent of the correlators except for the population n_0.

We now show some particular cases to illustrate these results. In all cases, the boundaries can be found from Eqs. (1.10) by imposing the conditions $P_k \geq 0$ and $P_k \leq 1$. As a result, the analogue inequalities for the correlations are obtained. Following this, the marginal probability distributions in the projected subspaces are provided though these boundary equations.

Subspace	Probability
$\mathcal{H}_N$	$\mathcal{P}(P_0, P_1, \ldots, P_N) = (1/A_N)\Theta(\mathcal{H}_N)$
$\mathcal{G}_N$	$\mathcal{P}_G(n_0, G^{(2)}, \ldots, G^{(N)}) = (\sqrt{\lvert\mathbb{F}\rvert}/A_N)\Theta(\mathcal{G}_N)$
$\mathcal{g}_N$	$\mathcal{P}_g(n_0, g^{(2)}, \ldots, g^{(N)}) = (J\sqrt{\lvert\mathbb{F}\rvert}/A_N)\Theta(\mathcal{g}_N)$

Table 1.1: Summary of notations for the various spaces introduced. $\mathcal{H}_N$ is the Hilbert space truncated to $N \in \mathbb{N}$ particles in the Fock basis, $\mathcal{G}_N$ is the corresponding space in the basis of unnormalized correlators $G^{(N)}$, and $\mathcal{g}_N$ in the space of Glauber correlators $g^{(n)}$. The original probability distribution (uniform) are A_N, the volume of the Hilbert space $\mathcal{H}_N$. $\mathbb{F}$ is the first fundamental form and J the Jacobian of the transformation between the unnormalised and normalised correlators. The expressions are given in Eqs. (1.12) and (1.13). Θ is the indicator function, which is nonzero only if exists there a physical state with such correlators.

1.1.2 THE TWO-PARTICLE HILBERT SPACE

We skip the discussion of the Hilbert space truncated to $N = 1$ here, which has already been completely characterised in the literature [12] and moreover it will be briefly revised in Chapter 2. The next simplest is the two-particle space $\mathcal{H}_2$. The basis of this space is given by $|0\rangle$, $|1\rangle$ and $|2\rangle$, so that the dimension is 3 (see the triangle or 2-simplex of side $\sqrt{2}$ in Fig. 1.1). Equations (1.10) that connect P_k and $g^{(k)}$ read in this case

$$P_0 = 1 - n_0 + \frac{n_0^2 g^{(2)}}{2}, \tag{1.16a}$$

$$P_1 = n_0(1 - n_0 g^{(2)}), \tag{1.16b}$$

$$P_2 = \frac{n_0^2 g^{(2)}}{2}, \tag{1.16c}$$

with $0 \leq P_k \leq 1$. As we discussed above, each point (state) on the simplex (Hilbert space) can be generated by the intersection of the plane and constant n_0 and $g^{(2)}$. In vector form, each state is described by

$$\{P_0, P_1, P_2\} = \left\{1 - n_0 + \frac{n_0^2 g^{(2)}}{2}, n_0 - n_0^2 g^{(2)}, \frac{n_0^2 g^{(2)}}{2}\right\} \tag{1.17}$$

The joint probability $\mathcal{P}_g$, i.e., the probability of finding a state with given $(n_0, g^{(2)})$ from a uniform sampling in the Hilbert space is:

$$\mathcal{P}_g(n_0, g^{(2)}) = n_0^2\, \Theta(\mathcal{g}_2), \tag{1.18}$$

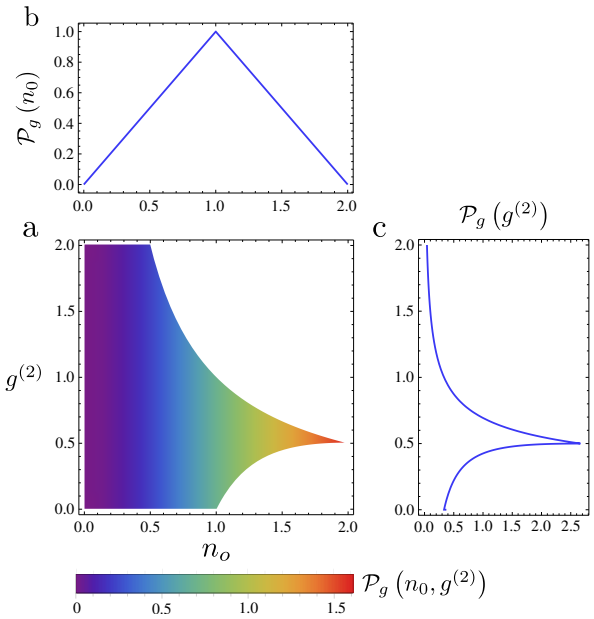

Figure 1.2: (a) Joint probability distribution $\mathcal{P}_g$ of finding a quantum state with mean population n_0 and $g^{(2)}$ from uniform distribution in $\mathcal{H}_2$. Both lower and upper boundaries are found. (b) Marginal distribution $\mathcal{P}_g(n_0)$ after integrating over $g^{(2)}$ and (c) Marginal distribution $\mathcal{P}_g(g^{(2)})$ after averaging over n_0. Reproduced from [Z1], with the permission of AIP Publishing.

where the indicator $\Theta\left(\mathcal{g}_2\right)$ vanishes if $\left(n_0, g^{(2)}\right) \notin \mathcal{g}_2$. There is no explicit dependency of $\mathcal{P}_g$ on $g^{(2)}$. However, the function $\Theta(\mathcal{g}_2)$ is zero in some regions of the correlator space and hence there must be some implicit dependency that induces the geometry of $\mathcal{g}_N$. The inequalities P_k that shape $\mathcal{H}_2$ give rise to upper and lower boundaries for the $(n_0, g^{(2)})$ space:

$$g^{(2)} \leq \frac{1}{n_0}, \tag{1.19a}$$

$$g^{(2)} \geq \frac{\lfloor n_0 \rfloor (2n_0 - \lfloor n_0 \rfloor - 1)}{n_0^2}. \tag{1.19b}$$

The lower boundary for $g^{(2)}$ in Eq. (1.19b) was already obtained in Ref. [5] and it is general for any $\mathcal{H}_N$. Here, in addition, an upper boundary is found (1.19a). This one is however particular for $\mathcal{H}_2$ and it varies as the truncation of the space grows. The constraints and the induced probability distribution $\mathcal{P}_g$ are shown in Fig. 1.2. For vanishing population $n_0 \to 0$, $g^{(2)}$ can reach arbitrary high values but the probability vanishes as it gets diluted in the $g^{(2)}$ axis due to the huge number of states. This is, the lesser the population, the greater the maximum $g^{(2)}$ can be. When the population is exactly zero, the only state is the vacuum $|0\rangle$. On the opposite side, the probability

density is maximised around the vertex $(2, 1/2)$, given by the state $|2\rangle$. The range of possible values of $g^{(2)}$ is hugely reduced and thus the density is extremely high. In intermediate cases, namely $n_0 = 0.5$, there are states with both antibunching and bunching. For $n_0 > 1$, all the states necessarily have $g^{(2)} > 0$, meaning that the contribution of $|2\rangle$ is different from zero above that population. On the other hand, for the most likely value of $g^{(2)}$, $1/2$, n_0 can run from 0 to 2 and, in the middle, values of $g^{(2)} < 1/2$ are allowed to have population greater than one. We already mentioned that for such population P_2 has to be non-zero. The (pure) states that lie on both the lower and upper boundaries are a superposition of two (out of three) Fock states

$$\sqrt{1 - \frac{n_0}{2}}\,|\mu\rangle + \sqrt{\frac{n_0}{2}}e^{i\theta}\,|\nu\rangle\ , \tag{1.20}$$

where $\mu, \nu = 0, 1, 2$ and $\mu \neq \nu$. The phase θ can be any real number. For instance, the superposition of $|0\rangle$ and $|1\rangle$ correspond to the horizontal axis from $n_0 = 0$ and $n_0 = 1$ (the qubit states). For $n_0 > 1$, the states defined in the lower boundary are superposition of $|1\rangle$ and $|2\rangle$. The upper boundary, when $g^{(2)} = 1/n_0$, has the states generated by $|0\rangle$ and $|2\rangle$.

The boundaries in $\mathcal{H}_2$ can also be written as:

$$n_0 \leq \frac{1 - \sqrt{1 - 2g^{(2)}}\theta(1 - 2g^{(2)})}{g^{(2)}}\,, \tag{1.21}$$

where $\theta(x)$ is the Heaviside function. Regarding the upper bound, for a given allowed population, $0 \leq n_0 \leq 2$, i.e.,

$$g^{(2)} \leq \frac{1}{n_0}\,. \tag{1.22}$$

Both marginal distributions, $\mathcal{P}_g(n_0)$ and $\mathcal{P}_g(g^{(2)})$, are obtained by integrating over the other observable. The first one provides the population distribution

$$\mathcal{P}_g(n_0) = \begin{cases} n_0 & \text{if } 0 \leq n_0 \leq 1 \\ 2 - n_0 & \text{if } 1 < n_0 \leq 2 \end{cases}\,, \tag{1.23}$$

and the other one provides the $g^{(2)}$ distribution

$$\mathcal{P}_g(g^{(2)}) = \begin{cases} \sqrt{\frac{8}{9}}\frac{(1-\sqrt{1-2g^{(2)}}-g^{(2)})^{\frac{3}{2}}}{(g^{(2)})^3} & \text{if } 0 \leq g^{(2)} \leq \frac{1}{2} \\ \frac{1}{3(g^{(2)})^3} & \text{if } g^{(2)} > \frac{1}{2} \end{cases}\,. \tag{1.24}$$

These two distributions are piecewise functions, and are shown in Fig. 1.2(b-c). A randomly picked state will most likely have a population equal to one (exclusively looking at this observable), whereas the most likely value for $g^{(2)}$ (examinating $\mathcal{P}_g(g^{(2)})$) is $1/2$. In the joint space $(n_0, g^{(2)})$, however, the maximum value is located at the edge $(2, 1/2)$. So that the most probable states are around the Fock state $|2\rangle$.

1.1.3 THE THREE-PARTICLE HILBERT SPACE

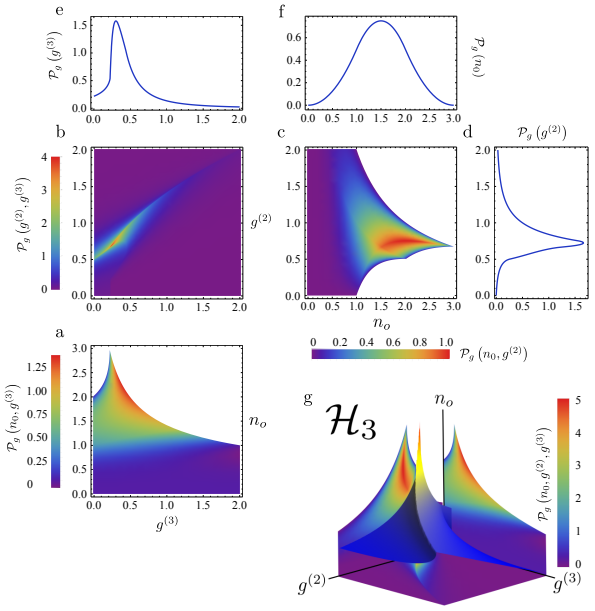

Figure 1.3: (a) Marginal probability distribution $\mathcal{P}_g(n_0, g^{(3)})$ (averaging over $g^{(2)}$) of finding a quantum state with the corresponding population and $g^{(3)}$ (starting with an uniform distribution in $\mathcal{H}_3$). The subspace has both lower and upper boundaries resembling g_2. (b) Distribution $\mathcal{P}_g(g^{(2)}, g^{(3)})$ after averaging over n_0. This subspace is defined by the possible choices of $(g^{(2)}, g^{(3)})$. (c) Distribution $\mathcal{P}_g(n_0, g^{(2)})$ after averaging over $g^{(3)}$. The single-parameter distributions are (d) $\mathcal{P}_g(g^{(2)})$, (e) $\mathcal{P}_g(g^{(3)})$ and (f) $\mathcal{P}_g(n_0)$. (g) The joint distribution for $\mathcal{H}_3$ is defined in a region of the 3D space, shown here through its upper boundary (together with the three projected subspaces, in 2D). Reproduced from [Z1], with the permission of AIP Publishing.

The underlying ideas discussed for $\mathcal{H}_2$ also apply to the 3-particle space $\mathcal{H}_3$. The main difference is that, since we are adding a fourth coordinate P_3, the natural representation requires a 4D space which entails a great difficulty when trying to visualise the whole space. From the correlators side, a new quantity is necessary: the 3-particle Glauber correlator $g^{(3)}$. It is thus displayed in a 3D space whose

coordinates are now $(n_0, g^{(2)}, g^{(3)})$. The geometrical representation issue is partially surpassed in this context.

Equations (1.10) read in this case

$$P_0 = 1 - n_0 + \frac{n_0^2 g^{(2)}}{2} - \frac{n_0^3 g^{(3)}}{6}\,, \tag{1.25a}$$

$$P_1 = n_0 - n_0^2 g^{(2)} + \frac{n_0^3 g^{(3)}}{2}\,, \tag{1.25b}$$

$$P_2 = \frac{n_0^2 g^{(2)}}{2} - \frac{n_0^3 g^{(3)}}{2}\,, \tag{1.25c}$$

$$P_3 = \frac{n_0^3 g^{(3)}}{6}\,. \tag{1.25d}$$

We can easily check that $\mathcal{H}_2$ is a subspace of $\mathcal{H}_3$ by taking $g^{(3)}$ to zero (which automatically leads to $P_3 = 0$). The distribution of states is found to be

$$\mathcal{P}_g(n_0, g^{(2)}, g^{(3)}) = \frac{n_0^5}{2}\Theta\left(\mathcal{g}_3\right)\,, \tag{1.26}$$

and as before, it is explicitly depends only on the population n_0, while the implicit dependence on $g^{(2)}$ and $g^{(3)}$ remains encoded within the indicator function $\Theta(\mathcal{g}_3)$. The boundaries for $(n_0, g^{(2)}, g^{(3)})$ are complex and can be expressed as constraints on one variable as a function of the two others. For $g^{(2)}$ as a function of n_0 and $g^{(3)}$:

$$g^{(2)} \leq \frac{n_0 g^{(3)}}{2} + \frac{1}{n_0}\,, \tag{1.27a}$$

$$g^{(2)} \geq \max\left(n_0 g^{(3)}, \frac{n_0 g^{(3)}}{3} + \frac{2}{n_0} - \frac{2}{n_0^2}\right)\,, \tag{1.27b}$$

and, for $g^{(3)}$ as a function of n_0 and $g^{(2)}$:

$$g^{(3)} \leq \min\left(\frac{g^{(2)}}{n_0}, \frac{3g^{(2)}}{n_0} - \frac{6}{n_0^2} + \frac{6}{n_0^3}\right)\,, \tag{1.28a}$$

$$g^{(3)} \geq \max\left(0, \frac{2g^{(2)}}{n_0} - \frac{2}{n_0^2}\right)\,, \tag{1.28b}$$

with $0 \leq n_0 \leq 3$ in both cases and $g^{(2)}, g^{(3)} \geq 0$. The system of inequalities holds for pairs of coordinates that are allowed, i.e., they are inside the space $\mathcal{g}$. Providing a pair that lies outside will produce unphysical boundaries such as $g^{(3)} < 0$. The valid combinations, in turn, produce the boundaries for the projected spaces, e.g., $(n_0, g^{(2)})$

or $(n_0, g^{(3)})$ subspaces. Additionally, these $(n_0, g^{(n)})$ ($n \geq 2$) boundaries are general for any subspace of $\mathcal{H}_N$ and will be provided later, derived from more general equations (see Appendix A.3). In particular, the upper boundary for $g^{(2)}$ is always proportional to $1/n_0$ which allows to have arbitrarily large superbunching when the population is vanishing.

The remaining (upper) boundary condition for n_0 as functions of $g^{(2)}$ and $g^{(3)}$ is condensed in the following expression

$$0 \leq n_0 \leq U(g^{(2)}, g^{(3)})\,. \tag{1.29}$$

The equation looks simple, but requires the definition of auxiliary functions $f_1(g^{(2)}, g^{(3)})$ and $f_2(g^{(3)})$, that can be found in the Appendix A.2 (cf. Eqs. (A.6)–(A.8)). With this, the function $U(g^{(2)}, g^{(3)})$ reads

$$U(g^{(2)}, g^{(3)}) \equiv \begin{cases} f_1(g^{(2)}, g^{(3)}) & \text{if } g^{(3)} \leq \frac{2}{9} \text{ and } g^{(2)} < f_2\left(g^{(3)}\right), \\ \frac{g^{(2)} - \sqrt{(g^{(2)})^2 - 2g^{(3)}}}{g^{(3)}} & \text{if } g^{(3)} \leq \frac{2}{9} \text{ and } g^{(2)} \geq f_2\left(g^{(3)}\right), \\ \min[f_1, \frac{g^{(2)}}{g^{(3)}}] & \text{if } g^{(3)} \geq \frac{2}{9} \text{ and } g^{(2)} < \sqrt{2g^{(3)}}, \\ \frac{g^{(2)} - \sqrt{(g^{(2)})^2 - 2g^{(3)}}}{g^{(3)}} & \text{if } g^{(3)} \geq \frac{2}{9} \text{ and } g^{(2)} \geq \sqrt{2g^{(3)}}\,. \end{cases} \tag{1.30}$$

and the natural lower boundary is $n_0 \geq 0$. The a priori arbitrary value $2/9$ actually comes from the $g^{(3)}$ of the Fock state $|3\rangle$. The full space (up to three particles) is completely characterized through these boundaries (as shown in Fig. 1.3) although the structure is still complicated to visualise. A simpler and usually more suitable representation is the projection into the pairwise subspaces, e.g., $(n_0, g^{(2)})$. They can be obtained by integrating over one of the three observables. We compute the exact expressions for the marginal probability distribution but they are bulky and not specially insightful (cf. Appendix A.2). The boundaries are also realized by states of the form of Eq. (1.20), this time with $0 \leq \mu, \nu \leq 3$ (still with $\mu \neq \nu$). This is true as well for the new projected spaces $(n_0, g^{(3)})$.

From Fig. 1.3, we see that the Hilbert space is bounded for the population but is not for the rest of the correlators. Normalised intensity correlations of all orders are independent from the population and, as a result, one can find states with antibunching at the two-particle level but extreme Super-Poissonian three-particle fluctuations. The reciprocal scenario, $g^{(2)} \gg 1$ and $g^{(3)} \ll 1$, is likewise possible. Of

course, as the population grows, the region of $(g^{(2)}, g^{(3)})$ that is accessible to physical states is reduced (the boundary is provided in terms of the function U). Near the vacuum ($n_0 \to 0$), on the contrary, any combination is allowed. In the vicinity, we can study in detail the behaviour of the boundary function U in the limits of small or huge arguments of the correlators. All the combinations are shown in the Table (1.2). The density of probability for this subspace, that quantifies the relative occurrence of all possible combinations, reads

$$\mathcal{P}_g(g^{(2)}, g^{(3)}) = \frac{1}{12}\left[U(g^{(2)}, g^{(3)})\right]^6 , \tag{1.31}$$

and is shown in Fig. 1.3(b).

$U(g^{(2)}, g^{(3)})$	$g^{(2)} \to 0$	$g^{(2)} \to \infty$
$g^{(3)} \to 0,$	$1 + \frac{g^{(2)}}{2} - \frac{g^{(3)}}{6}$	$\frac{1}{g^{(2)}} + \frac{2g^{(3)}}{(g^{(2)})^3}$
$g^{(3)} \to \infty$	$\frac{g^{(2)}}{g^{(3)}}$	*i)* $\frac{1}{g^{(2)}} + \frac{2g^{(3)}}{(g^{(2)})^3}$ *ii)* $\frac{g^{(2)}}{g^{(3)}}$

Table 1.2: Limiting cases of the population upper bound $U(g^{(2)}, g^{(3)})$ for all the possible combination of vanishing and diverging $g^{(2)}$ and $g^{(3)}$. In the bottom right cell, case i) applies to $(g^{(2)})^2 > 2g^{(3)}$ while case ii) applies to $(g^{(2)})^2 < 2g^{(3)}$. All cases except $g^{(2)} \to 0$ and $g^{(3)} \to 0$ lead to vanishing populations n_0.

Integrating a second time, the marginal probability distribution for n_0 in $\mathcal{H}_3$ can be computed from either equation (A.9) or (A.10) and yields

$$\mathcal{P}_g(n_0) = \begin{cases} \frac{n_0^2}{2} & \text{if } 0 \le n_0 \le 1\,, \\ -\frac{1}{2}\left(2n_0^2 - 6n_0 + 3\right) & \text{if } 1 < n_0 \le 2\,, \\ \frac{1}{2}\left(n_0^2 - 6n_0 + 9\right) & \text{if } 2 < n_0 \le 3\,, \end{cases} \tag{1.32}$$

that is plotted in panel (f) of Fig. 1.3. Similarly, the reduced probability distribution for $g^{(2)}$ is obtained and, again, the corresponding expression is bulky (cf. Eq. (A.11)) and has piecewise form. The analytical expression for $\mathcal{P}_g(g^{(3)})$ could not be obtained so that the one displayed in panel (e) comes from numerical integration. The whole family of marginal probability distribution (for all 2D and 1D subspaces) are shown in Fig. 1.3. The 2D cases are also displayed as

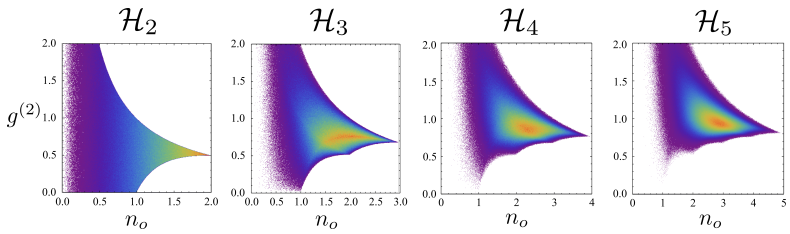

Figure 1.4: Distributions of states in the projected subspace $(n_0, g^{(2)})$ as obtained from Monte Carlo uniform sampling in $\mathcal{H}_N$ for $2 \leq N \leq 5$. The cases $N = 2$ and 3 do match with the aforementioned analytical solutions. Reproduced from [Z1], with the permission of AIP Publishing.

projections on their respective planes in the full 3D space, showing in full detail the convoluted structure of the three-particle Hilbert space $\mathcal{H}_3$.

1.1.4 THE N-PARTICLE HILBERT SPACE

The extension of the previous calculations, already intricate for $N = 3$, to higher dimensional spaces becomes hard to deal with and the complexity scales swiftly, making their interpretation difficult. For $N \geq 4$, the inequalities involve polynomials of degree greater than 3 and the roots cannot be obtained analytically (the method is, in principle, still applicable for quartic polynomials but these results are intractable). Nonetheless, some general results can be obtained for the projected subspaces and the marginal distributions.

For instance, all the marginal distributions for the population $\mathcal{P}_g(n_0)$ follow Irwin-Hall distributions (i.e., the distribution for the sum of N independent random variables with a uniform distribution):

$$\mathcal{P}_g(n_0) = \frac{1}{2(N-1)!} \sum_{k=0}^{N} (-1)^k \binom{N}{k} (n_0 - k)^{n-1} \mathrm{sgn}(n_0 - k)\,, \quad (1.33)$$

which, in the limit of large N, tends to a normal distribution. Other generalisations to all N (and subsequently to $\mathcal{H}_\infty$) are the boundaries of g_N in the projected subspaces $(n_0, g^{(n)})$. Their expressions are (the proofs are given in Appendix A.3 and Ref. [5]):

These boundaries, both from above and below, for the k-th order Glauber correlator, give the most general constrains that exist for the correlations of the quantum states. There is no upper boundary in the full Hilbert space, while there is a lower boundary as shown in Fig. 1.5.

$$g^{(k)} \leq \frac{(N-1)!}{(N-k)!} \frac{1}{n_0^{k-1}}\,, \quad (1.34a)$$

$$g^{(k)} \geq \frac{\lfloor n_0 \rfloor !}{(\lfloor n_0 \rfloor - k)! n_0^k} \left(1 + \frac{k(n_0 - \lfloor n_0 \rfloor)}{\lfloor n_0 \rfloor + 1 - k}\right)\,. \quad (1.34b)$$

The equations (1.34) are indeed the necessary conditions for $N = 3$ to provide physical upper boundaries to Eqs. (1.27)–(1.28). As a

straightforward consequence, from the boundaries (1.34) we can find the minimum and maximum values for $g^{(n)}$ for a given population n_0 in any truncated space $\mathcal{H}_N$. We have checked these results through numerical calculations. For several truncation numbers, N, we have performed Monte Carlo simulations, making random sampling on the $N-1$-simplex following a uniform distribution. In Figure 1.4, the projections in the $(n_0, g^{(2)})$ subspaces are shown. In all cases, the numerical results are in accordance with the analytical formulae. The marginal density probabilities $\mathcal{P}_g(n_0, g^{(2)})$ for $\mathcal{H}_2$ and $\mathcal{H}_3$ also agree with the expressions shown above.

The behaviour of the upper and lower boundaries is different as we increase the truncation number N. The upper one grows ceaselessly with N, meaning that, in the full harmonic oscillator space (without restrictions in the number of excitations), all $g^{(k)}$ are unbounded and can have arbitrary large values for any choice of the population n_0 which has no upper bound as well. Conversely, the lower bound does not depend on N. As a result, it remains after the limiting process $N \to \infty$ has taken place. The (pure) states that lie on the border are superpositions of consecutive Fock states $\sqrt{p}\,|n\rangle + \sqrt{(1-p)}e^{i\theta}\,|n+1\rangle)$ (for $0 < p < 1$). It is particularly interesting to see that this boundary allows to have states with $n_0 > 1$ and $g^{(2)} < 1/2$ (shaded region in Fig. 1.5). Along the discussion, we already have mentioned that any state with $n_0 > 1$ implies that at least one of the probabilities $P_{k>1}$ is different from zero. This contradicts the popular criterion for single-photon emission $g^{(2)} < 1/2$ [13–18], used to identify quantum states with single-particle contributions only. What $g^{(2)} < 1/2$ actually indicates is that the state has on average less than two particles. In the wake of this contradiction, more sophisticated criteria were proposed to properly bound the presence of the one-particle Fock state [19]. Amending the former criterion, a single-particle state must have $g^{(2)} = 0$, which is virtually impossible to reach in a experiment. Other alternative single-photon criteria are contemplated in Ref. [20].

Regarding the independence of any pair of Glauber correlators, although we find that all possible combinations are allowed, any particular choice limits the accessible values for the rest of the correlators. An illustrative case is when we take $g^{(k)} = 0$. From (1.5), we find that all the probabilities $P_{n \geq k}$ are then necessarily equal to zero. Hence, all $g^{(k+n)}$ (with $0 \leq n \leq N-n$) also vanish. The exact cancellation of $g^{(k)}$ automatically locates the state in the subspace $\mathcal{g}_{k-1}$. A dramatic case was already pointed out when discussing the 2-particle space $\mathcal{H}_2$. If $n_0 = 0$, then all $g^{(k)}$ are zero, exhausting any possible state except for the vacuum $|0\rangle$. In fact, the probability density is exactly zero if $n_0 = 0$. In truncated spaces, extremely large values of $g^{(k)}$

This insightful mapping of all the quantum states in the Hilbert space was surprisingly overlooked, despite the importance of $g^{(2)}$ and the population. It shows in particular that quantum states do exist in the shaded region, thereby invalidating a popular criterion used by experimentalists that $g^{(2)} < 1/2$ identifies a single-photon source.

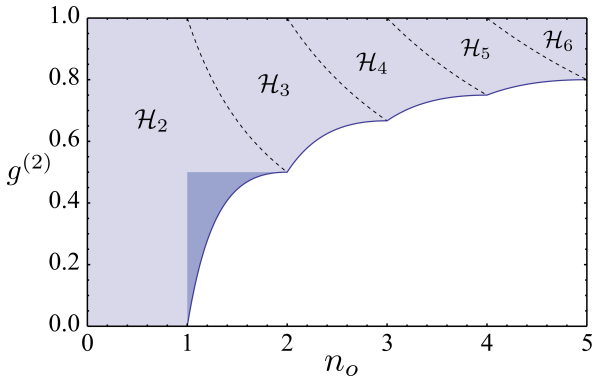

Figure 1.5: Structure of the harmonic oscillator Hilbert space in the $(n_0, g^{(2)})$ subspace. It displays a lower boundary but no upper boundary. The dashed lines are remainder of successive upper boundaries that exist in the N-truncated spaces $\mathcal{H}_N$. The shaded region shows the states with $g^{(2)} < 0.5$ and $n_0 > 1$. Reproduced from [Z1], with the permission of AIP Publishing.

indicate that the vacuum prevails over all the other states since the space is bounded from above and only states with vanishing mean population can access that region of the space. In the whole space $\mathcal{H}_\infty$, this statement does not always hold. We can devise states with both n_0 and $g^{(k)}$ as large as desired. For instance, the state $(1-p)\,|0\rangle + p\,|n\rangle$ has population $n_0 = np$ and $g^{(2)} = (n-1)/(np)$. Fixing the product $np = m$ and with m as large as we want and taking n much greater than unity, then $g^{(2)} \approx 1/p = n/m$, which can return a big number too. In that case, of course, p is small and the state is dominated by the vacuum but on average the number of particles is large (because n is large enough). In such an infinite space, trying to narrow down the kind of state from few observables may produce misleading conclusions. This is epitomised by the states with $g^{(2)} < 1/2$, which do not guarantee the so sought single-photon generation.

To finish with the discussion about the general quantum states of light, we can extend the Hilbert space to allow multimode states. For a general number of modes, the complete Hilbert space is given by the tensor product of an infinite number of copies of $\mathcal{H}_\infty$. Any Fock state is then written as

$$\left|n_1\, n_2 \ldots n_p\right\rangle = \left|n_1\right\rangle \otimes \left|n_2\right\rangle \otimes \ldots \left|n_p\right\rangle \,, \tag{1.35}$$

where n_q are the number of photons in the q-th mode. All the pure states are superposition of the Fock states. In terms of the creation operators, the state (1.35) is created from vacuum as

$$\left|n_1\, n_2 \ldots n_p\right\rangle = \prod_{q=1}^{p} \frac{a_q^{\dagger n_q}}{\sqrt{n_q!}} \left|0\right\rangle \,, \tag{1.36}$$

where the vacuum state is indeed $|0\rangle = \otimes_q |0_q\rangle$, i.e., the tensor product of q-mode vacuum states. A similar analysis can be done to link multimode correlators, for instance, $\langle a_1^\dagger a_2^\dagger a_2 a_1\rangle$ to the diagonal elements of the two-mode density matrix P_{n_1,n_2}, that is, the probability of being in the state $|n_1\, n_2\rangle$ but this goes beyond the scope of the Thesis.

1.2 TIME-RESOLVED PHOTON STATISTICS

So far we have discussed the inherent properties of the states, in particular, the set of correlators $g^{(k)}$, the k-photon fluctuations of the photon-number distribution. To study the photon emission in more detail, however, we also need the dynamics of the field. The following gives an overview of results already known in the literature but that we need to survey so as to be able to extend them later on. Firstly, we now allow the single time correlators to vary in time $G^{(k)}(t) = \xi^{-k}\langle : (I(t))^k : \rangle$, where $I(t)$ is the intensity field operator defined as

$$I(t) = \epsilon \int_V E^{(-)}(\vec{x}, t) E^{(+)}(\vec{x}, t) d\vec{x}\,, \tag{1.37}$$

where V is the volume of the detection region, ϵ is a normalisation constant to ensure that the operator has the proper dimensions, all the additional constants after integrating are gathered up in ξ and :: indicates normal ordering. For our purposes, we can restrict the discussion to single-mode fields, unless otherwise indicated. The intensity operator thus reduces to $I(t) = \xi\, a^\dagger(t) a(t)$. In that case, $G^{(k)} = \langle a^{\dagger k}(t) a^k(t)\rangle$ recovers the same shape that we have already discussed but including the variation in time. We do not show examples yet because we would need the equations of motion that will remain undefined until the next Chapter. The meaning of the correlators is general enough to be described without particular cases. $G^{(k)}(t)$ is the direct generalisation of $G^{(k)}(0)$ for $\rho(t)$, the instant k-photon fluctuations of the photon-number distribution $P_k(t) = \rho_{k,k}(t)$.

A more general kind of correlator is multi-time k-photon Glauber functions

$$G^{(k)}(t_1, t_2, \ldots, t_k) = \xi^{-k}\langle : I(t_1) I(t_2) \ldots I(t_k) : \rangle\,, \tag{1.38}$$

where we have not any particular order for times t_i (with $k = 1, \ldots, k$). We introduce the canonical time ordering, choosing the times $t_i \in (0, T)$ to satisfy the following order

$$0 < t_1 < t_2 < \ldots < t_k < T\,. \tag{1.39}$$

After unravelling and ordering the operators in (1.38) such that $a^\dagger(t_i)$ grow in time from left to right, e.g., $a^\dagger(t_1)a^\dagger(t_2)$, and $a(t_i)$ grow from right to left, i.e., $a(t_2)a(t_1)$, we got

$$G^{(k)}(t_1, t_2, \ldots, t_k) = \langle a^\dagger(t_1) \ldots a^\dagger(t_k) a(t_k) \ldots a(t_1) \rangle \,. \tag{1.40}$$

In the context of the photo-detection theory, these time-ordered Glauber correlators are closely related to the coincidence or non-exclusive probability function $\mathcal{P}(t_1, t_2, \ldots t_k) = \xi^k G^{(k)}(t_1, t_2, \ldots, t_k)$. They measure how likely is to detect k photons in the interval $(0, T)$, one at each time t_i, while other counts can take place between successive times. In this sense, $G^{(2)}(t_1, t_2) = \langle a^\dagger(t_1)a^\dagger(t_2)a(t_2)a(t_1)\rangle$ measures how likely is to detect a pair of photons, one at t_1 and the other at t_2, no matter how many photons are detected in between t_1 and t_2. Another associated function is the elementary or exclusive probability function $\mathcal{Q}(t_1, t_2, \ldots t_k)$. Having the same time interval and time instants, $\mathcal{Q}(t_1, t_2, \ldots t_k)$ gives the probability of counting k photons, one at each t_i, without having any other count between time intervals, that is, the consecutive counts correspond to successive photons. The computation of this function is typically more complicated than the non-exclusive one. However, it can be seen that both distributions are linked. For the moment, we define the symmetrised version of $\mathcal{P}$ and $\mathcal{Q}$, namely $\tilde{\mathcal{P}}$ and $\tilde{\mathcal{Q}}$, where we have taken into account the $k!$ possible permutations of the instants t_i. For example, $\tilde{\mathcal{P}}(t_1, t_2) = \theta(t_2 - t_1)\mathcal{P}(t_1, t_2) + \theta(t_1 - t_2)\mathcal{P}(t_2, t_1)$, where $\theta(x)$ is the Heaviside step function. These symmetrised functions do not change when we exchange any pair of times ($t_i \leftrightarrow t_j$). The non-exclusive distribution is naturally written in terms of the exclusive distributions as

$$\tilde{\mathcal{P}}(t_1, \ldots, t_n) = \sum_{s=n}^{\infty} \frac{1}{(s-n)!} \int_0^T \ldots \int_0^T \tilde{\mathcal{Q}}(t_1, \ldots, t_n, \tau_{n+1}, \ldots, \tau_s) \prod_{p=n+1}^{s} d\tau_p. \tag{1.41}$$

The inversion of the previous formula is possible and the details can be found in Ref. [21]. We can then write $\tilde{\mathcal{Q}}$ as

$$\tilde{\mathcal{Q}}(t_1, \ldots t_k) = \sum_{s=k}^{\infty} \frac{(-1)^{k-s}}{(s-k)!} \int_0^T \ldots \int_0^T \tilde{\mathcal{P}}(t_1, \ldots t_k, \tau_{k+1}, \ldots \tau_s) \prod_{p=k+1}^{s} d\tau_p. \tag{1.42}$$

and, in terms of the intensity operator, we have

$$\tilde{\mathcal{Q}}(t_1, \ldots t_k) = \left\langle : I(t_1) \ldots I(t_k) \exp\left(- \int_0^T I(\tau) d\tau \right) : \right\rangle , \tag{1.43}$$

whereas the unsymmetrical case, with the ordering (1.39), is

$$Q(t_1, \dots t_k) = \theta(t_1 < t_2 < \dots t_k)\, \tilde{Q}(t_1, \dots t_k)\,, \tag{1.44}$$

where $\theta(t_1 < t_2 < \dots < t_k) = \prod_{p=1}^{k} \theta(t_p - t_{p-1})$ is the multi-time version of the Heaviside function and t_0 is the initial time of the time window, namely $t_0 = 0$. Finally, if we are interested in the probability of detecting k photons in the time window $(0, T)$, this is, $p(k, 0, T)$, we shall integrate over the time instants t_i

$$p(k, 0, T) = \int_0^T \int_0^{t_k} \dots \int_0^{t_2} Q(t_1, \dots t_k) dt_1 \dots dt_{k-1} dt_k\,, \tag{1.45}$$

or, using the symmetrised function,

$$p(k, 0, T) = \frac{1}{k!} \int_0^T \int_0^T \dots \int_0^T \tilde{Q}(t_1, \dots t_k) dt_1 \dots dt_{k-1} dt_k\,. \tag{1.46}$$

Introducing the time-integrated intensity operator $\Omega = \int_0^T I(\tau) d\tau$, we can expressed the photon-counting probability as it usually appears in the literature under the name of Mandel's photon-counting formula

$$p(k, 0, T) = \frac{1}{k!} \left\langle : \Omega^k \exp(-\Omega) : \right\rangle\,, \tag{1.47}$$

that we will fully develop in Chapter 4.

The usual measurements regarding the Glauber correlator functions involve interferometry schemes. For instance, using a Mach-Zehnder interferometer (scheme shown in Fig. 1.6), the amplitude-amplitude or field-field correlations, i.e.,

$$g^{(1)}(t, \tau) = \frac{\langle E^{(-)}(t) E^{(+)}(t + \tau) \rangle}{\langle E^{(-)}(t) E^{(+)}(t) \rangle}\,, \tag{1.48}$$

can be measured. The setup has got two beams splitters. The signal is split in two (if the BS is balanced, the signal is distributed 50:50), then the light travels along the two paths. If the total length of each path is different, there will be a time delay $\tau = \Delta l / c$ between the split signal. The fields are admixed in the second beam splitter and finally the intensity is recorded at one of the output arms. If the signal is stationary, then the correlation functions will depend only on τ. After many measurements or/and long time integration, we average the intensity and from there infer the amplitude-amplitude or first-order coherence correlation function $g^{(1)}(\tau)$ for fixed τ. Repeating the process for different values of τ, $g^{(1)}(\tau)$ can, a priori, be reconstructed.

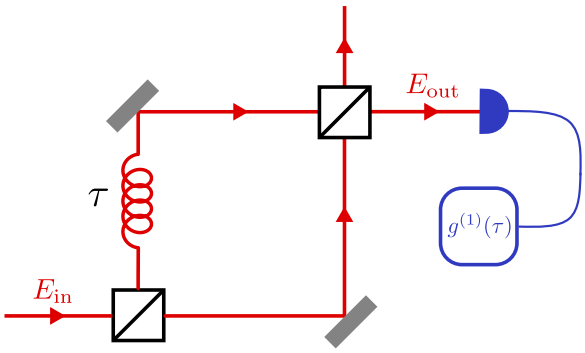

Figure 1.6: Typical scheme for the Mach-Zehnder interferometer. The input, namely E_{in}, is split in two and suffer a $\pi/2$ phase change. One of the signals travels across a delayed line and both merge and admix at the second beam splitter. After that, the output E_{out} is recorded at the detector and subsequently analysed to infer $g^{(1)}(\tau)$.

Through the Wiener-Khinchin theorem we can connect the normalised spectrum of the light $S(\omega)$ and the first-order coherent function $g^{(1)}(\tau)$ via the Fourier transform. It reads

$$S(\omega) = \frac{1}{2\pi}\int_{-\infty}^{\infty} g^{(1)}(\tau)e^{i\omega\tau}d\tau\,, \tag{1.49}$$

since, by definition, $g^{(1)}(-\tau) = (g^{(1)}(\tau))^*$, we can rewrite (1.49) as

$$S(\omega) = \frac{1}{\pi}\,\text{Re}\left\{\int_{0}^{\infty} g^{(1)}(\tau)e^{i\omega\tau}d\tau\right\}. \tag{1.50}$$

We can check the normalisation by integrating over all the frequencies

$$\int_{-\infty}^{\infty} S(\omega)d\omega = \frac{1}{2\pi}\int_{-\infty}^{\infty}\int_{-\infty}^{\infty} g^{(1)}(\tau)e^{i\omega\tau}d\tau d\omega\,, \tag{1.51}$$

remembering that $\int_{-\infty}^{\infty} e^{i\omega\tau}d\omega = 2\pi\delta(\tau)$, we finally get

$$\int_{-\infty}^{\infty} S(\omega)d\omega = \int_{-\infty}^{\infty} g^{(1)}(\tau)\delta(\tau)d\tau = g^{(1)}(0) = 1\,. \tag{1.52}$$

For a single mode and assuming that the system has reached the steady-state – implying that the signal is stationary – $g^{(1)}(\tau) = \langle a^\dagger(0)a(\tau)\rangle_{\text{ss}}/\langle a^\dagger a\rangle_{\text{ss}}$ (the subscript ss denotes that the average is performed on the steady-state solution). Then, the spectrum is recast as

$$S(\omega) = \frac{1}{\pi\langle a^\dagger a\rangle_{\text{ss}}}\,\text{Re}\left\{\int_{0}^{\infty} \langle a^\dagger(0)a(\tau)\rangle_{\text{ss}}\, e^{i\omega\tau}d\tau\right\}. \tag{1.53}$$

A second popular setup is the Hanbury Brown-Twiss interferometer

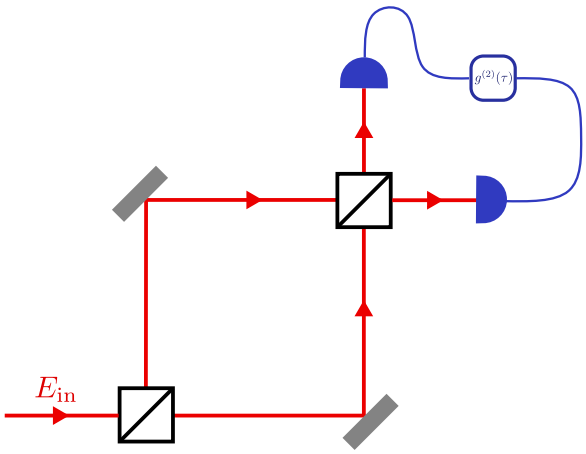

Figure 1.7: Scheme of the Hanbury Brown-Twiss intensity-intensity interferometer. The signal is split and the photon clicks (counts) are recorded at both outputs. Computing the cross-correlation of the intensities, the photon coincidences at multiple delay times τ are obtained, which are proportional to the second-order Glauber correlator $g^{(2)}(\tau)$.

(shown in Fig. 1.7). The measurements here are intensity-intensity correlations rather than amplitude-amplitude correlations. Therefore, they are associated to the second-order coherence $g^{(2)}(\tau)$ instead. The same setup as the Mach-Zehnder is used but it is not necessary to induce any delay between the two signals so that $\tau = 0$ within the interferometer. Splitting the signal and recording the counts at both arms, we can measure the coincidences separated by a given delay time τ. The second-order coherence is associated to the Glauber correlator [2]

$$g^{(2)}(t,\tau) = \frac{\langle E^{(-)}(t)E^{(-)}(t+\tau)E^{(+)}(t+\tau)E^{(+)}(t)\rangle}{\langle E^{(-)}(t)E^{(+)}(t)\rangle\langle E^{(-)}(t+\tau)E^{(+)}(t+\tau)\rangle}\,. \tag{1.54}$$

For a single-mode and stationary fields, the photon autocorrelation function reduces to

$$g^{(2)}(\tau) = \frac{\langle a^\dagger(0)a^\dagger(\tau)a(\tau)a(0)\rangle_{\text{ss}}}{\langle a^\dagger a\rangle^2_{\text{ss}}}\,, \tag{1.55}$$

which is the two-time 2-photon Glauber correlator, the straightforward generalisation of Eq. (A.3). This function is also symmetric when we change the sign of τ, i.e., $g^{(2)}(-\tau) = g^{(2)}(\tau)$ since the coincidences at previous times are exactly the same as the succeeding times, just exchanging the order of the photons (this may not be true for cross-correlations). It is closely related to the coincidence probability function $\tilde{\mathcal{P}}(t,t+\tau)$, however, it is normalised so that it will not depend on the average population (intensity) of the signal.

The interpretation is indeed the same. Having emitted a photon at $t = 0$, the probability of detecting a second photon on the interval $(\tau, \tau + d\tau)$, without specifying what happens in between, is given by $g^{(2)}(\tau)d\tau$. For $\tau \to \infty$, any correlation is washed out and the photons are uncorrelated, then, $\langle a^\dagger(0)a^\dagger(\tau)a(\tau)a(0)\rangle_{ss} \to \langle a^\dagger a\rangle_{ss}\langle a^\dagger a\rangle_{ss}$ and therefore $g^{(2)}(\tau \to \infty) \to 1$. We shall properly define photon antibunching as $g^{(2)}(0) < g^{(2)}(\tau)$. This is a stronger condition than simply $g^{(2)}(0) < 1$, which indicates the photon-number distribution has Sub-Poissonian fluctuation. As such, $g^{(2)}(\tau)$ cannot be understood as a proper probability density given that it is a non-normalisable function (this follows immediately from $g^{(2)}(\tau \to \infty) \to 1$) but we will show that it is closely related to exclusive probability distribution $w(\tau)$, called the Waiting Time Distribution (WTD), that provides the probability density for the inter-arrival time τ between successive photons, that is, how long the second photon takes to be finally emitted. Kim *at al.* derived in Ref. [22] a relation between both, which is easily formulated in the Laplace space and reads

$$\tilde{g}^{(2)}(s) = \frac{1}{R}\frac{\tilde{w}(s)}{1-\tilde{w}(s)}, \tag{1.56}$$

where the tilde denote the Laplace-transformed function $\tilde{g}^{(2)}(s) = \int_0^\infty g^{(2)}(\tau)e^{-s\tau}d\tau$ (and the same for $w(\tau)$) and R is the emission rate (probability per unit time to emit a photon). The inverse relation is

$$\tilde{w}(s) = \frac{\tilde{g}^{(2)}}{1/R + \tilde{g}^{(2)}}. \tag{1.57}$$

We then transform $\tilde{w}(s)$ back to the time domain. If the emission is uncorrelated then $g^{(2)} = 1$, which in the Laplace transform is $\tilde{g}^{(2)} = 1/s$. The WTD is then

$$w(\tau) = R\,e^{-R\tau}, \tag{1.58}$$

where the emission rate is usually written as $R = \gamma n_0$, where γ is one-photon decay rate and n_0, the mean number of photons, plays the role of the mean intensity. The WTD for an uncorrelated source is, expectedly, an exponential distribution, which is a characteristic feature of the Poisson process. Successive photons, though, remain always uncorrelated and will be emitted closer together on average as the photon rate grows. Later on, in the next Chapter, we present physical examples of $g^{(2)}(\tau)$ and then use Eq. (1.57) to obtain the corresponding $w(\tau)$, which were not computed before.

1.2.1 FREQUENCY-RESOLVED CORRELATIONS

The spectral properties of the light emitted by any dynamical system could bring precious information about the internal mechanisms that entangle or correlate the emission of pairs of photons (not necessarily successive) or more generally n-photons. Apparently this was already achieved studying the n-order Glauber correlators $g^{(n)}(t_1, \dots t_n)$ but, aside from the luminescence spectrum (1.50), we could not deduce how photons of frequencies ω_i (from 1 to n) correlated. In 1977, Eberly and Wódkiewicz proposed a theory to compute what they called the *physical spectrum* [23], that accounts for the spectral limitations of the photodetectors. This was subsequently applied to solve the frequency-filtered correlations of the Resonance Fluorescence by Knöll [24, 25], amongst other. We define the frequency-filtered field operator (for negative frequencies)

$$E_F^{(+)}(\vec{x}, t) \equiv \int_{-\infty}^{t} F(t - t_1) E^{(+)}(\vec{x}, t_1)\, dt_1\,, \tag{1.59}$$

that is the quantum counterpart of a filtered quantity in Signal Analysis where the original signal is convolved with the filter response F, here in time but it could be in space too. For the purpose of our analysis, we disregard the spatial dependence of the field and focus on the temporal resolution. The final results shall not vary dramatically for the cases of interest. Only the photon collection may be decreased which is translated into a worse detection efficiency ξ. Ultimately, the photon statistics are not affected by the amount of signal because $g^{(n)}$ are normalised quantities. Aside from these details, the frequency-resolved operator, namely ς_F, has the following form in term of the bare or (frequency) blind operator a:

$$\varsigma_F(t) = \int_{-\infty}^{t} F(t - t_1) a(t_1) dt_1\,. \tag{1.60}$$

and the adjoint operator is

$$\varsigma_F^\dagger(t) = \int_{-\infty}^{t} F^*(t - t_1) a^\dagger(t_1) dt_1\,, \tag{1.61}$$

As yet, we have not introduced any particular filter response function $F(t)$. In the frequency domain, the Fourier transform of the filter response is $\check{F}(\omega)$, given by

$$\check{F}(\omega) = \int_{-\infty}^{\infty} F(t) e^{i\omega t} dt\,, \tag{1.62}$$

or, inversely,

$$F(t) = \frac{1}{2\pi} \int_{-\infty}^{\infty} \check{F}(\omega) e^{-i\omega t} d\omega\,. \tag{1.63}$$

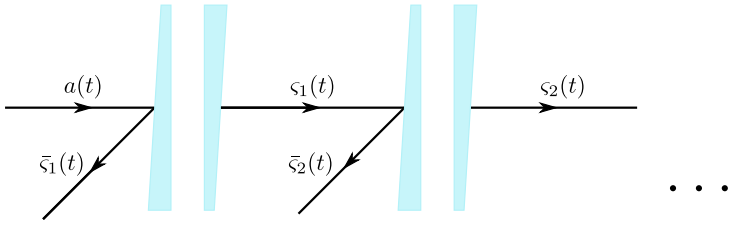

Figure 1.8: Possible scheme for the successive filters, represented here as Fabry-Perot etalons. The signal is split after impinging each interference filter, the transmitted (associated with the filtered operators ς) and the reflected (identified with the complementary filtered operators $\bar{\varsigma}$) parts, assuming there are no losses.

This defines the spectral shape of the filter which could come from a wide range of families. The response is expected to be causal if the filter only holds information about the past. Any realistic dynamical system must behave in this way. The arrival of a photon towards the filter cannot precede its emission. There are however some exceptions when we model the time uncertainty of the detector [26]. For frequency-resolved correlators, each filter will be causal and then we can extend the upper limit of the integral (1.60) to infinity.

The Lorentzian band-pass filter, for instance, has the response function

$$F_{\mathrm{L}}(t) = \frac{\Gamma}{2} e^{-(\Gamma/2 + i\omega_1)t}\theta(t)\,, \tag{1.64}$$

where Γ is the Full Width at Half Maximum (FWHM), ω_1 is the frequency corresponding to the maximum position and $\theta(t)$ is the Heaviside step function. In the frequency domain, the filter response reads

$$\check{F}_{\mathrm{L}}(\omega) = \frac{\Gamma/2}{\Gamma/2 + i(\omega - \omega_1)}\,. \tag{1.65}$$

In this case, the prefactor in (1.65) is chosen so that in the case of an infinitely broad filter ($\Gamma \to \infty$), we recover $\check{F}_{\mathrm{L}}(\omega) \to 1$, the Dirac delta in the time domain. Then, the filtered operator converges to the unfiltered one. Nevertheless, from the point of view of the transferred energy, the filter can absorb and emit an infinite amount of energy if the width Γ grows to infinity. The power spectrum is given by the modulus squared of the filter function $|\check{F}_{\mathrm{L}}(\omega)|^2$, which reads

$$|\check{F}_{\mathrm{L}}(\omega)|^2 = \frac{(\Gamma/2)^2}{(\Gamma/2)^2 + (\omega - \omega_1)^2}\,. \tag{1.66}$$

From (1.66) we find that the power spectrum is bounded between 0 and 1. We shall understand this as a measure of the probability

to accept a photon with frequency with frequency ω. As such, any photon with energy $\omega = \omega_1$ would never be rejected ($\check{F}_{\mathrm{L}}(\omega_1) = 1$). The main issue is that $|\check{F}_{\mathrm{L}}(\omega)|^2$ is not normalised. After integrating over the frequencies, we find $(2\pi)^{-1}\int_{-\infty}^{\infty}|\check{F}_{\mathrm{L}}(\omega)|^2 d\omega = \Gamma/4$. As the width Γ increases, the total transferred energy (or the filtered intensity) becomes larger and larger. An alternative choice of the prefactor is $\sqrt{\Gamma}$ instead of $\Gamma/2$. Then, the power spectrum is normalised but the infinitely-wide filter goes to zero rather than yielding the unfiltered operator back. We will keep the first definition (amplitude-normalised) for the filter response. Another useful filter is the Lorentzian band-stop filter. It can be seen as the complementary filter of (1.65). Its expression is

$$\check{F}_{\mathrm{CL}}(\omega) = 1 - \check{F}_{\mathrm{L}}(\omega) = \frac{i(\omega-\omega_1)}{\Gamma/2 + i(\omega-\omega_1)}\,, \tag{1.67}$$

and, in time domain, is

$$F_{\mathrm{CL}}(\omega) = \delta(t) - F_{\mathrm{L}}(t)\,. \tag{1.68}$$

If we assume that the amplitude normalisation rule can be applied for a particular filter $\check{F}$, then we are able to define the complementary filter $1-\check{F}$. For such family of filters, we have the following operator

$$\boxed{\bar{\varsigma}_F = \int_{-\infty}^{\infty}\big[\delta(t-t_1) - F_{\mathrm{L}}(t-t_1)\big]a(t_1)dt_1 = a(t) - \varsigma_F(t)\,,} \tag{1.69}$$

The introduction of such a complementary field was not, to the best of our knowledge, previously considered in the terms that we will now present and that will allow us to describe easily stop-band filters.

that we will call *complementary-field operator*. This identification makes possible to compute not only the filtered emission, that was already addressed by many authors, but also the rejected emission that, in some physical situations can be useful (as we devise in Ref. [Z4]). Both fulfil the identity $a(t) = \varsigma_F(t) + \bar{\varsigma}_F(t)$, that is, the total number of photons, either accepted or rejected by the filter, is conserved. Like the Fourier integral in Optics, the sum of the fields diffracted by an object and a slit with the complementary shape does return the incident field. In other words, the identity follows from the conservation of energy and could be useful to obtain the correlators of the complementary filter $\bar{F}$ from the bare and filtered correlators. This description naturally appears in the context of the frequency-resolved Monte Carlo [27]. In this scheme, the usual quantum-optical Monte Carlo method [28] is extended to include the frequency-resolved dynamics. In such scheme, one channel is clearly associated to the bare emission a and another one to the filtered emission ς_{F}. However, there is a third channel identified in Ref. [27] as *mixed emission*. This one indeed corresponds to the complementary-field emission $\bar{\varsigma}_F$. Therefore, performing the

Monte Carlo simulations automatically allows to simulate experimental realisations of photon detection for the bare or filtered emission, either the Lorentzian or the complementary Lorentzian.

If we substitute in Eq. (1.60) the operator $a(t)$ by another filtered one $\varsigma_{F'}$, we can obtain the doubly or second-order filtered operator that we will call $\varsigma^{(2)}$

$$\varsigma^{(2)}(t) = \int_{-\infty}^{\infty} F(t-t_1)\varsigma_{F'}(t_1)dt_1\,. \tag{1.70}$$

Substituting $\varsigma_{F'}$ and inserting the Fourier integral (1.63) for both filters, we end up with the following expression

$$\varsigma^{(2)}(t) = \int_{-\infty}^{\infty}\left(\frac{1}{2\pi}\int_{-\infty}^{\infty}\check{F}(\omega)\check{F}'(\omega)e^{-i\omega(t-s)}d\omega\right)a(s)ds\,. \tag{1.71}$$

That is, the effective response function of the second-order filter is the product of the filters responses in the frequency domain. For n consecutive filters, the same idea applies. In the Fourier space, the spectral response is the product of the functions $\check{F}_i$ (for $i = 1,\ldots,n$). However, if the function has to be amplitude-normalised (so that it converges to the Dirac delta), an additional prefactor has to be included. This may lead to unphysical situations if we understand the filter response as a physical target (such as a Fabry-Perot interferometer, also called etalon) that accepts photons from the source. In a series of n identical etalons (see Fig. 1.8), each one would reject or reflect some fraction of the signal (quantified by the reflectivity $1 \geq R \geq 0$) and then the transmitted signal will be proportional to $(1-R)^n$ (in absence of absorption). The amount of filtered signal will always be less than the incoming or unfiltered signal and is limited by the overlapping among the spectral functions. In the context of engineering, however, we can exploit the benefits of concatenating simpler filters to design a higher-order filter, in particular, using Lorentzian functions (each one with its width Γ_i and characteristic frequency ω_i). For instance, the non-Lorentzian filter

$$\check{F}_{\mathrm{N}}(\omega) = \left(\frac{\Gamma/2}{\Gamma/2 + i(\omega-\omega_1)}\right)^2, \tag{1.72}$$

that decays like ω^{-4}, much faster than a simple Lorentzian, and is the product of two identical Lorentzians. In this case, we shall consider two consecutive Lorentzian filters and then we would multiply the corresponding operator by the suitable normalisation constant and changing their width $\Gamma \to \Gamma/\sqrt{\sqrt{2}-1}$ so that the effective FWHM remains $\Gamma/2$ (same as the Lorentzian). Another well-known filter is

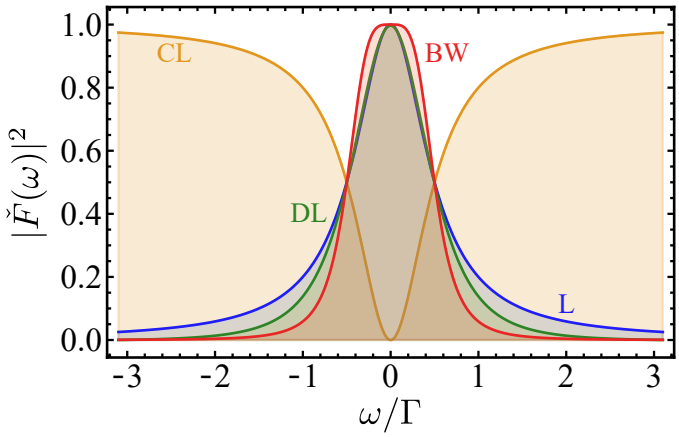

Figure 1.9: Squared amplitude of the four filters in question: Lorentzian (in blue), complementary (notch) Lorentzian (in orange), double Lorentzian (in green) and the second-order Butterworth filter (in red). The widths are chosen so that the FWHM is identical for all of them and the filter response at centered at zero for the sake of simplicity ($\omega_1 = 0$).

the second-order Butterworth filter

$$\check{F}_{\mathrm{B}}(\omega) = \frac{(\Gamma/2)^2}{(\Gamma/2)^2 + i\sqrt{2}\Gamma/2(\omega-\omega_1) - (\omega-\omega_1)^2}\,, \tag{1.73}$$

which also decays like ω^{-4} but is much flatter around the maximum, as it can be seen in Figure 1.9. The FWHM is exactly $\Gamma/2$ so it can be compared to Lorentzian filter right away. This filter can be generated by multiplying two Lorentzians, $\check{F}_{1,\mathrm{L}}$ and $\check{F}_{2,\mathrm{L}}$, with width $\Gamma' = \Gamma/\sqrt{2}$ and center frequencies $\omega_1' = \omega_1 + \Gamma'/2$ and $\omega_2' = \omega_1 - \Gamma'/2$. After the computation, we find that there is only a missing factor 2 which comes from the overlapping between the Lorentzian. The normalised operator associated to $\check{F}_{\mathrm{B}}$ is then twice the doubly-integrated operator $\varsigma^{(2)}(t)$ (choosing $\check{F} = \check{F}_{1,\mathrm{L}}$ and $\check{F}' = \check{F}_{2,\mathrm{L}}$).

1.2.2 DETECTED PHOTON STATISTICS

The properties of the photon statistics may be modified when we include in the detection picture detrimental effects such as, for instance, the time jitter and noise typical of detectors. In this Subsection, we derive the novel theory to include both sources of uncertainty in the detected emission (that appears in the publication [Z6]). For instance, an antibunched signal (ideally with $g^{(2)}(0) = 0$) would have its detected photon correlations lessened if an additional count takes place close to another one or if the timing jitter places two photons in the same time bin. These are, in fact, unavoidable issues in most

of the cases. In any detection scheme, typically the Hanbury Brown-Twiss, when photon coincidences are being recorded, the detection device plays a crucial role. The collection of single photons, with such low intensity, requires extremely-sensitive detectors. The most used ones in these situations are photomultiplier tubes but they have a low quantum efficiency. For this reason, avalanche photodiodes (in Geiger mode) are more suitable in this case. The main issue are their slow response and their large time jitter. Another drawback that limits the count rate is the noise contamination due to the afterpulsing, caused by the feedback following a previous count. Alternatively, a streak camera provides a direct observation of the series of photons impinging on the apparatus, allowing to measure not only 2-photon correlations but to perform real-time photon-number measurements (improved with novel techniques such the transition edge sensors).

The first source of contamination that we under study is the noise. The detector can indeed record counts even when there are no photons arriving to the detector. These are the well-known dark counts. Obviously, the correlations are affected by the dark counts and can spoil an antibunching measurement and thus thwart the true characterisation of the photon source. In the same way, the origin of the additional counts could come from the excitation source of the system, e.g., the laser light may arrive to the detector and contaminate the photon correlations.

We consider the total intensity operator as the sum of the source intensity $I(t)$ and the noise intensity $I'(t)$ (we will not specify the nature of the noise),

$$I^*(t) = I(t) + I'(t)\,, \tag{1.74}$$

and then the 2-photon Glauber correlator is

$$g^{*(2)}(t,\tau) = \frac{\langle : I^*(t)I^*(t+\tau) : \rangle}{\langle I^*(t)\rangle\langle I^*(t+\tau)\rangle}\,, \tag{1.75}$$

which for stationary signals (in the steady-state) reduces to

$$g^{*(2)}(\tau) = \frac{\langle : I^*(0)I^*(\tau) : \rangle}{\langle I^*(0)\rangle^2}\,. \tag{1.76}$$

Since the noise and the source remain uncorrelated at all times, we can split $\langle : I(0)I'(\tau) : \rangle$ (and the rest of the terms in the numerator) as $\langle I(0)\rangle\langle I'(0)\rangle$. Defining the noise-to-signal ratio $\eta \equiv \langle I'(0)\rangle / \langle I(0)\rangle$, we find the noise-contaminated photon statistics in terms of the original signal and noise correlations and the ratio η as

This expression allows one to describe exactly the impact of uncorrelated noise, of any type, to a quantum signal, which is a problem of great experimental relevance that is otherwise dealt with approximately.

$$\boxed{g^{*(2)}(\tau) = \frac{g^{(2)}(\tau) + 2\eta + \eta^2 g^{'(2)}(\tau)}{(1+\eta)^2}\,,} \tag{1.77}$$

where $g^{'(2)}(\tau) = \langle : I'(0)I'(\tau) : \rangle / \langle I'(0) \rangle^2$. If the source is perfectly antibunched, that is, $g^{(2)}(0) = 0$, then the effective $g^{*(2)}$ is clearly different from zero for $\eta > 0$. For Poissonian noise ($g^{'(2)} = 1$), for instance, $g^{*(2)}(0) = 0.5$ is reached when $\eta = \sqrt{2} - 1 \approx 0.42$ and tends monotonically to one as the noise intensity increases. The random counts due to shot noise spoils, as expected, the antibunching and turns the total signal into a Poisson-distributed (uncorrelated) noise. Likewise, for any bunched signal $g^{*(2)}(0)$ converges to one for strong enough noise ratios. Another kind of noise is thermal noise which has $g^{'(2)}(0) = 2$. The correlations worsen even faster, $g^{*(2)}(0)$ reaches 0.5 when $\eta = 1/3$ and make the signal uncorrelated (at the 2-photon level) for $\eta = 1$ and get bunched for greater values. The overall effect is more detrimental than the Poisson noise.

We can extend the computation of the total signal correlations to the n-photon level. The zero-delay n-Glauber correlator reads

$$g^{*(n)}(0) = \sum_{k=0}^{n} \binom{n}{k} \frac{\eta^{n-k}}{(1+\eta)^n} g^{(k)}(0)\, g^{'(n-k)}(0)\,, \tag{1.78}$$

which, if $g^{(n>1)}(0) = 0$, simplifies to

$$g^{*(n)}(0) = \frac{\eta^n g^{'(n)}(0)}{(1+\eta)^n} + \frac{n\,\eta^{n-1} g^{'(n-1)}(0)}{(1+\eta)^n}\,. \tag{1.79}$$

The antibunching, of course, is destroyed as the noise intensity grows. However, Poissonian and thermal noises behave in a different way when we go to higher orders. We compute the value of η for which $g^{*(n)}(0) = n!/n^n$ ($g^{(n)}$ of the n-Fock state). The Poisson noise has no analytical solution for $n > 2$, whereas the thermal does, it is $\eta = (n^{\frac{n}{n-1}} - 1)^{-1}$. In Table 1.3 are shown some cases. Comparing both kinds of noise, we observe that the correlators resemble (independently of the rest) the n-photon Fock state for growing (although with slow-paced rate) values if the noise is uncorrelated, while the thermal noise displays the opposite trend, the antibunching gets worse, faster as n is greater.

We consider now the time uncertainty in the detector. The cause can be either the dead time, which is the time gap after a count in which the detector cannot record a second one as a separated event, or a timing jitter effect. The resulting effect is that a photon that arrives at time t_0 is recorded by the detector at $t_0 + t$. The probability distribution that follows time t is $D^2_\Gamma(t)$, where Γ is the width of the distribution, proportional to inverse of characteristic jitter time (this is, how long t deviates from perfect time arrival). Even though the photon arrival time is not completely determined, we are assuming that each

n	η (poisson)	η (thermal)
2	0.412	0.333
3	0.439	0.238
4	0.455	0.187
5	0.468	0.154

Table 1.3: Numerical values for the noise-to-signal ratio η that are solution of $g^{*(n)}(0) = n!/n^n$, this is, when the total signal (perfectly-antibunched signal + noise) reaches the $g^{(n)}$ of the n-photon Fock state. Two types of noise are shown: Poissonian, with $g^{'(n)}(0) = 1$, and thermal, with $g^{'(n)}(0) = n!$.

photon is eventually detected. As a consequence, the probability distribution must fulfil

$$\int_{-\infty}^{\infty} D_\Gamma^2(t)dt = 1\,. \tag{1.80}$$

Even if the photons are always reported, the temporal structure of the emission is affected by the time uncertainty. We can evaluate its effect through the spectrum of emission, as provided in Ref. [23],

$$S_\Gamma^{(1)}(\omega, T) = \frac{1}{2\pi}\int_{-\infty}^{\infty}\int_{-\infty}^{\infty} D_\Gamma(T-t_1)D_\Gamma(T-t_2)e^{i\omega(t_2-t_1)}\times \\ \times\,\langle a^\dagger(t_1)a(t_2)\rangle dt_1 dt_2\,, \tag{1.81}$$

where ω and T are the frequency and time at which the photons are being detected. In the next Chapter, we will consider a particular case, the two-level system (2LS). For the moment, we will retain the theory as general as possible, so actually $a(t)$ can be any single-mode operator. We now integrate over all the frequencies Equation (1.81), yielding

$$S_\Gamma^{(1)}(T) = \int_{-\infty}^{\infty} D_\Gamma^2(T-t_1)\langle a^\dagger a\rangle(t_1)dt_1\,, \tag{1.82}$$

where we have used the property $2\pi\delta(t_1-t_2) = \int_{-\infty}^{\infty} e^{i\omega(t_1-t_2)}$. The detected population is then the convolution of the jitter probability function and the bare population. If the system has reached the steady-state, the bare population does not depend on time, i.e., $\langle a^\dagger a\rangle(t) = n_0$. In that case, the detected intensity is exactly n_0, which is a result that follows from the perfect detection assumption (remembering the normalisation of D_Γ) we made. In the same way, we can apply this formalism to the 2-photon correlator. We expect however that the correlator is affected even in the steady-state, since it is a measure of

the inter-arrival time between photons. The second-order correlator of the detected signal is then

$$S^{(2)}_{\Gamma_1\Gamma_2}(\omega_1, T_1; \omega_2, T_2) = \frac{1}{(2\pi)^2} \int D_{\Gamma_1}(T_1 - t_1) D_{\Gamma_1}(T_1 - t_4) \times$$
$$D_{\Gamma_2}(T_2 - t_2) D_{\Gamma_2}(T_2 - t_3) e^{i\omega_1(t_4 - t_1)} e^{i\omega_2(t_3 - t_2)} \times$$
$$\langle \mathcal{T}[a^\dagger(t_1) a^\dagger(t_2) a(t_3) a(t_4)] \rangle dt_1 dt_2 dt_3 dt_4 \quad (1.83)$$

where the time-ordering operator $\mathcal{T}$ ensures that all annihilation operators are ordered in increasing time from right to left and, conversely, the creation operators in increasing ordered from right to left and we omitted the integration limit (from $-\infty$ to ∞) for simplicity. Since we might look upon photon coincidences from distinct detectors, the widths Γ_1 and Γ_2 can be different. We however assume that both detectors are identical so $\Gamma_1 = \Gamma_2 = \Gamma$ for the sake of simplicity. Integrating over the frequencies ω_1 and ω_2 equation (1.83), we get $S^{(2)}_\Gamma(T_1; T_2)$, which reads now

$$S^{(2)}_\Gamma(T_1; T_2) = \int \int D^2_\Gamma(T_1 - t_1) D^2_\Gamma(T_2 - t_2) \times$$
$$\langle \mathcal{T}[a^\dagger(t_1) a^\dagger(t_2) a(t_2) a(t_1)] \rangle dt_1 dt_2 \,. \quad (1.84)$$

Notice that the correlation function that appears within the previous integral is indeed another way to express the symmetrised version of $G^{(2)}(t_1, t_2)$. There are two possible orderings, $t_1 > t_2$ and $t_2 > t_1$, and we can rewrite them as a single term $G^{(2)}(t, \tau) = \langle a^\dagger(t) a^\dagger(t + \tau) a(t + \tau) a(t) \rangle$, where $t \equiv \min(t_1, t_2)$ and $\tau \equiv |t_1 - t_2|$, the latter being the time delay between the photons. The detected time-resolved second-order correlator is then written as

$$S^{(2)}_\Gamma(T_1; T_2) = \int_{-\infty}^{\infty} \int_0^\infty G^{(2)}(t_1, \tau_1) [D^2_\Gamma(T_1 - t_1) D^2_\Gamma(T_2 - t_1 - \tau_1) +$$
$$D^2_\Gamma(T_1 - t_1 - \tau_1) D^2_\Gamma(T_2 - t_1)] d\tau_1 dt_1 \,. \quad (1.85)$$

The corresponding normalised correlator simply reads

$$g^{(2)}_\Gamma(T_1; T_2) = \frac{S^{(2)}_\Gamma(T_1; T_2)}{S^{(1)}_\Gamma(T_1) S^{(1)}_\Gamma(T_2)} \,. \quad (1.86)$$

In the steady-state, time t_1 is completely irrelevant and the function does depend only on the time delay τ, i.e., $G^{(2)} = G^{(2)}(\tau)$. The detected (jittered) 2-photon, consequently, would not be a function of T_1 and T_2 but of the time difference τ. Finally, the jittered $g^{(2)}_\Gamma(\tau)$ as function of the original $g^{(2)}(\tau)$ and the jitter function D_Γ reads

$$\boxed{g^{(2)}_\Gamma(\tau) = \int_0^\infty g^{(2)}(\tau') \int_{-\infty}^\infty [D^2_\Gamma(-t' - \tau') D^2_\Gamma(\tau - \tau') + D^2_\Gamma(-t') D^2_\Gamma(\tau - t' - \tau')] dt' d\tau' \,.} \quad (1.87)$$

This expression allows one to describe exactly the impact of jitter, of any type, to a quantum signal, which is a problem of great experimental relevance that is otherwise dealt with approximately in terms of simplified (Gaussian) deconvolution. Analytical results for the cases of most interest are given below.

The jittered Glauber correlator is, therefore, the original Glauber correlator weighted by the function that only depends on D_Γ and this is completely general as long as the solution corresponds to the steady-state. The jitter function D_Γ can be, in principle, any function describing the timing jitter response. We include now four possibilities together with a brief discussion on their physical origin. In order to compare them on equal footing, all the distributions must have the same variance so that the width Γ is common to the four cases (shown in Fig. 1.10).

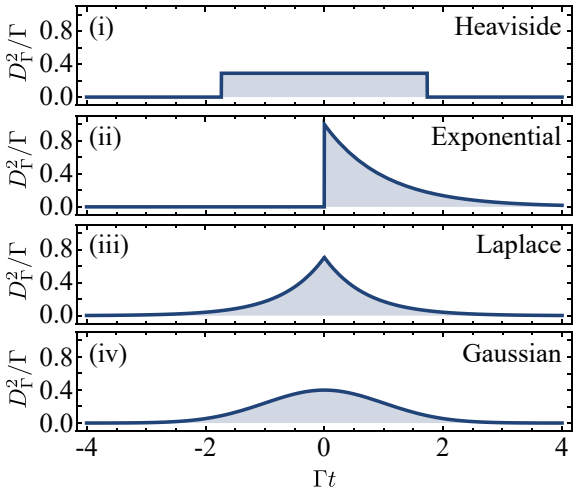

Figure 1.10: The four jitter functions discussed in the text, which are (i) Heaviside, (ii) one-sided exponential, (iii) two-side exponential (Laplace) and (iv) Gaussian. They describe the fluctuations distribution for the detected photon arrival time. Reproduced with permission from [Z6]. Copyright (2022) by the APS.

First, we consider the Heaviside-like function. This describes a device which has undefined time resolution within a fixed time window, that might correspond to a pixel of a CCD camera. It would randomly assign any value of the time window. The jitter function in this case reads

$$D_\Gamma(t) = \sqrt{\frac{\Gamma}{\sqrt{12}}}\theta\left(1-\frac{2\Gamma t}{\sqrt{12}}\right)\theta\left(1+\frac{2\Gamma t}{\sqrt{12}}\right), \tag{1.88}$$

where the nonzero region is $(-\sqrt{3}/\Gamma, \sqrt{3}/\Gamma)$.

Another possible function is the one-sided exponential, that corresponds to devices with memoryless dead time. After the collection (when the photodetector gets excited), the triggered signal could occur at any following time with the same probability per unit time. The jitter function is

$$D_\Gamma(t) = \sqrt{\Gamma}\theta(t)e^{-\Gamma t/2}. \tag{1.89}$$

If both the triggered signal and the excitation time have memoryless dead time, then the jitter function has to be a two-sided exponential (also known as the Laplace distribution), which reads

$$D_\Gamma(t) = \sqrt{\frac{\Gamma}{\sqrt{2}}} e^{-\Gamma|t|/\sqrt{2}}. \tag{1.90}$$

Unlike the previous case, the recorded arrival time can be either greater or smaller than the original one.

Finally, we consider the normal or Gaussian distribution. There are multiple reasons to choose this function since this type of fluctuations may arise in several steps of the detection process, e.g, noise in the electronics or a side effect after the photon arrival. The function has the following expression

$$D_\Gamma(t) = \sqrt{\frac{\Gamma}{\sqrt{2\pi}}} e^{-(\Gamma t/2)^2}. \tag{1.91}$$

To follow with the discussion we would need to specify a $g^{(2)}(\tau)$. The simplest example is a coherent source, such as an ideal laser, which emits uncorrelated photons. As such, $g^{(2)}(\tau) = 1$ for any τ. The resulting jitter autocorrelation functions are, in all cases, $g^{(2)}_\Gamma(\tau) = 1$. Since the photons are uncorrelated, shuffling them randomly will not induce any additional correlations. If the 2-photon Glauber correlator can be written as a sum of exponentials, this is, $g^{(2)}(\tau) = 1 + \sum_p l_p\, e^{-\lambda_p \tau}$ (such that $\mathrm{Re}\{\lambda_p\} > 0$), then, due to the linearity of the integral (1.87), we can express the jitter correlator as sum $g^{(2)}_\Gamma(\tau) = 1 + \sum_p l_p\, \mathcal{I}_p(\tau)$, where

$$\begin{aligned}\mathcal{I}_p(\tau) = \int_0^\infty e^{-\lambda_d \tau_1} \int_{-\infty}^\infty \big[D^2_\Gamma(-t_1-\tau_1) D^2_\Gamma(\tau-\tau_1) + \\ D^2_\Gamma(-t_1) D^2_\Gamma(\tau - t_1 - \tau_1)\big] dt_1 d\tau_1 .\end{aligned} \tag{1.92}$$

The particular values for both the coefficients l_p and the complex exponents λ_p have to be computed for each system but knowing the general expressions (1.92) beforehand allows us to automatically obtain the jitter counterpart of $g^{(2)}(\tau)$.

For the Heaviside jitter function (1.88), the integral (1.92) yields

$$\begin{aligned}\mathcal{I}^{(i)}_p(\tau) = -\frac{\Gamma^2 e^{-\lambda_p \tau}}{6\lambda_p^2} + \theta(\Gamma\tau - \sqrt{12}) \frac{\Gamma^2\, e^{-\lambda_p \tau} \cosh\left(\sqrt{12}\lambda_p/\Gamma\right)}{6\lambda_p^2} + \\ \theta(\sqrt{12} - \Gamma\tau)\left[\frac{e^{-\sqrt{12}\lambda_p/\Gamma}\,\Gamma^2 \cosh(\lambda_p \tau)}{6\lambda_p^2} + \frac{\Gamma}{\sqrt{3}\lambda_p} - \frac{\Gamma^2\,\tau}{6\lambda_p}\right],\end{aligned} \tag{1.93}$$

while for the one-sided exponential (1.89) it is

$$\mathcal{I}_p^{(ii)}(\tau) = \frac{\Gamma}{\Gamma^2 - \lambda_p^2}\left(\Gamma e^{-\lambda_p \tau} - \lambda_p\, e^{-\Gamma \tau}\right), \tag{1.94}$$

whereas the two-sided exponential (1.90) has the following expression

$$\begin{aligned}\mathcal{I}_p^{(iii)}(\tau) = &\frac{1}{2\left(\lambda_p + \sqrt{2}\Gamma\right)^2\left(\lambda_p^2 - 2\Gamma^2\right)^2}\\ &\Big\{8\Gamma^4(2\Gamma^2 + 2\sqrt{2}\Gamma\lambda_p + \lambda_p^2)\, e^{-\lambda_p\tau} -\\ &\Gamma\lambda_p\big[8\Gamma^5\tau + 4\sqrt{2}\Gamma^4(2\lambda_p\tau + 3) + 24\Gamma^3\lambda_p -\\ &4\sqrt{2}\Gamma^2\lambda_p^2(\lambda_p\tau - 1) - 2\Gamma\lambda_p^3(\lambda_p\tau + 2) - \sqrt{2}\lambda_p^4\big] e^{-\sqrt{2}\Gamma\tau}\Big\},\end{aligned} \tag{1.95}$$

and, finally, for the Gaussian function (1.91), we have

$$\mathcal{I}_p^{(iv)}(\tau) = \frac{1}{2} e^{\lambda_p^2/\Gamma^2 - \lambda_p\tau}\,\mathrm{erfc}\left(\frac{\lambda_p}{\Gamma} - \frac{\Gamma\tau}{2}\right) + \frac{1}{2} e^{\lambda_p^2/\Gamma^2 + \lambda_p\tau}\,\mathrm{erfc}\left(\frac{\lambda_p}{\Gamma} + \frac{\Gamma\tau}{2}\right), \tag{1.96}$$

where $\mathrm{erfc}(x) = \frac{2}{\sqrt{\pi}}\int_x^\infty e^{-t^2} dt$ is the complementary error function. These integrals have much simpler expressions if the delay time is zero ($\tau = 0$), which are

$$\mathcal{I}_p^{(i)}(0) = \frac{\sqrt{12}\Gamma\lambda_p - \Gamma^2\left(1 - e^{-\sqrt{12}\lambda_p/\Gamma}\right)}{6\lambda_p^2}, \tag{1.97a}$$

$$\mathcal{I}_p^{(ii)}(0) = \frac{\Gamma}{\Gamma + \lambda_p}, \tag{1.97b}$$

$$\mathcal{I}_p^{(iii)}(0) = \frac{\Gamma(4\Gamma + \sqrt{2}\lambda_p)}{2(\sqrt{2}\Gamma + \lambda_p)^2}, \tag{1.97c}$$

$$\mathcal{I}_p^{(iv)}(0) = e^{\lambda_p^2/\Gamma^2}\mathrm{erfc}(\lambda_p/\Gamma). \tag{1.97d}$$

From these last equations, we find that in the limit $\Gamma \to 0$, all the cases go to zero, that is, $\mathcal{I}_p(0) \to 0$. Then, the jittered Glauber correlator simply reads $g_\Gamma^{(2)}(0) = 1$. For large time jitter $1/\Gamma$, all the photons are scrambled and the correlations are lost, resulting in a uncorrelated stream of photons. On the opposite limit ($\Gamma \to \infty$), when the time jitter vanishes, all the integrals (1.97) tend to one. Therefore, as expected, we recover the bare photon correlations.

In the next Chapter, we compute the correlations of a single-photon emitter under for different regimes of excitation. In all the cases, the antibunching is perfect ($g^{(2)}(0) = 0$). We will then apply this theory and discuss the effect on the antibunching induced by the time jitter.

2

LIGHT-MATTER INTERACTIONS

2.1 TWO-LEVEL SYSTEM: SINGLE-PHOTON EMITTER

Let us introduce a system consisting of two levels, also called qubit. The lower state is often called ground state and we identify it as $|0\rangle$. The corresponding energy of the ground state is ω_0, however, in order to simplify further computations, we will take this energy as a reference for the next ones. As such, we assume, unless noticed otherwise, that $\omega \to \omega - \omega_0$. The excited state, denoted as $|1\rangle$, naturally has a greater energy $\omega_1 > \omega_0$. We define the transition or lowering/rising operators $\sigma = |0\rangle\langle 1|$ and $\sigma^\dagger = |1\rangle\langle 0|$, respectively. Together with $\hat{n}_\sigma = \sigma^\dagger\sigma = |1\rangle\langle 1|$, which provides the probability of being in the excited state, the state is completely specified. These three elements form an algebra equivalent to that of the spin one half and is often referred to as a pseudo-spin algebra (and not a spin algebra because fermion statistics may not be obeyed among different qubits). The transition between these two states has characteristic frequency or energy $\omega_\sigma = \omega_1 - \omega_0$ and can be mediated by many different mechanisms, which we can classify in two categories, radiative or non-radiative. If any electromagnetic field is involved and photon absorption or emission is taking place, then the process is radiative. If not, it is non-radiative. The backbone of the present work is studying the generation of light, thus, we are especially interested in the first kind of processes. Nevertheless, neglecting the non-radiative processes sometimes leads to inaccurate or plainly mistaken results.

A non-interacting qubit has the following Hamiltonian:

$$H_0 = \omega_\sigma \sigma^\dagger \sigma \,, \tag{2.1}$$

and the most general description of the quantum state of the qubit is given in terms of its density matrix

$$\rho = \rho_{00}\,|0\rangle\langle 0| + \rho_{01}\,|1\rangle\langle 0| + \rho_{10}\,|0\rangle\langle 0| + \rho_{11}\,|1\rangle\langle 1| \,. \tag{2.2}$$

Since the density matrix is hermitian $\rho^\dagger = \rho$, its matrix elements fulfil $\rho_{ji} = \rho^*_{ij}$. In particular, the diagonal elements are necessarily real. Since the probability of being in the i-th state $\rho_{ii} = P_i$, they must

be positive and the sum has to be equal to one, $\mathrm{tr}(\rho) = \sum_i P_i = 1$. Alternatively, the state is represented using a regular matrix

$$\rho = \begin{pmatrix} \rho_{00} & \rho_{01} \\ \rho_{10} & \rho_{11} \end{pmatrix} . \tag{2.3}$$

The correlation functions that can be computed are just three and the rest of them are zero, since $\sigma^n = 0$ and $\left(\sigma^\dagger\sigma\right)^n = \sigma^\dagger\sigma$, for $n > 1$:

$$\langle\sigma\rangle = \mathrm{tr}(\rho\sigma) = \rho_{01} , \tag{2.4a}$$

$$\langle\sigma^\dagger\rangle = \mathrm{tr}\left(\rho\sigma^\dagger\right) = \rho_{10} = \langle\sigma\rangle^* , \tag{2.4b}$$

$$\langle\sigma^\dagger\sigma\rangle = \mathrm{tr}\left(\rho\sigma^\dagger\sigma\right) = \rho_{11} , \tag{2.4c}$$

which, together with the trace norm $\mathrm{tr}(\rho) = 1$, allow us to rewrite ρ as

$$\rho = \begin{pmatrix} 1 - \langle\sigma^\dagger\sigma\rangle & \langle\sigma\rangle^* \\ \langle\sigma\rangle & \langle\sigma^\dagger\sigma\rangle \end{pmatrix} . \tag{2.5}$$

The same kind of substitution or mapping applies to more general and interesting systems such as qudits (with more than one excited state) or even to infinite dimensional systems as the harmonic oscillator (see Chapter 1).

The temporal evolution of the qubit state is given by the Liouville-Von Neumann equation, quantum counterpart of the Liouville equation [29] or, equivalently, the Heisenberg equation [30] for the density matrix ρ

$$\dot{\rho}(t) = -i[H_0, \rho(t)] , \tag{2.6}$$

where $\dot{\rho}(t)$ is the time derivative of $\rho(t)$. The formal solution of this equation is $\rho(t) = e^{-iH_0t}\rho(0)e^{iH_0t}$. This exponential factor is called then evolution operator $U(t) = e^{-iH_0t}$. Applied to the matrix elements, we get $U(t)\,|\mu\rangle\,\langle\nu|\,U^\dagger(t) = e^{-i\omega_\sigma(\mu-\nu)t}\,|\mu\rangle\,\langle\nu|$ (for $\mu, \nu = 0, 1$). The free evolution of the state adds an unitary exponential to the ket $|\mu\rangle \to e^{-i\omega_\sigma\mu t}\,|\mu\rangle$. In the same manner, the correlation functions have the following expressions:

$$\langle\sigma\rangle(t) = \mathrm{tr}(\rho(t)\sigma) = \rho_{10}(0)\, e^{i\omega_\sigma t} , \tag{2.7a}$$

$$\langle\sigma^\dagger\rangle(t) = \mathrm{tr}\left(\rho(t)\sigma^\dagger\right) = \rho_{01}(0)\, e^{-i\omega_\sigma t} , \tag{2.7b}$$

$$\langle\sigma^\dagger\sigma\rangle(t) = \mathrm{tr}\left(\rho(t)\sigma^\dagger\sigma\right) = \rho_{11}(0) . \tag{2.7c}$$

As expected, without any interaction, the probabilities $P_i(t) = P_i(0)$ remain equal at all time t. The next step is to include interactions,

that is, to couple the qubit (matter) to the Electromagnetic (EM) field (light). In our level of approximation, the light-matter interaction is well described by the dipole interaction Hamiltonian [31]. Defining the electric dipole moment operator $\hat{\vec{d}}$ and the quantity $\vec{d} = \langle 0|\,\hat{\vec{d}}\,|1\rangle$ – the dipole moment associated to this transition – we can write the interaction Hamiltonian as

$$H_{\text{int}} = -\left[\vec{E}(t)\cdot\vec{d}\right]\sigma - \left[\vec{E}(t)\cdot\vec{d}^{*}\right]\sigma^{\dagger}\,, \tag{2.8}$$

where $\vec{E}(t) = \vec{E}_0 e^{-i\omega t} + \text{c.c}$ is the electric field of a monochromatic EM waves with (complex) amplitude $\vec{E}_0$ and frequency ω. The next approximation is to assume that the frequencies of the transition and wave are close enough, i.e., $\omega \approx \omega_\sigma$, so that none of the remaining levels are excited. In the interaction picture the hamiltonian is

$$UH_{\text{int}}U^{\dagger} = -\left[\vec{E}(t)\cdot\vec{d}\right]e^{-i\omega_\sigma t}\sigma - \left[\vec{E}(t)\cdot\vec{d}\right]e^{i\omega_\sigma t}\sigma^{\dagger}\,. \tag{2.9}$$

After expanding the electric field, it reads

$$UH_{\text{int}}U^{\dagger} = -\left[(\vec{E}_0\cdot\vec{d})\,e^{-i(\omega+\omega_\sigma)t} + (\vec{E}_0^{*}\cdot\vec{d})\,e^{i(\omega-\omega_\sigma)t}\right]\sigma + \text{h.c.}\,. \tag{2.10}$$

The exponential with sum $\omega+\omega_\sigma$ oscillates rapidly as compared to the other one with the difference $\omega-\omega_\sigma \approx 0$. Thus, we can neglect the first term and change ω_σ by ω. This approximation is known as the Rotating Wave Approximation (RWA). Then, keeping only the term proportional to $e^{-i\omega t}$ is $\vec{E}(t) \approx i\omega\vec{A}_0 e^{-i\omega t} = \vec{E}_0 e^{-i\omega t}$.

With all this, the final form of the interaction Hamiltonian is

$$H_{\text{int}} \approx -\left(\vec{E}_0\cdot\vec{d}^{*}\right)e^{-i\omega t}\sigma^{\dagger} - \left(\vec{E}_0^{*}\cdot\vec{d}\right)e^{i\omega t}\sigma\,, \tag{2.11}$$

or, introducing the abbreviated notation $\Omega_\sigma = -\left(\vec{E}_0\cdot\vec{d}^{*}\right)$, we finally get

$$H_{\text{int}} = \Omega_\sigma e^{-i\omega t}\sigma^{\dagger} + \Omega_\sigma^{*} e^{i\omega t}\sigma\,. \tag{2.12}$$

This is the light-matter interaction Hamiltonian in the electric dipole and RWA and we assume these two approximations to be valid all along this Thesis. In general, this Hamiltonian has the form $H_{\text{int}} = -\vec{E}(\vec{x_0},t)\cdot\hat{\vec{d}}$ for each emitter, placed at the position x_0, that is coupled to the EM field at this same point. The effective coupling Ω_σ is treated as a c-number instead of a quantum operator, so the theory is semiclassical. Within the fully-quantised model, the electric field is treated as an operator, i.e., $\vec{E}(t) \to \hat{\vec{E}}(t) = \vec{E}_0\,a(t) + \text{h.c.}$, where a is a bosonic operator associated to a specific EM mode. The full quantum interaction Hamiltonian is then

$$H_{\text{int}} = g\,a^{\dagger}\sigma + g^{*}\,\sigma^{\dagger}a\,, \tag{2.13}$$

where g is the coupling strength between the EM mode and the qubit. The full system Hamiltonian, the free evolution and the interaction, reads

$$H = \omega a^\dagger a + \omega_\sigma \sigma^\dagger \sigma + g\, a^\dagger \sigma + g^*\, \sigma^\dagger a\,. \tag{2.14}$$

If the operator a corresponds to a cavity mode, i.e., the system is confined, rather than a free space mode, the model is known as the Jaynes–Cummings model [32], that was first introduced to study the differences between the semiclassical and quantum theories of light-matter interactions.

With the semiclassical theory, it is only possible to explain the stimulated emission and absorption of photon by atoms, nuclei or any other matter system. It was not until the quantum nature of light was considered that the spontaneous emission was well understood. However, some apparent contradictions may arise when combining irreversible processes such as losing photon forever and quantum mechanics, where the unitarity, and therefore reversibility, is a cornerstone of the theory. A proper formulation and treatment of the problem was correctly tackled when the open quantum system formalism [33, 34] was introduced and subsequently applied in the quantum-optical context. The derivation and further explanations of the formalism can be found in Refs. [21, 35, 36]. The outline of the formalism is that the system and the environment (reservoir), described by the corresponding density matrix ρ, are split into parts and then the reservoir degrees of freedom are averaged and explicitly eliminated for the dynamics. To simplify the computations some approximations are usually made. For our kind of systems – the quantum-optical ones – there are two main assumptions or approximations. Firstly, we assume that the system and reservoir interaction is weak so that they are disentangled at all times. This strong statement is known as the *Born approximation*. In other words, the correlations between system and reservoir are small enough to be neglected. The second major assumption is the *Markov approximation*. The equation of motion, the master equation, is then memoryless and simplifies to a regular differential operator equation. The justification of this simplification is similar to the previous one. The time scale of the bath-system correlations compared to the dynamics of the system are short enough to disregard any memory effect.

The master equation of a Two-Level System (2LS) coupled to a photonic bath in thermal equilibrium is given by

$$\dot{\rho} = -i[H_\sigma, \rho] + \frac{\gamma_\sigma}{2}\bar{N}\mathcal{L}_\sigma\rho + \frac{\gamma_\sigma}{2}(\bar{N}+1)\mathcal{L}_{\sigma^\dagger}\rho\,, \tag{2.15}$$

where γ_σ is the decay rate of the emitter and $\bar{N}$ is the mean number of photons of the thermal bath. We have also introduced here the popular notation in open quantum systems [37], the Lindblad terms $\mathcal{L}_c\rho = 2c\rho c^\dagger - c^\dagger c\rho - \rho c^\dagger c$ (where c is the suitable operator). The first term represents the Hamiltonian or coherent evolution of the system. The remaining ones, given by the Lindblad terms, are associated to the incoherent or non-hermitian evolution. They represent the losses and gains (or other processes) that cannot be described through the Hamiltonian formalism. The Lindbladian $\mathcal{L}_\sigma\rho$ unidirectionally connects the excited state $|1\rangle$ to the ground state $|0\rangle$. It explains the irreversible decay of the qubit in presence of the environment. Conversely, the Lindbladian $\mathcal{L}_{\sigma^\dagger}\rho$ links the ground state with the excited state in the opposite direction. The thermal reservoir, like in classical Thermodynamics, can transfer energy in both ways. A thermal photon can be absorbed by the system and therefore get excited. This excitation process is known as *incoherent pumping*.

Now, we would like to remark a few points. In the first place, as mentioned at the beginning of the Section, the system could be coupled not only to the EM field. The total bath could be more general. For instance, emitters embedded in crystals usually couple to the vibrational degrees of freedom, known as phonons. The steps can be repeated with these different baths so that new Lindblad terms may appear. In particular, the total decay and pumping rates may not be $\gamma_\sigma(\bar{N}+1)$ and $\gamma_\sigma\bar{N}$ but something more generic. We shall define the arbitrary rates γ_σ and P_σ that are not restricted by the inequality $P_\sigma < \gamma_\sigma$ (unlike for a free cavity mode, where $P_a > \gamma_a$ leads to a divergence). Anther incoherent process is pure dephasing, given by $\frac{\gamma_\phi}{2}\mathcal{L}_{\sigma^\dagger\sigma}\rho$. Rather than destroy or create excitations, the effect of dephasing is the loss of coherence, turning a pure state into a mixed state.

In a similar way, a master equation can be derived for a cavity mode (with bosonic operators a and $a^\dagger$) coupled to free-space EM field with minimal changes. Other possibilities are exciton states in semiconductors, light-matter hybrid systems such as exciton-polaritons, qubits embedded in cavities (Jaynes-Cummings or Dicke models) or opto-mechanical systems, etc. For all of them, we end up, within the *Born-Markov approximation*, with a master equation of the type

$$\dot{\rho} = \mathcal{L}\rho = -i[H,\rho] + \sum_c \frac{\gamma_c}{2}\mathcal{L}_c\rho\,. \tag{2.16}$$

where the superoperator $\mathcal{L}$ is called Liouvillian, which shapes the evolution of the density matrix.

In the next Section, we proceed to solve the master equation, whether looking at the elements of the density matrix or through

the correlations between operators computed from tracing them over the density matrix. In Chapter 1, we find that there is a complete correspondence between the space of correlations and the Hilbert space. Solving the problem in one basis allows us to have access to the other.

Before continuing this discussion, an important caveat has to be addressed. The correlation functions and the subsequent photon statistics thereof all along the text refer to the bare system. Technically, the measured quantities in an experiment comes from the detected incoming EM field E_{det} (whether the free-space field, an optical fibre or any other device that sends the light towards the detectors). However, this alarming issue is overcome by analysing the source-field dynamics which, in our Born-Markov approximation scenario, simply reduces the source-field correspondence to $E_{\text{det}}(t) = \varepsilon\,\sigma(t - r/c)$ [38, 39], where r is the source-detector distance and ε is a constant which depends on the light-matter coupling and the specific geometry of the problem, among other. So, in the end, the detected field is proportional to the source delayed signal. If the distance between source and detector is small, we can also neglect the time delay. We assume this approximation holds hereafter.

2.2 SOLVING SINGLE-PHOTON CORRELATIONS

Under many circumstances, the dynamics of a qubit are well described by the family of master equations presented in this previous Section. We will use this first example to conclude our discussion about the quantum nature of spontaneous decay of the emitter. In absence of pumping, the master equation reads

$$\dot{\rho} = -i\omega_\sigma[\sigma^\dagger\sigma, \rho] + \frac{\gamma_\sigma}{2}\mathcal{L}_\sigma\rho\,. \tag{2.17}$$

There are several ways to proceed now. Typically, one would write down the equations for the density matrix coefficients ρ_{ij} or for the correlators $\langle\sigma^{\dagger\mu}\sigma^\nu\rangle = \text{tr}\left(\rho\sigma^{\dagger\mu}\sigma^\nu\right)$. Taking the second path, the equations of motion for the correlators are

$$\frac{d}{dt}\langle\sigma^{\dagger\mu}\sigma^\nu\rangle = -\left[(\mu+\nu)\gamma_\sigma/2 - i(\mu-\nu)\omega_\sigma\right]\langle\sigma^{\dagger\mu}\sigma^\nu\rangle\,, \tag{2.18}$$

whose solution is

$$\langle\sigma^{\dagger\mu}\sigma^\nu\rangle(t) = e^{-\left[(\mu+\nu)\gamma_\sigma/2 - i(\mu-\nu)\omega_\sigma\right]t}\langle\sigma^{\dagger\mu}\sigma^\nu\rangle(0)\,. \tag{2.19}$$

The conservation of the trace implies that $\langle\sigma^{\dagger 0}\sigma^0\rangle = \text{tr}(\rho) = 1$. The initial condition for the correlators depend on the initial state $\rho(0)$.

Taking the state $\rho(0) = |1\rangle\langle 1|$, the initial conditions are $\langle \sigma^{\dagger\mu}\sigma^{\nu}\rangle(0) = \delta_{\mu,\nu}$. Then, the solution is

$$\langle \sigma^{\dagger}\sigma\rangle(t) = e^{-\gamma_\sigma t}\,, \tag{2.20}$$

and the rest are zero. Remembering the relations (2.4), we can reconstruct the density matrix.

$$\rho(t) = \begin{pmatrix} 1 - e^{-\gamma_\sigma t} & 0 \\ 0 & e^{-\gamma_\sigma t} \end{pmatrix}. \tag{2.21}$$

This is in accordance with the prediction of the semi-classical model. The probability of being excited at any time t decays exponentially. Ultimately, the qubit gets inevitably de-excited. The characteristic time of the decay is inversely proportional to γ_σ, which is the linewidth of the transition. In presence of pumping, either coherent or incoherent, the final state ($t \to \infty$) would be different. The qubit continuously emits and absorbs photons. Thus, the system has a non-zero average population when reaching the steady-state. The state at $t \to \infty$ is not $\rho(t \to \infty) \to |0\rangle\langle 0|$. We now derive what it is.

2.2.1 STEADY-STATE SOLUTION: SPECTRA AND PHOTON STATISTICS

The most general master equation that includes losses, both coherent (2.12) and incoherent pumping and dephasing is

$$\begin{aligned}\dot{\rho} = &-i[\omega_\sigma\sigma^{\dagger}\sigma + \Omega_\sigma\sigma^{\dagger}e^{-i\omega_L t} + \Omega_\sigma\sigma e^{i\omega_L t}, \rho] + \\ &\frac{\gamma_\sigma}{2}\mathcal{L}_\sigma\rho + \frac{P_\sigma}{2}\mathcal{L}_{\sigma^{\dagger}}\rho + \frac{\gamma_\phi}{2}\mathcal{L}_{\sigma^{\dagger}\sigma}\rho\,,\end{aligned} \tag{2.22}$$

The explicit time dependence can be removed by transforming the system into its Rotating Frame, giving

$$\dot{\rho} = -i[\Delta_\sigma\sigma^{\dagger}\sigma + \Omega_\sigma\sigma^{\dagger} + \Omega_\sigma\sigma, \rho] + \frac{\gamma_\sigma}{2}\mathcal{L}_\sigma\rho + \frac{P_\sigma}{2}\mathcal{L}_{\sigma^{\dagger}}\rho + \frac{\gamma_\phi}{2}\mathcal{L}_{\sigma^{\dagger}\sigma}\rho\,, \tag{2.23}$$

where $\Delta_\sigma = \omega_\sigma - \omega_L$ is the detuning between the emitter and the laser. The correlator equations read

$$\begin{aligned}\frac{d}{dt}\langle \sigma^{\dagger\mu}\sigma^{\nu}\rangle = &-\big[(\mu+\nu)\Gamma_\sigma/2 - i(\mu-\nu)\Delta_\sigma - \\ &(\mu-\nu)^2\gamma_\phi/2\big]\langle \sigma^{\dagger\mu}\sigma^{\nu}\rangle + \mu\nu P_\sigma\langle \sigma^{\dagger(1-\mu)}\sigma^{1-\nu}\rangle + \\ &i\Omega_\sigma\big[\mu + 2\nu(1-\mu)\big]\langle \sigma^{\dagger(1-\mu)}\sigma^{\nu}\rangle - \\ &i\Omega_\sigma\big[\nu + 2\mu(1-\nu)\big]\langle \sigma^{\dagger\mu}\sigma^{1-\nu}\rangle\,,\end{aligned} \tag{2.24}$$

where $\Gamma_\sigma = \gamma_\sigma + P_\sigma$ is the effective linewidth. The incoherent pumping broadens the transition. The set of linear differential equations can be handled using vector notation. We arrange the correlators as $\vec{c} = (1, \langle\sigma\rangle, \langle\sigma^\dagger\rangle, \langle\sigma^\dagger\sigma\rangle)^{\mathrm{T}}$. Now the system of differential equations is written as

$$\frac{d}{dt}\vec{c} = M\,\vec{c}\,, \tag{2.25}$$

where the matrix M is called the regression matrix and has the following shape

$$M = \begin{pmatrix} 0 & 0 & 0 & 0 \\ -i\Omega_\sigma & -(\Gamma_\sigma + \gamma_\phi)/2 - i\Delta_\sigma & 0 & 2i\Omega_\sigma \\ i\Omega_\sigma & 0 & -(\Gamma_\sigma + \gamma_\phi)/2 + i\Delta_\sigma & -2i\Omega_\sigma \\ P_\sigma & i\Omega_\sigma & -i\Omega_\sigma & -\Gamma_\sigma \end{pmatrix}. \tag{2.26}$$

The first element of $\vec{c}$ is always one and can be eliminated from the vector. However, there are correlators connected to it. In order to preserve this matrix element, we can include an additional vector $\vec{b}$ to the equation. The new system of equations is then

$$\frac{d}{dt}\vec{c} = M\,\vec{c} + \vec{b}\,, \tag{2.27}$$

with

$$M = \begin{pmatrix} -(\Gamma_\sigma + \gamma_\phi)/2 - i\Delta_\sigma & 0 & 2i\Omega_\sigma \\ 0 & -(\Gamma_\sigma + \gamma_\phi)/2 + i\Delta_\sigma & -2i\Omega_\sigma \\ i\Omega_\sigma & -i\Omega_\sigma & -\Gamma_\sigma \end{pmatrix}, \tag{2.28}$$

and

$$\vec{b} = \begin{pmatrix} -i\Omega_\sigma \\ i\Omega_\sigma \\ P_\sigma \end{pmatrix}. \tag{2.29}$$

This kind of equation, an inhomogeneous matrix differential equation with constant coefficients, can always be formally solved as $\vec{c}(t) = -M^{-1}\vec{b} + e^{Mt}(\vec{c}(0) + M^{-1}\vec{b})$, where M^{-1} denoted the matrix inverse (we have assumed that it exist), $\vec{c}(0)$ is the initial condition and e^{Mt} is the matrix exponential. The way to deal with e^{Mt} is explained in Chapter 3. Assuming that it vanishes at $t \to \infty$, we find that the steady-state correlators are given by

$$\vec{c}_{\mathrm{ss}} = \vec{c}(t \to \infty) = -M^{-1}\vec{b}\,. \tag{2.30}$$

Another and faster approach is to take the time derivative to zero (equilibrium condition) in Eq. (2.27), which yields the algebraic linear system $M\vec{c}_{\rm ss} + \vec{b} = 0$. The solution is straightforward if the matrix M has inverse, hence, $\vec{c}_{\rm ss} = -M^{-1}\vec{b}$.

Now we turn to computing correlators that depend on multiple times. Although the following procedure is quite general, we will focus on steady-state solutions (non-equilibrium scenarios fulfil the same equations). In this regime, the initial or first time t does not play any role given that in the steady-state there is no origin, only time differences matter. We shall use the time intervals τ_i between the i-th and $(i+1)$-th events instead. The cornerstone of the following computations is the Quantum Regression Theorem [40, 41]. Any two-time (or n-time) correlator can be computed from the same equations of motion for the density matrix or, equivalently, from the correlator equations (as long as the system is coupled to Markovian baths).

As proved in Ref. [36], given a master equation ($\dot{\rho} = \mathcal{L}\rho$), any two-time correlator evolves in time τ as

$$\langle O_1(0)O_2(\tau)O_3(0)\rangle = \mathrm{tr}\Big\{O_2(0)e^{\mathcal{L}\tau}\big[O_3(0)\rho_{\rm ss}\,O_1(0)\big]\Big\}\,, \tag{2.31}$$

where ss denotes steady-state and we have fixed the initial time at $t = 0$. The operators O_i are chosen so that the average (2.31) is in fact normal-ordered. For instance, with $O_1 = \sigma^\dagger$, $O_2 = \sigma$ and $O_3 = 1$, we compute $G^{(1)}(\tau) = \langle\sigma^\dagger(0)\sigma(\tau)\rangle$. Another useful quantity is the second-order Glauber correlator, for which we have $O_1 = \sigma^\dagger$, $O_2 = \sigma^\dagger\sigma$ and $O_3 = \sigma$. Alternatively, if we identified a set of operators c_i such that their respective correlators follow the equations of motion

$$\frac{d}{dt}\langle c_i(t)\rangle = \sum_j M_{i,j}\langle c_j(t)\rangle\,, \tag{2.32}$$

then, any 2-time correlator $\langle O_1(0)c_i(\tau)O_3(0)\rangle$ satisfies the following equation

$$\frac{d}{d\tau}\langle O_1(0)c_i(\tau)O_3(0)\rangle = \sum_j M_{i,j}\langle O_1(0)c_j(\tau)O_3(0)\rangle\,. \tag{2.33}$$

Building a vector $\vec{c} = (c_1, c_2, \ldots)^{\rm T}$, we can rewrite Eq. (2.33) as

$$\frac{d}{d\tau}\langle O_1(0)\vec{c}(\tau)O_3(0)\rangle = M\langle O_1(0)\vec{c}(\tau)O_3(0)\rangle\,, \tag{2.34}$$

where M is, again, the regression matrix. The formal solution of (2.34) is succinctly expressed in terms of the matrix exponential as

$$\langle O_1(0)\vec{c}(\tau)O_3(0)\rangle = e^{M\tau}\langle O_1(0)\vec{c}(0)O_3(0)\rangle\,. \tag{2.35}$$

The generalisation for n times immediately follows from this. For instance, for three times, we have

$$\langle O_1(0)O_2(\tau_1)\vec{c}(\tau_1+\tau_2)O_3(\tau_1)O_4(0)\rangle\,. \tag{2.36}$$

Since only $\vec{c}$ depends on τ_2, the rest of the correlators can be treated constant (in time τ_2). Then, the equation of motion is formally identical to (2.34) and, mutatis mutandis, the formal solution is the same

$$\begin{aligned}\langle O_1(0)O_2(\tau_1)\vec{c}(\tau_1+\tau_2)O_3(\tau_1)O_4(0)\rangle = \\ e^{M\tau_2}\langle O_1(0)O_2(\tau_1)\vec{c}(\tau_1)O_3(\tau_1)O_4(0)\rangle\,,\end{aligned} \tag{2.37}$$

and, in turn, $\langle O_1(0)O_2(\tau_1)\vec{c}(\tau_1)O_3(\tau_1)O_4(0)\rangle$ has its own set of equations. Renaming $\vec{c'} = O_2\,\vec{c}\,O_3$, then

$$\frac{d}{d\tau_1}\langle O_1(0)\vec{c}'(\tau_1)O_3(0)\rangle = M'\langle O_1(0)\vec{c}'(\tau_1)O_3(0)\rangle\,. \tag{2.38}$$

The matrices M and M' are not necessarily the same because some elements of $\vec{c}'$ might not be in $\vec{c}$ and vice versa. The procedure is to start from the end, the last time τ_n, back-propagate to $\tau_n = 0$ and repeat for the previous time τ_{n-1} and so on.

The two-level system is completely described by the three correlators σ, $\sigma^\dagger$ and $\sigma^\dagger\sigma$ (plus the trace 1). We have already defined the averaged correlators $\vec{c} = \langle\vec{c}\rangle = (\langle\sigma\rangle, \langle\sigma^\dagger\rangle, \langle\sigma^\dagger\sigma\rangle)^{\mathrm{T}}$ and the equation of motion (2.27). Then, applying the Quantum Regression Theorem, we get the equation for $\langle\sigma^\dagger(0)\vec{c}\sigma(0)\rangle$ as

$$\frac{d}{d\tau}\langle\sigma^\dagger(0)\vec{c}(\tau)\sigma(0)\rangle = M\langle\sigma^\dagger(0)\vec{c}(\tau)\sigma(0)\rangle + \langle\sigma^\dagger\sigma\rangle\vec{b}\,, \tag{2.39}$$

which is a variant of the previous equation when there is an inhomogeneous term. Remembering that $\sigma^2 = \sigma^{\dagger 2} = 0$, then $\sigma^\dagger\vec{c}\sigma = 0$ and the solution of the differential equation reads

$$\langle\sigma^\dagger(0)\vec{c}(\tau)\sigma(0)\rangle = -\langle\sigma^\dagger\sigma\rangle\left(1-e^{M\tau}\right)\left(M^{-1}\vec{b}\right) = \langle\sigma^\dagger\sigma\rangle\left(1-e^{M\tau}\right)\vec{c}_{\mathrm{ss}}\,. \tag{2.40}$$

One remarkable feature of this solution is that $\langle\sigma^\dagger(0)\vec{c}(0)\sigma(0)\rangle = 0$, hence $G^{(2)}(0) = 0$ for any possible matrix M. This may not be surprising given that any state spanned by $|0\rangle$ and $|1\rangle$ has all $g^{(n)}(0) = 0$. The non-zero delay Glauber correlators is given by

$$\begin{aligned}\langle\sigma^\dagger(0)\sigma^\dagger(\tau)\sigma(\tau)\sigma(0)\rangle &= \left[\langle\sigma^\dagger\sigma\rangle\left(1-e^{M\tau}\right)\vec{c}_{\mathrm{ss}}\right]_3 = \\ &= \langle\sigma^\dagger\sigma\rangle^2 - \langle\sigma^\dagger\sigma\rangle\left[e^{M\tau}\vec{c}_{\mathrm{ss}}\right]_3\end{aligned} \tag{2.41}$$

where $[]_i$ denotes the i-th element of the vector. Assuming that the matrix M has an eigenvalue decomposition, i.e., $M = EDE^{-1}$, where E is a matrix whose columns are the eigenvectors and D is a diagonal matrix with the eigenvalues λ_i. The matrix exponential then has simple form $e^{M\tau} = Ee^{D\tau}E^{-1}$. After expanding the matrix product, we can rearrange the equation, now yielding

$$\langle\sigma^\dagger(0)\sigma^\dagger(\tau)\sigma(\tau)\sigma(0)\rangle = \langle\sigma^\dagger\sigma\rangle^2 + \langle\sigma^\dagger\sigma\rangle \sum_{p=1}^{3} l_p\, e^{\lambda_p} \tag{2.42}$$

where $l_p = \sum_{q=1}^{3}(E)_{3,p}(E^{-1})_{p,q}(-\vec{c}_{\rm ss})_q$. Therefore, we find

$$g^{(2)}(\tau) = \frac{\langle\sigma^\dagger(0)\sigma^\dagger(\tau)\sigma(\tau)\sigma(0)\rangle}{\langle\sigma^\dagger\sigma\rangle^2} = 1 + \frac{1}{\langle\sigma^\dagger\sigma\rangle}\sum_{p=1}^{3} l_p\, e^{\lambda_p\tau}\,. \tag{2.43}$$

In a similar way, we obtain $g^{(1)}(\tau)$

$$g^{(1)}(\tau) = \frac{\langle\sigma^\dagger(0)\sigma(\tau)\rangle}{\langle\sigma^\dagger\sigma\rangle} = \frac{|\langle\sigma\rangle|^2}{\langle\sigma^\dagger\sigma\rangle} - \frac{1}{\langle\sigma^\dagger\sigma\rangle}\sum_{p=1}^{3} \ell_p\, e^{\lambda_p\tau}\,, \tag{2.44}$$

where $\ell_p = \sum_{q=1}^{3}(E)_{1,p}(E^{-1})_{p,q}(\vec{v}_{\rm ss})_q$ and

$$\vec{v}_{\rm ss} = \langle\sigma^\dagger\vec{c}\rangle - \langle\sigma^\dagger\rangle\vec{c}_{\rm ss} = \begin{pmatrix} \langle\sigma^\dagger\sigma\rangle - |\langle\sigma\rangle|^2 \\ -\langle\sigma^\dagger\rangle^2 \\ -\langle\sigma^\dagger\rangle\langle\sigma^\dagger\sigma\rangle \end{pmatrix}. \tag{2.45}$$

The spectrum (1.53) is then

$$S(\omega) = \frac{1}{\pi\langle\sigma^\dagger\sigma\rangle}\,\mathrm{Re}\left\{\int_0^\infty \left(|\langle\sigma\rangle|^2 + \sum_{p=1}^{3}\ell_p\, e^{\lambda_p\tau}\right)e^{i\omega\tau}d\tau\right\}. \tag{2.46}$$

If we split ℓ_p and λ_p into their real and imaginary part as $\ell_p = L_p + iK_p$ and $\lambda_p = -\gamma_p/2 - i\omega_p$ (the real part gives the width of the transition γ_p and the imaginary part, the frequency of the transition), then the spectrum reads [42]

$$S(\omega) = \frac{|\langle\sigma\rangle|^2}{\langle\sigma^\dagger\sigma\rangle}\delta(\omega) + \frac{1}{\pi\langle\sigma^\dagger\sigma\rangle}\sum_p \left(L_p\frac{\gamma_p/2}{(\gamma_p/2)^2 + (\omega-\omega_p)^2} - K_p\frac{\omega-\omega_p}{(\gamma_p/2)^2 + (\omega-\omega_p)^2}\right), \tag{2.47}$$

The spectrum is split into two parts, the coherent (Rayleigh) scattering that has an infinitely narrow shape and the incoherent (fluorescence)

part which consists of the sum of Lorentzian profiles (proportional to L_p) and, secondly, the dispersive parts (proportional to K_p). The origin of these are different. The first one corresponds to the elastic scattering by the emitter of the laser (if there is any). Since the photons are not absorbed, the lineshape is inherited from the source (an ideal laser would have an infinitely narrow linewidth). The second one, conversely, comes from the absorption and subsequent emission of the photons. It depends on the dynamics of the emitter and its interaction with the EM field. Since we are in the Rotating Frame of the laser, the Fourier transform is rigidly displaced as $\omega \to \omega - \omega_{\rm L}$. Then, the Dirac delta is actually centered at $\omega = \omega_{\rm L}$.

Having the regression matrix (2.26), the steady-state of the 2LS system is

$$\vec{c}_{\rm ss} = \begin{pmatrix} \dfrac{2i(2P_\sigma - \Gamma_\sigma)(\Gamma_\sigma + \gamma_\phi - 2i\Delta_\sigma)\Omega_\sigma}{\left[\Gamma_\sigma(\Gamma_\sigma+\gamma_\phi)^2 + 4\Delta_\sigma^2\right] + 8(\Gamma_\sigma+\gamma_\phi)\Omega_\sigma^2} \\ -\dfrac{2i(2P_\sigma - \Gamma_\sigma)(\Gamma_\sigma + \gamma_\phi + 2i\Delta_\sigma)\Omega_\sigma}{\left[\Gamma_\sigma(\Gamma_\sigma+\gamma_\phi)^2 + 4\Delta_\sigma^2\right] + 8(\Gamma_\sigma+\gamma_\phi)\Omega_\sigma^2} \\ \dfrac{P_\sigma\left[(\Gamma_\sigma+\gamma_\phi)^2 + 4\Delta_\sigma^2\right] + 4(\Gamma_\sigma+\gamma_\phi)\Omega_\sigma^2}{\left[\Gamma_\sigma(\Gamma_\sigma+\gamma_\phi)^2 + 4\Delta_\sigma^2\right] + 8(\Gamma_\sigma+\gamma_\phi)\Omega_\sigma^2} \end{pmatrix}, \tag{2.48}$$

which is the most general solution within our level of approximation.

We however consider two special cases, the incoherent 2LS ($\Omega_\sigma = \Delta_\sigma = \gamma_\phi = 0$) and the coherent 2LS ($P_\sigma = \gamma_\phi = 0$). For the first case, the correlators reduce to

$$\vec{c}_{\rm ss} = \begin{pmatrix} 0 \\ 0 \\ \frac{P_\sigma}{\Gamma_\sigma} \end{pmatrix}, \tag{2.49}$$

and the regression matrix is completely diagonal with eigenvalues $\lambda = (-\Gamma_\sigma/2, -\Gamma_\sigma/2, -\Gamma_\sigma)$. The computation of the spectrum and $g^{(2)}(\tau)$ is straightforward. The coefficients l_p are

$$l_{1,2} = 0\,, \quad l_3 = \frac{P_\sigma}{\Gamma_\sigma}\,, \tag{2.50}$$

so that it yields

$$g^{(2)}_{P_\sigma}(\tau) = 1 - e^{-\Gamma_\sigma \tau}\,. \tag{2.51}$$

The Glauber correlator displays perfect antibunching since $g^{(2)}(0) = 0$ and $g^{(2)}(0) < g^{(2)}(\tau)$. The coherence time, that is, the characteristic

time in which the anticorrelation is still strong, is proportional to $1/\Gamma_\sigma$. For huge values of P_σ, the intensity $\langle\sigma^\dagger\sigma\rangle$ grows but, on the contrary, the coherence time decreases and photons are more likely to be emitted closer in time.

On the other hand, the coefficients ℓ_p are

$$\ell_1 = \frac{P_\sigma}{\Gamma_\sigma}\,, \quad \ell_{2,3} = 0\,. \tag{2.52}$$

Hence, the luminescence spectrum of the incoherent 2LS is

$$S_{P_\sigma}(\omega) = \frac{1}{\pi}\frac{\Gamma_\sigma/2}{(\Gamma_\sigma/2)^2+\omega^2}\,. \tag{2.53}$$

The spectrum is simply a Lorentzian centered at the frequency of the emitter. Its effective width is $\Gamma_\sigma = \gamma_\sigma + P_\sigma$, so the incoherent pumping is broadening the emission (as compared to spontaneous emission).

The next case is the two-level system driven by a laser (of frequency ω_L). The regression matrix is not diagonal any more. We obtain the eigenvalues from the characteristic polynomial which is cubic in this case. The roots with detuning Δ_σ are given in Appendix A.5. We reproduce here the case when the emitter is driven at resonance $\Delta_\sigma = 0$. Then, the eigenvalues are

$$\lambda_1 = -\gamma_\sigma\,, \quad \lambda_{2,3} = -\frac{3\gamma_\sigma}{4} \mp \gamma_\mathrm{M}\,, \tag{2.54}$$

where $\gamma_\mathrm{M} = \frac{1}{4}\sqrt{\gamma_\sigma^2 - 64\Omega_\sigma^2}$. Unlike the incoherent 2LS, depending on the range of parameters, the behaviour of the correlators qualitatively change. The eigenvalues undergo a transition when $\Omega_\sigma = \gamma_\sigma/8$. For $\Omega_\sigma < \gamma_\sigma/8$, all eigenvalues are real while, conversely, above this threshold two of the roots have non-zero imaginary part since $\gamma_\mathrm{M} = i\Omega_+$ where $\Omega_+ = \frac{1}{4}\sqrt{64\Omega_\sigma^2 - \gamma_\sigma^2}$ and which, as compared to the Rabi case, can be called Mollow splitting. In Appendix A.5, a more general condition for the transition is given together with the general Mollow splitting. The steady-state solution is

$$\vec{c}_\mathrm{ss} = \begin{pmatrix} -\frac{2i\Omega_\sigma}{\gamma_\sigma^2+8\Omega_\sigma^2} \\ \frac{2i\Omega_\sigma}{\gamma_\sigma^2+8\Omega_\sigma^2} \\ \frac{4\Omega_\sigma^2}{\gamma_\sigma^2+8\Omega_\sigma^2} \end{pmatrix}\,. \tag{2.55}$$

The coefficients l_p are

$$l_1 = 0\,, \quad l_{2,3} = -\frac{2\Omega_\sigma^2}{\gamma_\sigma^2+8\Omega_\sigma^2}\left(1 \mp \frac{3\gamma_\sigma}{8\gamma_\mathrm{M}}\right)\,, \tag{2.56}$$

so the second-order Glauber correlator is

$$g^{(2)}_{\Omega_\sigma}(\tau) = 1 - e^{-\frac{3\gamma_\sigma}{4}\tau}\left[\cosh(\gamma_M\tau) + \frac{3\gamma_\sigma}{24\gamma_M}\sinh(\gamma_M\tau)\right]. \quad (2.57)$$

The coefficients ℓ_p are

$$\ell_1 = \frac{2\Omega_\sigma^2}{\gamma_\sigma^2 + 8\Omega_\sigma^2}, \quad \ell_{2,3} = \pm\frac{\gamma_\sigma^2\Omega_\sigma^2(\gamma_\sigma \mp 4\gamma_M) \mp 8\Omega_\sigma^4(4\gamma_M \mp 5\gamma_\sigma)}{4\gamma_M(\gamma_\sigma^2 + 8\Omega_\sigma^2)^2}. \quad (2.58)$$

After computing the coefficients L_p and K_p, we obtain for both regimes the following spectrum

$$S_{\Omega_\sigma}(\omega) = \frac{\gamma_\sigma^2}{\gamma_\sigma^2 + \Omega_\sigma^2}\delta(\omega) + \frac{1}{\pi}\frac{32\gamma_\sigma\Omega_\sigma^2(\gamma_\sigma^2 + 2\Omega_\sigma^2 + \omega^2)}{(\gamma_\sigma^2 + 4\omega^2)\left[\gamma_\sigma^4 + \gamma_\sigma^2(5\omega^2 + 16\Omega_\sigma^2) + 4(\omega^2 - 4\Omega_\sigma^2)^2\right]}. \quad (2.59)$$

This is the spectrum of resonance fluorescence, that was first provided by Mollow [43].

Now that we have the emission spectrum and the 2-photon Glauber correlator in our hands, we can analyse both regimes and find the differences. The spectrum in the limit of weak driving ($\Omega_\sigma \ll \gamma_\sigma$) can be approximated as

$$S_{\Omega_\sigma}(\omega) \approx \left(1 - \frac{8\Omega_\sigma^2}{\gamma_\sigma^2}\right)\delta(\omega) + \frac{8\Omega_\sigma^2}{\gamma_\sigma^2}\frac{4\gamma_\sigma^3}{\pi(\gamma_\sigma^2 + 4\omega^2)^2}, \quad (2.60)$$

and $g^{(2)}(\tau)$ as

$$g^{(2)}_{\Omega_\sigma}(\tau) \approx (1 - e^{-\gamma_\sigma/2\,\tau})^2. \quad (2.61)$$

On the other hand, when the driving strength is large ($\Omega_\sigma \gg \gamma_\sigma$), we find

$$S_{\Omega_\sigma}(\omega) \approx \frac{1}{\pi}\left(\frac{\gamma_\sigma}{\gamma_\sigma^2 + 4\omega^2} + \frac{3\gamma_\sigma}{9\gamma_\sigma^2 + 16(\omega - 2\Omega_\sigma)^2} + \frac{3\gamma_\sigma}{9\gamma_\sigma^2 + 16(\omega + 2\Omega_\sigma)^2}\right), \quad (2.62)$$

and

$$g^{(2)}_{\Omega_\sigma}(\tau) \approx 1 - e^{-\frac{3\gamma_\sigma}{4}\tau}\cos(2\Omega_\sigma\,\tau). \quad (2.63)$$

Another property derived from the autocorrelation function $g^{(2)}(\tau)$ is the waiting time distribution $w(\tau)$, already defined in Eq. (1.57). We start by computing $w(\tau)$ for the incoherent 2LS. The emission rate is then $R = \gamma_\sigma n_\sigma = \gamma_\sigma P_\sigma / \Gamma_\sigma$ (where $n_\sigma = \langle \sigma^\dagger \sigma \rangle$). After inverting the Laplace transform, we get the WTD for the incoherently-driven 2LS as

$$w_{\rm inc}(\tau) = \frac{\gamma_\sigma P_\sigma}{\gamma_\sigma - P_\sigma}\left(e^{-P_\sigma \tau} - e^{-\gamma_\sigma \tau}\right), \tag{2.64}$$

while the coherent counterpart, with counting rate $R = \frac{4\gamma_\sigma \Omega_\sigma}{\gamma_\sigma^2 + 8\Omega_\sigma^2}$, is

$$w_{\rm coh}(\tau) = \frac{\gamma_\sigma \Omega_\sigma^2}{\gamma_{\rm M}^2} e^{-\gamma\tau/2} \sinh^2(\gamma_{\rm M}\tau). \tag{2.65}$$

Although immediate results from Eq. (1.57), the waiting time distributions for the 2LS system under coherent and incoherent drivings, and their derived results like Eqs. (2.66), appear to be original results not found in the literature.

As a consequence of the antibunching the initial value of the WTDs is $w(0) = 0$ (as we can see in Fig. 2.1). The most likely value is around $\gamma_\sigma \tau \approx -\log(n_\sigma^p)$, where $p = 1$ for the incoherent case and $p = 2$ for the coherent one, that becomes exact for $n_\sigma \to 0$. For stronger intensities, above the transition, $w_{\rm coh}(\tau)$, like $g^{(2)}(\tau)$, exhibits oscillations due to the laser-atom dressing. From these distributions

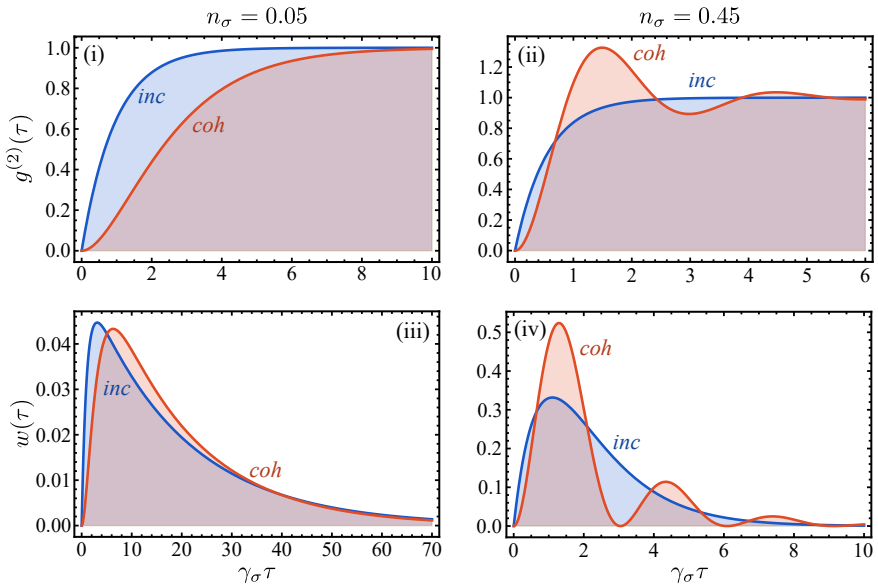

Figure 2.1: Pairwise photon correlations, non-exclusive ($g^{(2)}(\tau)$) on the first row and exclusive ($w(\tau)$) on the second one, for different types of pumping (incoherent driving in blue and coherent driving in red). Pumping rates are fixed so that in both cases the amount of photons per unit time is identical. On the left-hand side, the emission rate is low ($n_\sigma = 0.05$) while the remaining column correspond to the high population ($n_\sigma = 0.45$).

we can compute the mean and variance of inter-arrival time, $\langle\tau\rangle$ and $(\Delta\tau)^2 = \langle\tau^2\rangle - \langle\tau\rangle^2$, respectively. The mean time is then

$$\langle\tau\rangle_{\text{inc}} = \frac{1}{P_\sigma} + \frac{1}{\gamma_\sigma} = (\gamma_\sigma n_\sigma)^{-1}\,, \tag{2.66a}$$

$$\langle\tau\rangle_{\text{coh}} = \frac{2}{\gamma_\sigma} + \frac{\gamma_\sigma}{4\Omega_\sigma^2} = (\gamma_\sigma n_\sigma)^{-1}\,, \tag{2.66b}$$

$$\tag{2.66c}$$

which are both equal to the inverse of the emission rate as expected. In order to compare both cases, incoherent and coherent 2LS's, we parametrise the pumping rates P_σ and Ω_σ in terms of the population n_σ, i.e.,

$$P_\sigma = \frac{\gamma_\sigma n_\sigma}{1 - n_\sigma}\,, \tag{2.67}$$

where the population runs from 0 to 1 in this case and

$$\Omega_\sigma = \sqrt{\frac{\gamma_\sigma^2 n_\sigma}{4(1 - 2n_\sigma)}}\,, \tag{2.68}$$

where the population has to fulfil $0 < n_\sigma < 1/2$. The time variance is

$$(\Delta\tau)^2_{\text{inc}} = \langle\tau\rangle^2_{\text{inc}}\left[1 + 2n_\sigma(n_\sigma - 1)\right], \tag{2.69a}$$

$$(\Delta\tau)^2_{\text{coh}} = \langle\tau\rangle^2_{\text{coh}}\left[1 + 6n_\sigma(2n_\sigma - 1)\right]. \tag{2.69b}$$

The photon arrival time variance, conveniently normalised to the mean squared, shows two maxima at the (open) boundaries that would correspond to $(\Delta\tau)^2 = \langle\tau\rangle^2$. For $n_\sigma \to 0$, the excited level has very small chances to get populated, entailing that the photon flux is extremely small so the mean time between them is huge compared to the correlation time (proportional to γ_σ). The second limit $n_\sigma \to 1$ implies an infinite amount of energy and cannot be approached. In between, we find a minimum, which is located exactly at the midpoint of interval, $n_\sigma = 1/2$ for $(\Delta\tau)^2_{\text{inc}}$ and $n_\sigma = 1/4$ for $(\Delta\tau)^2_{\text{coh}}$. At half the available population, the deviation from the Poisson process is maximum.

Since we have the expressions for the 2-photon correlations for the 2LS under incoherent (2.51) and coherent (2.57) excitation, we are able to apply the detection theory (excluding frequency filtering, that will be addressed later on) and discuss the photon statistics of a single-photon emitter. We take the corresponding exponents λ_p and coefficients l_p and compute the sum $g^{(2)}_\Gamma(\tau) = 1 + \sum_p l_p \mathcal{I}^{(i)}_p(\tau)$

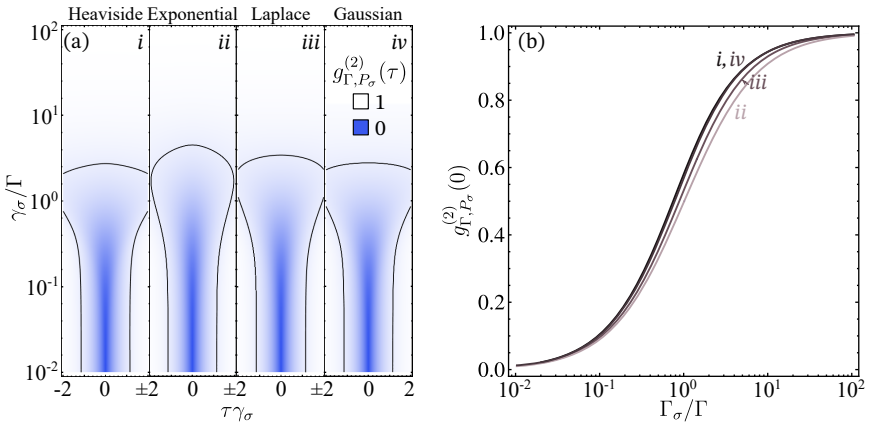

Figure 2.2: Detected photon correlations for the incoherently driven 2LS. (a) Time dependent 2-photon Glauber correlator considering the four jitter functions discussed in the text: (i) Heaviside, (ii) Exponential, (iii) Laplace and (iv) Gaussian. The black contours represent the isolines $g^{(2)}_{\Gamma,P_\sigma}(\tau) = 0.9$. (b) Zero delay correlation as a function of jitter characteristic time width. The pumping rate is taken to be vanished ($P_\sigma \to 0$). Adapted with permission from [Z6]. Copyright (2022) by the APS.

for any of the jitter functions: (i) Heaviside, (ii) One-sided exponential, (iii) Two-sided exponential or Laplace and (iv) Gaussian, whose expressions are found in the previous Chapter. The immediate and most noticeable effect of the time jitter is the spoilt photon statistics, which results in $g^{(2)}_\Gamma \neq 0$. When the time width is small ($1/\Gamma \to 0$), the jitter disappears and perfect antibunching recovered. For big jitter ($1/\Gamma \to \infty$) the effective photon statistics are Poissonian (uncorrelated), as the large time uncertainty completely randomises the arrival time of the photons. In Figs. 2.2 and 2.3 the incoherent and coherent cases (both the weak and strong driving regimes) are shown, respectively. The more detrimental functions are the Heaviside and Gaussian functions, followed by the Laplace distribution and, lastly, the one-sided exponential. It turns out that the flatness of these distributions, which scrambles more photons in a short time scale, affects more the statistics than the fatter tails of exponential distributions, that are more likely to return larger deviations. The Heitler regime is more resilient to losing its statistical properties than the Mollow regime. In the middle we find the incoherently-driven 2LS. The coherence time of the first one is the greatest of the three, so it is less likely to find photons in the same time interval than the incoherent case (even with the same intensity). The Mollow case, on the other hand, displays not only shorter coherence times but has laser-induced oscillations. This explain its fragility under time disordering.

This calculation of the impact of jitter on the emission of a 2LS highlights at least two important results:

i *the availability of closed-form formulas (obtained in the previous chapter) to describe the loss of antibunching exactly as opposed to approximate deconvolution procedures.*

ii *the fundamental differences brought by the type of driving, with the Heitler regime being the more robust one.*

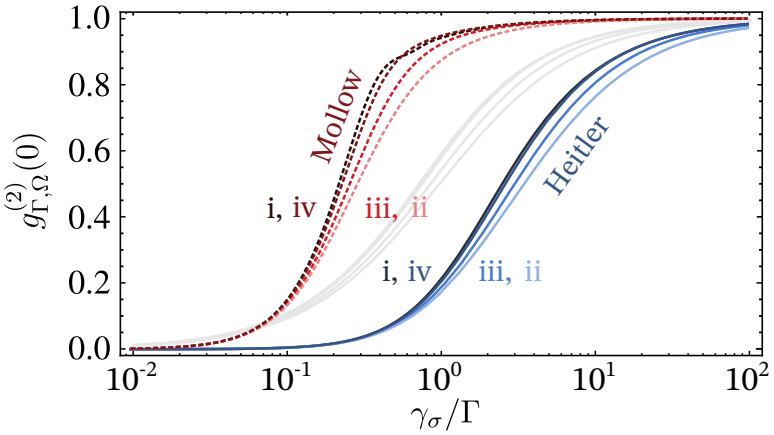

Figure 2.3: Detected photon correlations for the coherently driven 2LS. Zero delay correlation as a function of jitter characteristic time width for the Heitler case (solid bluish lines) and the Mollow regime (dashed reddish lines), superimposed with the incoherently driven 2LS (shown in the previous figure). Adapted with permission from [Z6]. Copyright (2022) by the APS.

The behaviour and shape of all these quantities is completely different in these limits. For weak intensities (Heitler regime, studied in Ref. [44]), the spectrum is dominated by the coherent scattering and the incoherent contribution has a non-Lorentzian profile (it decays as ω^{-4} and is thus narrower). Although the resonance fluorescence (incoherent) fraction seems to be negligible compared to the scattered laser light, it is the interplay (interference) between these processes what actually yields the properties of the two-level system [45] (extended to detuning and dephasing in Ref. [46]). As devised in Ref. [45], we can split the two components of the signal (coherent + incoherent) directly at the operator level, that is, $\sigma = \langle\sigma\rangle + \delta\sigma$ (mean field and fluctuations). The absence of either contribution results in photon statistics different from $g^{(n)}(0) = 0$, for $n \geq 2$. The fluctuations comprise photon processes of all orders due to the non-linear nature of the emitter. At low intensities, however, the two-photon scattering is dominant. This is confirmed by inspecting the squeezing properties of the fluctuations. In fact the Wigner representation of the state is well approximated by a displaced squeezed thermal state [47]. We can see that by first computing the exact expression. The Wigner representation [48–50] applied to any photonic state generated by the 2LS yields

$$W_\sigma(x,p) = \rho_{0,0}W_{0,0}(x,p) + \rho_{0,1}W_{0,1}(x,p) + \rho_{1,0}W_{1,0}(x,p) + \rho_{1,1}W_{1,1}(x,p)\,, \quad (2.70)$$

where x and p are the average values of the electric field operators $\hat{x} = (a^\dagger + a)/\sqrt{2}$ and $\hat{p} = i(a^\dagger - a)/\sqrt{2}$. In terms of the correlators it is written as

$$W_\sigma(x,p) = \big(1 - \langle\sigma^\dagger\sigma\rangle\big)W_{0,0}(x,p) + \langle\sigma\rangle W_{0,1}(x,p) + \langle\sigma\rangle^* W_{1,0}(x,p) + \langle\sigma^\dagger\sigma\rangle W_{1,1}(x,p)\,, \quad (2.71)$$

where the functions $W_{n,m}$ are the Wigner representation of the matrix elements $|m\rangle\langle n|$ corresponding for the Harmonic Oscillator (equivalent to a single bosonic mode), as defined in [49], whose explicit expressions are

$$W_{0,0}(x,p) = \frac{1}{\pi}\, e^{-(x^2+p^2)}\,, \quad (2.72)$$

$$W_{1,0}(x,p) = \frac{1}{\pi}\,\sqrt{2}(x + i\,p)e^{-(x^2+p^2)} = \big[W_{0,1}(x,p)\big]^*\,, \quad (2.73)$$

$$W_{1,1}(x,p) = \frac{1}{\pi}\,(2x^2 + 2p^2 - 1)e^{-(x^2+p^2)}\,, \quad (2.74)$$

$$(2.75)$$

and the correlators are given in Eq. (2.55). As shown in Fig. 2.4, the Wigner function starts being a Gaussian distribution slightly displaced from the center (the displacement is precisely $\sqrt{2}\,\mathrm{Im}\{\langle\sigma\rangle\}$) and exhibiting a small degree of squeezing, so that the resulting shape of the distribution is elliptical rather than round (symmetrical). We can then compare the state with the Gaussian displaced squeezed thermal state [51]. The approximate parameters, expanding W up to second order, are $\alpha = -\frac{2\sqrt{2}\Omega_\sigma}{\gamma_\sigma}$ and $r = -\frac{4\Omega_\sigma^2}{\gamma_\sigma^2}$ (the minus sign indicates that the squeezing angle as to be $\theta = \pi$ rather than $\theta = 0$). Around the transient regime, the shape is asymmetric and non-convex, that are characteristics of non-Gaussian states which, in turn, is linked to the non-classicality of the state [52]. Far above the threshold, the state is centered again and displays a ring-like shape. The state is in fact a balanced mixture of $|0\rangle$ and $|1\rangle$, that is, $\rho \approx \frac{1}{2}\big(|0\rangle\langle 0| + |1\rangle\langle 1|\big)$.

We can also compare the Heitler regime with the incoherent case when $P_\sigma \to 0$. The dynamics of the incoherent 2LS when the pumping is small resembles the spontaneous emission. The reloading time after the first photon is emitted, is much longer than the decay time, so each photon does not get disturbed by the others. In contrast, in the Heitler regime, photons result from the two processes and it is the interference between both that produces the antibunching for the the total emission. The luminescence spectrum is much richer. The incoherent part has got a non-Lorentzian profile considerably narrower than for the incoherent case. The coherence time of $g^{(2)}(\tau)$

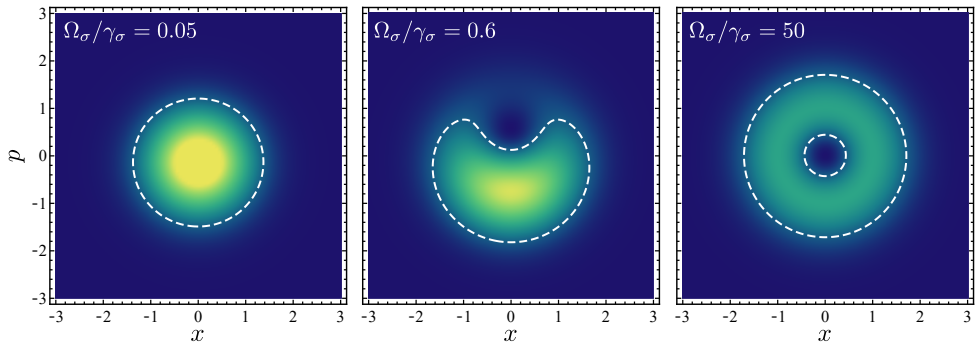

Figure 2.4: Wigner representation of the coherently-driven 2LS for low (left), intermediate (center) and strong (right) driving. The white dashed curves correspond to the isolines $W_\sigma = 0.05$.

is longer too. It takes $\tau \approx 0.69/\gamma_\sigma$ for the incoherent 2LS to reach $g^{(2)}(\tau) = 1/2$, while this same point is reached at $\tau \approx 2.45/\gamma_\sigma$ for the coherent case. The regime when $\Omega_\sigma > \gamma_\sigma/8$ can be called the Mollow regime. The spectrum displays the distinctive triplet shape, one central peaks (with the greatest intensity) and two satellites or side-peaks centered at $\omega = \pm\Omega_+$. The second-order coherence function does not grow monotonically to 1 but exhibits an oscillatory behaviour (whose characteristic frequency is Ω_+). The energy level structure that explains this transition was given by Cohen-Tannoudji and Reynoud [53], presenting a dressed-state picture where the eigenstates of the system are laser-atom (laser-qubit) hybrids, that is, $|\pm\rangle$. Since the laser field has an infinite number of states, our new light-matter coupled level structure is an infinite ladder of this kind of states $|n, \pm\rangle$. The splitting between the levels of the same manifold n is precisely Ω_+. The four allowed transitions between two consecutive manifolds are $|+\rangle \to |+\rangle$, $|-\rangle \to |-\rangle$, $|+\rangle \to |-\rangle$ and $|-\rangle \to |+\rangle$. The first two are degenerated, i.e., the transition frequency is exactly ω_L (zero in the Rotating frame) and hence both contribute to the central peak that has twice the intensity. The last two have the energies $\omega_L \pm \Omega_+$ ($\pm\Omega_+$ in the rotating frame), respectively and they give rise to the satellites. When the laser is strong enough, the elastically scattered light is negligible and the emission is dominated by these processes. The fluctuations is this limiting case do shown $g^{(2)}(0) = 0$ without any interference mechanism involved. In this limit, the dispersive part K_p vanish and the spectrum is exactly represented by three Lorentzians. More interesting underlying properties that reveal the rich and vast landscape within this system, deceptively called simple, are found through the study of its frequency-resolved correlations [54]. If we directly start from the integrated filtered operators, the computation of these quantities would be incredibly hard and limited to a

scarce amount of cases, such as the spontaneous emission of dots and cavities free of any external driving. Although they may look irrelevant, we will develop an interesting theory around it which allows to understand and apprehend the effects of frequency-filtering on the photo-detection (see Chapter 4). For other situations, we shall follow an alternative path. Those complicated integrals can be substituted by a physical entity that we call a sensor and whose correlators are equivalent to them. The sensor operators, independently of the nature of the system (2LS or cavity), are indeed the filtered operators ς and $\varsigma^\dagger$ (up to a constant, see Appendix A.4). The sensor is coupled either though a vanishing coherent coupling ($\epsilon(\sigma^\dagger\varsigma + \text{h.c.})$, with $\epsilon \to 0$), as originally proposed in Ref. [55], or though unidirectional coupling (cascade formalism, employed in Refs. [5] and [56]), used to develop the frequency-resolved Monte Carlo technique [27]. We will outline the procedure followed in the original case that served as the main inspiration and also as an example of the perturbational approach that we describe in the next Chapter.

2.2.2 BEYOND THE TWO-LEVEL SYSTEM

Until now we have considered only the simplest but most paradigmatic single-photon emitter: a system with just two levels. This automatically ensures that bare correlations (without detection) are always $g^{(n)}(0) = 0$. However, the single photon generation is not restricted to such types of systems or sometimes this level of approximation is not enough to faithfully describe the dynamics. We shall update the system to allow a more complex structure. In semiconductor quantum dots, the excitation ladder consists of a fundamental state with no excitons $|0\rangle$, then single-exciton levels $|X_i\rangle$ ($i = \text{H}, \text{V}$, for the different polarisations) and, on top, the two-exciton or biexciton state $|2X\rangle$. More energetic states are discarded. The vertical and horizontal exciton levels, namely $|X_\text{V}\rangle$ and $|X_\text{H}\rangle$, are slightly detuned due to the fine structure [57] and the interaction between the two excitons produces the biexciton bound state (whose binding energy $-E_b$), with less energy than the sum of the exciton energies.

The decay processes link the biexciton $|2X\rangle$ to intermediate states $|X_{\text{H,V}}\rangle$ and these to the ground state $|0\rangle$. We could eliminate the degeneracy between the horizontal and vertical transitions. The biexciton, ignoring the small fine structure splitting, de-excites to any of them. With an ultrafast laser pulse tuned to half the biexciton energy (two-photon excitation) the upper level gets *excited*. Then, after some free evolution, there is a second (polarised) pulse resonant with the transition $|2X\rangle \leftrightarrow |X_\text{H}\rangle$ that allows to eliminate the other decay chan-

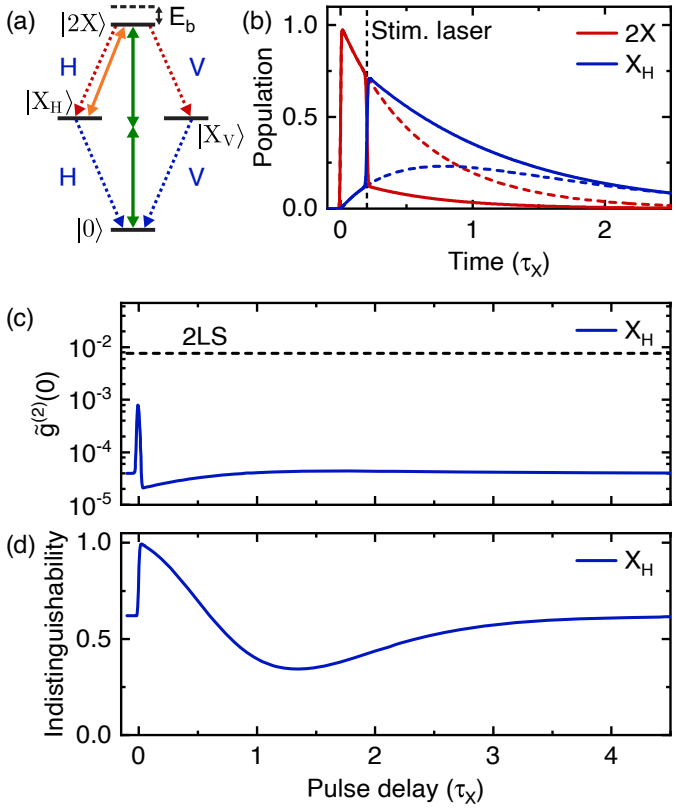

Figure 2.5: (a) Level structure of an excitonic system. The decay processes are represented by the dotted arrows while the solid arrows denote the laser-induced transitions. (b) Numerical simulation of the system. The population of the biexciton and exciton with the stimulation pulse starting at $t = 0.2\tau_X$ (τ_x is the lifetime of the exciton) are given by the solid lines while the case without the second laser pulse are represented by the dashed lines. (c) and (d) display the time-integrated second-order coherence function and the indistinguishability as a function of delay between the pulses (the black dashed line corresponds to 2LS with the same pulse). Adapted with permission from [Z5]. Copyright (2022) by the APS.

nel and populate only the desired exciton state through *stimulated* de-excitation. The system then naturally decays into the ground state, emitting a single photon in the process. The combination of the 2-photon excitation of the biexciton and the resonant excitation brings together two highly sought features for the single photon emission: good single-photon purity (strong antibunching) and high indistinguishability, measured by the Hong-Ou-Mandel (HOM) visibility [58]. The first ensures strong suppression of more-than-one photon events, while the second confirms the degree of monochromaticity of the source. In addition, the resulting brightness (how likely it is to emit and detect the photon) is much greater than in other schemes.

The system reduces to a three level system (we drop the label H from now on). We shall demonstrate the validity of the model by solving the Hamiltonian dynamics (no lossy treatment is needed to prove it). The 3-level system Hamiltonian is the following

$$H = \omega_X |X\rangle \langle X| + (2\omega_X - E_b) |2X\rangle \langle 2X| + \Omega_x(t) e^{-i\omega_L t}(|X\rangle \langle 0| + |2X\rangle \langle X|) + \text{h.c.}, \quad (2.76)$$

where ω_X is the exciton energy, E_b the binding energy and the laser frequency matches the condition $\omega_L = \omega_X - E_b/2$. We assume that the pulse $\Omega_x(t)$ is square, so it remain constant until $t = T$ and, after that, the laser is switched off. In the Rotating Frame, the Hamiltonian reads, now in matrix form:

$$H = \begin{pmatrix} 0 & \Omega_x & 0 \\ \Omega_x & E_b/2 & \Omega_x \\ 0 & \Omega_x & 0 \end{pmatrix}. \quad (2.77)$$

The initial state is assumed to be $|\psi(0)\rangle = |0\rangle$. The dynamics of the state is given in terms of the time evolution operator $U(t)$ yielding $|\psi(t)\rangle = U(t) |\psi(0)\rangle = e^{-iHt} |\psi(0)\rangle$. Using the eigenvalue decomposition (the matrix is hermitian, therefore such a decomposition always exists), we write the Hamiltonian matrix as $H = EDE^{-1}$ and then the evolution operator as $U(t) = Ee^{-iDt}E^{-1}$, where D is the diagonal matrix of the eigenvalues and E the eigenvector matrix. The state is then expressed as a superimposition of excitonic states as

$$|\psi(t)\rangle = c_1(t) |0\rangle + c_2(t) |X\rangle + c_3(t) |2X\rangle , \quad (2.78)$$

where the coefficients $c_i(t)$ are found by projecting the eigenvectors of U onto the exciton states. That is, $c_i(t) = \sum_{p=1}^{3} c_{i,p} e^{-i\epsilon_p t}$, where $c_{i,p} = E_{i,p}(E^{-1}c(0))_p$ and $c_i(0) = \delta_{i,1}$. The eigenvalues are

$$\epsilon_1 = 0, \quad \epsilon_{2,3} = \frac{1}{4}\left(E_b \mp \sqrt{E_b^2 + 32\Omega_x^2}\right), \quad (2.79)$$

and the coefficients can be found in Table 2.1.

The population of each state, following the Born rule, is then

$$P_0(t) = |c_1(t)|^2, \quad P_X(t) = |c_2(t)|^2, \quad P_{2X}(t) = |c_3(t)|^2, \quad (2.80)$$

where $P_X(t)$ has particularly a simple expression for any set of parameters:

$$P_X(t) = \frac{16\Omega_x^2}{E_b^2 + 32\Omega_x^2} \sin^2\left(\frac{t}{4}\sqrt{E_b^2 + 32\Omega_x^2}\right). \quad (2.81)$$

i \ p	1	2	3
1	$1/2$	$\frac{1}{4}\left(1+\frac{E_b}{\sqrt{E_b^2+32\Omega_x^2}}\right)$	$\frac{1}{4}\left(1-\frac{E_b}{\sqrt{E_b^2+32\Omega_x^2}}\right)$
2	0	$-\frac{2\Omega_x}{\sqrt{E_b^2+32\Omega_x^2}}$	$\frac{2\Omega_x}{\sqrt{E_b^2+32\Omega_x^2}}$
3	$-1/2$	$\frac{1}{4}\left(1+\frac{E_b}{\sqrt{E_b^2+32\Omega_x^2}}\right)$	$\frac{1}{4}\left(1-\frac{E_b}{\sqrt{E_b^2+32\Omega_x^2}}\right)$

Table 2.1: Coefficients $c_{i,p}$ that appear in the expressions of $c_i(t)$, that go together with the exponentials $e^{-i\epsilon_p t}$, where ϵ_p are the eigenenergies of the Hamiltonian.

These equations justify the two-photon approximation for an emitter of experimental relevance that goes beyond the 2LS. Based on the underlying theoretical picture, highly indistinguishable bright and pure single-photon emission could be demonstrated experimentally.

Under weak driving, i.e., $\Omega_x \ll E_b$, the population of $|X\rangle$ goes to zero at any time whereas the ground and biexciton states display Rabi oscillations, with frequency $\Omega_x^{(2)} \equiv 2\Omega_x^2/E_b$, as if the intermediate state did not exist:

$$\boxed{P_0(t) \approx \cos^2\left(\Omega_x^{(2)}t\right), \quad P_X(t) \approx 0, \quad P_{2X}(t) = \sin^2\left(\Omega_x^{(2)}t\right).} \tag{2.82}$$

So that with a π-pulse, that is, $T = \pi/(2\Omega_x^{(2)})$, the higher state gets a population equal to one. This justifies the two-photon excitation approximation that directly couples the ground and biexciton states. The effective Hamiltonian in the rotating frame then read

$$H = \frac{[\Omega_e(t)]^2}{2E_b}(|0\rangle\langle 2X| + \text{h.c}) + \frac{\Omega_s(t)}{2}(|X\rangle\langle 2X| + \text{h.c}), \tag{2.83}$$

where $\Omega_{e,s}(t)$ are the time-dependent amplitude of the excitation and stimulation lasers, respectively, that define the profile of the pulses. The excitation and stimulation times are expected to be much smaller than the decay times of the exciton and biexciton, τ_X and τ_{2X}, respectively. Adding to the model the radiative decay of the exciton states and performing the numerical simulation, validates the two pulses scheme (see Figure 2.5). We find a near-unity population P_{2X} right after the first pulse. The biexciton starts to de-excite and the single-exciton level contribution grows due to spontaneous emission (the dashed lines show the natural decay in absence of the stimulation pulse) and when the second pulse takes place, after a given time delay, P_{2X} goes to zero and the population is transferred to $|X_H\rangle$. Ultimately, the exciton de-excites and emits a single photon. The purity of the single-photon emission is quantified using the time-integrated second-order Glauber correlator [59], that has the following expression:

$$\tilde{g}^{(2)}(0) = \frac{2\int_0^T\int_0^T dtd\tau\langle a^\dagger(t)a^\dagger(t+\tau)a(t+\tau)a(t)\rangle}{\left(\int_0^T dt\langle a^\dagger(t)a(t)\rangle\right)^2}, \tag{2.84}$$

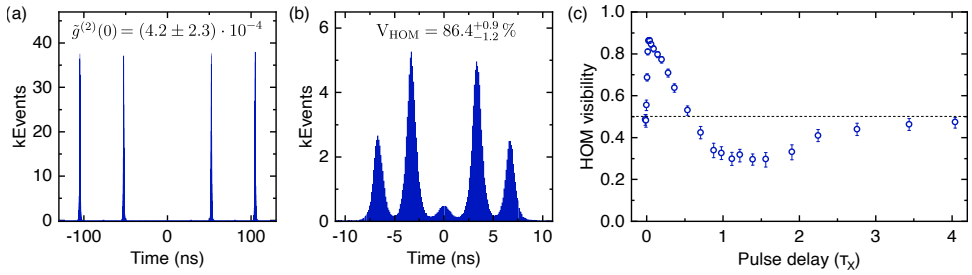

Figure 2.6: Experimental realisation of the scheme. (a) Autocorrelation histogram of the exciton emission after th stimulation pulse took place. b) Correlation histogram of the exciton emission measured with an unbalanced Mach-Zehnder interferometer. (c) HOM visibility of the exciton emission as a function of the stimulation pulse delay. The dashed line marks the HOM visibility without the stimulation pulse. Adapted with permission from [Z5]. Copyright (2022) by the APS.

where T is the time window of integration and the indistinguishability is measured through the HOM visibility

$$V_{\mathrm{HOM}} = |\tilde{g}^{(1)}(0)|^2 = \frac{2\int_0^T \int_0^T dt d\tau |\langle a^\dagger(t+\tau)a(t)\rangle|^2}{\left(\int_0^T dt \langle a^\dagger(t)a(t)\rangle\right)^2}. \tag{2.85}$$

The indistinguishability as a function of the delay between the pulses grows from 62.0%, that is the limit arising from the two-photon cascade (given by the ratio $\gamma_{2X}/(\gamma_X + \gamma_{2X})$, that compares decay of the first photon to the whole two-photon cascaded emission), up to 99.4% induced by the stimulation of the second pulse. Then, for greater delays, the visibility decreases until it reaches a minimum around $1.4\tau_X$. The stimulation laser backfires scheme and the biexciton turns out to be partially re-excited. For even longer delay, the indistinguishability asymptotically goes to the initial value. The 2-photon correlator $\tilde{g}^{(2)}(0)$ remain two orders of magnitude lower than the 2LS threshold in the same ranges. This theoretical proposal was experimentally confirmed with a semiconductor InGaAs quantum dot. The measured autocorrelation function is $\tilde{g}^{(2)}(0) = (4.2 \pm 2.3) \cdot 10^{-4}$, which is almost two order of magnitude the value reported for resonant excitation [60]. The maximum HOM visibility, measured using an unbalanced Mach-Zehnder interferometer, is $V_{\mathrm{HOM}} = 86.4\%$, which disagree with the theoretical predictions. Such deviations may be explained by the limited stability of the studied samples and the lack of dephasing in the theoretical model, that would reduce the predicted maximum visibility. However, the experimental results seem to be in accordance with the theoretical curve of HOM visibility (see Figures 2.5 and 2.6).

3

PERTURBATION THEORY FOR OPEN QUANTUM SYSTEMS

3.1 THEORY

Under some circumstances, the Hamiltonian of a system can be separated as $H = H_0 + \epsilon H_I$, where ϵ is assumed to be small. This means that the addition of the second term, usually called perturbation, essentially does not modify the original or unperturbed system (described by the first term H_0). Examples of this situation exsit in a fair amount, including weakly coupled (sub)systems or low pumped light sources. In most cases, the dynamics of the system is governed by a master equation of the type shown in Eq. (2.16).

We can directly compute the correlators, e.g., for one 2LS and two bosonic modes $\{\mu,\nu,m,n,p,q\} \equiv \langle \sigma^{\dagger\mu}\sigma^{\nu}s_1^{\dagger m}s_1^{n}s_2^{\dagger p}s_2^{q}\rangle$, then the density matrix's dynamics is described by

$$\partial_t\{\mu,\nu,m,n,p,q\} = \sum_{\mu',\nu',m',n',p',q'} \mathcal{M}^{\mu',\nu',m',n',p',q'}_{\mu,\nu,m,n,p,q}\{\mu',\nu',m',n',p',q'\}, \quad (3.1)$$

where $0 \leq \mu,\nu \leq 1$ and $m,n,p,q \geq 0$. These multi-index (but linear) relations are the generalization of Eq. (2.32). We can rearrange (flatten) all the indices as a single index, then we map the multi-index structure into a regular correlator vector $\vec{c}$ and the generalised matrix as a regular one. So we build up a simpler linear system

$$\frac{d}{dt}\langle\vec{c}(t)\rangle = M\,\langle\vec{c}(t)\rangle, \quad (3.2)$$

where $\langle\vec{c}\rangle = (\{0,0,0,0,0,0\},\ldots)^{\mathrm{T}}$ represents the correlators vector and M is a matrix of constant values (it does not depend on time) resulting from the reshaping of the array $\mathcal{M}$ as the matrix M, which is the regression matrix introduced in Ref. [42]. As we already mentioned, the equation shown above is not exclusive of a particular problem. Thus, the following method is useful in many different situations.

These equations show that correlators are often coupled to each other in a way that the whole set of them (an infinite number) is

required to completely solve the problem, either the dynamics or the steady-state ($t \to \infty$). The order of approximation depends on the truncation needed to make the solution converge. However, we do not need the *whole* solution if we consider the limit of vanishing parameters (namely, $\epsilon \to 0$). This lets us find the solution recursively, in a expansion-like way. For this purpose, we define the subsets

$$C_k = \left\{ \{\mu, \nu, m, n, p, q\} \,\middle|\, \text{leading order } k, \text{ for } k \geq 0 \right\}, \tag{3.3}$$

so any correlator contained in the k-th subset is proportional to ϵ^k (limiting the computations to the leading order). Following this, the full set of correlators can be split as $\langle \vec{c} \rangle = (\langle \vec{c}_0 \rangle, \epsilon \langle \vec{c}_1 \rangle, \epsilon^2 \langle \vec{c}_2 \rangle, \dots)^{\mathrm{T}}$. This manifold separation will let us solve recursively each subset C_k from the previous one. Now we divide the full matrix M into blocks $M_{i,j}$, where each block connects the i-th subset to the j-th one (then the dimensions of each matrix is $m_i \times m_j$, where m_j is the number of elements contained in the j-th subset). Additionally, the elements from C_k that are linked to 1 (density matrix trace), which is usually included as the first element of $\langle \vec{c}_0 \rangle$, can be gathered in the vector $\vec{b}_k$ (often only $\vec{b}_0$ has non-zero elements). We define $\vec{c} = \langle \vec{c} \rangle$ whose elements are the expectation values of the operators in $\vec{c}$.

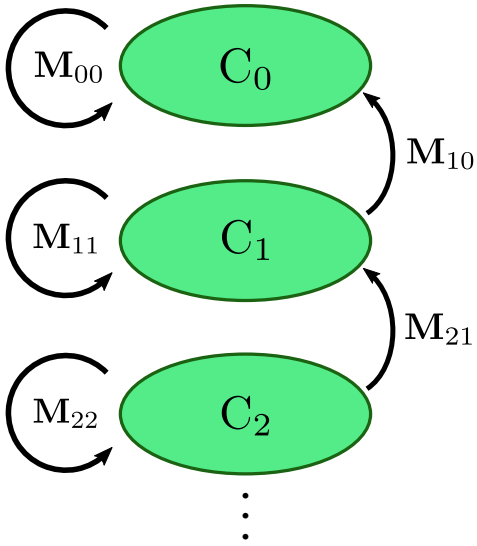

Figure 3.1: Ladder-like structure of the perturbed correlator sets. Each set C_k includes all the correlation functions proportional to ϵ^k. Whereas the matrices $M_{k,k}$ describes the internal dynamics of the k-th set, $M_{k,k-1}$ feed the set with the previous ones.

The matrix equation can be written, for each manifold, as $\dot{\vec{c}}_k(t) = M_{k,k}\vec{c}_k(t) + \sum_{i \neq k} M_{k,i}\vec{c}_i(t) + \vec{b}_k$. Nevertheless, in most cases only contiguous subsets ($i = k \pm 1$) directly contribute to $\vec{c}_k$ to first order.

We discard $C_{i>k}$ subsets because they are supposed to depend on higher powers of ϵ at their leading order. Keeping only the leading order terms for each manifold leads to the following set of equations (schematically represented in Fig. 3.1):

$$\epsilon^0 \; : \; \dot{\vec{c}}_0(t) = M_{0,0}\,\vec{c}_0(t) + \vec{b}_0\,, \tag{3.4a}$$

$$\epsilon^1 \; : \; \dot{\vec{c}}_1(t) = M_{1,1}\,\vec{c}_1(t) + M_{1,0}\,\vec{c}_0(t) + \vec{b}_1\,, \tag{3.4b}$$

$$\epsilon^2 \; : \; \dot{\vec{c}}_2(t) = M_{2,2}\,\vec{c}_2(t) + M_{2,1}\,\vec{c}_1(t) + \vec{b}_2\,, \tag{3.4c}$$

$$\vdots$$

$$\epsilon^k \; : \; \dot{\vec{c}}_k(t) = M_{k,k}\,\vec{c}_k(t) + M_{k,k-1}\,\vec{c}_{k-1}(t) + \vec{b}_k\,, \tag{3.4d}$$

$$\vdots$$

The steady-state solution is reached when $\dot{\vec{c}} = 0$, so that each manifold follows $\dot{\vec{c}}_k = 0$. Starting from the zeroth manifold we find its solution which is just: $\vec{c}_{0,ss} = -\left(M_{0,0}\right)^{-1}\vec{b}_0$. For higher orders, the idea is similar so the steady-state solution can be written as:

$$\vec{c}_{k,ss} = -\left(M_{k,k}\right)^{-1}\left(M_{k-1,k}\,\vec{c}_{k-1,ss} + \vec{b}_k\right)\,. \tag{3.5}$$

Then, starting from the unperturbed correlations, all of them enclosed in the o-th order subset C_0, any higher correlator can be obtained by solving iteratively the recursive equations until reaching the desired order.

3.1.1 CORRELATOR DYNAMICS: NON-ZERO DELAY

Even if the system has reached the steady-state, such important properties as the emission spectrum $S(\omega)$ or the non-zero delay 2-photon correlation $g^{(2)}(\tau)$, which are dynamical properties of the system, need to be resolved in time (actually, the dynamics are two-time dependent but for systems that are already in the steady-state only the delay $\tau = t' - t$ is relevant so we can simply choose $t = 0$). The way to proceed mainly relies on the Quantum Regression Theorem (3.45). Hitherto, we have tackled the time-independent problem: the steady-state solution for $\vec{c}$. The time-dependent case requires a more sophisticated technique. Now we must distinguish the o-th order equation from the rest since the inhomogeneous term $\vec{b}_0$ does not depend on time while for higher orders we have to deal with time-dependent terms. For $k = 0$, the solution can be easily obtained and reads:

$$\vec{c}_0(t) = \vec{c}_{0,ss} + e^{M_{0,0}t}\left[\vec{c}_0(0) - \vec{c}_{0,ss}\right]\,, \tag{3.6}$$

where $\vec{c}_{0,ss} = -(M_{0,0})^{-1}\vec{b}_0$ now denotes the steady-state solution and $\vec{c}_0(0)$ is the initial condition. To simplify computations further, we define $\Delta\vec{c}_k(t) = \vec{c}_k(t) - \vec{c}_{k,ss}$ where $\vec{c}_{k,ss} = -(M_{k,k})^{-1} M_{k,k-1}\vec{c}_{k-1,ss}$ for $k \geq 1$ corresponds to the steady-state solution. For instance, the previous equation can be written as

$$\Delta\vec{c}_0(t) = e^{M_{0,0}t}\Delta\vec{c}_0(0), \tag{3.7}$$

and the equation for the k-th subset can also be rearranged to be written in terms of $\Delta\vec{c}_k$:

$$\Delta\dot{\vec{c}}_k(t) = M_{k,k}\,\Delta\vec{c}_k(t) + M_{k,k-1}\,\Delta\vec{c}_{k-1}(t)\,, \tag{3.8}$$

where we assume that $\vec{b}_k(k \geq 1)$ vanishes.

For $k \geq 1$, as pointed out above, the equation of motion for $\vec{c}_k$ has to be solved using another strategy. We apply the Laplace transform to both sides of the equation (3.8) and taking advantage of the following property $\mathcal{L}\{f'(t)\}(s) = s\tilde{f}(s) - f(0)$ ($f'(t)$ is the time derivative of $f(t)$, $\mathcal{L}$ denotes Laplace transformation and $\tilde{f}(s) = \mathcal{L}\{f(t)\}(s)$), we obtain:

$$s\,\Delta\tilde{c}_k(s) - \Delta\vec{c}_k(0) = M_{k,k}\,\Delta\tilde{c}_k(s) + M_{k,k-1}\,\Delta\tilde{c}_{k-1}(s), \tag{3.9}$$

where $\Delta\tilde{c}_k(s)$ represents the vector of the Laplace transform for each element of $\Delta\vec{c}_k(t)$. This matrix equation can be formally solved for $\Delta\tilde{c}_k(s)$, it gives:

$$\Delta\tilde{c}_k(s) = \frac{1}{sI - M_{k,k}}\left\{\Delta\vec{c}_k(0) + M_{k,k-1}\,\Delta\tilde{c}_{k-1}(s)\right\}, \tag{3.10}$$

where I represents the identity matrix with the adequate dimension. This equation is the dynamical analogous of the recursive equation given above in the previous section. The first term gives the intrinsic dynamics of the n-th subset while the second one additionally feeds the correlations from lower manifolds (and eventually inherited from the non-perturbed correlations). To get a clearer vision of the problem, we need to develop the method in full detail. We start with the first two manifolds. The case $k = 0$ was previously solved and we can calculate its Laplace transform. Assuming that $M_{0,0}$ admits eigenvalue decomposition, equation (3.7) can be written as:

$$\Delta\vec{c}_0(t) = E_0\, e^{D_0 t} E_0^{-1}\Delta\vec{c}_0(0), \tag{3.11}$$

where D_0 is the diagonal matrix consisting of the eigenvalues of $M_{0,0}$ ($\{d_p^{(0)}\}$, for $m_0 \geq p \geq 1$) and E_0 is a matrix whose columns are the

eigenvectors associated to $M_{0,0}$. Therefore, the i-th element of $\Delta\vec{c}_0(t)$ can be expressed as:

$$\left(\Delta\vec{c}_0(t)\right)_i = \sum_{p=1}^{m_0} L_{ip}^{(0)}\, e^{d_p^{(0)}t}, \tag{3.12}$$

where the elements $L_{ip}^{(0)}$ are defined as:

$$L_{ip}^{(0)} = (E_0)_{ip} \sum_{q=1}^{m_0} \left(E_0^{-1}\right)_{pq} \left(\Delta\vec{c}_0(0)\right)_q \,, \tag{3.13}$$

and $(E_0)_{ip}$ is the matrix element that is located at the i-th row and p-th column. This notation is common to every matrix that appears in the text unless otherwise indicated. Now it is easy to compute the Laplace transform (of course, the transform does converge only if each eigenvalue fulfils $\mathrm{Re}\{d_p^{(0)}\} < 0$). Applying it to (3.12) returns:

$$\left(\Delta\tilde{c}_0(s)\right)_i = \sum_{p=1}^{m_0} L_{ip}^{(0)} \frac{1}{s - d_p^{(0)}} \,. \tag{3.14}$$

The next step is to solve the case $k = 1$. We assume, from now on, that each matrix $M_{k,k}$ does admit an eigenvalue decomposition. Thus, E_n and D_n represent the eigenvector matrix and the eigenvalue (diagonal) matrix of $M_{k,k}$, respectively. Its eigenvalues are denoted by $d_p^{(k)}$, where p goes from 1 to m_k. Then, we can write equation (3.10) as:

$$\begin{aligned} \Delta\tilde{c}_1(s) \; &= E_1 \frac{1}{sI - D_1} E_1^{-1} \left\{ \Delta\vec{c}_1(0) + M_{1,0}\, \Delta\tilde{c}_0(s) \right\} \\ &= E_1 \frac{1}{sI - D_1} E_1^{-1} \Delta\vec{c}_1(0) + E_1 \frac{1}{sI - D_1} Q_1\, \Delta\tilde{c}_0(s) \,, \end{aligned} \tag{3.15}$$

where $Q_k = E_k^{-1} M_{k,k-1}$ (for $k \geq 0$). Now each contribution is clearly differentiated, however, it is highly convenient to write down the i-th component of this equation:

$$\begin{aligned} \left(\Delta\tilde{c}_1(s)\right)_i = &\sum_{p=1}^{m_1} L_{ip}^{(1)} \frac{1}{s - d_p^{(1)}} + \\ &\sum_{p=1}^{m_1} \sum_{q=1}^{m_0} \sum_{q'=1}^{m_0} (E_1)_{ip}\, (Q_1)_{pq'}\, L_{q'q}^{(0)} \frac{1}{s - d_p^{(1)}} \frac{1}{s - d_q^{(0)}} \,, \end{aligned} \tag{3.16}$$

where

$$L_{ip}^{(1)} = (E_1)_{ip} \sum_{q'=1}^{m_1} \left(E_1^{-1}\right)_{pq'} \left(\Delta\vec{c}_1(0)\right)_{q'} \,. \tag{3.17}$$

The second term of equation (3.16) can be further simplified. Since we expect that eigenvalues from every manifold are all different from each other (if not, these ones can be treated separately and would appear as extra-terms for successive manifolds), the product of fractions is written as a sum of simple fractions, i.e.,

$$\frac{1}{s-d_p^{(1)}}\frac{1}{s-d_q^{(0)}} = \frac{1}{d_p^{(1)}-d_q^{(0)}}\left(\frac{1}{s-d_p^{(1)}} - \frac{1}{s-d_q^{(0)}}\right). \tag{3.18}$$

Thus, after substituting this in the previous equation, $(\Delta\tilde{c}_1(s))_i$ takes the following form:

This equation provides the general solution for the perturbative treatment of single-time quantum correlations in an open system. This is the backbone for explicit calculations when turning to particular cases, as shown in Section 3.2.

$$\boxed{(\Delta\tilde{c}_1(s))_i = \sum_{p=1}^{m_1}\left(L_{ip}^{(1)} + \sum_{q=1}^{m_0} R_{ipq}\right)\frac{1}{s-d_p^{(1)}} + \sum_{q=1}^{m_0}\left(-\sum_{p=1}^{m_1} R_{ipq}\right)\frac{1}{s-d_q^{(0)}},} \tag{3.19}$$

where

$$R_{ipq}^{(1)} = (E_1)_{ip}\sum_{q'=1}^{m_0}(Q_1)_{pq'}L_{q'q}^{(0)}\frac{1}{d_p^{(1)}-d_q^{(0)}}. \tag{3.20}$$

Then, the dynamics are described by $\mu_1 = m_0 + m_1$ terms, μ_1 eigenvalues and their corresponding coefficients, which we now summarize in a compact form as $\lambda_p^{(1)}$ (from $d_1^{(0)}$ to $d_{m_1}^{(1)}$) and $\ell_p^{(1)}$ (ordered in the same way), respectively. The procedure for $k > 1$ is quite straightforward following the same steps as before. The general form is:

$$(\Delta\tilde{c}_k(s))_i = \sum_{p=1}^{\mu_k}\ell_{ip}^{(k)}\frac{1}{s-\lambda_p^{(k)}}, \tag{3.21}$$

or, substituting $\Delta\tilde{c}_k$ and including the steady-state term,

$$(\tilde{c}_k(s))_i = \frac{(\vec{c}_{k,ss})_i}{s} + \sum_{p=1}^{\mu_k}\ell_{ip}^{(k)}\frac{1}{s-\lambda_p^{(k)}}, \tag{3.22}$$

where we have used the Laplace transform identity $\mathcal{L}\{1\}(s) = 1/s$ and introduced the notation

$$\lambda^{(k)} = \left(d_1^{(0)},\ldots,d_{m_0}^{(0)},d_1^{(1)},\ldots,d_{m_1}^{(1)},\ldots,d_1^{(k)},\ldots,d_{m_k}^{(k)}\right), \tag{3.23}$$

i.e., the collection of eigenvalues from the o-th to k-th manifold in growing order; $\mu_k = \sum_{0\le j\le k} m_j$ and

$$\ell_{ip}^{(k)} = \begin{cases} -\sum_{1\le q\le m_n} R_{iqp}^{(k)}, & 1 \le p \le \mu_{k-1} \\ L_{ip'}^{(k)} + \sum_{1\le q\le\mu_{k-1}} R_{ip'q}^{(k)}, & \mu_{k-1}+1 \le p \le \mu_k \end{cases}, \tag{3.24}$$

where $p' = p - \mu_{k-1}$ and we also have defined:

$$L_{ip}^{(k)} = (E_k)_{ip} \sum_{q'=1}^{m_k} \left(E_k^{-1}\right)_{pq'} (\Delta \vec{c}_k(0))_{q'} \,, \tag{3.25}$$

and

$$R_{ipq}^{(k)} = (E_k)_{ip} \sum_{q'=1}^{\mu_{k-1}} (Q_k)_{pq'} \, \ell_{q'q}^{(k-1)} \, \frac{1}{d_p^{(k)} - \lambda_q^{(k-1)}} \,. \tag{3.26}$$

Finally, after inverting the Laplace transform:

$$(\vec{c}_k(t))_i = (\vec{c}_{k,ss})_i + \sum_{p=1}^{\mu_k} \ell_{ip}^{(k)} e^{\lambda_p^{(k)} t} \,, \tag{3.27}$$

or in vector form

$$\vec{c}_k(t) = \vec{c}_{k,ss} + \sum_{p=1}^{\mu_k} \vec{\ell}_p^{(k)} e^{\lambda_p^{(k)} t} \,, \tag{3.28}$$

where the vector $\vec{\ell}_p^{(k)}$ is formed of the elements $\ell_{ip}^{(k)}$ (i from 1 to m_k).

For 2-time correlators the solution is obtained in the same way. There are slight differences which, however, do not alter the essence of the method. We introduce the short notation for the two-time averages $\vec{v}(\tau) = \langle O_1(0)\vec{c}(\tau)O_3(0)\rangle$. The initial condition $\vec{v}_k(0)$ is given by the steady-state solution for $\langle O_1\vec{c}_k O_3\rangle$. Assuming that $\langle O_1 O_3\rangle$ is included in C_n, the total order in ϵ of $\vec{v}_k(0) = \langle O_1\vec{c}_k O_3\rangle(\infty)$ will be $k' = k + n$. This means that we would need to additionally compute another set of correlators, namely $\vec{c}'$, split in subsets C'_k (up to $k' = k + n$). Moreover, $\vec{c}'_{k'}$ and $\vec{v}_k$ correspond to different sets in most cases. However, aside from these subtleties, the equations of motion are identical:

$$\epsilon^0 \;:\; \dot{\vec{v}}_0(\tau) = M_{0,0}\, \vec{v}_0(\tau) + \vec{b}'_0 \,, \tag{3.29a}$$

$$\epsilon^1 \;:\; \dot{\vec{v}}_1(\tau) = M_{1,1}\, \vec{v}_1(\tau) + M_{1,0}\, \vec{v}_0(\tau) \,, \tag{3.29b}$$

$$\epsilon^2 \;:\; \dot{\vec{v}}_2(\tau) = M_{2,2}\, \vec{v}_2(\tau) + M_{2,1}\, \vec{v}_1(\tau) \,, \tag{3.29c}$$

$$\vdots$$

$$\epsilon^k \;:\; \dot{\vec{v}}_k(\tau) = M_{k,k}\, \vec{v}_k(\tau) + M_{k,k-1}\, \vec{v}_{k-1}(\tau) \,, \tag{3.29d}$$

$$\vdots$$

where $\vec{b}'_0 = (\langle O_1 O_3\rangle_{ss})\, \vec{b}_0$. Since $\vec{b}'_0$ is not the inhomogeneous counterpart of the steady-state recursive equation for $\vec{c}'_k$, then we have

$\Delta\vec{v}_k(\tau) = \vec{v}_k(0) - (\langle O_1 O_3\rangle_{ss})\,\vec{c}_{k,ss}$ instead. Formally, the solution for $\vec{c}_k(t)$ and $\vec{v}_k(\tau)$ are identical:

This equation provides the general solution for the perturbative treatment of two-time quantum correlations in an open system.

$$\boxed{\vec{v}_k(\tau) = (\langle O_1 O_3\rangle_{ss})\,\vec{c}_{k,ss} + \sum_{p=1}^{\mu_k} \hat{\ell}_p^{(k)} e^{\lambda_p^{(k)}\tau}\,,} \tag{3.30}$$

where the vector $\hat{\ell}_p^{(k)}$ has the following components $(\hat{\ell}_p^{(k)})_i = \tilde{\ell}_{ip}^{(k)}$

$$\tilde{\ell}_{ip}^{(k)} = \begin{cases} -\sum_{1\le q\le m_k} \tilde{R}_{iqp}^{(k)}\,, & 1 \le p \le \mu_{k-1} \\ \tilde{L}_{ip'}^{(k)} + \sum_{1\le q\le \mu_{k-1}} \tilde{R}_{ip'q}^{(k)}\,, & \mu_{k-1}+1 \le p \le \mu_k \end{cases}, \tag{3.31}$$

with

$$\tilde{L}_{ip}^{(k)} = (E_k)_{ip} \sum_{q'=1}^{m_k} \left(E_k^{-1}\right)_{pq'} (\Delta\vec{v}_k(0))_{q'}\,, \tag{3.32}$$

and

$$\tilde{R}_{ipq}^{(k)} = (E_k)_{ip} \sum_{q'=1}^{\mu_{k-1}} (Q_k)_{pq'}\, \tilde{\ell}_{q'q}^{(k-1)}\, \frac{1}{d_p^{(k)} - \lambda_q^{(k-1)}}\,. \tag{3.33}$$

Sometimes, for instance, when calculating the emission spectrum, it is more useful to directly give the Fourier transform of the correlator $\langle a^\dagger(t) a(t+\tau)\rangle$ rather than its temporal series. By substituting $s \to i\omega + \eta$ in equation (3.22) (here $\eta \to 0^+$ is a vanishing constant to ensure convergence), the Laplace transform is turned into a Fourier transform

$$(\check{c}_k(\omega))_i = \frac{(\vec{c}_{k,ss})_i}{i\omega + \eta} + \sum_{p=1}^{\mu_k} \ell_{ip}^{(k)} \frac{1}{i\omega - \lambda_p^{(k)}}\,. \tag{3.34}$$

The constant η can be taken to zero without any trouble for the second term since the convergence is clear ($\mathrm{Re}\{\lambda\} > 0$), while for the first one we should be careful when computing the limit:

$$\begin{aligned} \lim_{\eta\to 0^+} \frac{1}{i\omega+\eta} &= \lim_{\eta\to 0^+} \frac{-i\omega}{\omega^2+\eta^2} + \frac{\eta}{\omega^2+\eta^2} \\ &= \frac{1}{i\omega} + \pi\,\delta(\omega)\,. \end{aligned} \tag{3.35}$$

This result is also found applying by the Sokhotski–Plemelj theorem to the Fourier integral.

Combining now equations (1.49), (3.34) and (3.35), and taking $O_1 = a^\dagger$ and $O_2 = 1$, with $\ell_{ip}^{(k)} = L_{ip}^{(k)} + iK_{ip}^{(k)}$ and same for $\lambda_p^{(k)} = -\gamma_p/2 - i\omega_p$, we get

$$S(\omega) = \frac{|\langle a\rangle_{ss}|^2}{\langle a^\dagger a\rangle_{ss}}\delta(\omega) + \frac{1}{\pi\langle a^\dagger a\rangle_{ss}}\sum_{p=1}^{\mu_k}\frac{(\gamma_p/2)L_{ip}^{(k)}}{(\gamma_p/2)^2+(\omega-\omega_p)^2} + \frac{(\omega-\omega_p)K_{ip}^{(k)}}{(\gamma_p/2)^2+(\omega-\omega_p)^2}\,, \tag{3.36}$$

which is the general expression for the luminescence expression (not only for the 2LS, as computed in Eq. (2.47)). This way we naturally separate the coherent part of the spectrum (infinite lifetime) from the incoherent one. Of course, the delta peak corresponds to the frequency of the coherent source ω_L, that in the Rotating Frame is centered at $\omega = 0$ but, undoing the frame transformation, corresponds to $\omega = \omega_L$. This applies to the incoherent spectrum as well.

This method allows to calculate perturbed dynamics by substantially reducing the problem complexity and saving memory space since matrix block expansion returns much smaller matrices, which also facilitates operations such as inversion or diagonalization. Another recurring issue when working with vanishing quantities is the convergence. The parameters must be small enough to ensure good results but still over a certain threshold to avoid numerical instabilities. The spirit of our method is to compute the correlations as a series expansion. In this way, the perturbation parameter, namely ϵ, does not explicitly appear throughout the whole computation. Our choice of the value for ϵ is completely irrelevant as long as it is small to be perturbative and does not determine the convergence at all.

3.1.2 APPLICABILITY OF THE METHOD IN THE DENSITY MATRIX BASIS

Although the majority of the results are obtained in the correlator space, we can also apply this series expansion directly on the master equation: $\dot\rho(t) = \mathcal{L}\rho(t)$. We now separate the Liouvillian superoperator as $\mathcal{L} = \mathcal{L}_0 + \epsilon\,\mathcal{L}_1$ and write the density matrix as $\rho = \sum_k \epsilon^k \rho^{(k)}$ (for $k \geq 0$). Then, we substitute this expansion in the master equation and gather up all the terms with the same power of ϵ, yielding

$$\dot\rho^{(0)}(t) = \mathcal{L}_0\,\rho^{(0)}(t) \qquad (\text{if } k = 0)\,, \tag{3.37a}$$

$$\dot\rho^{(k)}(t) = \mathcal{L}_0\,\rho^{(k)}(t) + \mathcal{L}_1\,\rho^{(k-1)}(t) \qquad (\text{if } k > 0)\,. \tag{3.37b}$$

This set of equations reproduces exactly the dynamics, however, we are not interested in solving the whole density matrix but only getting the leading order of each matrix element, for instance, $\rho_{mn,pq} = |m\rangle\langle n| \otimes |p\rangle\langle q|$, if we had two subsystems. To do so, we first transform the matrix equation into a vector equation. We define the vectorized density matrix $\vec{\rho}$ and the corresponding Liouvillian matrix L. Then, the last equations turns into:

$$\dot{\vec{\rho}}^{(0)}(t) = L_0\,\vec{\rho}^{(0)}(t) \qquad (\text{if } k = 0)\,, \tag{3.38a}$$

$$\dot{\vec{\rho}}^{(k)}(t) = L_0\,\vec{\rho}^{(k)}(t) + L_1\,\vec{\rho}^{(k-1)}(t) \qquad (\text{if } k > 0)\,, \tag{3.38b}$$

For instance, we assume the following rules $\rho_{\mu\nu} \sim \epsilon^{\mu+\nu}\,\rho_{\mu\nu}$ for the 2LS density matrix (so that, $\mu, \nu = 0, 1$). Then, we would like to identify all the elements whose leading order is $k = \mu + \nu$ with $\vec{\rho}^{(k)}$, gather them into a reduced vector $\vec{\rho}'^{(k)}$ and solve their corresponding dynamics separately. Now, in order to reduce the dimensionality of the problem, it is useful to know the position of the non-zero matrix elements of the vector $\vec{\rho}^{(k)}$, that we name $j_p^{(k)}$ (with $1 \leq p \leq n_k$, where n_k is the dimension of $\vec{\rho}'^{(k)}$). We define the projection matrices T_k, which send the matrix elements from the full vector space to the reduced space. That is, for $\vec{\rho} = (\rho_{00},\ \rho_{01},\ \rho_{10},\ \rho_{11})^{\mathrm{T}}$, we have the reduced vectors

$$\vec{\rho}'^{(0)} = T_0\vec{\rho} = (\rho_{00})^{\mathrm{T}}\,, \tag{3.39a}$$

$$\vec{\rho}'^{(1)} = T_1\vec{\rho} = (\rho_{01}\ \rho_{10})^{\mathrm{T}}\,, \tag{3.39b}$$

$$\vec{\rho}'^{(2)} = T_2\vec{\rho} = (\rho_{11})^{\mathrm{T}}\,. \tag{3.39c}$$

From these rules, we are able to find the actual shape of these matrices. They must be $n_k \times (N+1)^2$ matrices, where N is total number of excitations of the truncated Hilbert space. The i-th row has only non-zero entries at its $j_i^{(k)}$-th position. For the case at hand,

$$T_0 = \begin{pmatrix} 1 & 0 & 0 & 0 \end{pmatrix}, \quad T_1 = \begin{pmatrix} 0 & 1 & 0 & 0 \\ 0 & 0 & 1 & 0 \end{pmatrix}, \quad T_2 = \begin{pmatrix} 0 & 0 & 0 & 1 \end{pmatrix}. \tag{3.40}$$

The opposite mapping that returns the reduced vector to the original space is given by the transposed matrix T_k^{T}. Additionally, we can define the projection operator as $T_k^{\mathrm{T}}\,T_k$, which is a $(N+1)^2$ diagonal square matrix with ones at the positions $j_p^{(k)}$ and zeros elsewhere. This operator leaves $\vec{\rho}^{(k)}$ untouched while it sends to zero any other $\vec{\rho}^{(k')}$. Then, we can left-multiply (3.38) by T_k and introduced $T_k^{\mathrm{T}}\,T_k$ in

between L_0 and $\vec{\rho}^{\,(k)}(t)$ and $T_{k-1}^{\mathrm{T}}\,T_{k-1}$ in between L_1 and $\vec{\rho}^{\,(k-1)}(t)$. We get:

$$T_0\dot{\vec{\rho}}^{\,(0)}(t) = \left(T_0\,L_0\,T_0^{\mathrm{T}}\right)T_0\vec{\rho}^{\,(0)}(t) \quad (\text{if } k=0)\,, \tag{3.41a}$$

$$T_k\dot{\vec{\rho}}^{\,(k)}(t) = \left(T_k\,L_0\,T_k^{\mathrm{T}}\right)T_k\,\vec{\rho}^{\,(k)}(t) + \left(T_k\,L_1\,T_{k-1}^{\mathrm{T}}\right)T_{k-1}\,\vec{\rho}^{\,(k-1)}(t) \quad (\text{if } k>0)\,, \tag{3.41b}$$

which, after defining $L_{k,k} = T_k\,L_0\,T_k^{\mathrm{T}}$ and $L_{k,k-1} = T_k\,L_1\,T_{k-1}^{\mathrm{T}}$ and substituting $\vec{\rho'}^{\,(k)} = T_k\vec{\rho}^{\,(k)} \to \vec{\rho}^{\,(k)}$ for simplicity, leads to:

$$\dot{\vec{\rho}}^{\,(0)}(t) = L_{0,0}\,\vec{\rho}^{\,(0)}(t) \qquad (\text{if } k=0)\,, \tag{3.42a}$$

$$\dot{\vec{\rho}}^{\,(k)}(t) = L_{k,k}\,\vec{\rho}^{\,(k)}(t) + L_{k,k-1}\,\vec{\rho}^{\,(k-1)}(t) \qquad (\text{if } k>0)\,, \tag{3.42b}$$

that is formally equivalent to Eq. (3.4) and can be solved almost identically as shown in the previous Subsections. From there, we find the time evolution of the reduced vectors:

$$\vec{\rho}^{\,(k)}(t) = \sum_p \vec{\ell}_p^{\,(k)} e^{\lambda_p^{(k)} t}\,, \tag{3.43}$$

where the elements of $\vec{\ell}_p^{\,(k)}$ are $\ell_{ip}^{(k)}$. The whole density matrix is obtained applying the inverse mapping T_k^{T} and reshaping the vector as a matrix (which we will denote as $[\![\cdot]\!]$). After that, we get the final result:

$$\boxed{\rho(t) = \sum_k \sum_{p=1}^{\mu_k} [\![T_k^{\mathrm{T}}\vec{\ell}_p^{\,(k)}]\!]\, e^{\lambda_p^{(k)} t}\,.} \tag{3.44}$$

This equation provides the counterpart of Eq. (3.19) but at the level of the density matrix. While no illustrations will be provided here for this case, the formalism is complete with this formula and its accompanying results (cf. Eq. (3.53)).

Nevertheless, there is a subtle change when solving the steady-state case. For $k=0$, the linear system is homogeneous and the matrix cannot be inverted. One way to overcome this problem and get the non-trivial solution is to look for the null-space of $L_{0,0}$. Since the matrix admits an eigenvalue decomposition, its kernel corresponds to the non-trivial eigenvectors of the eigenvalue 0. For the usual configurations, this eigenvalue is non-degenerate, i.e., the steady-state solution is unique and its normalization must be chosen so that, after reshaping the vector, the trace of the density matrix is 1.

Remembering that, in this basis and assuming the system has already reached the steady-state, the Quantum Regression Theorem takes the following form

$$\langle O_1(0)O_2(\tau)O_3(t)\rangle = \mathrm{Tr}\Big\{O_2(0)e^{\mathcal{L}\tau}\big(O_3(0)\rho_{\mathrm{ss}}O_1(0)\big)\Big\}\,. \tag{3.45}$$

We are dropping time dependence of O_1, O_2 and O_3 for clarity. We define $v_{O_1O_3}(\tau) = e^{\mathcal{L}\tau}(O_3\rho_{\rm ss}O_1) = e^{\mathcal{L}\tau}v_{O_1O_3}(0)$ and calculate its derivative with respect to τ:

$$\partial_\tau v_{O_1O_3}(\tau) = \mathcal{L}\, e^{\mathcal{L}\tau} v_{O_1O_3}(0) = \mathcal{L} v_{O_1O_3}(\tau)\,. \tag{3.46}$$

Since $v_{O_1O_3}(0)$ is proportional to ρ_{ss}, we can decompose it as a sum $v_{O_1O_3}(0) = \sum_k \epsilon^k v^{(k)}_{O_1O_3}(0)$ and do the same for $v_{O_1O_3}(\tau)$. After plugging this into Eq. (3.46) and separating the different powers

$$\partial_\tau v^{(k)}_{O_1O_3}(\tau) = \mathcal{L}_0 v^{(k)}_{O_1O_3}(\tau) + \mathcal{L}_1 v^{(k-1)}_{O_1O_3}(\tau)\,, \tag{3.47}$$

or, vectorizing the equation ($v_{O_1O_3} \to \vec{v}_{O_1O_3}$ and $\mathcal{L}_i \to L_i$),

$$\partial_\tau \vec{v}^{(k)}_{O_1O_3}(\tau) = L_0 \vec{v}^{(k)}_{O_1O_3}(\tau) + L_1 \vec{v}^{(k-1)}_{O_1O_3}(\tau)\,. \tag{3.48}$$

This equation can be solved following the same procedure as Eq. (3.38). However, we should be careful when solving this equation. It may be the case that $v^{(k)}_{O_1O_3}(0) = O_3\rho^{(k)}_{ss}O_1 = 0$ for some $k < k_0$. This means that O_1 and O_3 acting on ρ_{ss} are lowering indices (connecting to lower order matrix elements). For instance, for a single cavity mode, symbolically $(a\rho_{mn}a^\dagger) \to \rho_{m-1,n-1}$, which is non zero only if $m, n \geq 1$. Then, both $\rho^{(0)}$ and $\rho^{(1)}$ do not contribute to $v_{AB}(\tau)$ (with $O_1 = a^\dagger$ and $O_3 = a$) and the first term to appear is $v^{(2)}_{O_1O_3}(\tau)$, so $k_0 = 2$ here. Applying the projection matrices on the vector $\vec{v}^{(2)}_{O_1O_3}(\tau)$, only $T_0\vec{v}^{(2)}_{O_1O_3}(\tau)$ is different from zero. As a general statement, if O_1 and O_3 act on the perturbed part of ρ, the first non-vanishing term of $\vec{v}_{O_1O_3}$ is $\vec{v}^{(k_0)}_{O_1O_3}$ (k_0 depends on the specific choice of O_1 and O_3 and usually is the total number of operators in O_1 and O_3) and the reduced vectors of $\vec{v}^{(k)}_{O_1O_3}$ are calculated as $\vec{v}'^{(k)}_{O_1O_3} = T_{k-k_0}\vec{v}^{(k)}_{O_1O_3}$. Applying T_{k-k_0} on Eq. (3.48), introducing the projection matrices $T^{\rm T}_{k-k_0}T_{k-k_0}$ in between L and $\vec{v}_{O_1O_3}$ and changing $k \to k + k_0$, we get

$$\partial_\tau \vec{v}^{(k+k_0)}_{O_1O_3}(\tau) = L_{k,k}\vec{v}^{(k+k_0)}_{O_1O_3}(\tau) + L_{k,k-1}\vec{v}^{(k+k_0-1)}_{O_1O_3}(\tau) \qquad (\text{for } k \geq 0)\,. \tag{3.49}$$

where we have substituted $\vec{v}'^{(k)}_{O_1O_3} \to \vec{v}^{(k)}_{O_1O_3}$ for brevity. Now the question is how many orders are required to calculate (3.45). For $\tau = 0$, we have $O_2(O_3\rho_{ss}O_1)$ inside the trace. For the single mode and using $O_1 = a^\dagger$, $O_2 = a^\dagger a$ and $O_3 = a$, symbolically we have

$$a^\dagger a\left(a\rho_{mn}a^\dagger\right) \to a\,(\rho_{m-1,n-1})a^\dagger \to \rho_{m-2,n-2}\,. \tag{3.50}$$

That is, $m, n \geq 2$ is needed to find non zero elements. The operations inside the bracket were previously considered, as k must be at least $k_0 = 2$. This necessarily means that $O_2 v_{O_1O_3}^{(k+k_0)}(\tau)$ does not vanish only if $k \geq K$, where $K = 2$ in this particular case. For the general case, K is equal to the number of operators in O_2. Then, the leading order of (3.45) is

$$\langle O_1(t)O_2(t+\tau)O_3(t)\rangle = \sum_{k=0}^{K} \mathrm{Tr}\Big\{O_2\, v_{O_1O_3}^{(k+k_0)}(\tau)\Big\} = \mathrm{Tr}\Big\{O_2\, v_{O_1O_3}^{(K+k_0)}(\tau)\Big\}, \quad (3.51)$$

where $v_{O_1O_3}^{(K+k_0)}$ is expressed in terms of $\vec{v}_{O_1O_3}^{(K+k_0)}(\tau)$ and solved using Eq. (3.30) (applied to (3.48))

$$v_{O_1O_3}^{(K+k_0)}(\tau) = [\![T_K^{\mathrm{T}} \vec{v}_{O_1O_3}^{(K+k_0)}(\tau)]\!] = \sum_{p=1}^{\mu_K} [\![T_K^{\mathrm{T}} \hat{\iota}_p^{(K+k_0)}]\!] e^{\lambda_p^{(K)}\tau} \quad (3.52)$$

and, bringing together (3.51) and (3.52),

$$\langle O_1(t)O_2(t+\tau)O_3(t)\rangle = \sum_{p=1}^{\mu_K} \mathrm{Tr}\Big\{O_2\, [\![T_K^{\mathrm{T}} \hat{\iota}_p^{(K+k_0)}]\!]\Big\} e^{\lambda_p^{(K)}\tau}. \quad (3.53)$$

3.1.3 FREQUENCY-FILTERED CORRELATIONS: THE SENSOR METHOD

In the Section 1.2.1, we have introduced the frequency-filtered photon correlations. These quantities are described in terms of convolutions of the unfiltered correlations with the spectral response of the filter. These multi-time integrals are, generally speaking, hard to solve, either analytically or numerically. Indeed, only a few cases can be solved straight from these integrals. However, there is an alternative way to compute these correlators: *the sensor method*.

Following the ideas established by del Valle *et al.* [55], we couple the unfiltered system, namely a (it could represent any system such as a 2LS or a cavity), to n sensors (ς_j, for $j = 1, ..., n$). This always allows to describe the filtered system perturbatively. The system-sensor Hamiltonian is of the general form

$$H = H_a + \sum_j \left[\omega_j \varsigma_j^\dagger \varsigma_j + \epsilon(a^\dagger \varsigma_j + \varsigma_j^\dagger a)\right], \quad (3.54)$$

where H_a is the system Hamiltonian (containing only system variable) and the coupling constant ϵ is taken to be as little as possible

(eventually, $\epsilon \to 0$). The sensors have got a decay rate Γ and the lossy dynamics is described by the master equation

$$\dot{\rho} = -i[H,\rho] + \sum_c \frac{\gamma_c}{2}\mathcal{L}_c\rho + \frac{\Gamma}{2}\sum_{j=1,2}\mathcal{L}_{\varsigma_j}\rho\,, \tag{3.55}$$

with the c operators that act only in the system subspace.

In the supplemental material of Ref. [55], it is proved that solving this dynamical system in the limit of vanishing coupling ($\epsilon \to 0$) is equivalent to computing the photon correlations via averaged time-convoluted field operators, which we define in Eq. (1.60) (for a Lorentzian filter F_L). An alternative justification of the method can be found in Appendix A.4. Although notations may slightly differ, the equivalence is clear, making the following changes: $M_{0,0} \to M$, $\vec{c}_0 \to \mathcal{O}$, $\langle \vec{c}_0 \varsigma_1^{\dagger\mu_1}\varsigma_1^{\nu_1}\varsigma_2^{\dagger\mu_1}\varsigma_2^{\nu_1}\rangle \to [\mu_1\nu_1,\mu_2\nu_2]$ and $M_{k,k-1}$ combines $T_\pm$ (adding $a^\dagger$ or a to $\vec{c}_0$) and subtracting $\varsigma^\dagger$ or ς.

The zeroth-order equation is just $\partial_t\langle\vec{c}_0\rangle = M_{0,0}\langle\vec{c}_0\rangle$. It is convenient to write the equation separating the unity from the rest of the correlators as $\langle\vec{c}_0\rangle = (1\ \langle\vec{c'}_0\rangle)^{\mathrm{T}}$, which yields the equation

$$\partial_t\begin{pmatrix}1\\ \langle\vec{c}_0\rangle\end{pmatrix} = \begin{pmatrix}0 & 0\\ \vec{b}_0 & M'_{0,0}\end{pmatrix}\begin{pmatrix}1\\ \langle\vec{c}_0\rangle\end{pmatrix} \tag{3.56}$$

which, in the steady-state regime, has the solution

$$\begin{pmatrix}1\\ \langle\vec{c}_0\rangle_{\mathrm{ss}}\end{pmatrix} = \begin{pmatrix}1\\ -(M'_{0,0})^{-1}\,\vec{b}_0\end{pmatrix}. \tag{3.57}$$

The next set is composed of $\langle\vec{c}_1\rangle = (\langle\varsigma_j^\dagger\vec{c}_0\rangle\ \langle\vec{c}_0\varsigma_j\rangle)^{\mathrm{T}}$ and the equation of motion is $\partial_t\langle\vec{c}_1\rangle = M_{1,1}\langle\vec{c}_1\rangle + M_{1,0}\langle\vec{c}_0\rangle$. We find

$$\partial_t\begin{pmatrix}\langle\varsigma_j^\dagger\vec{c}_0\rangle\\ \langle\vec{c}_0\varsigma_j\rangle\end{pmatrix} = \begin{pmatrix}M_{0,0}-z_j^*I & 0\\ 0 & M_{0,0}-z_jI\end{pmatrix}\begin{pmatrix}\langle\varsigma_j^\dagger\vec{c}_0\rangle\\ \langle\vec{c}_0\varsigma_j\rangle\end{pmatrix} + i\epsilon\begin{pmatrix}\langle a^\dagger\vec{c}_0\rangle\\ -\langle\vec{c}_0\,a\rangle\end{pmatrix}, \tag{3.58}$$

with $z_j \equiv \Gamma/2 + i\,\omega_j$. Now, we introduce the matrices $\mathrm{T}_\pm$ that send $\langle\vec{c}_0\rangle$ to $\langle a^\dagger\vec{c}_0\rangle$ and $\langle\vec{c}_0\,a\rangle$, respectively. The previous equation can be written as

$$\partial_t\begin{pmatrix}\langle\varsigma_j^\dagger\vec{c}_0\rangle\\ \langle\vec{c}_0\varsigma_j\rangle\end{pmatrix} = \begin{pmatrix}M_{0,0}-z_j^*I & 0\\ 0 & M_{0,0}-z_jI\end{pmatrix}\begin{pmatrix}\langle\varsigma_j^\dagger\vec{c}_0\rangle\\ \langle\vec{c}_0\varsigma_j\rangle\end{pmatrix} + \begin{pmatrix}i\epsilon\,\mathrm{T}_+\\ -i\epsilon\,\mathrm{T}_-\end{pmatrix}\langle\vec{c}_0\rangle, \tag{3.59}$$

which has the steady-state ($t \to \infty$)

$$\begin{pmatrix} \langle \varsigma_j^\dagger \vec{c}_0 \rangle_{\rm ss} \\ \langle \vec{c}_0 \varsigma_j \rangle_{\rm ss} \end{pmatrix} = \begin{pmatrix} -i\epsilon [M_{0,0} - z_j^* I]^{-1} \, \mathrm{T}_+ \langle \vec{c}_0 \rangle_{\rm ss} \\ i\epsilon [M_{0,0} - z_j I]^{-1} \, \mathrm{T}_- \langle \vec{c}_0 \rangle_{\rm ss} \end{pmatrix} . \tag{3.60}$$

For $k \geq 2$, the equations are solved recursively, following the instructions written above, and whose expressions can be found in Appendix. A.4. It is easy to check that these results coincide with Ref. [55]. A change of basis or picture also allows us to solve this problem in terms of density matrix elements while maintaining the same ladder-like structure (as shown above and in [61]), making clear the equivalent formalism developed in [62] can be straightforwardly obtained through a transformation from the correlation function frame. In the same way, 2-time correlations are solved and proved to be equivalent. This, together with the fact that exact perturbation value, namely ϵ, does only appear in the expansion after the corresponding algebraic manipulations, makes this approach very stable and versatile.

3.2 ILLUSTRATIONS OF THE PERTURBATION THEORY

Having the theory presented, we turn now to illustrations of the method by applying it to particular cases.

3.2.1 N-EMITTERS WITHIN A CAVITY: DICKE MODEL

The Dicke model [63] was introduced to study the interaction of light and matter, particularly the phenomenon of superradiance. This concept was introduced by Dicke [64] when studying the interaction of N 2LS with the EM field. In the initial state all of them are excited and eventually will decay due to the presence of the field. Under certain circumstances, the emission displays an extraordinary enhancement of the intensity that does not correspond to N-emitters being de-excited independently (like the radioactive decay). Instead, the ensemble behaves as a single collective mode that emits coherently. This is called the superrandiant phase as the system undergoes a phase transition from the normal phase which bears many similarities with lasing (strong coherence and intensity). The model consists of an array of N emitters σ_j coupled to a cavity mode a so the Hamiltonian reads

$$H = \omega_a a^\dagger a + \omega_\sigma \sum_{j=1}^{N} \sigma_j^\dagger \sigma_j + g(a^\dagger + a) \sum_{j=1}^{N} \left(\sigma_j^\dagger + \sigma_j \right) . \tag{3.61}$$

In our level of approximation (RWA), we can eliminate the counter-rotating terms. The model is then usually called the Tavis-Cummings model (an extension of the Jaynes-Cummings model). We include coherent excitation, that is, a laser feeding the cavity mode with frequency ω_{L} and amplitude Ω_a. In the Rotating Frame, the Hamiltonian becomes

$$H = \Delta_a a^\dagger a + \Delta_\sigma \sum_{j=1}^{N} \sigma_j^\dagger \sigma_j + g \sum_{j=1}^{N} \left(a^\dagger \sigma_j + \sigma_j^\dagger a \right) + \Omega_a \left(a^\dagger + a \right), \quad (3.62)$$

where $\Delta_a = \omega_a - \omega_{\mathrm{L}}$ and $\Delta_\sigma = \omega_\sigma - \omega_{\mathrm{L}}$ are the cavity and emitter detuning with respect of the laser. The dissipative dynamics is governed by the master equation

$$\dot{\rho} = -i\,[H, \rho] + \frac{\gamma_a}{2} \mathcal{L}_a \rho + \frac{\gamma_\sigma}{2} \sum_{j=1}^{N} \mathcal{L}_{\sigma_j} \rho\,. \quad (3.63)$$

We now proceed to solve the correlators equations.

We define $\{m, n, \mu_1, \nu_1, \ldots, \mu_N, \nu_N\} \equiv \langle a^{\dagger m} a^m \sigma_1^{\dagger \mu_1} \sigma_1^{\nu_1} \ldots \sigma_N^{\dagger \mu_N} \sigma_N^{\nu_N} \rangle$, where $m, n \geq 0$ and $\mu_j, \nu_j = 0, 1$ $(j = 1, \ldots, N)$ whose dynamics, as usual, are given by the equations

$$\partial_t \{m, n, \mu_1, \nu_1, \ldots, \mu_N, \nu_N\} = \sum M^{m,n,\mu_1,\nu_1,\ldots,\mu_N,\nu_N}_{m',n',\mu_1',\nu_1',\ldots,\mu_N',\nu_N'} \{m', n', \mu_1', \nu_1', \ldots, \mu_N', \nu_N'\} \quad (3.64)$$

where this multi-index array M is zero except when the following rules are fulfilled. For $N = 2$, we have

$$\mathcal{M}^{m,n,\mu_1,\nu_1,\mu_2,\nu_2}_{m,n,\mu_1,\nu_1,\mu_2,\nu_2} = i\Delta_a\,(m - n) + i\Delta_\sigma \sum_j (\mu_j - \nu_j) - \frac{\gamma_a}{2}(m + n) - \frac{\gamma_\sigma}{2} \sum_j (\mu_j + \nu_j)\,, \quad (3.65a)$$

$$\mathcal{M}^{m,n,\mu_1,\nu_1,\mu_2,\nu_2}_{m-1,n,\mu_1,\nu_1,\mu_2,\nu_2} = i\Omega_a m\,, \quad (3.65b)$$

$$\mathcal{M}^{m,n,\mu_1,\nu_1,\mu_2,\nu_2}_{m,n-1,\mu_1,\nu_1,\mu_2,\nu_2} = -i\Omega_a n\,, \quad (3.65c)$$

$$\mathcal{M}^{m,n,\mu_1,\nu_1,\mu_2,\nu_2}_{m+1,n,1-\mu_1,\nu_1,\mu_2,\nu_2} = ig\mu_1 \text{ (and same for } \mu_2)\,, \quad (3.65d)$$

$$\mathcal{M}^{m,n,\mu_1,\nu_1,\mu_2,\nu_2}_{m,n+1,\mu_1,1-\nu_1,\mu_2,\nu_2} = -ig\nu_1 \text{ (and same for } \nu_2)\,, \quad (3.65e)$$

$$\mathcal{M}^{m,n,\mu_1,\nu_1,\mu_2,\nu_2}_{m-1,n,1-\mu_1,\nu_1,\mu_2,\nu_2} = igm(1 - \mu_1) \text{ (and same for } \mu_2)\,, \quad (3.65f)$$

$$\mathcal{M}^{m,n,\mu_1,\nu_1,\mu_2,\nu_2}_{m,n-1,\mu_1,1-\nu_1,\mu_2,\nu_2} = -ign(1 - \nu_1) \text{ (and same for } \nu_2)\,, \quad (3.65g)$$

$$\mathcal{M}_{\substack{m,n,\mu_1,\nu_1,\mu_2,\nu_2 \\ m+1,n,\mu_1,1-\nu_1,\mu_2,\nu_2}} = -2ig\mu_1(1-\nu_1) \text{ (and same for } \mu_2)\,, \tag{3.65h}$$

$$\mathcal{M}_{\substack{m,n,\mu_1,\nu_1,\mu_2,\nu_2 \\ m,n+1,1-\mu_1,\nu_1,\mu_2,\nu_2}} = 2ig\nu_1(1-\mu_1) \text{ (and same for } \nu_2)\,. \tag{3.65i}$$

These equations relate the correlations in a way that an infinite number of them is needed to be solved completely. Nevertheless, in the regime of low pumping ($\Omega_a \ll \gamma_a, \gamma_\sigma, g$) these equations can be solved recursively. We assume that $\langle a^{\dagger m} a^m \sigma_1^{\dagger\mu_1}\sigma_1^{\nu_1}\ldots\sigma_N^{\dagger\mu_N}\sigma_N^{\nu_N}\rangle \sim \Omega_a^k$, where $k = m+n+\mu_1+\nu_1+\ldots+\mu_N+\nu_N$. For instance, the first manifold is made up of $\langle a\rangle$, $\langle a^\dagger\rangle$, $\langle\sigma_j\rangle$ and $\langle\sigma_j^\dagger\rangle$. Gathering these correlators, we get the equations

$$\frac{d}{dt}\langle a\rangle = -i\Omega_a - \left(\frac{\gamma_a}{2}+i\Delta_a\right)\langle a\rangle - ig\sum_j\langle\sigma_j\rangle\,, \tag{3.66a}$$

$$\frac{d}{dt}\langle\sigma_j\rangle = -\left(\frac{\gamma_\sigma}{2}+i\Delta_\sigma\right)\langle\sigma_j\rangle - ig\langle a\rangle\,. \tag{3.66b}$$

These equations can be further simplified. Since each emitter is identical to the other, each correlator $\langle\sigma_j\rangle$ has to be exactly the same. We can make the following assumption, defining the bright state operator $\Sigma = \frac{1}{N}\sum_j\sigma_j$. Then, instead of having $N+1$ coupled equations we reduce the problem to just a pair. That is,

$$\frac{d}{dt}\langle a\rangle = -i\Omega_a - \left(\frac{\gamma_a}{2}+i\Delta_a\right)\langle a\rangle - igN\langle\Sigma\rangle\,, \tag{3.67a}$$

$$\frac{d}{dt}\langle\Sigma\rangle = -\left(\frac{\gamma_\sigma}{2}+i\Delta_\sigma\right)\langle\Sigma\rangle - ig\langle a\rangle\,. \tag{3.67b}$$

The equations for $\langle a^\dagger\rangle$ and $\langle\Sigma^\dagger\rangle$ are obtained by taking the conjugate of these equations. For higher manifold correlations, the reduced equations are given in the Appendix A.6. Again, the rest of correlators can be obtained by taking the complex conjugate of this set of equations.

From the first manifold we obtain the mean fields

$$\langle a\rangle = \frac{-2i\Omega_a(\gamma_a+2i\Delta_a)}{4g^2N+(\gamma_a+2i\Delta_a)(\gamma_\sigma+2i\Delta_\sigma)}\,, \tag{3.68}$$

$$\langle\Sigma\rangle = \frac{-4g\Omega_a}{4g^2N+(\gamma_a+2i\Delta_a)(\gamma_\sigma+2i\Delta_\sigma)}\,, \tag{3.69}$$

while the cavity and emitters population are

$$\langle a^\dagger a\rangle_N = \frac{\Omega_a^2\tilde{\Gamma}_\sigma^2}{16g^4N^2+8g^2N\left(\gamma_a\gamma_\sigma-4\Delta_a\Delta_\sigma\right)+\tilde{\Gamma}_a^2\tilde{\Gamma}_\sigma^2}, \tag{3.70}$$

$$\langle\Sigma^\dagger\Sigma\rangle_N = \frac{\Omega_a^2 g^2}{16g^4N^2+8g^2N\left(\gamma_a\gamma_\sigma-4\Delta_a\Delta_\sigma\right)+\tilde{\Gamma}_a^2\tilde{\Gamma}_\sigma^2}, \tag{3.71}$$

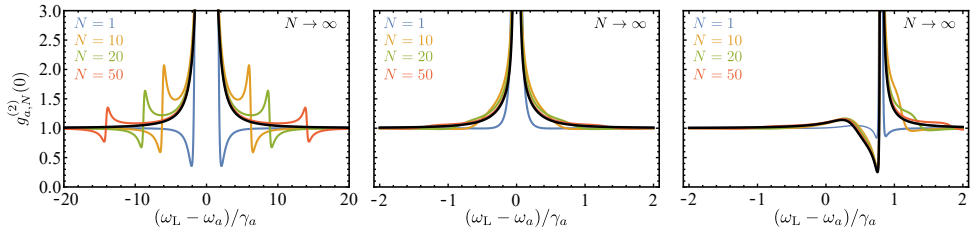

Figure 3.2: 2-photon cavity autocorrelation function for zero time delay for the Dicke model at vanishing driving. The overall behaviour of $g^{(2)}_{a,N}(0)$ changes as the number of emitters within the cavity increases ($N = 1, 10, 20, 50$ shown here, together with the limit $N \to \infty$). Left-hand figure at resonance ($\omega_a = \omega_\sigma$) and strong coupling ($g = 2\gamma_a$), the center one also at resonance but weak coupling ($g = 0.2\gamma_a$) and the right-hand figure shows the blue-shifted emitters $\omega_\sigma - \omega_a = 0.8\gamma_a$ in weak coupling. Parameters: $\gamma_a = 1$, $\gamma_\sigma = 0.01$, i. e., same parameters as Ref. [65].

where $\tilde{\Gamma}_i^2 \equiv \gamma_i^2 + 4\Delta_i^2$ (for $i = a, \sigma$). Similarly, the 2-particle Glauber correlator $g_a^{(2)} = \langle a^{\dagger 2} a^2 \rangle / \langle a^\dagger a \rangle^2$ for zero delay time is

This along with other analytical results illustrate the power of our perturbative theory, by providing the general closed-form expressions for all N of quantities that were previously obtained only in the limit $N \to \infty$ or numerically (using the scattering matrix [65]).

$$
\begin{aligned}
g^{(2)}_{a,N}(0) = \Big\{ & \left[16g^4N^2 + 8g^2N\left(\gamma_a\gamma_\sigma - 4\Delta_a\Delta_\sigma\right) + \tilde{\Gamma}_a^2\tilde{\Gamma}_\sigma^2\right] \times \\
& \left[16g^4N^2 - 8g^2\left(\gamma_{11}\gamma_\sigma - 4\Delta_{11}\Delta_\sigma\right) + \tilde{\Gamma}_{11}^2\tilde{\Gamma}_\sigma^2\right] \Big\} \Big/ \\
& \Big\{ \tilde{\Gamma}_a^2\tilde{\Gamma}_\sigma^2\tilde{\Gamma}_{11}^2 + 16g^4\big[(N-1)^2\gamma_a^2 + 2(N-1)N\gamma_a\gamma_\sigma + \\
& 4\Delta_a^2 - 8N\Delta_a\Delta_{11} + N^2(\gamma_\sigma^2 + 4\Delta_{11}^2)\big] + \\
& 8g^2\big[(N-1)\gamma_a^3\gamma_\sigma + \gamma_a^2\big([2N-1]\gamma_\sigma^2 + \\
& 4\Delta_\sigma[\Delta_{11} - N\Delta_a]\big) - 4\Delta_a(\gamma_\sigma^2\Delta_{1N} + 4\Delta_\sigma\Delta_{11}\Delta_{N-1,N}) + \\
& \gamma_a\gamma_\sigma\big(4[N-1]\Delta_a^2 + N\tilde{\Gamma}_\sigma^2\big)\big] \Big\}\,,
\end{aligned}
\tag{3.72}
$$

where we have introduced the notation $\gamma_{ij} \equiv i\,\gamma_a + j\,\gamma_\sigma$ and $\Delta_{ij} \equiv i\,\Delta_a + j\,\Delta_\sigma$ (i and j being integers). Additionally, we define $\tilde{\Gamma}_{ij}^2 \equiv \gamma_{ij}^2 + 4\Delta_{ij}^2$. For increasing number of emitters in the cavity, the collective bright state is allowed to have more and more excitation and eventually converges to a boson-like state ($N \to \infty$) that, however, keeps some of the intrinsic non-linearities of the emitter. This is indeed reflected is the 2-photon correlation in the limit $N \to \infty$, yielding

$$
g^{(2)}_{a,N\to\infty}(0) = \left[16g^4 - 8g^2(\gamma_\sigma\gamma_{11} - 4\Delta_\sigma\Delta_{11}) + \tilde{\Gamma}_\sigma^2\tilde{\Gamma}_{11}^2\right] / (\tilde{\Gamma}_\sigma^2\tilde{\Gamma}_{11}^2)\,, \tag{3.73}
$$

instead of $g_a^{(2)}(0) = 1$, expected for coupled boson modes under coherent driving. The 2-photon correlations shows strong features for any N, both bunching and antibunching depending on the frequency

of the driving source (see Fig. 3.2). For weak driving, this was already reported in the Jaynes-Cummings scenario [66] (for $N = 1$) and for non-linear bosonic system ($N \to \infty$), for instance, two coupled photonic modes with Kerr non-linearities [67] or exciton-polaritons [68, 69]. In between, we can place the Dicke model. Making reasonable assumptions (bright state approximation) under weak driving, we are able to replicate the results from [65]. The major asset of our method is that we could provide analytical expressions for an arbitrary number of emitters N rather than only the limit $N \to \infty$ (equivalent to Eq. (3.73)) and compute, if needed, higher order corrections. Besides, the computation of photon correlations using the scattering matrix requires an exhaustive counting of all the possible one and two photon scattering events. In the end, it turns out to be completely equivalent to our more simple method.

3.2.2 INCOHERENT JC MODEL

We make here a little revision of the simplest model for light-matter interaction, the Jaynes-Cummings model, under incoherent driving, studied in depth in Refs. [70, 71], where the solution of the correlators are presented as a series of recursive equations. Fixing a cut-off, one can obtain the solution to the desired level of approximation. With our method, we can replicate these results and even generalise some of them keeping only the leading order without needing to unravel the recursive equations.

The Hamiltonian has the same form as the Dicke model (3.62), fixing $N = 1$ and $\Omega_a = 0$. The incoherent pumping is inserted into the system dynamics by adding to the Liouvillian the terms $\frac{P_\sigma}{2}\mathcal{L}_{\sigma^\dagger}\rho$ and $\frac{P_a}{2}\mathcal{L}_{a^\dagger}\rho$. Subsequently, the effective decay rates are modified due to the presence of the incoherent (thermal) bath: $\Gamma_\sigma \equiv \gamma_\sigma + P_\sigma$ and $\Gamma_a \equiv \gamma_a - P_a$.

The small parameter corresponds here to the pumping rate, either P_σ or P_a, hence we always stay in the *linear regime*, following the classification introduced in Ref. [70]. Since the results for cavity-driven and emitter-driven cases are qualitatively different, we will present them separately. By inspecting the correlator equations, we notice that all the linking terms jump from k to $k \pm 2$. Thus, some subsets may be left unconnected and would not contribute to the dynamics. The method has to be slightly modified to incorporate these contributions. As pointed out above, in absence of feeding terms, the first subset remains isolated and all the correlators vanish, therefore, the mean fields $\langle a \rangle = \langle \sigma \rangle = 0$ in the steady-state. Besides this, the following steps are the same.

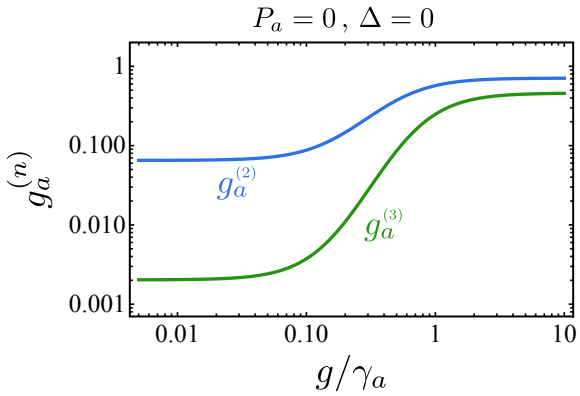

Figure 3.3: Two and three photon statistics of the light emitted by the dot-pumped incoherent Jaynes–Cummings model at resonance ($\omega_a = \omega_\sigma$) depending on the cavity-dot coupling strength g. Chosen parameters: $\gamma_a = 1$, $\gamma_\sigma = 0.1$, $P_a = 0$ and $P_\sigma = 0.01\,\gamma_\sigma$.

The first non-zero correlators are the total populations. For the dot-driven case ($P_a = 0$), we have

$$n_a = \frac{4g^2 P_\sigma \Gamma_1}{\Gamma_1^2(4g^2 + \Gamma_a\Gamma_\sigma) + 4\Gamma_a\Gamma_\sigma\Delta^2}\,, \tag{3.74a}$$

$$n_\sigma = \frac{4g^2 P_\sigma \Gamma_1 + P_\sigma\Gamma_a(\Gamma_+^2 + 4\Delta^2)}{\Gamma_1^2(4g^2 + \Gamma_a\Gamma_\sigma) + 4\Gamma_a\Gamma_\sigma\Delta^2}\,, \tag{3.74b}$$

where $\Delta = \omega_\sigma - \omega_a$ is the detuning between the emitter and cavity frequencies and we have defined $\Gamma_k \equiv k\,\Gamma_a + \Gamma_\sigma$ (for $k \in \mathbb{N}$). To make a fairer comparison, we introduce the quantity from Ref. [70]

$$\kappa_\sigma \equiv \frac{4g^2}{\Gamma_a\left(1 + \frac{4\Delta^2}{\Gamma_1^2}\right)}\,, \tag{3.75}$$

reminding that we did not include dephasing effects (so $\gamma_\phi = 0$) and $\Gamma_a = \gamma_a$ (since $P_a = 0$). Then, the populations (3.74) read

$$n_a = \frac{\kappa_\sigma}{\Gamma_1\,(\kappa_\sigma + \Gamma_\sigma)} P_\sigma\,, \tag{3.76a}$$

$$n_\sigma = \frac{\kappa_\sigma + \Gamma_1}{\Gamma_1\,(\kappa_\sigma + \Gamma_\sigma)} P_\sigma\,. \tag{3.76b}$$

In a similar way, we can obtain the correlators for the cavity-driven case. In the low pumping regime, some correlators are symmetric under the exchange $a \leftrightarrow \sigma$. Thus, $n_a \leftrightarrow n_\sigma$ if we change $P_\sigma \to P_a$ (so $P_\sigma = 0$). However, this symmetry does not hold for higher

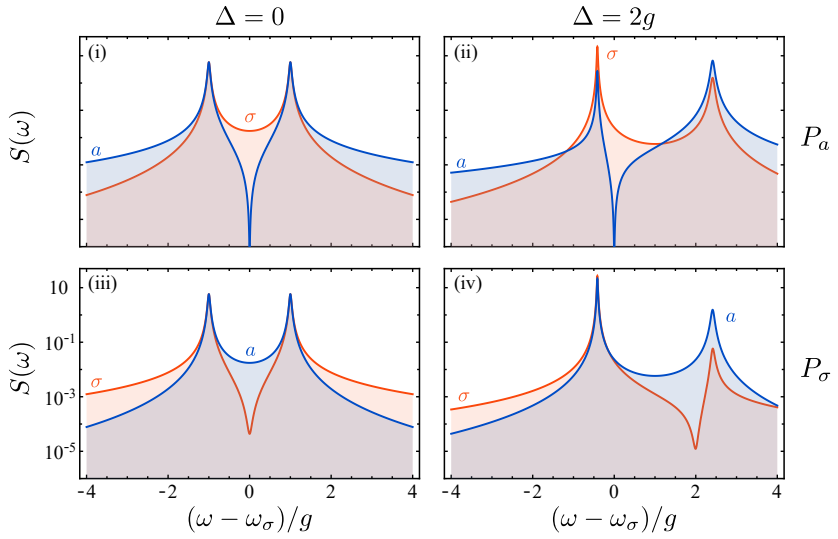

Figure 3.4: Luminescence spectra from both the cavity and dot emission, shown in blue and red, respectively. For weak driving, only the first manifold is effectively excited and two peaks are shown in the spectrum, corresponding to the transitions from the dressed states (in strong coupling, the position of the peaks are $\pm R_r$). When the cavity-emitter detuning is zero ($\Delta = 0$), both peaks are symmetric. On the other hand, the detuning ($\Delta = 2g$ here) not only displaces the position of the peaks but unbalances the proportion yielding an asymmetrical spectrum. Chosen parameters: $g = 1$, $\gamma_a = 0.1$, $\gamma_\sigma = 0.01$, and the pumping rates are $P_a = 0$ and $P_\sigma = 0.01\,\gamma_\sigma$ for the first row and $P_a = 0.01\gamma_a$ and $P_\sigma = 0$ for the second.

correlators. For the dot-driven case, the 2nd and 3rd-order photon Glauber correlator are:

$$g_a^{(2)} = \frac{2\Gamma_3[\Gamma_1^2(4g^2+\Gamma_a\Gamma_\sigma)+4\Gamma_a\Gamma_\sigma\Delta^2]}{\Gamma_1[\Gamma_3^2(4g^2+\Gamma_a\Gamma_1)+4\Gamma_a\Gamma_1\Delta^2]}, \tag{3.77a}$$

$$g_a^{(3)} = \frac{6\Gamma_3\Gamma_5[\Gamma_1^2(4g^2+\Gamma_a\Gamma_\sigma)+4\Gamma_a\Gamma_\sigma\Delta^2]^2}{\Gamma_1^2\prod_{k=1,2}[\Gamma_{2k+1}^2(4g^2+\Gamma_a\Gamma_k)+4\Gamma_a\Gamma_k\Delta^2]}, \tag{3.77b}$$

which are shown in Fig. 3.3. The counterpart of $g_a^{(2)}$ for the cavity-driven case, is shown in Appendix A.8. The resulting photon statistics behave very differently depending on the pumped target as can be seen in Fig. 3.5. While the outcoming signal from a dot-driven system is antibunched under a wide range of parameters, the opposite configuration always provides bunched, nearly chaotic, light. When the system is dot driven and weakly coupled, the photon statistics of the cavity partially resemble the emitter perfect antibunching, displaying small values of $g_a^{(2)}(0)$ and $g_a^{(3)}(0)$, limited due to the possibility of exciting higher energy levels.

These results also illustrate the power of our perturbative theory, by providing the general closed-form expressions, now for the τ dynamics, of important correlations in the Jaynes–Cumming model that were previously only obtained at $\tau = 0$ (Refs. [70, 71]).

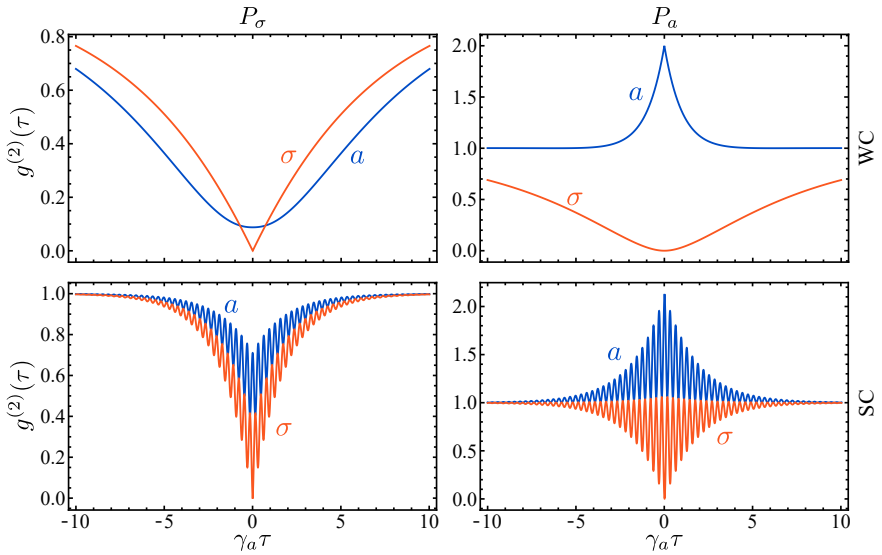

Figure 3.5: Two-photon autocorrelation functions for the cavity and the emitter under incoherent driving as a function of the delay time τ (cavity in blue and emitter in red). The first row corresponds to the weak coupling (WC) regime ($g = 0.01$) and the second one to strong coupling (SC) regime ($g = 1$). The left column shows the cases of dot excitation, whereas the right column contains the cavity excited cases. Chosen parameters: $\Delta = 0$, $\gamma_a = 0.1$, $\gamma_\sigma = 0.01$, and the pumping rates are $P_a = 0$ and $P_\sigma = 0.01\,\gamma_\sigma$ for the first row and $P_a = 0.01\gamma_a$ and $P_\sigma = 0$ for the second.

The luminescence spectra can be easily computed too (shown for several cases in Fig. 3.4). In the low pumping regime ($P_i \to 0$), there are only two non-zero contributions, corresponding to the eigenvalues, split into their real and imaginary parts:

$$\omega_{1,2} = \omega_a + \frac{\Delta}{2} \pm \mathrm{R}_r\,, \tag{3.78a}$$

$$\frac{\gamma_{1,2}}{2} = \frac{\Gamma_a + \Gamma_\sigma}{4} \mp \mathrm{R}_i\,, \tag{3.78b}$$

where $\mathrm{R}_{r,i}$ are the real and imaginary part of the complex Rabi splitting

$$\mathrm{R} = \mathrm{R}_r + i\,\mathrm{R}_i = \sqrt{g^2 - \left(\frac{\Gamma_-}{4} + i\frac{\Delta}{2}\right)^2}\,, \tag{3.79}$$

and $\Gamma_- \equiv \Gamma_a - \Gamma_\sigma$. The spectrum is written as Eq. (3.36). The coefficients L_p and K_p for the cavity and dot can be found in Appendix A.8. As expected, the spectrum only have two peaks, that correspond to the transitions between the first manifold states to the ground state when the system in the strong coupling regime ($g \gg \gamma_a, \gamma_\sigma$). However, the resonant and detuned cases have different shapes. If the detuning is zero, the peaks are symmetric. Otherwise, the weight of the

Lorentzians L_p is unbalanced. The kind of pumping, P_a or P_σ, also changes the contribution of the dispersive part K_p, that produces a deep dip in between the peaks. All these results are in accordance with the ones discussed in Refs. [70, 71].

Additionally, we can obtain the non-zero delay 2nd-order correlator. It can be written as

$$g_i^{(2)}(\tau) = 1 + \sum_p l_p^{(i)} e^{-\lambda_p \tau}\,, \tag{3.80}$$

for either the cavity or the dot ($i = a, \sigma$). The eigenvalues are

$$\lambda_{1,2} = \Gamma_1/2 \pm i\sqrt{2}\mathrm{R}^{(+)}\,, \tag{3.81a}$$
$$\lambda_{3,4} = \Gamma_1/2 \pm i\sqrt{2}\mathrm{R}^{(-)}\,, \tag{3.81b}$$

and

$$\mathrm{R}^{(\pm)} = \sqrt{g^2 + \left(\frac{\Delta}{2}\right)^2 - \left(\frac{\Gamma_-}{4}\right)^2 \pm \sqrt{\chi_+\chi_-}}\,, \tag{3.82}$$

where $\chi_\pm = (g \pm \Gamma_-/4)^2 + (\Delta/2)^2$. In the same way as the zero delay 2-photon correlator function, the time dependent case, i.e., $g_a^{(2)}(\tau)$ manifest some resemblance, in weak coupling, with the dot emission but also incorporates its own dynamics and thus it has less pronounced antibunching but similar coherence time. In the strong coupling regime, however, the statistics are much closer to 1. In the time domain we observe the oscillations in all the cases. Such oscillations are consequence of the strong coupling between the cavity and the emitter and remain as long as $\mathrm{R}^{(\pm)}$ are real, that is, when the system is in the strong coupling regime. This description is valid only if the pumping rate are small enough. If this is not the case, like in the regular perturbation theory, we could extend the series expansion to higher orders and compute the corrections.

3.2.3 FREQUENCY-FILTERED INCOHERENT 2LS

We solve the frequency-filtered correlations for a qubit coupled to a bath. Then, it has a channel to decay and a second one to be pumped. Following the sensor method, we couple a cavity mode to the emitter and, in order to compute second-order filtered quantities, we also coupled a second cavity to the first one. The full Hamiltonian reads

$$H = \omega_\sigma \sigma^\dagger\sigma + \omega_1 \varsigma_1^\dagger\varsigma_1 + \omega_2 \varsigma_2^\dagger\varsigma_2 + \epsilon(\varsigma_1^\dagger\sigma + \varsigma_2^\dagger\varsigma_1 + \mathrm{h.c.})\,, \tag{3.83}$$

where ω_i are the frequency of the sensors. The lossy evolution of the system is given by the master equation

$$\dot{\rho} = -i[H,\rho] + \frac{\gamma_\sigma}{2}\mathcal{L}_\sigma\rho + \frac{P_\sigma}{2}\mathcal{L}_{\sigma^\dagger}\rho + \frac{\Gamma_1}{2}\mathcal{L}_{\varsigma_1}\rho + \frac{\Gamma_2}{2}\mathcal{L}_{\varsigma_2}\rho\,. \tag{3.84}$$

We let the filters widths be, a priori, different. In practice, the second-order filters we choose are the double Lorentzian (1.72) and the Butterworth filter (1.73), so we will fix $\Gamma_1 = \Gamma_2 = \Gamma$ to build the filter up in terms of Lorentzians. Henceforth, we choose the same width Γ for both. Moreover the filter frequencies are parametrised as $\omega_1 = \omega_2 = \omega_\sigma + \Delta_1$ for the double Lorentzian and as $\omega_{1,2} = \omega_\sigma + \Delta_1 \pm \Gamma/2$ for the Butterworth filter. We additionally consider the Lorentzian band-stop filter (which we already referred to as the complementary filter). From the integral (1.69), we found out that we can express its correlator by means of the unfiltered and the Lorentzian (band-pass) filter ones. The coefficient that connects the sensor and integrated correlators is $\zeta = \frac{i\Gamma}{2\epsilon}$ so that any correlator has its corresponding integrated counterpart by changing $\langle \varsigma^{\dagger m}\varsigma^n\rangle \to \zeta^{*m}\zeta^n\,\langle \varsigma^{\dagger m}\varsigma^n\rangle$. The complementary operator will be $\bar{\varsigma} = a - \zeta\varsigma$. The complementary filter has then the mean field $\langle\bar{\varsigma}\rangle = \langle a\rangle - \zeta\langle\varsigma\rangle$, the mean population

$$\langle\bar{\varsigma}^\dagger\bar{\varsigma}\rangle = \langle a^\dagger a\rangle - \zeta^*\langle\varsigma^\dagger a\rangle - \zeta\langle a^\dagger\varsigma\rangle + |\zeta|^2\langle\varsigma^\dagger\varsigma\rangle\,, \tag{3.85}$$

and the two-photon Glauber correlator

$$\begin{aligned}
&\langle\bar{\varsigma}^\dagger(0)(\bar{\varsigma}^\dagger\bar{\varsigma})(\tau)\bar{\varsigma}(0)\rangle = \\
&\langle a^\dagger(0)(a^\dagger a)(\tau)a(0)\rangle - \zeta\langle a^\dagger(0)(a^\dagger a)(\tau)\varsigma(0)\rangle - \\
&\zeta^*\langle\varsigma^\dagger(0)(a^\dagger a)(\tau)a(0)\rangle - \zeta\langle a^\dagger(0)(a^\dagger\varsigma)(\tau)a(0)\rangle - \\
&\zeta^*\langle a^\dagger(0)(\varsigma^\dagger a)(\tau)a(0)\rangle + |\zeta|^2\langle\varsigma^\dagger(0)(a^\dagger a)(\tau)\varsigma(0)\rangle + \\
&|\zeta|^2\langle a^\dagger(0)(\varsigma^\dagger\varsigma)(\tau)a(0)\rangle + \zeta^2\langle a^\dagger(0)(a^\dagger\varsigma)(\tau)\varsigma(0)\rangle + \\
&\zeta^{*2}\langle\varsigma^\dagger(0)(\varsigma^\dagger a)(\tau)a(0)\rangle + |\zeta|^2\langle\varsigma^\dagger(0)(a^\dagger\varsigma)(\tau)a(0)\rangle + \\
&|\zeta|^2\langle a^\dagger(0)(\varsigma^\dagger a)(\tau)\varsigma(0)\rangle - \zeta|\zeta|^2\langle a^\dagger(0)(\varsigma^\dagger\varsigma)(\tau)\varsigma(0)\rangle - \\
&\zeta^*|\zeta|^2\langle\varsigma^\dagger(0)(\varsigma^\dagger\varsigma)(\tau)a(0)\rangle - \zeta|\varsigma|^2\langle\varsigma^\dagger(0)(a^\dagger\varsigma)(\tau)\varsigma(0)\rangle - \\
&\quad\zeta^*|\zeta|^2\langle\varsigma^\dagger(0)(\varsigma^\dagger a)(\tau)\varsigma(0)\rangle + |\zeta|^4\langle\varsigma^\dagger(0)(\varsigma^\dagger\varsigma)(\tau)\varsigma(0)\rangle\,,
\end{aligned} \tag{3.86}$$

which, at $\tau = 0$, has the following form

$$\begin{aligned}
\langle\bar{\varsigma}^{\dagger 2}\bar{\varsigma}^2\rangle = \langle a^{\dagger 2}a^2\rangle - 2\zeta\langle a^{\dagger 2}\varsigma a\rangle - 2\zeta^*\langle a^\dagger\varsigma^\dagger a^2\rangle + \zeta^2\langle a^{\dagger 2}\varsigma^2\rangle + \\
4|\zeta|^2\langle a^\dagger\varsigma^\dagger\varsigma a\rangle + \zeta^{*2}\langle\varsigma^{\dagger 2}a^2\rangle - 2\zeta|\zeta|^2\langle\varsigma^{\dagger 2}\varsigma a\rangle - \\
2\zeta^*|\zeta|^2\langle a^\dagger\varsigma^\dagger\varsigma^2\rangle + |\zeta|^4\langle\varsigma^{\dagger 2}\varsigma^2\rangle\,.
\end{aligned} \tag{3.87}$$

Here, $a = \sigma$ and $\varsigma = \varsigma_1$. Remembering that $\sigma^2 = 0$, $\langle \bar{\varsigma}^{\dagger 2} \bar{\varsigma}^2 \rangle$ reduces to

$$\begin{aligned}\langle \bar{\varsigma}^{\dagger 2} \bar{\varsigma}^2 \rangle = {} & 4|\zeta|^2 \langle \sigma^\dagger \varsigma_1^\dagger \varsigma_1 \sigma \rangle + \zeta^{*2} \langle \varsigma_1^{\dagger 2} \sigma^2 \rangle - 2\zeta |\zeta|^2 \langle \varsigma_1^{\dagger 2} \varsigma_1 \sigma \rangle - \\ & 2\zeta^* |\zeta|^2 \langle \sigma^\dagger \varsigma_1^\dagger \varsigma_1^2 \rangle + |\zeta|^4 \langle \varsigma_1^{\dagger 2} \varsigma_1^2 \rangle \,. \end{aligned} \tag{3.88}$$

Our assumption is again that each correlator $\langle \sigma^{\dagger \mu} \sigma^\nu \varsigma_1^{\dagger m} \varsigma_1^n \varsigma_2^{\dagger p} \varsigma_2^q \rangle$ is proportional to ϵ^k, with $k = m + n + 2p + 2q$. Gathering all the required correlators into C_k and solving the subsets up to $k = 8$ (to solve $\langle \varsigma_2^{\dagger 2} \varsigma_2^2 \rangle$), the first sensor population is then

$$\langle \varsigma_1^\dagger \varsigma_1 \rangle_{\mathrm{L}} = \frac{4 P_\sigma \tilde{\Gamma}_1}{\Gamma \Gamma_\sigma (\tilde{\Gamma}_1^2 + 4\Delta_1^2)} \,, \tag{3.89}$$

which corresponds to the (band-pass) Lorentzian filter, whence the subscript L. In the same way, the second sensor population is

$$\langle \varsigma_2^\dagger \varsigma_2 \rangle = \frac{8 P_\sigma \left[\tilde{\Gamma}_1 (\tilde{\Gamma}_1 \tilde{\Gamma}_2 + 2\Delta_1^2) + 2\tilde{\Gamma}_1 \Delta_2^2 - 4\Gamma \Delta_1 \Delta_2 \right]}{\Gamma \Gamma_\sigma (\tilde{\Gamma}_1^2 + 4\Delta_1^2)(\tilde{\Gamma}_1^2 + 4\Delta_2^2) \left[\Gamma^2 + (\Delta_1 - \Delta_2)^2 \right]} \,, \tag{3.90}$$

where $\tilde{\Gamma}_k \equiv \Gamma_\sigma + k\,\Gamma$ (not to be confused with Γ_k from the previous Section). For the double Lorentzian (DL) and the Butterworth (BW), after the corresponding substitutions, the sensor population read

$$\langle \varsigma_2^\dagger \varsigma_2 \rangle_{\mathrm{DL}} = \frac{8 P_\sigma (\tilde{\Gamma}_1^2 \tilde{\Gamma}_2 + 4\Gamma_\sigma \Delta_1^2)}{\Gamma^3 \Gamma_\sigma (\tilde{\Gamma}^2 + 4\Delta^2)^2} \,, \tag{3.91}$$

$$\begin{aligned}\langle \varsigma_2^\dagger \varsigma_2 \rangle_{\mathrm{BW}} = {} & 4 P_\sigma \left[\Gamma^3 + \tilde{\Gamma}_1 (\Gamma - 2\Delta)^2/2 - 4\Gamma \Delta_1^2 + \right. \\ & \left. \tilde{\Gamma}_1^2 \tilde{\Gamma}_2 + \tilde{\Gamma}_1 (\Gamma + 2\Delta_1)^2/2 \right] / \\ & \left[\Gamma^3 \Gamma_\sigma (\tilde{\Gamma}_1^2 + (\Gamma - 2\Delta_1)^2)(\tilde{\Gamma}_1^2 + (\Gamma + 2\Delta_1)^2) \right] . \end{aligned} \tag{3.92}$$

We can change the effective width Γ in order to have the same FWHM for all the cases. For (3.91), we substitute $\Gamma \to \Gamma_{\mathrm{DL}} = \Gamma / \sqrt{\sqrt{2} - 1}$ and, for (3.92), we replace $\Gamma \to \Gamma_{\mathrm{BW}} = \Gamma / \sqrt{2}$.

From equation (3.85) we compute the complementary filter population, that reads

$$\langle \bar{\varsigma}_1^\dagger \bar{\varsigma}_1 \rangle_{\mathrm{CL}} = \frac{P_\sigma \Gamma_\sigma \tilde{\Gamma}_1 + 4 P_\sigma \Delta_1^2}{\Gamma_\sigma (\tilde{\Gamma}_1^2 + 4\Delta_1^2)} \,. \tag{3.93}$$

The 2-photon correlators are already too complicated to be written here for any frequency Δ_1. Nevertheless, since the emission is characterised by a single Lorentzian, the most interesting setup would be to place the filter frequency right at the center of the spectrum, that is, $\Delta_1 = 0$. The behaviour for another choice of Δ_1 is similar to

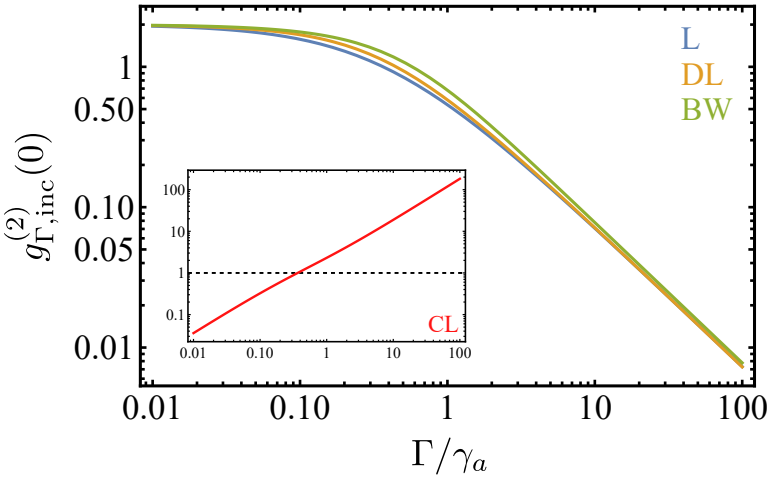

Figure 3.6: Filtered emission (at resonance) of the incoherently-driven 2LS. The second-order Glauber correlator at zero delay for three different (band-pass) filters: Lorentzian (L), double Lorentzian (DL) and second-order Butterworth (BW), all of them with the same FWHM Γ. In inset, the complementary (notch) Lorentzian filter is displayed.

the resonance case. For the Lorentzian band-pass, the second-order Glauber correlator reads

$$g^{(2)}_{\Gamma,\mathrm{L}}(0) = \frac{2\Gamma_\sigma}{\tilde{\Gamma}_3}\,, \tag{3.94}$$

whereas the band-stop filter reads

$$g^{(2)}_{\Gamma,\mathrm{CL}}(0) = 2\Gamma\left(\frac{1}{\Gamma_\sigma}+\frac{1}{\tilde{\Gamma}_3}\right). \tag{3.95}$$

The second-order filter cases are

$$g^{(2)}_{\Gamma,\mathrm{DL}}(0) = 2+\frac{3\Gamma}{4}\left(\frac{285}{\tilde{\Gamma}_2}-\frac{42}{\tilde{\Gamma}_2^2}-\frac{192\Gamma^3}{\tilde{\Gamma}_3^4}-\frac{224\Gamma^2}{\tilde{\Gamma}_3^3}-\frac{252\Gamma}{\tilde{\Gamma}_3^2}\right), \tag{3.96}$$

and

$$g^{(2)}_{\Gamma,\mathrm{BW}}(0) = 2+\frac{6\Gamma}{125}\left(\frac{567}{\tilde{\Gamma}_2}-\frac{210\Gamma}{\tilde{\Gamma}_2^2}+\frac{492\Gamma+158\Gamma_\sigma}{\Gamma_\sigma^2+6\Gamma\Gamma_\sigma+18\Gamma^2}-\frac{200(4\Gamma_\sigma+15\Gamma)}{\Gamma_\sigma^2+6\Gamma\Gamma_\sigma+10\Gamma^2}\right). \tag{3.97}$$

The behaviour of the three band-pass filters is similar (see Fig. 3.6). The filtered Glauber correlator converges to 2 for small widths ($\Gamma\to 0$), so that they lead to thermalisation, while we recover perfect antibunching when $\Gamma\to\infty$. However, for intermediate values ($\Gamma\gtrsim 0.1\gamma_\sigma$), the loss of

antibunching is slightly greater for the BW filter. The tails decay much faster than for the Lorentzian filter and thus overlaps less with the Lorentzian profile of the spectrum. In the middle, one has the double Lorentzian, which also decays as ω^{-4} but spreads more beyond the FWHM (see Fig. 1.9). The notch filter, on the contrary, does not follow this description and, instead, covers the whole range of possible values of $g^{(2)}$. Infinitely small widths return $g^{(2)} = 0$, something we could expect from the complementary shape of the filter. On the other hand, a broadband notch filter rejects a massive fraction of the signal, leading to vanishing population and therefore producing a vacuum-induced superbunching, i.e., $g^{(2)} \gg 1$. The shape of all the curves, however, does not qualitatively change with the pumping P_σ and merely speeds up or slows down the loss of anticorrelation. The correlation function grows, like it does for decreasing values of Γ, as the pumping increases, since the effective width of the spectrum does so. This is qualitatively different from what was found in Ref. [72], in which $g^{(2)}(0)$ exhibits a significant depletion around $P_\sigma = \gamma_\sigma$.

The time dependent case can also be obtained through this method. Both the band-pass and the band-stop Lorentzian filter are written in terms of exponentials

$$\boxed{g^{(2)}(\tau) = 1 + \sum_p l_p \, e^{-\lambda_p \tau}} \,, \tag{3.98}$$

whose the exponents are

$$\lambda_1 = \Gamma_\sigma \,, \quad \lambda_2 = \tilde{\Gamma}_1/2 \,, \quad \lambda_3 = \Gamma \,. \tag{3.99}$$

For the Lorentzian, the coefficients that go with the exponentials are

$$l_{1,\mathrm{L}} = -\frac{\Gamma^2}{\Gamma_-^2} \,, \tag{3.100a}$$

$$l_{2,\mathrm{L}} = -\frac{2\Gamma\Gamma_\sigma(\Gamma_\sigma - 5\Gamma)}{\Gamma_-^2 \tilde{\Gamma}_3} \,, \tag{3.100b}$$

$$l_{3,\mathrm{L}} = 1 - \frac{\Gamma\Gamma_\sigma}{\Gamma_-^2} - \frac{3\Gamma}{\tilde{\Gamma}_3} \,, \tag{3.100c}$$

where we have defined $\Gamma_- \equiv \Gamma_\sigma - \Gamma$. For the complementary Lorentzian, we have

$$l_{1,\mathrm{CL}} = -\frac{\Gamma^2}{\Gamma_-^2} \,, \tag{3.101a}$$

$$l_{2,\mathrm{CL}} = \frac{\Gamma}{\tilde{\Gamma}_3} + \frac{\Gamma(5\Gamma_\sigma - 3\Gamma)}{\Gamma_-^2} \,, \tag{3.101b}$$

$$l_{3,\mathrm{CL}} = \frac{2\Gamma}{\Gamma_\sigma} + \frac{\Gamma}{\tilde{\Gamma}_3} - \frac{\Gamma(3\Gamma_\sigma - 2\Gamma)}{\Gamma_-^2} \,. \tag{3.101c}$$

This result and its accompanying expressions (3.99)–(3.103), as well as its particular cases (3.94)–(3.97), give another illustration of the power of the perturbative theory, by providing exact, closed-form expressions for how various types of filters affect two-photon correlations. While the effects do not turn out to be strong qualitative ones in the simple cases considered here (as seen in Figs. 3.6 and 3.7), this shows how exact results can be obtained for arbitrary types of filters.

The Butterworth filter, on the other hand, has the following exponents

$$\lambda_1 = \Gamma_\sigma\,, \quad \lambda_{2,3} = \tilde{\Gamma}_1/2 \pm i\,\Gamma/2\,, \quad \lambda_{4,5} = \Gamma \pm i\,\Gamma\,, \quad \lambda_6 = \Gamma\,, \tag{3.102}$$

and the coefficients

$$l_{1,\mathrm{BW}} = -\frac{16\Gamma^6}{(4\Gamma^3 - 2\Gamma^2\Gamma_\sigma + \Gamma_\sigma^3)^2}\,, \tag{3.103a}$$

$$\begin{aligned} l_{2,\mathrm{BW}} = -\Big\{ & 4(1-i)\Gamma^3\Gamma_\sigma(\tilde{\Gamma}_1 - i\Gamma)\big[(34+66i)\Gamma^3 + 10(2+3i)\Gamma_\sigma\Gamma^2 - \\ & 3(3+i)\Gamma_\sigma^2\Gamma - \Gamma_\sigma^3\big]\Big\} \Big/ \Big\{\tilde{\Gamma}_2^2(\Gamma_\sigma^2 + 6\Gamma\Gamma_\sigma^2 + 10\Gamma^2)(\Gamma - i\Gamma_-) \\ & (\Gamma_- - i\Gamma)^2(3i\Gamma + \tilde{\Gamma}_3)\Big\} = (l_{3,\mathrm{BW}})^*\,, \end{aligned} \tag{3.103b}$$

$$\begin{aligned} l_{4,\mathrm{BW}} = \frac{1}{10}\Big\{ & \Gamma_\sigma(\tilde{\Gamma}_1 - i\Gamma)\big[(40-32i)\Gamma^4 + (10-62i)\Gamma^3\Gamma_\sigma - \\ & (2+24i)\Gamma^2\Gamma_\sigma^2 + (5+7i)\Gamma\Gamma_\sigma^3 + (2+i)\Gamma_\sigma^4\big]\Big\} \Big/ \\ & \Big\{\tilde{\Gamma}_2^2(\Gamma_- - i\Gamma)^2(\tilde{\Gamma}_3 + i\Gamma)(\tilde{\Gamma}_3 + 3i\Gamma)\Big\} = (l_{5,\mathrm{BW}})^*\,, \end{aligned} \tag{3.103c}$$

$$l_{6,\mathrm{BW}} = \frac{\Gamma_\sigma(\Gamma_\sigma^2 + 2\Gamma_\sigma\Gamma + 2\Gamma^2)(5\Gamma_\sigma^3 + 6\Gamma_\sigma^2\Gamma - 94\Gamma_\sigma\Gamma^2 - 80\Gamma^3)}{5\tilde{\Gamma}_2^2(\Gamma_\sigma^4 + 4\Gamma_\sigma^3\Gamma - 8\Gamma_\sigma\Gamma^3 + 20\Gamma^4)}\,. \tag{3.103d}$$

The $g^{(2)}(\tau)$ for the remaining filter, however, cannot be written like the rest, i.e., as a sum of exponentials. Most of the times when the roots of the same or different sets do coincide, the eigenvectors are linearly independent. This happens when we take some limiting cases, e.g., if $\Delta_1 \to 0$. In such cases, the coefficients l_p are convergent and stay finite after taking the limit. The double Lorentzian is a counter example since it exhibits divergences if $\Delta_2 \to \Delta_1$ (and $\Gamma_2 \to \Gamma_1$). This case shares the roots of Eq. (3.99). Some roots are double or triple but they do not correspond to different eigenvectors. In the Laplace space, if the roots have 2-fold degeneracy (like $\lambda_2 = \tilde{\Gamma}_1/2$, in this case), the complete solution is given by

$$\frac{b_0 + b_1 s}{(s+\lambda_2)^2}\,, \tag{3.104}$$

and, inverting the Laplace transform, we get

$$\big[b_1 + (b_0 - \lambda_2 b_1)\tau\big]e^{-\lambda_2\tau}\,. \tag{3.105}$$

If it is 3-fold degenerate (as $\lambda_3 = \Gamma$), the solution is

$$\frac{c_0 + c_1 s + c_2 s^2}{(s+\lambda_3)^3}\,, \tag{3.106}$$

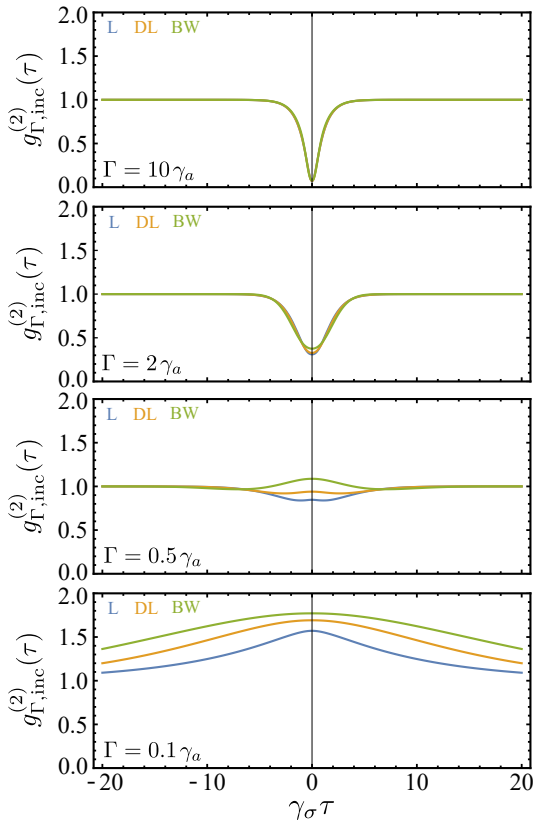

Figure 3.7: Time-dependent filtered emission (at resonance) of the incoherently-driven 2LS for three different (band-pass) filters, Lorentzian (L), double Lorentzian (DL) and Butterworth (BW); shown for several values of Γ.

or, in the time domain,

$$\big[c_2 + (c_1 - \lambda_3 c_2)\tau + (c_0 - \lambda_3 c_1 + \lambda_3^2 c_2)\tau^2/2)\big] e^{-\lambda_3 \tau}\,. \tag{3.107}$$

For a general n-degenerate root (without linearly independent solutions), the time-domain solution is an $(n-1)$-th polynomial of τ times the corresponding exponential. So the 2-photon Glauber correlator for the double Lorentzian has the following form

$$\begin{aligned} g^{(2)}_{\Gamma,\mathrm{DL}}(\tau) = 1 + a_0\, e^{-\Gamma_\sigma \tau} + \big[b_1 + (b_0 - \lambda_2 b_1)\tau\big] e^{-\tilde{\Gamma}_1/2\tau} + \\ \big[c_2 + (c_1 - \lambda_3 c_2)\tau + (c_0 - \lambda_3 c_1 + \lambda_3^2 c_2)\tau^2/2)\big] e^{-\Gamma\tau}\,, \end{aligned} \tag{3.108}$$

where

$$a_0 = -\frac{4\Gamma^6}{\Gamma_-^4 \tilde{\Gamma}_2^2}\,, \tag{3.109a}$$

$$b_0 = \frac{\Gamma^2}{486}\left(\frac{530}{\Gamma_-} - \frac{99\Gamma}{\Gamma_-^2} - \frac{288\Gamma^2}{\Gamma_-^3} + \frac{432\Gamma^4}{\Gamma_-^4} - \frac{22400}{\tilde{\Gamma}_2} - \frac{2640\Gamma}{\tilde{\Gamma}_2^2} + \frac{21870}{\tilde{\Gamma}_3} + \frac{18711\Gamma}{\tilde{\Gamma}_3^2} + \frac{17496\Gamma^2}{\tilde{\Gamma}_3^3} + \frac{34992\Gamma^3}{\tilde{\Gamma}_3^4}\right), \tag{3.109b}$$

$$b_1 = \frac{\Gamma}{486}\left(\frac{368}{\Gamma_-} + \frac{63\Gamma}{\Gamma_-^2} - \frac{288\Gamma^2}{\Gamma_-^3} + \frac{432\Gamma^3}{\Gamma_-^4} + \frac{52120}{\tilde{\Gamma}_2} - \frac{7728\Gamma}{\tilde{\Gamma}_2^2} - \frac{52488}{\tilde{\Gamma}_3} - \frac{45927\Gamma}{\tilde{\Gamma}_3^2} - \frac{40824\Gamma^2}{\tilde{\Gamma}_3^3} - \frac{34992\Gamma^3}{\tilde{\Gamma}_3^4}\right), \tag{3.109c}$$

$$c_0 = \frac{\Gamma^2}{486}\left(1215 - \frac{661\Gamma}{\Gamma_-} - \frac{81\Gamma^2}{\Gamma_-^2} + \frac{360\Gamma^3}{\Gamma_-^3} - \frac{216\Gamma^4}{\Gamma_-^4} + \frac{68944\Gamma}{\tilde{\Gamma}_2} - \frac{10572\Gamma^2}{\tilde{\Gamma}_2^2} - \frac{71199\Gamma}{\tilde{\Gamma}_3} - \frac{62451\Gamma^2}{\tilde{\Gamma}_3^2} - \frac{52488\Gamma^3}{\tilde{\Gamma}_3^3} - \frac{34992\Gamma^4}{\tilde{\Gamma}_3^4}\right), \tag{3.109d}$$

$$c_1 = 3\Gamma + \frac{\Gamma^2}{972}\left(-\frac{1942}{\Gamma_-} + \frac{72\Gamma}{\Gamma_-^2} + \frac{1008\Gamma^2}{\Gamma_-^3} - \frac{864\Gamma^3}{\Gamma_-^4} + \frac{235951}{\tilde{\Gamma}_2} - \frac{35070\Gamma}{\tilde{\Gamma}_2^2} - \frac{240570}{\tilde{\Gamma}_3} - \frac{210924\Gamma}{\tilde{\Gamma}_3^2} - \frac{186624\Gamma^2}{\tilde{\Gamma}_3^3} - \frac{139968\Gamma^3}{\tilde{\Gamma}_3^4}\right), \tag{3.109e}$$

$$c_2 = 1 + \frac{\Gamma}{972}\left(-\frac{800}{\Gamma_-} + \frac{18\Gamma}{\Gamma_-^2} + \frac{288\Gamma^2}{\Gamma_-^3} - \frac{432\Gamma^3}{\Gamma_-^4} + \frac{103589}{\tilde{\Gamma}_2} - \frac{15114\Gamma}{\tilde{\Gamma}_2^2} - \frac{104976}{\tilde{\Gamma}_3} - \frac{91854\Gamma}{\tilde{\Gamma}_3^2} - \frac{81648\Gamma^2}{\tilde{\Gamma}_3^3} - \frac{69984\Gamma^3}{\tilde{\Gamma}_3^4}\right). \tag{3.109f}$$

The first noticeable effect of the filter is the loss of antibunching. At $\tau = 0$, none of the filtered $g^{(2)}(0)$ is exactly zero any longer. Such a feature is shared by every filter and the reason is that any information gained in the frequency (energy) domain, namely $\Delta\omega$, does affect the information in time of the signal. In other words, we are losing certainty in time. In signal analysis, this is known as the bandwidth theorem. Given a Fourier transform mainly defined in a range of frequencies $\Delta\omega$, then, in time, the signal is spread over a range of length $\Delta t \propto 1/\Delta\omega$. The explanation is summarised in the equation $\Delta\omega\,\Delta t \geq 1$. In Quantum Mechanics, the generalisation of this theorem is the Heisenberg uncertainty principle. The theorem would read $\Delta E\,\Delta\tau \geq \hbar$, so that the more defined is the energy, the greater is

the time uncertainty. Due to the spectral response of the detector, each frequency is not captured with the same probability. The time resolution is limited by the bandwidth. Then, two photons emitted close together could be seen by the detector as if they arrived at the same time. Thus, the antibunching is spoilt by the limited time resolution. The time dynamics is also modified by the filtering process (see Fig. 3.7), which is evident when inspecting the time-dependent expressions as computed above: a single exponential turns into multi-exponential quantities. The noticeable kink, the discontinuity of the first derivative at $\tau = 0$, is smoothed down in presence of the filter, that introduces its own dynamics in the picture and also some mixed terms, which manifest the interplay between source and filter.

3.2.4 FREQUENCY-FILTERED COHERENT 2LS

We now tackle a similar problem changing the kind of excitation. Under coherent pumping (e.g., a laser) and after expanding the Hilbert space to include the sensors ς_i ($i = 1, 2$), the Hamiltonian in the Rotating Frame reads

$$H = \Delta_\sigma \sigma^\dagger \sigma + \Omega_\sigma(\sigma^\dagger + \sigma) + \sum_{j=1,2} \Delta_j \varsigma_j^\dagger \varsigma_j + \epsilon(\varsigma_1^\dagger \sigma + \varsigma_2^\dagger \varsigma_1 + \text{h.c.}), \quad (3.110)$$

where $\Delta_j = \omega_j - \omega_L$ is the detuning between the 2LS/sensors and the laser. From Chapter (2) we already know that the coherent excitation brings a much more complicated structure than the incoherently-pumped case. Even the simplest filter, the Lorentzian, makes this evident and reinforces the necessity of an accurate description through spectral measurements of the multiphoton correlations. The filtered spectrum is given the by sensor population (up to a constant). The whole expression is lengthy so we show a few cases of interest. If the system is driven at resonance ($\Delta_\sigma = 0$), the first sensor population reads

$$\begin{aligned}\langle \varsigma_1^\dagger \varsigma_1 \rangle_L = 16\Omega_\sigma^2 \Big\{ &\Gamma(\gamma_{11}^2 + 4\Delta_1^2)^2(\gamma_{12}^2 + 4\Delta_1^2)^2 + 8\Omega_\sigma^2 \big[\Gamma \gamma_{11}^2 \gamma_{12} \\ &\gamma_{32} + 4\Delta_1^2(2\Gamma^3 + 16\Gamma^2\gamma_\sigma + 23\Gamma\gamma_\sigma^2 + 8\gamma_\sigma^3) - 16\Delta_1^4 \gamma_{12}\big] + \\ &128\Omega_\sigma^4 \gamma_{11}(\Gamma^2 + 4\Delta_1^2)\Big\} \Big/ \Big\{ \Gamma(\Gamma^2 + 4\Delta_1^2)(\gamma_{11}^2 + 4\Delta_1^2) \\ &(\gamma_\sigma^2 + 8\Omega_\sigma^2)\big[\Gamma^4 + 6\Gamma^3\gamma_\sigma + 12\Gamma\gamma_\sigma(\gamma_\sigma^2 + 2\Delta_1^2 + 8\Omega_\sigma^2) + \\ &\Gamma^2(13\gamma_\sigma^2 + 8\Delta_1^2 + 32\Omega_\sigma^2) + 4\gamma_\sigma^4 + 16(\Delta_1^2 - 4\Omega_\sigma^2)^2 + \\ &4\gamma_\sigma^2(5\Delta_1^2 + 16\Omega_\sigma^2)\big]\Big\}, \end{aligned} \quad (3.111)$$

where $\gamma_{jk} = j\,\Gamma + k\,\gamma_\sigma$ and the bar notation denotes s negative sign, i.e., $\bar{k} \equiv -k$. The complementary filter has the following expression:

$$\begin{aligned}\langle \bar{\varsigma}_1^\dagger \bar{\varsigma}_1 \rangle_{\mathrm{CL}} = 16\Omega_\sigma^2 \Big\{ & \Delta_1^2(\gamma_{12}^2 + 4\Delta_1^2)(\gamma_{11}^2 + 4\Delta_1)^2 + 2\Omega_\sigma^2 \big[\Gamma^2\gamma_{11}^2\gamma_{12}^2 + \\ & 4\Delta_1^2(2\Gamma^2 + 8\Gamma^3\gamma_\sigma + 17\Gamma^2\gamma_\sigma^2 + 20\Gamma\gamma_\sigma^3 + 8\gamma_\sigma^4)\big] + \\ & 32\Omega_\sigma^4(\Gamma^2 + 4\Delta_1^2)(\gamma_{11}\gamma_{22} + 8\Delta_1^2)\Big\} \Big/ \\ & \Big\{ (\Gamma^2 + 4\Delta_1^2)(\gamma_{11}^2 + 4\Delta_1^2)(\gamma_\sigma^2 + 8\Omega_\sigma^2)\big[\Gamma^4 + 6\Gamma^3\gamma_\sigma + \\ & 12\Gamma\gamma_\sigma(\gamma_\sigma^2 + 2\Delta_\sigma^2 + 8\Omega_\sigma^2) + \Gamma^2(13\gamma_\sigma^2 + 32\Omega_\sigma^2 + 8\Delta_\sigma^2) \\ & + 4\gamma_\sigma^2 + 4(\Delta_1^2 - 4\Omega_\sigma^2)^2 + 4\gamma_\sigma^2(5\Delta_\sigma^2 + 16\Omega_\sigma^2)\big]\Big\}. \end{aligned} \tag{3.112}$$

The second-order filtered correlations are obtained, again, coupling the first sensor to a second one. The following expressions are even more cumbersome so we only show the filtered observables when the filters and both at resonance (so that $\Delta_1 = \Delta_2 = 0$ for the Double Lorentzian and $\Delta_1 = -\Delta_2 = \Gamma/2$ for the Butterworth filter), which are

$$\begin{aligned}\langle \varsigma_2^\dagger \varsigma_2 \rangle_{\mathrm{DL}} = 64\Omega_\sigma^2 \Big\{ & \gamma_{12}^2(\gamma_{11}^2 + 4\Delta_\sigma^2)^2 + 8\Omega_\sigma^2\gamma_{12}(2\Gamma^3 + 5\Gamma^2\gamma_\sigma + \\ & 5\Gamma\gamma_\sigma^2 + 4\Delta_\sigma^2\gamma_{32}) + 64\Omega_\sigma^4\Gamma\gamma_{21}\Big\} \Big/ \\ & \Big\{ \Gamma^4(\gamma_\sigma^2 + 4\Delta_\sigma^2 + 8\Omega_\sigma^2)\big[\gamma_{12}(\gamma_{11}^2 + 4\Delta_\sigma^2) + 16\gamma_{11}\Omega_\sigma^2\big]^2 \Big\}, \end{aligned} \tag{3.113}$$

$$\begin{aligned}\langle \varsigma_2^\dagger \varsigma_2 \rangle_{\mathrm{BW}} = 64\Omega_\sigma^2 \Big\{ & (\Gamma^2 + 2\Gamma\gamma_\sigma + 2\gamma_\sigma^2)\big[2\Gamma^2 + 2\Gamma(\gamma_\sigma - 2\Delta_\sigma) + \\ & \gamma_\sigma^2 + 4\Delta_\sigma^2\big]\big[2\Gamma^2 + 2\Gamma(\gamma_\sigma + 2\Delta_\sigma) + \gamma_\sigma^2 4\Delta_\sigma^2\big] + \\ & 8\Omega_\sigma^2\gamma_\sigma(10\Gamma^3 + 15\Gamma^2\gamma_\sigma + 8\Gamma\gamma_\sigma^2 + 2\gamma_\sigma^2) + \\ & 32\Omega_\sigma^2\Delta_\sigma^2(3\Gamma^2 + 4\Gamma\gamma_\sigma + 2\gamma_\sigma^2) + 64\Gamma\gamma_{21}\Omega_\sigma^4\Big\} \Big/ \\ & \Big\{ \Gamma^4(\gamma_\sigma^2 + 4\Delta_\sigma^2 + 8\Omega_\sigma^2)\big[4\Gamma^6 + 16\Gamma^5\gamma_\sigma + 32\Gamma^4\gamma_\sigma^2 + \\ & 2\gamma_\sigma^2(\gamma_\sigma^2 + 4\Delta_\sigma^2 + 8\Omega_\sigma^2)^2 + 2\Gamma\gamma_\sigma(\gamma_\sigma^2 + 4\Delta_\sigma^2 + 8\Omega_\sigma^2) \\ & (5\gamma_\sigma^2 + 4\Delta_\sigma^2 + 16\Omega_\sigma^2) + \Gamma^2(5\gamma_\sigma^2 + 4\Delta_\sigma^2 + 16\Omega_\sigma^2)^2 + \\ & 4\Gamma^3\gamma_\sigma(9\gamma_\sigma^2 + 4\Delta_\sigma^2 + 24\Omega_\sigma^2)\big]\Big\}. \end{aligned} \tag{3.114}$$

At resonance $\Delta_1 = 0$, we get the Lorentzian filter 2-photon correlations as

$$g^{(2)}_{\Gamma,\mathrm{L}}(0) = \Big\{(\gamma_\sigma^2 + 4\Delta_\sigma^2 + 8\Omega_\sigma^2)\big[\gamma_{12}(\gamma_{11}^2 + 4\Delta_\sigma^2) + 16\gamma_{11}\Omega_\sigma^2\big] \big[\gamma_{11}\gamma_{12}\gamma_{32}(\gamma_{21}^2 + 4\Delta_\sigma^2)(\gamma_{31}^2 + 4\Delta_\sigma^2)\big] + 8\Gamma\Omega_\sigma^2(51\Gamma^4 + 104\Gamma^3\gamma_\sigma + 83\Gamma^2\gamma_\sigma^2 + 30\Gamma\gamma_\sigma^3 + 4\gamma_\sigma^4 + 12\gamma_{11}\gamma_{34}\Delta_\sigma^2 + 4\Delta_\sigma^2\gamma_\sigma\Gamma) + 192\Gamma^2\gamma_{21}\Omega_\sigma^2\Big\} \Big/ \Big\{\big[\gamma_{12}(\gamma_{11}^2 + 4\Delta_\sigma^2) + 8\Gamma\Omega_\sigma^2\big]^2 \big[\gamma_{11}(\gamma_{21}^2 + 4\Delta_\sigma^2) + 8\gamma_{21}\Omega_\sigma^2\big]\big[\gamma_{32}(\gamma_{31}^2 + 4\Delta_\sigma^2) + 16\gamma_{31}\Omega_\sigma^2\big]\Big\}, \tag{3.115}$$

and the Lorentzian notch filter correlations are

$$g^{(2)}_{\Gamma,\mathrm{CL}}(0) = \Big\{(\gamma_\sigma^2 + 4\Delta_\sigma^2 + 8\Omega_\sigma^2)\big[\gamma_{12}(\gamma_{11}^2 + 4\Delta_\sigma^2) + 16\gamma_{12}\Omega_\sigma^2\big]\gamma_{11}\gamma_{12} \gamma_{32}(\gamma_{21}^2 + 4\Delta_\sigma^2)(\gamma_{31}^2 + 4\Delta_\sigma^2) + 8\Omega_\sigma^2\big[159\Gamma^5 + 500\Gamma^4\gamma_\sigma + 647\Gamma^3\gamma_\sigma^2 + 418\Gamma^2\gamma_\sigma^3 + 132\Gamma\gamma_\sigma^4 + 16\gamma_\sigma^5 + 4\Delta_\sigma^2(21\Gamma^3 + 42\Gamma^2\gamma_\sigma + 44\Gamma\gamma_\sigma^2 + 14\gamma_\sigma^3)\big] + 64\Omega_\sigma^4\Gamma\gamma_{21}\gamma_{15,8}\Big\} \Big/ \Big\{64\gamma_{12}^2\Omega_\sigma^4\big[\gamma_{11}(\gamma_{21}^2 + 4\Delta_\sigma^2) + 8\Omega_\sigma^2\gamma_{21}\big] \big[\gamma_{32}(\gamma_{31}^2 + 4\Delta_\sigma^2) + 16\Omega_\sigma^2\gamma_{31}\big]\Big\}. \tag{3.116}$$

The expressions of the 2-photon correlator for the DL and BW filters are analytical but impossible to handle without the help of a computer. Therefore, we only include the approximated expressions when the driving strength is weak enough and both the 2LS and the filter are at resonance ($\Delta_\sigma = \Delta_1 = 0$). After taking the limit $\Omega_\sigma \to 0$, they read

$$g^{(2)}_{\Gamma,\mathrm{DL}}(0) \approx \frac{\gamma_\sigma^2\gamma_{32}^2}{4\gamma_{11}^4}, \tag{3.117}$$

and

$$g^{(2)}_{\Gamma,\mathrm{BW}}(0) \approx \frac{\gamma_\sigma^2\gamma_{11}^2}{(\Gamma^2 + \gamma_{11}^2)^2}. \tag{3.118}$$

For completeness, we also compute the limit $\Omega_\sigma \to 0$ for Eqs. (3.115) and (3.116), yielding

$$g^{(2)}_{\Gamma,\mathrm{L}}(0) \approx \frac{\gamma_\sigma^2}{\gamma_{11}^2}, \tag{3.119}$$

and

$$g^{(2)}_{\Gamma,\mathrm{CL}}(0) \approx \frac{\gamma_\sigma^2\gamma_{11}^2}{\Omega_\sigma^4}. \tag{3.120}$$

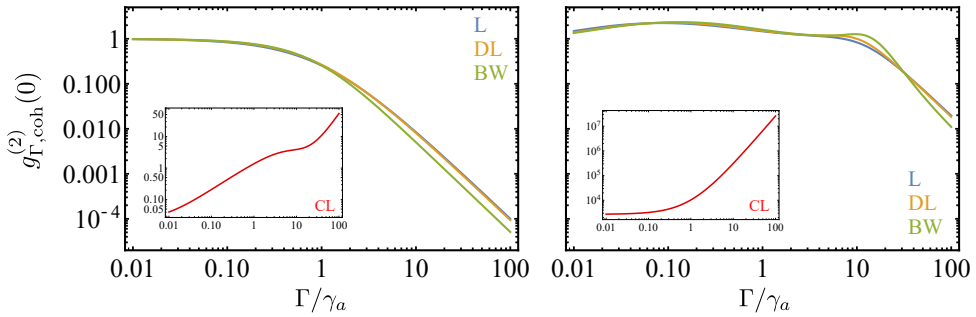

Figure 3.8: 2-photon correlations of the coherently-driven 2LS system in the Heitler (left) and Mollow (right) regimes. The four kinds of filters are shown: Lorentzian (blue), double Lorentzian (yellow), Butterworth (green) and complementary (notch) Lorentzian (in inset, red). The weak driving case recovers the perfect antibunching monotonously but faster for the Butterworth filter. On the contrary, the notch filter returns extreme bunching even for narrow filters, eliminating the Rayleigh peak. In the Mollow regime, given the richer structure of the spectrum, the autocorrelation function exhibits bunching for intermediate values of Γ (having a maximum around $\Gamma/\gamma_\sigma = 0.1$) and have a noticeable change of slope near $\Gamma/\gamma_\sigma = 10$. After the satellites are filtered in, $g^{(2)}_\Gamma(0)$ moves towards zero rapidly.

When $\Gamma \to 0$ so the (band-pass) filters are infinitely narrow, the photon correlations turns to 1 because they only accepts photons from the infinitely narrow laser. In the opposite limit $\Gamma \to \infty$ and the filters collect all the photons and the blind or unfiltered statistics are then recovered, giving $g^{(2)}_{\Gamma\to\infty}(0) \to 0$. If the filter is placed at any other frequency $\Delta_1 \neq 0$, $g^{(2)}_\Gamma(0) \to 2$, as $\Gamma \to 0$, instead of 1 because the laser light is filtered out. The complementary or notch filter has a different behaviour as we already mentioned, nonetheless, the situation is slightly different because of the delta peak of the spectrum. A narrow filter, centered at the laser frequency, will let pass all the photons except those that come from the laser. The resulting statistics correspond to the bare fluctuations (insets of Fig. 3.8), that is, the unfiltered light without the coherent scattered light (Rayleigh peak). These fluctuations are indeed bunched in the weak driving regime and turn antibunched in the Mollow regime. For broad notch filters, most of the signal becomes blocked and eventually it is rejected entirety and no photons are detected. Since the population goes to zero and vacuum dominates, the normalised Glauber correlator explodes to infinity, the same as for the incoherently-pumped case. The overall effect that we find is, again, the partial loss of antibunching as a consequence of the spectral resolution.

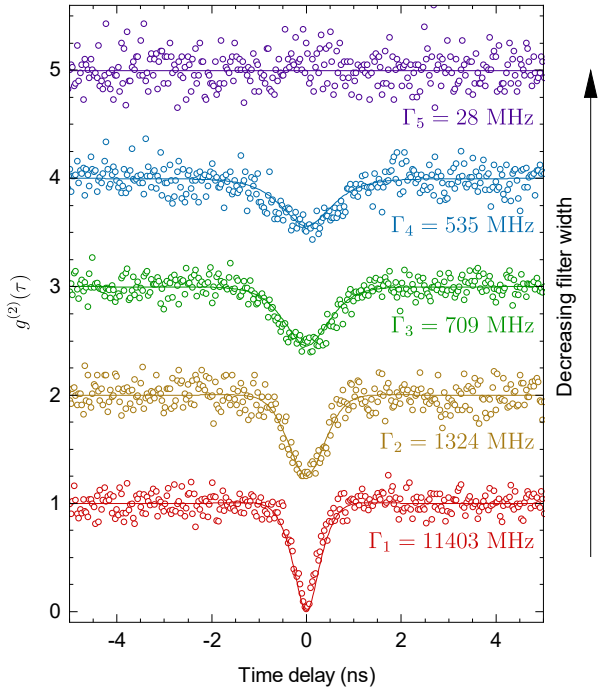

Figure 3.9: Actual measurements, from the group of Technische Universität München (Ref. [Z2]), of the filtered 2-photon autocorrelation function of a single-photon emitter in the weak driving regime for decreasing filter widths Γ_i. The circles correspond to the experimental data while the theoretical results are shown as solid lines. Adapted with permission from [Z2]. Copyright (2020) by the APS.

Except for the Lorentzian band-pass filter at resonance, the expressions for the non-zero delay Glauber correlator are extremely lengthy and clearly unpractical so we will not include them. These results provide the counterparts of exact, closed-form filtered $g^{(2)}_{\Gamma}$ of a 2LS but now for coherent driving. The particular case of a Lorentzian filter was used by two experimental groups to fit their data. One case [Z2] is shown in Fig. 3.9. The exact expression of the coefficients l_p for $g^{(2)}_{\Gamma,\mathrm{L}}(\tau)$ is found in the Appendix A.9. The weak-driving limit leads, for the Lorentzian filter, to the following exponents

$$\lambda_1 = \gamma_\sigma\,, \quad \lambda_2 = \gamma_\sigma/2\,, \quad \lambda_3 = \Gamma/2\,, \quad \lambda_4 = \gamma_{11}/2\,, \quad \lambda_5 = \Gamma\,, \tag{3.121}$$

with their corresponding coefficients

$$l_{1,\mathrm{L}} \approx \frac{\Gamma^4}{\gamma_{11}^2\gamma_{1\bar{1}}^2}\,, \quad l_{2,\mathrm{L}} \approx -\frac{2\Gamma^2}{\gamma_{11}\gamma_{1\bar{1}}}\,, \quad l_{3,\mathrm{L}} \approx \frac{2\Gamma\gamma_\sigma}{\gamma_{11}\gamma_{1\bar{1}}}\,, \tag{3.122}$$

$$l_{4,\mathrm{L}} \approx -\frac{2\Gamma^3\gamma_\sigma}{\gamma_{11}^2\gamma_{1\bar{1}}^2}\,, \quad l_{5,\mathrm{L}} \approx \frac{\Gamma^2\gamma_\sigma^2}{\gamma_{11}^2\gamma_{1\bar{1}}^2}\,. \tag{3.123}$$

In the same limit, the exponents and coefficient for $g^{(2)}_{\Gamma,\mathrm{CL}}(\tau)$ are

$$\lambda_1 \approx \gamma_\sigma\,, \quad \lambda_2 \approx \gamma_{11}/2\,, \quad \lambda_3 \approx \Gamma\,, \tag{3.124}$$

and

$$l_{1,\mathrm{CL}} = \frac{\gamma_\sigma^4\gamma_{11}^2}{64\gamma_{1\bar{1}}^2\Omega_\sigma^4}\,, \quad l_{2,\mathrm{CL}} = -\frac{\Gamma\gamma_\sigma^3\gamma_{11}^2}{32\gamma_{1\bar{1}}^2\Omega_\sigma^4}\,, \quad l_{3,\mathrm{CL}} = \frac{\Gamma^2\gamma_\sigma^2\gamma_{11}^2}{64\gamma_{1\bar{1}}^2\Omega_\sigma^4}\,. \tag{3.125}$$

The time dependency of the 2-photon correlation function, as the bare statistics, varies qualitatively from the Heitler to the Mollow but, overall, the loss of the perfect antibunching holds in any case. We already discussed that the origin of the antibunching depends on the strength of the driving. For weak driving, it is the interplay between the mean field and fluctuation what yields $g^{(2)}(0) = 0$. The filtering process affects these contributions and spoil the perfect cancellation of not only $g^{(2)}(0)$ but also of all the higher order correlations, that is, $g^{(n)}(0)$. The filtered statistics in the Heitler regime were indeed measured by two different groups, [73] and [Z2]. This verifies the loss of antibunching and the underlying mechanism that produce the single-photon emission in resonance fluorescence, predicted by the theory. The measurements of $g^{(2)}_{\Gamma,\Omega_\sigma}$ from Ref. [Z2], using an epitaxial quantum dot as the 2LS, together with the best fitting of the analytical expressions of the (Lorentzian) filtered $g^{(2)}_{\Gamma,\Omega_\sigma}(\tau)$ are shown in Figure 3.9. The theory of frequency-resolved correlators applied to this case is thus in agreement with the actual measurements.

4

PHOTON COUNTING

Until now, the statistical properties under study were coincidences of n-tuples of photons or the time intervals between consecutive or non-consecutive photons. However, it is not possible to quantify how many photon clicks are actually recorded from those measurements. In an experiment, the photons are sent to a photo-detector, that produces the transduction of the EM signal into electrical currents. At the microscopic level, the photons impinging on the apparatus excite the electrons (or other types of carriers) and produce a photo-current. In the process, such weak signal usually has to be amplified to be finally measured. We have briefly mentioned actual detection devices in 1.2.2 and discussed their influence on the photon statistics but, here, the relevant point is that a priori we can assign to each quanta of light a minimal current and thus count how many photons are arriving to the detector. If one photon generates the same photo-current independently of the rest, the probability to detect n photons in the time window $(t, t+T]$ is given by the Mandel formula [21, 36, 74]:

$$p(n,T;t) = \frac{1}{n!}\left\langle : \Omega^n \exp(-\Omega) : \right\rangle , \tag{4.1}$$

here :: denotes normal ordering and Ω is the time-integrated intensity operator defined as

$$\Omega = \xi\gamma \int_t^{t+T} \left(a^\dagger a\right)(t')\, dt' , \tag{4.2}$$

where ξ is a parameter that takes into account the detection efficiency (it is bounded between 0 and 1), γ is the emission rate of the system and a, $a^\dagger$ are the operators related to the light field (but not necessarily EM mode operators). If we plug this into Eq. 4.1, after unravelling the exponential and sorting out all the operators, we get

$$p(n,T;t) = \frac{(-1)^n}{n!}\sum_{k=0}^{\infty}\frac{(-\xi\gamma)^{n+k}}{k!}\times \int_t^{t+T}\dots\int_t^{t+T} G^{(n+k)}(t_1,\dots,t_{n+k})dt_1\dots dt_{n+k} , \tag{4.3}$$

or, in a succinct form,

$$p(n,T;t) = (-1)^n \sum_{k=0}^{\infty}\frac{(-1)^{n+k}\left\langle : \Omega^{n+k} : \right\rangle}{n!k!} . \tag{4.4}$$

This last equation can be easily inverted, so we can express the time-integrated intensity moments as

$$\langle : \Omega^k : \rangle = \sum_{n=k}^{\infty} \frac{n!}{(n-k)!}\, p(n, T; t)\,, \tag{4.5}$$

and from here, we can identify $\langle : \Omega^k : \rangle$ as the factorial moments of the distribution $p(n, T; t)$. With them, we are able to compute the central moments such as the mean and variance,

$$\mu = \sum_n n p(n) = \langle : \Omega^1 : \rangle\,, \tag{4.6a}$$

$$\Sigma^2 = \sum_n n^2 p(n) - \mu^2 = \langle : \Omega^2 : \rangle + \langle : \Omega^1 : \rangle - \langle : \Omega^1 : \rangle^2\,, \tag{4.6b}$$

respectively. An interesting quantity to analyse the deviations of the emission from an uncorrelated Poissonian stream is the variance normalised to the mean intensity, i.e., Σ^2/μ. Any Poisson distribution will return $\Sigma^2/\mu = 1$, no matter how dim or how strong the emission intensity is. Moreover, as we will see, it can be computed exactly for all the system presented below as it only requires to have knowledge of the population and 2-photon Glauber correlator. Of course, a deeper understanding would demand the study of all the moments and, in the end, the probability distribution itself, but in many situations such a goal is impossible to attain.

In order to compute these averages, we need to look into the m-time Glauber correlators which appear above. They have the following expression

$$\begin{aligned} G^{(m)}(t_1, ..., t_m) &= \theta(t_1 < t_2 < ... < t_m) \times \\ &\left\langle a^\dagger(t_1)...a^\dagger(t_m)a(t_m)...a(t_1) \right\rangle + (\text{other time orderings})\,. \end{aligned} \tag{4.7}$$

Note that each correlator consists of $m!$ terms since there are $m!$ possible orderings. However, all operators within the average are identical and, therefore, each term will return the same result after the integration. We are considering the time ordering $t_1 < t_2 < \cdots < t_m$, unless stated otherwise. Inserting this expression into Eq. (4.3) leads to

$$\begin{aligned} p(n, T; t) = \frac{(-1)^n}{n!} \sum_{k=0}^{\infty} \frac{(-\xi\gamma)^{n+k}(n+k)!}{k!} \\ \int_t^{t+T} ... \int_t^{t3} \int_t^{t2} \left\langle a^\dagger(t_1)...a^\dagger(t_{n+k})a(t_{n+k})...a(t_1) \right\rangle dt_1 dt_2 ... dt_{n+k}\,. \end{aligned} \tag{4.8}$$

Any multi-time correlation function, having the time ordering fixed, can be calculated through the Quantum Regression Theorem (see Eq. (2.33)). We then apply this idea to $G^{(m)}$. We choose, without loss of generality, time origin $t_0 = t = 0$ and define the vector

$$\vec{v}_m(t_1, ..., t_m) \equiv \langle a^\dagger(t_1) \dots a^\dagger(t_{m-1})\, \vec{c}(t_m)\, a(t_{m-1}) \dots a(t_1) \rangle\,, \quad (4.9)$$

and it is easy to check that, if $[\langle \vec{c}(t) \rangle]_{i_1} = \langle a^\dagger a(t) \rangle$, then $[\vec{v}_m(t_1, ..., t_m)]_{i_1} = G^{(m)}(t_1, ..., t_m)$ (where $[...]_i$ denotes the i-th component of the vector within the brackets). Using the Regression Theorem, we get the equation of motion for $\vec{v}_m(t_1, ..., t_m)$ as

$$\partial_{t_m} \vec{v}_m(t_1, ..., t_m) = \mathrm{M}\, \vec{v}_m(t_1, ..., t_m)\,. \quad (4.10)$$

The formal solution of this vector differential equation, considering the propagation of t_m from the previous time t_{m-1}, is

$$\begin{aligned} \vec{v}_m(t_1, ..., t_m) = \; & e^{\mathrm{M}(t_m - t_{m-1})}\, \vec{v}_m(t_1, ..., t_{m-1}, t_m = t_{m-1}) = \\ & e^{\mathrm{M}(t_m - t_{m-1})}\, \langle a^\dagger(t_1) ... a^\dagger(t_{m-2}) (a^\dagger \vec{c}\, a)(t_{m-1}) a(t_{m-2}) ... a(t_1) \rangle = \\ & e^{\mathrm{M}(t_m - t_{m-1})}\, \mathcal{C}\, \vec{v}_{m-1}(t_1, ..., t_{m-1})\,. \end{aligned} \quad (4.11)$$

In the last line, we have introduced the matrix $\mathcal{C}$ which maps $\langle \vec{c}(t) \rangle$ into $\langle (a^\dagger \vec{c}\, a)(t) \rangle$. Equivalently, the dynamics of $\vec{v}_{m-1}(t_1, ..., t_{m-1})$ are governed by the equation

$$\partial_{t_{m-1}} \vec{v}_{m-1}(t_1, ..., t_{m-1}) = \mathrm{M}\, \vec{v}_{m-1}(t_1, ..., t_{m-1})\,, \quad (4.12)$$

whose solution is formally identical to (4.11)

$$\vec{v}_{m-1}(t_1, ..., t_{m-1}) = e^{\mathrm{M}(t_{m-1} - t_{m-2})}\, \mathcal{C}\, \vec{v}_{m-2}(t_1, ..., t_{m-2})\,. \quad (4.13)$$

Inserting this in Eq. (4.11) leads to

$$\vec{v}_m(t_1, ..., t_m) = e^{\mathrm{M}(t_m - t_{m-1})}\, \mathcal{C}\, e^{\mathrm{M}(t_{m-1} - t_{m-2})}\, \mathcal{C}\, \vec{v}_{m-2}(t_1, ..., t_{m-2})\,. \quad (4.14)$$

Repeating this procedure down to $\vec{v}_1(t_1) = \langle \vec{c}(t_1) \rangle = e^{\mathrm{M}t_1} \langle \vec{c}\,(0) \rangle$ (solving Eq. (2.32)), we find the nested equation

$$\begin{aligned} \vec{v}_m(t_1, ..., t_m) &= e^{\mathrm{M}(t_m - t_{m-1})}\, \mathcal{C}\, e^{\mathrm{M}(t_{m-1} - t_{m-2})}\, \mathcal{C} \dots \mathcal{C}\, e^{\mathrm{M}(t_2 - t_1)}\, \mathcal{C} \langle \vec{c}(t_1) \rangle \\ &= \left(\prod_{k=0}^{m-2} e^{\mathrm{M}(t_{m-k} - t_{m-k-1})}\, \mathcal{C} \right) \langle \vec{c}\,(t_1) \rangle \\ &= \left(\prod_{k=0}^{m-2} e^{\mathrm{M}(t_{m-k} - t_{m-k-1})}\, \mathcal{C} \right) e^{\mathrm{M}t_1} \langle \vec{c}\,(0) \rangle\,. \end{aligned} \quad (4.15)$$

Thus, the m-photon Glauber correlator, given a particular time ordering, has the following expression

This expression of general validity (for a Markovian system) provides a tractable starting point to compute the multi-time m-photon correlators.

$$G^{(m)}(t_1,...,t_m) = \left[\left(\prod_{k=0}^{m-2} e^{\mathrm{M}(t_{m-k}-t_{m-k-1})}\,\mathcal{C}\right) e^{\mathrm{M}t_1}\langle\vec{c}\,(0)\rangle\right]_{i_1}. \tag{4.16}$$

For small times, that is, $t_k \to 0$, we can approximate $G^{(m)}$ taking $t_k - t_{k-1} \to 0$. The exponentials are, in this limit, $e^{\mathrm{M}(t_k-t_{k-1})} \approx 1 + \mathrm{M}(t_k - t_{k-1})$. Substituting this in Eq. (4.16) and keeping only the zeroth and linear terms,

$$G^{(m)}(t_1,...,t_m) \overset{t_k\to 0}{\approx} \left[\mathcal{C}^{m-1}\langle\vec{c}\,(0)\rangle\right]_{i_1} + \sum_{k=1}^{m-1}(t_k - t_{k-1})\left[\mathcal{C}^{m-1-k}\,\mathrm{M}\,\mathcal{C}^{k}\langle\vec{c}\,(0)\rangle\right]_{i_1}, \tag{4.17}$$

where $t_0 = t = 0$. Then, we are able to compute the time-integrated correlator for small time T (this necessarily implies that intermediate time steps t_k must be small as well):

$$\begin{aligned}\langle:\Omega_m:\rangle \approx m!\,(\xi\gamma)^m \int_0^T\int_0^{t_m}\!\!...\int_0^{t_2}\Big[&\mathcal{C}^{m-1}\langle\vec{c}\,(0)\rangle + \sum_{k=1}^{m-1}(t_k - t_{k-1})\,\mathcal{C}^{m-1-k}\,\mathrm{M}\,\mathcal{C}^{k}\langle\vec{c}\,(0)\rangle\Big]_{i_1} dt_1...dt_m = \\ &m!\,(\xi\gamma)^m\left[\mathcal{C}^{m-1}\langle\vec{c}\,(0)\rangle\right]_{i_1}\left(\int_0^T\int_0^{t_m}\!\!...\int_0^{t_2} dt_1...dt_m\right) + \\ &m!\,(\xi\gamma)^m\sum_{k=1}^{m-1}\left[\mathcal{C}^{m-1-k}\,\mathrm{M}\,\mathcal{C}^{k}\langle\vec{c}\,(0)\rangle\right]_{i_1}\times \\ &\left(\int_0^T\int_0^{t_m}\!\!...\int_0^{t_2}(t_k - t_{k-1})\,dt_1...dt_m\right).\end{aligned} \tag{4.18}$$

The integral accompanying the zeroth term returns $\frac{T^m}{m!}$ while the one that goes with the linear terms, for any $m > k > 0$, gives $\frac{T^{m+1}}{(m+1)!}$. Meanwhile, it is easy to see that $\left[\mathcal{C}^{m-1}\langle\vec{c}\,(0)\rangle\right]_{i_1} = \langle a^{\dagger m}a^m\rangle(0) = G^{(m)}(0)$. So, keeping only the first term, we find that for small integration time T

$$\langle:\Omega_m:\rangle \overset{T\to 0}{\approx} (\xi\gamma\,T)^m\,\langle a^{\dagger m}a^m\rangle(0) + O(T^{m+1}). \tag{4.19}$$

From this result, we can calculate the photon-counting probabilities from short integration times. Using Eq. (4.19) in Eq. (4.4)

$$p(n, T\to 0) \approx \frac{(-1)^n}{n!}\sum_{k=0}^{\infty}\frac{(-\xi\gamma T)^{n+k}}{k!}G^{(n+k)}(0), \tag{4.20}$$

or, inversely,

$$(\xi\gamma T)^k G^{(k)}(0) \approx \sum_{n=0}^{\infty} \frac{(n+k)!}{n!} p(k+n, T\to 0)\,. \tag{4.21}$$

These formulae resemble Equation (1.10) which relate the diagonal elements of the density matrix P_n and the Glauber correlators $G^{(m)}$. Having this in mind, it is possible to infer the m-photon correlators from photon-counting experiments.

In the following Sections, we will derive some results for system with Continuous Wave (CW) excitation and we will study in detail the particular case without any kind of excitation, also known as Spontaneous Emission (SE), emphasising the role of the spectral response of the detector.

4.1 INCOHERENTLY PUMPED 2LS

Now, we consider a 2LS under incoherent driving. The dynamics of the system are governed by the master equation (2.22) with decay and pumping rates γ_σ and P_σ and the rest of the parameters taken to zero. We can easily derive the equation of motion for the correlators from Eq. (2.24). It is interesting to reproduce them again prior to finding the multi-time m-photon Glauber correlators. The correlator equations are

$$\partial_t\langle\sigma\rangle = -(\Gamma_\sigma/2 + i\omega_\sigma)\langle\sigma\rangle\,, \tag{4.22a}$$
$$\partial_t\langle\sigma^\dagger\rangle = -(\Gamma_\sigma/2 - i\omega_\sigma)\langle\sigma^\dagger\rangle\,, \tag{4.22b}$$
$$\partial_t\langle\sigma^\dagger\sigma\rangle = -\Gamma_\sigma\langle\sigma^\dagger\sigma\rangle + P_\sigma\,. \tag{4.22c}$$

These equations are uncoupled, thus, they can be solved independently. We are particularly interested in the last one, which bears all the information of the m-photon correlators.

Defining the vector $\vec{c} = (1\ \langle\sigma^\dagger\sigma\rangle)^{\mathrm{T}}$, the matrices

$$\mathrm{M} = \begin{pmatrix} 0 & 0 \\ P_\sigma & -\Gamma_\sigma \end{pmatrix} \quad \text{and} \quad \mathcal{C} = \begin{pmatrix} 0 & 1 \\ 0 & 0 \end{pmatrix}, \tag{4.23}$$

and using the Quantum Regression Theorem (4.16) for Incoherent 2LS (in the steady-state), we find that any Glauber correlator, for a particular time ordering, can be written as:

$$G^{(m)}(t_1,\ldots,t_m) = n_\sigma^m \prod_{p=0}^{m-1}\left(1 - e^{-\Gamma_\sigma(t_{p+1}-t_p)}\right), \tag{4.24}$$

This result connecting the m-th order correlation of a two-level system to second-order ones only—that we will find remains valid for coherent driving—reveals a strong feature of the 2LS, rooting its multiphoton emission to the dynamics of two photons exclusively.

where $n_\sigma = P_\sigma/\Gamma_\sigma$ is the steady-state population of the system. The normalised correlators are

$$g^{(m)} = \frac{G^{(m)}(t_1,...,t_m)}{\prod_{p=1}^{m} G^{(1)}(t_p)} = \prod_{p=1}^{m-1}\left(1 - e^{-\Gamma_\sigma(t_{p+1}-t_p)}\right) = \prod_{p=1}^{m-1} g^{(2)}(t_{p+1}-t_p). \tag{4.25}$$

This factorisation property of the m-photon correlators is unique and the main characteristic of single-photon emitters. Not only that, each factor is a copy of $g^{(2)}$. Thus, the correlations only involve pairs of photons separated by the time interval τ. The explanation is simple. The system can be excited once each time so that, after emitting one photon, the system is deterministically in the ground state. Some reloading time is needed until it is re-excited and can emit again. If the two-level system is excited coherently instead, the mechanism is slightly different due to the coherent evolution but the factorization property still holds.

To obtain the probabilities $p(n, T; t)$, we need to solve nested integrals for any order m. Fortunately, these integrals have closed-form solutions:

$$\begin{aligned}
\mathcal{J}_{m<2} &= (n_\sigma T)^m\,, \\
\mathcal{J}_{m\geq 2} &= \frac{n_\sigma^m}{\Gamma_\sigma^m}\int_t^{t+T}\!\!\!\dots\int_t^{t3}\int_t^{t2} n_\sigma^m \prod_{p=1}^{m-1}\left(1 - e^{-\Gamma_\sigma(t_{p+1}-t_p)}\right) dt_1 dt_2 ... dt_m \\
&= \frac{n_\sigma^m}{\Gamma_\sigma^m}\left(L_m^{-(2m-1)}(-\Gamma_\sigma T) - e^{-\Gamma_\sigma T} L_{m-2}^{-(2m-1)}(\Gamma_\sigma T)\right)\,,
\end{aligned} \tag{4.26}$$

where $L_m^{(k)}(x)$ are the generalized Laguerre polynomials (m are positive integers and k can be any real number). The mean and variance are easily computed from these integrals and, in the limit $T \to \infty$, they yield the following normalised variance

$$\left(\Sigma^2/\mu\right)(T\to\infty) \to 1 - 2\xi n_\sigma(1-n_\sigma)\,, \tag{4.27}$$

which clearly deviates from 1 for any possible population (excluding the limits $n_\sigma = 0$ and $n_\sigma = 1$).

The probability of collecting n photons from the incoherent 2LS in a time window of length T is therefore:

$$p(n,T) = \frac{(-1)^n}{n!}\sum_{k=0}^{\infty}\frac{(-\xi\gamma_\sigma)^{n+k}(n+k)!}{k!}\mathcal{J}_{n+k}(\Gamma_\sigma T)\,, \tag{4.28}$$

or, after making a change of notation,

$$p(n,T) = \frac{(-1)^n}{n!}\sum_{k=0}^{\infty}\frac{(-y)^{n+k}(n+k)!}{k!}\mathcal{J}'_{n+k}(x)\,, \tag{4.29}$$

where $x \equiv \Gamma_\sigma T$, $y \equiv \gamma_\sigma \xi\, n_\sigma/\Gamma_\sigma$ and $\mathcal{J}'_m(x) = (n_\sigma/\Gamma_\sigma)^{-m}\,\mathcal{J}_m(x)$. Although the integrals in Eq. (4.26) have analytical solution and so do the photon-counting probabilities, it turns out that, in this current form, they are numerically unstable. For long integration time T, the summation does not converge. This makes difficult to computationally generate the probability distribution.

A way to surpass this issue or at least improve the rate of convergence is to transform the expressions in Eq. (4.26) into something more tractable. Inspecting the series expansion of $\mathcal{J}_m$, we notice that they have an easy expression. For $m > 1$,

$$\mathcal{J}'_m(x) = -\sum_{n\geq 2m-1}\binom{n-m-1}{m-2}\frac{(-x)^n}{n!}\,, \tag{4.30}$$

which can be identified with a more familiar function,

$$\mathcal{J}'_m(x) = \frac{x^{2m-1}}{(2m-1)!}\,{}_1F_1(m-1;2m;-x)\,, \tag{4.31}$$

the confluent hypergeometric function of the first kind ${}_1F_1(a;b;x)$, also known as Kummer's function of first kind. It is noticeable that this formulation is also valid for limiting cases $m = 0, 1$. However, for $m = 0$, it is preferable to substitute it by 1 straightforwardly.

Now we present the limiting cases when the integration time is either small or very large, this is, $x \ll 1$ or $x \gg 1$.

If the argument x is small, then Eq. (4.31) has the following expression

$$\mathcal{J}'_m(x) \approx \frac{x^{2m-1}}{(2m-1)!} - (k-1)\frac{x^{2m}}{(2m)!}\,, \tag{4.32}$$

which, after substituting in Eq. (4.29), yields

$$\begin{aligned} p(n,T\to 0) \approx & \frac{\sqrt{\pi}y^n x^{2n-1}}{4^{n+1}n!}\Big[\frac{8n-4(n-1)x}{\Gamma(n+1/2)}\,{}_0F_1\big(n+1/2,-\frac{x^2y}{4}\big)+ \\ & \frac{(x-2)x^2y}{\Gamma(n+3/2)}\,{}_0F_1\big(n+3/2,-\frac{x^2y}{4}\big)\Big] \\ \approx & \frac{x^{2n-1}y^n}{(2n)!}[2n-(n-1)x]\,, \end{aligned} \tag{4.33}$$

where ${}_0F_1(a;x)$ is a particular case of the generalised hypergeometric function. Remembering that $x = \Gamma_\sigma T$ and $y = \xi\gamma_\sigma n_\sigma/\Gamma_\sigma$, then

$$p(n, T \to 0) \approx \frac{1}{(2n-1)!}(\xi\gamma_\sigma n_\sigma T)^n(\Gamma_\sigma T)^{n-1}\left(1 - \frac{n-1}{2n}\Gamma_\sigma T\right). \quad (4.34)$$

On the other hand, when the integration time is large enough, Eq. (4.31) can be approximated as

$$\mathcal{J}'_m(x) \approx \frac{x^m}{m!}\left(1 - \frac{m(m-1)}{x}\right), \quad (4.35)$$

and, plugging this in Eq. (4.29), we get

$$p(n, T \to \infty) \approx \frac{1}{n!}(xy)^n e^{-xy}\left(1 - \frac{n(n-1)}{x} + 2ny - xy^2\right) \quad (4.36)$$

and, finally, it has the following expression

$$p(n, T \to \infty) \approx \frac{1}{n!}(\xi\gamma_\sigma n_\sigma T)^n e^{-\xi\gamma_\sigma n_\sigma T}\left(1 - \frac{n(n-1)}{\Gamma_\sigma T} + 2n\frac{\xi\gamma_\sigma n_\sigma}{\Gamma_\sigma} - \frac{\xi^2\gamma_\sigma^2 n_\sigma^2 T}{\Gamma_\sigma}\right). \quad (4.37)$$

If we define a Poisson distribution $p_0(n, T) = 1/n!\lambda^n e^{-\lambda}$ with parameter $\lambda = \bar{I}T$, where $\bar{I} = \xi\gamma_\sigma n_\sigma$ is the detected mean intensity, we can rewrite Eq. (4.37) as a sum of these probabilities

$$p(n, T \to \infty) \approx \left(1 + 2n\frac{\bar{I}}{\Gamma_\sigma}\right)p_0(n, T) - (n-1)\frac{\bar{I}}{\Gamma_\sigma}p_0(n-1, T) - (n+1)\frac{\bar{I}}{\Gamma_\sigma}p_0(n+1, T). \quad (4.38)$$

The distribution above, when plotted around its maximum, resembles a regular Poisson distribution whose parameter is $\lambda' = \beta\lambda = \beta\bar{I}T$ (with $1 > \beta > 0$) and that has been displaced such that $n \to n - m$ (with $m > 0$). The mean and variance of this displaced Poisson distribution are now $m + \beta\bar{I}T$ and $\beta\bar{I}T$, respectively. Since these moments have to coincide with the *exact* ones after taking the limit $T \to \infty$, the values for these parameters are

$$m = 2\frac{\bar{I}}{\Gamma_\sigma}\bar{I}T \quad \text{and} \quad \beta = 1 - 2\frac{\bar{I}}{\Gamma_\sigma}. \quad (4.39)$$

There is a caveat, it is important to remark that the approximation only holds for $n > m$ given that $p_0(n, T)$ is exclusively defined for positive integers (including $n = 0$). Nonetheless, the major contributions to

n	$p(n, T \to 0)$	$p(n, T \to \infty)$
0	$1 - \bar{I}T$	$e^{-\bar{I}T}(1 - \bar{I}^2 T/\Gamma_\sigma)$
1	$\bar{I}T - \frac{1}{3}(\bar{I}T)^2\Gamma_\sigma T$	$\bar{I}T\, e^{-\bar{I}T}(1 - 2\bar{I}/\Gamma_\sigma + \bar{I}^2 T/\Gamma_\sigma)$
2	$\frac{1}{3!}(\bar{I}T)^2\Gamma_\sigma T(1 - \Gamma_\sigma T/4)$	$\frac{1}{2!}(\bar{I}T)^2 e^{-\bar{I}T}(1 - 2/(\Gamma_\sigma T) + 4\bar{I}/\Gamma_\sigma + \bar{I}^2 T/\Gamma_\sigma)$
3	$\frac{1}{5!}(\bar{I}T)^3(\Gamma_\sigma T)^2(1 - \Gamma_\sigma T/3)$	$\frac{1}{3!}(\bar{I}T)^3 e^{-\bar{I}T}(1 - 6/(\Gamma_\sigma T) + 6\bar{I}/\Gamma_\sigma + \bar{I}^2 T/\Gamma_\sigma)$

Table 4.1: Incoherently pumped 2LS's photon-counting distribution $p(n, T)$ for two limiting cases $T \to 0$ and $T \to \infty$, respectively. The mean intensity is $\bar{I} = \xi\gamma_\sigma n_\sigma$.

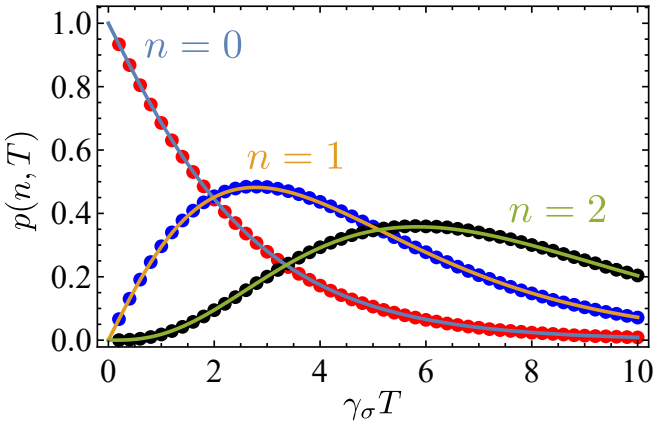

Figure 4.1: Probability of detecting $n = 0$ (blue), $n = 1$ (yellow) and $n = 2$ (green) in the time window $(0, T)$ for the incoherently driven 2LS, with $\xi = 1$ and $P_\sigma = 0.1\gamma_\sigma$. The circles are obtained from Monte Carlo simulations.

this distribution are far away from this lower bound and hence they are not affected.

As yet, only the limiting cases have been considered. In order to find a suitable and more accessible solution, we can make use of the Laplace transform. We will change the variable x (time) to the Laplace space variable s. The integrals in Eq. (4.31) have a particularly simple expression for their Laplace transform.

$$\mathcal{L}\left\{\mathcal{J}'_m\right\}(s) = \frac{1}{s^{m+1}(s+1)^{m-1}} - \delta_{m,0}\,, \tag{4.40}$$

where $\delta_{m,0}$ is the Kronecker delta. Using this result, we find the following expression for the Laplace transform of the photon-counting probabilities:

$$\tilde{p}(n, s) = \mathcal{L}\left\{p(n, T)\right\}(s) = y^n \frac{(s+1)^2}{(s^2 + s + y)^{n+1}} - \delta_{n,0}\,. \tag{4.41}$$

Despite this simple expression for $\tilde{p}(n, s)$, the inversion of Laplace transform is still very complicated. There are several ways to do that,

which are, of course, equivalent. The simplest is to decompose the denominator of Eq. (4.41) as a sum of fractions of k-th order. The poles are $s_\pm = -\frac{1}{2} \pm \frac{\alpha}{2}$, where $\alpha = \sqrt{1-4y}$. The roots are always real since $y < 1/4$ and are located in the negative-real half-plane of the s-space (i.e., $\mathrm{Re}(s) < 0$). After the decomposition, it yields

$$\frac{1}{(s^2+s+y)^{n+1}} = \sum_{k=0}^{n} (-1)^k \binom{n+k}{k} \left[\frac{1}{\alpha^{n+k+1}} \frac{1}{(s-s_+)^{n+1-k}} + \frac{1}{(-\alpha)^{n+k+1}} \frac{1}{(s-s_-)^{n+1-k}} \right]. \quad (4.42)$$

Now, the inversion of Eq. (4.42) is easy to do now since $\mathcal{L}^{-1}\{(s-a)^{-(n+1)}\}(x) = x^n e^{-ax}/n!$. Thus, the inversion gives

$$\tilde{f}_n(s) = \frac{e^{s_+ x}}{\alpha^{2n+1}} \sum_{k=1}^{n} (-1)^k \binom{n+k}{k} \frac{(\alpha x)^{n-k}}{(n-k)!} - \frac{e^{s_- x}}{\alpha^{2n+1}} \sum_{k=1}^{n+1} (-1)^k \binom{n+k}{k} \frac{(-\alpha x)^{n-k}}{(n-k)!}. \quad (4.43)$$

These sums can be further simplified and written in terms of modified Bessel functions of the second kind $K_\nu(x)$ (where $\nu > 0$)

$$f_n(x) = \frac{e^{-x/2} x^n \sqrt{-\alpha x}\, K_{n+1/2}(-\alpha x/2)}{\alpha^{n+1}\sqrt{\pi}\, n!} - \frac{e^{-x/2}(-x)^n \sqrt{\alpha x}\, K_{n+1/2}(\alpha x/2)}{\alpha^{n+1}\sqrt{\pi}\, n!} \quad (4.44)$$

Now, we focus on the numerator $(s+1)^2$. Reminding the property of the derivatives, $\mathcal{L}\{\partial_x f(x)\} = s\tilde{f}(s) - f(0)$ and $\mathcal{L}\{\partial_x^2 f(x)\} = s^2\tilde{f}(s) - sf(0) - f'(0)$, where $\tilde{f}(s) = \mathcal{L}\{f\}$. Then,

$$(s+1)^2 \tilde{f}_n(s) = \mathcal{L}\{\partial_x^2 f_n(x) + 2\partial_x f_n(x) + f_n(x)\} + (s+2) f_n(0) + \partial_x f_n(0). \quad (4.45)$$

Since all the functions $f_n(x)$ and their first derivative vanish at $x = 0$, with the exception of $n = 0$, so that $f_n(0) = 0$ and $\partial_x f_n(0) = \delta_{n,0}$, we can simply invert the Laplace transform of $\tilde{p}(n,s)$

$$\tilde{p}(n,s) = y^n \mathcal{L}\{\partial_x^2 f_n(x) + 2\partial_x f_n(x) + f_n(x)\}, \quad (4.46)$$

so, after computing the derivatives of $f_n(x)$, we finally get

$$p(n,T) = \frac{e^{-x/2}\sqrt{\pi}(xy)^n}{4\alpha^{n-1}(\alpha x)^{3/2}\, n!} \{[16n^2 + 8n(x+1) + x(\alpha^2 x + x + 4)] \times I_{n+1/2}(\alpha x/2) + 2\alpha x(x+2n) I_{n+3/2}(\alpha x/2)\}. \quad (4.47)$$

This provides the photon counting probability of detecting n photons in any time window T of an incoherently driven 2LS, for all drivings. This shows that strong correlations are maintained even at large times where one could expect them to wash out.

We show below some particular cases

$$p(0,T) = (2\alpha)^{-1}\left[(1-2y+\alpha)e^{-(1-\alpha)x/2} - (1-2y-\alpha)e^{-(1+\alpha)x/2}\right], \tag{4.48a}$$

$$p(1,T) = y(2\alpha^3)^{-1}\left\{\left[(1-4y-2\alpha y+\alpha)x-4y\right]e^{-(1-\alpha)x/2} - \left[(1-4y+2\alpha y-\alpha)x-4y\right]e^{-(1+\alpha)x/2}\right\}, \tag{4.48b}$$

$$p(2,T) = y^2(4\alpha^5)^{-1}\left\{\left[\alpha^2(1+\alpha-2y)x^2-2(\alpha^2+2\alpha y+\alpha)x+4+8y\right]e^{-(1-\alpha)x/2} - \left[\alpha^2(1-\alpha-2y)x^2 - 2(\alpha^2-2\alpha y-\alpha)x+4+8y\right]e^{-(1+\alpha)x/2}\right\}, \tag{4.48c}$$

that are shown in Fig. 4.1 together with the Monte Carlo simulations for the photo-counting experiment.

Another associated function which is interesting to calculate is the probability-generating function $\mathcal{G}(z)$. Independently of the coordinate space, either x or s, its definition is

$$\mathcal{G}(z,x) = \sum_{n=0}^{\infty} p(n,x)z^n\,, \tag{4.49}$$

or

$$\tilde{\mathcal{G}}(z,s) = \sum_{n=0}^{\infty} \tilde{p}(n,s)z^n\,, \tag{4.50}$$

and the convergence of this function is guaranteed only if $|z|<1$. The relation with the photon-counting probabilities is straightforward

$$p(n,x) = \frac{1}{n!}\partial_z^n \mathcal{G}(0,x)\,, \tag{4.51}$$

and formally identical for $\tilde{\mathcal{G}}(z,s)$. Inserting Eq. (4.41) into Eq. (4.50) leads to

$$\tilde{\mathcal{G}}(z,s) = \frac{s+1-y(1-z)}{s^2+s+y(1-z)}\,, \tag{4.52}$$

and, after inverting the Laplace transform, yields

$$\mathcal{G}(z,x) = \frac{1}{A_+-A_-}\left(A_+^2 e^{-A_- x} - A_-^2 e^{-A_+ x}\right), \tag{4.53}$$

where $A_\pm = (1\pm\alpha(z))/2$ and $\alpha(z) = \sqrt{1-4y(1-z)}$. Noticing that $\mathcal{G}(z,x)$ is solution of the second-order linear differential equation

$$\partial_x^2\mathcal{G}(z,x) + \partial_x\mathcal{G}(z,x) + y(1-z)\mathcal{G}(z,x) = 0\,, \tag{4.54}$$

with initial conditions $\mathcal{G}(z,0) = 1$ and $\partial_x \mathcal{G}(z,0) = -y(1-z)$, we can identify, inspecting each term of the series of $\mathcal{G}$, the equation of motion of the photon-counting probabilities. For all $n \geq 0$, $p(n,x)$ satisfies

$$\partial_x^2 p(n,x) + \partial_x p(n,x) + y\, p(n,x) - y\, p(n-1,x) = 0\,, \tag{4.55}$$

with initial conditions $p(n,0) = \delta_{n,0}$ and $\partial_x p(n,0) = y(\delta_{n,1} - \delta_{n,0})$. Remembering that $x = \Gamma_\sigma T$ and $y = \xi\gamma_\sigma n_\sigma/\Gamma_\sigma = \bar{I}/\Gamma_\sigma$, (4.55) is also written as

$$\partial_T^2 p(n,T) + \Gamma_\sigma\, \partial_T p(n,T) + \Gamma_\sigma \bar{I}\, p(n,T) - \Gamma_\sigma \bar{I}\, p(n-1,T) = 0\,, \tag{4.56}$$

and, at $T = 0$, $p(n,0) = \delta_{n,0}$ and $\partial_T p(n,0) = \bar{I}(\delta_{n,1} - \delta_{n,0})$. Solving these equations of motion numerically, we have an alternative way to generate the photon-counting distribution up to a fixed number of photons.

4.2 COHERENTLY PUMPED 2LS

We keep the same 2LS but change the incoherent pumping by coherent source, namely a laser of frequency ω_L and amplitude Ω_σ. In the Rotating Frame, the Master Equation (2.22) reduces to

$$\partial_t \rho = -i[\Delta_\sigma \sigma^\dagger\sigma + \Omega_\sigma(\sigma^\dagger + \sigma), \rho] + \frac{\gamma_\sigma}{2}\mathcal{L}_\sigma \rho\,, \tag{4.57}$$

Again, we show the equations of motion, which read

$$\partial_t \langle\sigma\rangle = -\left(\gamma_\sigma/2 + i\,\Delta_\sigma\right)\langle\sigma\rangle + 2i\,\Omega_\sigma\langle\sigma^\dagger\sigma\rangle - i\,\Omega_\sigma\,, \tag{4.58a}$$

$$\partial_t \langle\sigma^\dagger\rangle = -\left(\gamma_\sigma/2 - i\,\Delta_\sigma\right)\langle\sigma^\dagger\rangle - 2i\,\Omega_\sigma\langle\sigma^\dagger\sigma\rangle + i\,\Omega_\sigma\,, \tag{4.58b}$$

$$\partial_t \langle\sigma^\dagger\sigma\rangle = -\gamma_\sigma\langle\sigma^\dagger\sigma\rangle + i\,\Omega_\sigma\langle\sigma\rangle - i\,\Omega_\sigma\langle\sigma^\dagger\rangle\,. \tag{4.58c}$$

From these equations, we can identify the vector $\langle\vec{c}\rangle = (1\ \langle\sigma\rangle\ \langle\sigma^\dagger\rangle\ \langle\sigma^\dagger\sigma\rangle)^{\mathrm{T}}$ and the matrices

$$\mathrm{M} = \begin{pmatrix} 0 & 0 & 0 & 0 \\ -i\,\Omega_\sigma & -\gamma_\sigma/2 - i\,\Delta_\sigma & 0 & 2i\,\Omega_\sigma \\ i\,\Omega_\sigma & 0 & -\gamma_\sigma/2 + i\,\Delta_\sigma & -2i\,\Omega_\sigma \\ 0 & i\,\Omega_\sigma & -i\,\Omega_\sigma & -\gamma_\sigma \end{pmatrix}, \tag{4.59}$$

and

$$\mathcal{C} = \begin{pmatrix} 0 & 0 & 0 & 1 \\ 0 & 0 & 0 & 0 \\ 0 & 0 & 0 & 0 \\ 0 & 0 & 0 & 0 \end{pmatrix}. \tag{4.60}$$

Then, using the Quantum Regression Theorem (4.16), we compute the m-photon Glauber correlators. We previously found that in the incoherent case, they can be expressed as a product of the second-order correlator for different time delays τ_p. In the coherently-driven 2LS, this still holds. Since this factorization property is true, independently of the nature of the Liouvillian, the m-order Glauber correlators are also written as

$$G^{(m)}(t_1,\ldots,t_m) = n_\sigma^m \prod_{p=1}^{m-1} G^{(2)}(\tau_p)\,, \tag{4.61}$$

where $\tau_p = t_{p+1} - t_p$ and the two-photon autocorrelation function $G^{(2)}(\tau)$ has the following form

$$G^{(2)}(\tau) = n_\sigma^2 \left(1 + \sum_{p=1}^{3} l_p\, e^{-\lambda_p \tau}\right)\,, \tag{4.62}$$

where the exact coefficients and exponents are in Appendix A.5 and n_σ is the steady-state total population that, for any detuning, reads

$$n_\sigma = \frac{4\Omega_\sigma^2}{\gamma_\sigma^2 + 4\Delta_\sigma^2 + 8\Omega_\sigma^2}\,. \tag{4.63}$$

The resonant case $\Delta_\sigma = 0$ has already been discussed in Chapter 2 and the required formulae can be found there, that is, (2.54) and (2.56).

Despite of the significant simplification of $G^{(m)}$, the integration of these quantities is hard task and we cannot deduce any closed-form formula. We present the exact solution only for the first cases:

$$\langle : \Omega^1 : \rangle = \xi\gamma_\sigma n_\sigma T\,, \tag{4.64a}$$

$$\langle : \Omega^2 : \rangle = (\xi\gamma_\sigma n_\sigma)^2 \Bigg[T^2 - \frac{6\gamma_\sigma}{\gamma_\sigma^2 + 8\Omega_\sigma^2}\,T + 2\,\frac{7\gamma_\sigma^2 - 16\Omega_\sigma^2}{(\gamma_\sigma^2 + 8\Omega_\sigma^2)^2} - 4\,e^{-(\frac{3\gamma_\sigma}{4}+\gamma_M)T}\,\frac{4\gamma_M - 3\gamma_\sigma}{\gamma_M(4\gamma_M + 3\gamma_\sigma)^2} - (\gamma_M \to -\gamma_M)\Bigg]\,, \tag{4.64b}$$

$$\langle : \Omega^3 : \rangle = (\xi\gamma_\sigma n_\sigma)^3 \Bigg[T^3 - \frac{18\gamma_\sigma}{\gamma_\sigma^2 + 8\Omega_\sigma^2}\,T^2 + \frac{6(23\gamma_\sigma^2 - 32\Omega_\sigma^2)}{(\gamma_\sigma^2 + 8\Omega_\sigma^2)^2}\,T - \frac{432\gamma_\sigma(\gamma_\sigma^2 - 4\Omega_\sigma^2)}{(\gamma_\sigma^2 + 8\Omega_\sigma^2)^3} + 3\,e^{-(\frac{3\gamma_\sigma}{4}+\gamma_M)T}\Big(\frac{(4\gamma_M - 3\gamma_\sigma)^2}{2\gamma_M^2(4\gamma_M + 3\gamma_\sigma)^2}\,T + \frac{(4\gamma_M - 3\gamma_\sigma)^2(20\gamma_M + 3\gamma_\sigma)}{2\gamma_M^3(4\gamma_M + 3\gamma_\sigma)^2}\Big) + (\gamma_M \to -\gamma_M)\Bigg]\,, \tag{4.64c}$$

and the rest of the subsequent correlators have the same structure: an k-polynomial and two exponentials (with exponents $-\frac{3\gamma_\sigma}{4} \mp \gamma_M$)

followed by $(k-2)$-polynomials which, moreover, do transform to each other under the exchange $\gamma_M \to -\gamma_M$. We can compute the asymptotic behaviour of the normalised variance, which reads

$$\left(\Sigma^2/\mu\right)(T\to\infty) \to 1 - 6\xi n_\sigma(1-2n_\sigma)\,, \tag{4.65}$$

that is different from 1 in any case ($0 < n_\sigma < 1/2$).

Then, investigating the short and long time behaviour of the first correlators $\langle: \Omega^k :\rangle$, we are able to figure out a closed-form solution for both limiting cases ($T \to 0$ and $T \to \infty$). On one hand, in the short integration time limit, for $k \geq 1$,

$$\langle: \Omega^k :\rangle(T\to 0) \approx k!(\bar{I}T)^k \frac{(\mathcal{Y}\gamma_\sigma^2 T^2)^{k-1}}{2^{k-1}(3k-2)!}\left[1 - \frac{3}{2}\frac{k-1}{3k-1}\gamma_\sigma T\right]\,, \tag{4.66}$$

and, of course, $\langle: \Omega^0 :\rangle = 1$. We have defined $\bar{I} = \xi\gamma_\sigma n_\sigma$ which is, again, the mean detected intensity and $\mathcal{Y} = (\gamma_\sigma^2 + 8\Omega_\sigma^2)/\gamma_\sigma^2$. Inserting (4.68) in (4.4) and taking the limit $T \to 0$ leads to $p(0, T\to 0) \approx 1 - \bar{I}T$ and, for $n \geq 1$, to

$$p(n, T\to 0) \approx (\bar{I}T)^n(\mathcal{Y}\gamma_\sigma^2 T^2)^{n-1}\frac{2(3n-1) - 3(n-1)\gamma_\sigma T}{2^n(3n-1)!}\,. \tag{4.67}$$

On the other hand, the expression for long time integration is

$$\langle: \Omega^k :\rangle(T\to\infty) \approx (\bar{I}T)^k\left(1 - \frac{3k(k-1)}{\mathcal{Y}\gamma_\sigma T}\right)\,, \tag{4.68}$$

For the coherent driving case, we were not able to obtain formulas valid for all time windows, unlike the incoherent driving case. The limits that are obtained here also show, however, that strong quantum departures are maintained also in this case at large times.

Computing the sum (4.4) using the previous equation, we find

$$\boxed{\begin{aligned} p(n, T\to\infty) \approx \left(1+6n\frac{\bar{I}}{\mathcal{Y}}\right)p_0(n,T) - 3(n-1)\frac{\bar{I}}{\mathcal{Y}}p_0(n-1,T) - \\ 3(n+1)\frac{\bar{I}}{\mathcal{Y}}p_0(n+1,T)\,, \end{aligned}} \tag{4.69}$$

where $p_0(n,T)$ is the Poisson distribution.

4.3 INCOHERENTLY PUMPED CAVITY

Now, we change the kind of system. We analyse the emission of a cavity (harmonic oscillator), that can have an arbitrarily large number of excitations. As a consequence, the cavity can have perfect antibunching or any positive value for $g^{(2)}(0)$. Under incoherent pumping, the dynamics of the cavity are described by the master equation

$$\partial_t\rho = -i\omega_a[a^\dagger a, \rho] + \frac{\gamma_a}{2}\mathcal{L}_a\rho + \frac{P_a}{2}\mathcal{L}_{a^\dagger}\rho\,, \tag{4.70}$$

where the pumping and decay rates are P_a and γ_a, respectively. From the master equation (4.70), we obtain the equations of motion for the diagonal correlators $G^{(n)}(t) = \langle a^{\dagger n} a^n \rangle$ are

$$\partial_t G^{(n)}(t) = -n\Gamma_a G^{(n)}(t) + n^2 P_a G^{(n-1)}(t)\,, \tag{4.71}$$

where the effective linewidth is $\Gamma_a \equiv \gamma_a - P_a$. This set of coupled equations can be exactly solved up to any order n truncating the space of correlators. The correlator vector is $\vec{c} = (1,\ \langle a^\dagger a\ \rangle,\ \ldots \langle a^{\dagger n} a^n\ \rangle)^{\mathrm{T}}$, with corresponding matrices

$$M = \begin{pmatrix} 0 & 0 & 0 & \ldots & 0 \\ P_a & -\Gamma_a & 0 & & \vdots \\ 0 & 4P_a & -2\Gamma_a & & \\ \vdots & & & \ddots & \\ 0 & \ldots & & n^2 P_a & -n\Gamma_a \end{pmatrix} \tag{4.72}$$

and

$$\mathcal{C} = \begin{pmatrix} 0 & 1 & 0 & \ldots & 0 \\ \vdots & 0 & 1 & & \vdots \\ & & & \ddots & \\ 0 & & & & 1 \\ 0 & \ldots & & 0 & 0 \end{pmatrix}. \tag{4.73}$$

Thus, any correlator (involving up to n photons) follows from this. For instance, single-time correlations in the steady-state follow from $\vec{c}(t \to \infty)$, where $\vec{c}(t) = e^{\mathrm{M}t}\vec{c}(0)$. That is, $G^{(n)} = n!(P_a/\Gamma_a)^n = n!\,\bar{n}^n$, where $\bar{n} = P_a/\Gamma_a$ is the mean photon population, and the normalised ones are then $g^{(n)} = n!$, the very same any thermal state has. Other multi-time correlations (hereafter, we are assuming the system has reached the steady-state) such as $g^{(2)}(t_1, t_2)$ are computed through Eq. (4.16). In the steady state, such functions only depend on time differences $\tau_p = t_{p+1} - t_p$ rather than on the times t_p themselves. Thus, $G^{(2)}(t_1, t_2)$ can be actually written as $G^{(2)}(\tau_1)$, where $\tau_1 = t_2 - t_1$. The first multi-time correlators, for a particular time ordering, are

$$g^{(2)}(\tau_1) = 1 + e^{-\Gamma_a \tau_1}\,, \tag{4.74a}$$

$$g^{(3)}(\tau_1, \tau_2) = g^{(2)}(\tau_1) g^{(2)}(\tau_2) + 2\, e^{-\Gamma_a(\tau_1+\tau_2)}\,, \tag{4.74b}$$

$$\begin{aligned} g^{(4)}(\tau_1, \tau_2, \tau_3) = {} & g^{(3)}(\tau_1, \tau_2) g^{(2)}(\tau_3) + g^{(2)}(\tau_1) g^{(3)}(\tau_2, \tau_3) \\ & - g^{(2)}(\tau_1) g^{(2)}(\tau_2) g^{(2)}(\tau_3) \\ & + 4 g^{(2)}(\tau_2)\, e^{-\Gamma_a(\tau_1+\tau_2+\tau_3)}\,, \end{aligned} \tag{4.74c}$$

These interesting connections between the n-th order photon correlations with two-photon correlations are to be contrasted with those we found earlier for the two-level system.

and the rest of correlators are computed the same way. As we can see, the factorisation property that we found for the 2LS does not hold for the cavity, at least for this particular case. However, we can rearrange the Glauber functions as sum of products of the lower order correlators. In this way, they reveal a more complicated structure that correlates each photon not only with its first neighbours but with the rest of them. Reminding that $\tau_p = t_{p+1} - t_p > 0$, the time-integrated intensity operator moments, considering all the time orderings, are

$$\langle : \Omega^k : \rangle = k!(\xi\gamma_a)^k \int_0^T \cdots \int_0^{t_2} G^{(k)}(t_1, t_2, \dots t_k) dt_1 dt_2 \dots dt_k \,, \tag{4.75}$$

and the first cases are

$$\langle : \Omega^0 : \rangle = 1 \,, \tag{4.76a}$$
$$\langle : \Omega^1 : \rangle = \xi\gamma_a \bar{n} T \,, \tag{4.76b}$$
$$\langle : \Omega^2 : \rangle = (\xi\gamma_a\bar{n})^2 \Gamma_a^{-2} \left(\Gamma_a^2 T^2 + 2\Gamma_a T - 2 + 2\, e^{-\Gamma_a T}\right) , \tag{4.76c}$$
$$\langle : \Omega^3 : \rangle = (\xi\gamma_a\bar{n})^3 \Gamma_a^{-3} \left[\Gamma_a^3 T^3 + 6\Gamma_a^2 T^2 + 6\Gamma_a T - 24 + (18\Gamma_a T + 24) e^{-\Gamma_a T}\right] , \tag{4.76d}$$
$$\langle : \Omega^4 : \rangle = (\xi\gamma_a\bar{n})^4 \Gamma_a^{-4} \left[\Gamma_a^4 T^4 + 12\Gamma_a^3 T^3 + 48\Gamma_a^2 T^2 - 336 + (108\Gamma_a^2 T^2 + 360\Gamma_a T + 312) e^{-\Gamma_a T} + 24 e^{-2\Gamma_a T}\right] , \tag{4.76e}$$

from which we easily compute the variance-mean ratio when $T \to \infty$, that is

$$\left(\Sigma^2/\mu\right)(T \to \infty) \to 1 + 2\xi\bar{n}(1 + \bar{n}) \,, \tag{4.77}$$

which is always greater than 1 and, unlike the previous cases, the population $\bar{n} > 0$ has no upper bound (shown together with the rest of the cases in Fig. 4.4). Thus, from the point of view of the photo-counting distribution, the emission is Super-Poissonian.

Although we cannot deduce a closed-form expression for any time window T, it is possible to analyse both the short and long time behaviour. For $T \to 0$ and $n > 1$, we find that

$$\langle : \Omega^k : \rangle (T \to 0) \approx k!(\bar{I}T)^k \left(1 - \frac{k-1}{6}\, \Gamma_a T\right) , \tag{4.78}$$

where $\bar{I} = \xi\gamma_a\bar{n}$ is the detected mean intensity. On the other hand, for long time integration we can neglect the terms proportional to the exponential $e^{-\Gamma_a T}$. That is,

$$\langle : \Omega^k : \rangle (T \to \infty) \approx (\bar{I}T)^k \left[1 + \frac{k(k-1)}{\Gamma_a T}\right] . \tag{4.79}$$

Having these expressions in mind, the photon-counting probabilities can be computed through Eq. (4.4). For short time $T \to 0$, this is

$$p(0, T \to 0) \approx 1 - \bar{I}T \, \frac{6 + \bar{I}T(6 + \Gamma_a T)}{6(1 + \bar{I}T)^2} \approx 1 - \bar{I}T \,, \tag{4.80}$$

$$\begin{aligned} p(n \geq 1, T \to 0) &\approx (\bar{I}T)^n \, \frac{6 + 6\bar{I}T + (1 - n + 2\bar{I}T)\Gamma_a T}{6(1 + \bar{I}T)^{n+2}} \\ &\approx (\bar{I}T)^n \left[1 - (n+1)\bar{I}T - (n-1)\frac{\Gamma_a T}{6}\right] . \end{aligned} \tag{4.81}$$

The first term of Eq. (4.80) is clearly identified with a thermal distribution $p_{\text{th}}(n) = (1 - \theta)\theta^n \approx \theta^n$ (for $\theta = \bar{I}T \ll 1$). This means that for short times before other dynamical effects or mechanisms gain in significance, $p(n, T)$ clones the probabilities $P_n = \rho_{n,n}$ modulo the integration factor $\xi\gamma_a T$, which is in accordance with Eq. (4.20).

The other limit investigated is $T \to \infty$, the probability of detecting n photons is

$$\begin{aligned} p(n, T \to \infty) \approx \frac{1}{n!}(\bar{I}T)^n e^{-\bar{I}T} \Big[&\left(1 - 2n\bar{I}/\Gamma_a\right) + \\ &n(n-1)(\Gamma_a T)^{-1} + \bar{I}^2 T/\Gamma_a \Big] , \end{aligned} \tag{4.82}$$

or, after defining the Poisson distribution with the same mean number of detected photons $p_0(n, T) = \frac{1}{n!}(\bar{I}T)^n e^{-\bar{I}T}$, we can rewrite Eq. (4.82) as a function of Poisson distributions

$$\begin{aligned} p(n, T \to \infty) \approx &\left(1 - 2n\frac{\bar{I}}{\Gamma_a}\right) p_0(n, T) + (n-1)\frac{\bar{I}}{\Gamma_a} p_0(n-1, T) + \\ &(n+1)\frac{\bar{I}}{\Gamma_a} p_0(n+1, T) \,. \end{aligned} \tag{4.83}$$

Interestingly enough, this formula bears resemblance with Eq. (4.38), differing only in the sign of $\bar{I}/\Gamma_a$. Following this, in the same manner, we can try to approximate this distribution as a displaced Poisson distribution. Changing $n \to n + m$, with $m \geq 0$, and $\bar{I}T \to \beta\bar{I}T$ and making their mean and variance to match, we find that the best fit for m and β are

$$m = 2\,\frac{\bar{I}}{\Gamma_a}\,\bar{I}T \quad \text{and} \quad \beta = 1 + 2\,\frac{\bar{I}}{\Gamma_a} \,. \tag{4.84}$$

The interpretation of this result is the following. The intensity, that is, the mean number of photons per unit time, is proportional to the mean number of excitations of the emitter (averaged over the time window T too). The fluctuations of the intensity are, however, affected by the correlations between all the photons. As such, the shape of

This figure summarizes the departures from the classical case of the various systems studied and shows that not only correlations survive at long times, but they are actually maximum there.

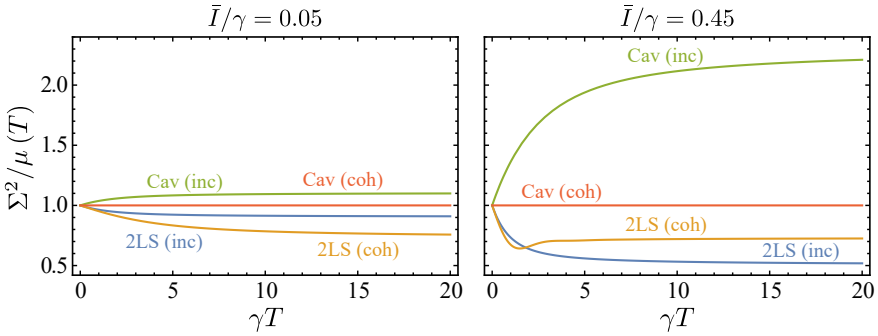

Figure 4.2: Variance normalised to the mean, namely Σ^2/μ for the photon-counting probabilities for the four cases discussed as a function of the integration time T, assuming perfect detection, i.e., $\xi = 1$. On the left hand side, when the intensity (population) is small ($\bar{I} = 0.05\gamma$) and, on the right when the mean intensity is greater ($\bar{I} = 0.45\gamma$). The decay rates are fixed to unity, i.e., $\gamma_\sigma = \gamma_a = 1$. All the curves promptly saturate to asymptotes, shown in Fig. 4.4.

the photon-counting distribution will be strongly dependent on the dynamical aspects of the emission. We have seen that the short-time behaviour can be inferred from the averaged single-time correlators $n!(\xi\gamma)^n \int_0^T G^{(n)}(t)dt$ (which simplifies to $(\xi\gamma T)^n G^{(n)}(0)$ if the system has already reached the steady-state). The correlations in this regime have not been developed yet due to the scarce time intervals between the emitted photons, compared to their characteristic time scale. This raises another interesting question: can we infer $G^{(n)}$ from photon-counting measurements? In principle, the answer is affirmative. We *barely* need some apparatus that collect photons and, if possible, a way to make all the photons to arrive at it, that is, to have good efficiency. The actual realisation is however more problematic. Not only the efficiency is a worrisome issue but also the response of the detector. In the next sections we will try elucidate the effect on the counting statistics.

Resuming the previous discussion, we have also analysed the long-time behaviour of the photon-counting distribution. One would expect that in this limit, correlations are washed out and do not play a role given that $g^{(n)}(t \to \infty) \to 1$, this is, photons separated by a long time interval remain uncorrelated. From that, we could conclude that any photon-counting distribution would be approximated better and better by a Poisson distribution. However, we find out several examples that contradict this guess. Both incoherently-driven 2LS's and cavity's photon-counting distributions do resemble an ordinary Poisson distribution but, in fact, cannot be fitted with it. The best approach is a combination of Poisson distributions, (4.38) and (4.83),

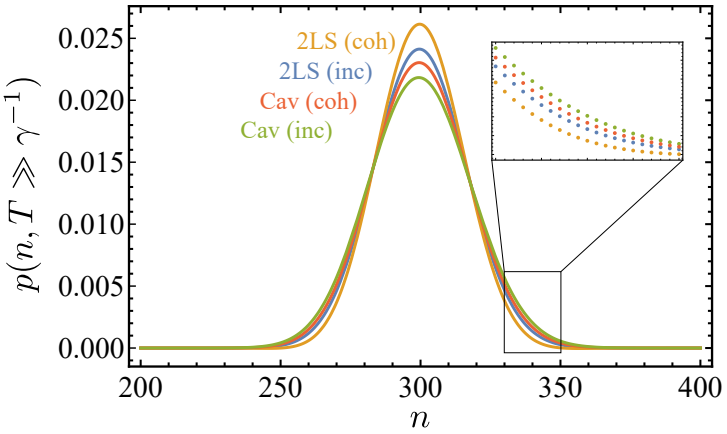

Figure 4.3: Photon-counting probabilities for the four cases discussed so far in the limit of long integration time ($\gamma T \gg 1$). The mean intensity is fixed to be $\bar{I} = 0.05\gamma$ and $\xi = 1$, where the decay rate is $\gamma_\sigma = \gamma_a = 1$ and the integration time is $T = 6000$. In inset, a zoom displaying the behaviour of tails of the distributions.

which are, in turn, approximated around their modes by displaced Poisson distributions (changing the origin $n \to n \mp m$ and the parameter $\bar{I}T \to \beta\bar{I}T$). This fact immediately discards the idea of losing or blurring the effect of correlations in the long term on the counting statistics. Taking a simple look to the first distribution moments can confirm this statement.

4.4 COHERENTLY PUMPED CAVITY

The cavity under coherent excitation, for instance, a laser with frequency ω_L has the following Hamiltonian (in the Rotating Frame):

$$H = \Delta_a a^\dagger a + \Omega_a (a^\dagger + a)\,, \tag{4.85}$$

and the master equation

$$\partial_t \rho = -i[H, \rho] + \frac{\gamma_a}{2}\mathcal{L}_a \rho\,. \tag{4.86}$$

The correlator equations are computed from the master equation (4.86) and read

$$\begin{aligned}\partial_t \langle a^{\dagger m} a^n \rangle = &- \left[(m+n)\gamma_a/2 - i\Delta_a(m-n)\right]\langle a^{\dagger m} a^n\rangle + \\ &i\Omega_a m \langle a^{\dagger m-1} a^n\rangle - i\Omega_a n \langle a^{\dagger m} a^{n-1}\rangle\,.\end{aligned} \tag{4.87}$$

This set of coupled equations is usually difficult to solve if m and n are large. However, using the ansatz $a(t) = e^{-(\gamma_a/2 + i\Delta_a)t} a(0) + \alpha$,

where $\alpha = i\Omega_a/(\gamma_a/2 + i\Delta_a)$ and $t \geq 0$, all correlators equations are automatically satisfied. This still holds even when each operator is evaluated at different times, for instance,

$$\langle a^\dagger(t_1)a(t_2)\rangle = e^{-(\gamma_a/2(t_1+t_2)}e^{i\Delta_a(t_1-t_2)}\langle a^\dagger a\rangle(0) + \alpha^* e^{-(\gamma_a/2+i\Delta_a)t_2}\langle a\rangle(0) + \alpha e^{-(\gamma_a/2-i\Delta_a)t_1}\langle a^\dagger\rangle(0) + |\alpha|^2\,, \quad (4.88)$$

which in the limit $t_p \to \infty$ tends to $\langle a^\dagger(t_1)a(t_2)\rangle \to |\alpha|^2$. Translated to the Fourier space, the spectrum corresponds to a Dirac delta centered at $\omega = \omega_L$ (undoing the Rotating Frame Transformation). This implies the cavity is emitting monochromatic light once it has reached the steady-state.

Furthermore, in this limit, the cavity operator $a(t)$ can be substituted by a c-number, i.e., $a(t \to \infty) \to \alpha$. Then, all the correlators $G^{(m)}(t_1, \ldots, t_m)$ are simply $|\alpha|^{2m}$. Following that, the time-integrated correlations are

$$\langle : \Omega^k : \rangle = k!(\xi\gamma_a)^k|\alpha|^{2k}\int_0^T\int_0^{t_k}\cdots\int_0^{t_2} dt_1 \ldots dt_k\,, \quad (4.89)$$

where the k-fold integral has already appeared in the previous sections and it was found to be equal to $T^k/k!$. Then,

$$\langle : \Omega^k : \rangle = (\xi\gamma_a|\alpha|^2 T)^k = \left(\frac{4\xi\gamma_a\Omega_a^2}{\gamma_a^2 + 4\Delta_a^2}\,T\right)^k = (\bar{I}T)^k\,, \quad (4.90)$$

where, again, $\bar{I} = (4\xi\gamma_a\Omega_a^2)/(\gamma_a^2 + 4\Delta_a^2)$ is the mean detected intensity. With this particularly simple shape, the photon-counting probabilities are

$$p(n, T) = \frac{1}{n!}(\bar{I}T)^n e^{-\bar{I}T}\,, \quad (4.91)$$

which is genuinely a Poisson distribution. The normalised variance, given the Poisson distribution, is simply $\Sigma^2/\mu = 1$.

The four cases, all studied under CW excitation, display different behaviours both in the short and long integration time regimes (the latter shown in Fig. 4.3). First, the few-photon quantities such as the variance-mean ratio differ from the Poisson case (except for the coherent cavity). Greater values are found for the incoherent cavity displaying Super-Poissonian behaviour ($\Sigma^2/\mu > 1$) in the photo-detection scenario, in accordance with the system observables such as $g^{(2)} > 1$. The 2LS, which has $g^{(2)}(0) = 0$, exhibits Sub-Poissonian statistics, this is, $\Sigma^2/\mu < 1$ from the point of view of the detection distribution. The largest deviations are found to be when the population reaches the midpoint of the allowed range of n_σ (see Figure 4.4)

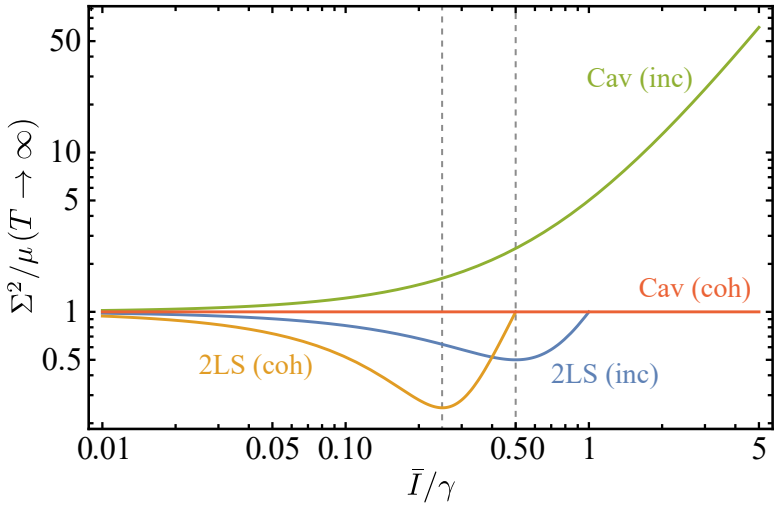

This figure gives the optimum driving to maximize the 2LS's departure from the classical (uncorrelated) case, and shows that the thermal state's long time correlations increase without bounds with temperature.

Figure 4.4: Asymptotic long-time behaviour of the variance-mean ratio for the four cases studied in the text. The coherently driven cavity can display $\Sigma^2/\mu = 1$, while the other three cases deviate from that value. The thermal emission of the incoherently pumped cavity exhibits Super-Poissonian behaviour and grows without limit as the signal intensifies. On the other hand, the single-photon emitters have Sub-Poissonian behaviours. The maximum deviation appears when the intensity is exactly half the maximum accessible population (0.25 for the coherent case and 0.5 the incoherent one, assuming that $\xi = 1$), marked by the vertical dashed lines.

and the global minimum is $\Sigma^2/\mu = 0.25$ by the coherently driven 2LS. These two polynomials, (4.27) and (4.65), are in fact exactly the same as (2.69), the inter arrival time variances. Identically, this also holds for the thermal emission. We identify (4.77) with (A.97) (making the substitution $n_{\infty,\mathrm{th}} \to \bar{n}$).

For short times, for instance, the incoherently driven 2LS has $p(2, T \to 0)$ that is proportional to T^3 rather than T^2 (as the cavity distribution does). This is a direct consequence of the structure of the 2LS, that cannot have more than one excitation at the same time. The reloading process after the first photon breaks down the Poisson picture of the emission in which the probability per unit time is proportional to $\bar{I}$ (it would automatically lead to zero). The re-excitation, is indeed a Poisson process whose probability per unit time goes like P_σ for the incoherently driven case. It is then a two step procedure, the emission is delayed until the excitation successfully takes place. That explains the discrepancy between the 2LS and the cavity.

4.5 N-PHOTON SPONTANEOUS EMISSION

Another case of interest is a cavity or $M \geq N$-emitter prepared at $t = 0$ to hold the state $\rho(0) = |N\rangle\langle N|$ and that is allowed to freely radiate the photons out without any type of stimulation. Under these conditions, the state evolves following the master equation:

$$\dot{\rho} = -i\,\omega_a[a^\dagger a, \rho] + \frac{\gamma_a}{2}\mathcal{L}_a\rho\,, \tag{4.92}$$

where ω_a is the characteristic frequency of the cavity, γ_a is the decay rate and $\mathcal{L}_a = 2a\rho a^\dagger - a^\dagger a\rho - \rho a^\dagger a$ is the Lindblad operator associated with the cavity losses. From this master equation, we can calculate the equation of motion for any correlator $\langle a^{\dagger m} a^n\rangle(t) = \mathrm{Tr}\{\rho(t) a^{\dagger m} a^n\}$, that is

$$\partial_t\langle a^{\dagger m} a^n\rangle(t) = -\left[\left(\frac{\gamma_a}{2} - i\,\omega_a\right) m + \left(\frac{\gamma_a}{2} + i\,\omega_a\right) n\right]\langle a^{\dagger m} a^n\rangle(t)\,, \tag{4.93}$$

which have the following solution

$$\langle a^{\dagger m} a^n\rangle(t) = \langle a^{\dagger m} a^n\rangle(0)\,\exp\left\{[-(m+n)\gamma_a/2 + i(m-n)\omega_a]t\right\}\,, \tag{4.94}$$

for $t \geq 0$ and zero otherwise. Since the initial state is diagonal and has N excitations, $\langle a^{\dagger m} a^n\rangle(0)$ vanishes if $m \neq n$ or $m, n > N$. Then, the non-zero correlators are $\langle a^{\dagger m} a^m\rangle(0) = N!/(N-m)!$ (for $0 \leq m \leq N$) and evolve in time as

$$\langle a^{\dagger m} a^m\rangle(t) = \frac{N!}{(N-m)!}\,e^{-m\gamma_a t}\,. \tag{4.95}$$

For subsequent calculations, we will make use of the multi-time correlators $\langle A_n^\dagger(t_1', \ldots, t_n') A_n(t_1, \ldots, t_n)\rangle$, where $A_n(t_1, \ldots, t_n) = \prod_{k=1}^n a(t_k)$ is a product of time-ordered operators from right to left ($t_n \geq \ldots \geq t_1 \geq 0$). The conjugate operator $A_n^\dagger$ would be ordered the other way around. To simplify further computations, we assume that $t_m' \geq t_m$ and $t_m, t_m' \geq t_{m-1}, t_{m-1}'$ for every m.

Using the Quantum Regression theorem, for $m = 1$, we have

$$\partial_{t_1'}\langle a^\dagger(t_1') a(t_1)\rangle = -\left(\gamma_a/2 - i\,\omega_a\right)\langle a^\dagger(t_1') a(t_1)\rangle \tag{4.96}$$

which, fixing the initial condition at $t_1' = t_1$ and making use of Eq. (4.95) after that, has the solution

$$\begin{aligned}\langle a^\dagger(t_1') a(t_1)\rangle &= \langle a^\dagger(t_1) a(t_1)\rangle\, e^{-(\gamma_a/2 - i\omega_a)(t_1' - t_1)} \\ &= \langle a^\dagger a\rangle(0)\, e^{-\gamma_a t_1} e^{-(\gamma_a/2 - i\omega_a)(t_1' - t_1)} \\ &= \langle a^\dagger a\rangle(0)\, e^{-(\gamma_a/2 - i\omega_a)t_1'} e^{-(\gamma_a/2 + i\omega_a)t_1}\,.\end{aligned} \tag{4.97}$$

We would have chosen the alternative time order, the result would been exactly the same. As we will see, this structure is maintained throughout successive orders. For $m = 2$,

$$\partial_{t_2'}\langle a^\dagger(t_1')a^\dagger(t_2')a(t_2)a(t_1)\rangle = -(\gamma_a/2 - i\,\omega_a)\,\langle a^\dagger(t_1')a^\dagger(t_2')a(t_2)a(t_1)\rangle \tag{4.98}$$

that, after fixing the initial condition at $t_2' = t_2$, leads to

$$\langle a^\dagger(t_1')a^\dagger(t_2')a(t_2)a(t_1)\rangle = \langle a^\dagger(t_1')a^\dagger(t_2)a(t_2)a(t_1)\rangle\, e^{-(\gamma_a/2 - i\omega_a)(t_2' - t_2)}\,. \tag{4.99}$$

Now we need the time evolution for t_1' and t_2, using the equations

$$\partial_{t_1'}\langle a^\dagger(t_1')a^\dagger(t_2)a(t_2)a(t_1)\rangle = - (\gamma_a/2 - i\,\omega_a)\,\langle a^\dagger(t_1')a^\dagger(t_2)a(t_2)a(t_1)\rangle\,, \tag{4.100}$$

$$\partial_{t_2}\langle a^\dagger(t_1)a^\dagger(t_2)a(t_2)a(t_1)\rangle = -\gamma_a\langle a^\dagger(t_1)a^\dagger(t_2)a(t_2)a(t_1)\rangle \tag{4.101}$$

and (4.95) too, we can finally find

$$\langle a^\dagger(t_1')a^\dagger(t_2')a(t_2)a(t_1)\rangle = \langle a^{\dagger 2}a^2\rangle(0)\, e^{-(\gamma_a/2 - i\omega_a)(t_1' + t_2')} e^{-(\gamma_a/2 + i\omega_a)(t_1 + t_2)}\,. \tag{4.102}$$

This procedure may be repeated for successive k and lead to the general form for $0 \leq k \leq N$

$$\begin{aligned}
&\langle a^\dagger(t_1')...a^\dagger(t_m')a(t_m)...a(t_1)\rangle \\
&= \langle a^{\dagger m}a^m\rangle(0)\,\left(\prod_{k'=1}^{m} e^{-(\gamma_a/2 - i\omega_a)t_{k'}'}\right)\left(\prod_{k=1}^{m} e^{-(\gamma_a/2 + i\omega_a)t_k}\right) \\
&= \frac{N!}{(N-m)!}\,\left(\prod_{k'=1}^{m} e^{-(\gamma_a/2 - i\omega_a)t_{k'}'}\right)\left(\prod_{k=1}^{m} e^{-(\gamma_a/2 + i\omega_a)t_k}\right)\,,
\end{aligned} \tag{4.103}$$

or, as a rule of thumb, each time we have an operator $a(t)$, we do the substitution $a(t \geq 0) \to e^{-(\gamma_a/2 + i\,\omega_a)t}\,a(0)$. This fact allows to to calculate (4.2) very easily

$$\begin{aligned}
\Omega(0;T) &= \xi\gamma_a \int_0^T (a^\dagger a)(t)dt = \xi\gamma_a \left(\int_0^T e^{-\gamma_a t}dt\right)(a^\dagger a)(0) \\
&= \xi\left(1 - e^{-\gamma_a T}\right)(a^\dagger a)(0)\,,
\end{aligned} \tag{4.104}$$

or, any (normal-ordered) average of Ω up to $k = N$

$$\langle : \Omega^k : \rangle = \xi^k \left(1 - e^{-\gamma_a T}\right)^k \langle a^{\dagger k} a^k \rangle(0) = \xi^k \left(1 - e^{-\gamma_a T}\right)^k \frac{N!}{(N-k)!}. \tag{4.105}$$

Then, the probability of detecting n out of N photons in the time window $(0, T]$ is

This result, that provides the photon-counting from SE as a binomial distribution, thereby identifies the time-resolved quantum efficiency of the detection process. This is further generalized by Eq. (4.113).

$$\begin{aligned} p(n;T) &= \frac{1}{n!} \sum_{k=0}^{\infty} (-1)^k \frac{\langle : \Omega^{n+k} : \rangle}{k!} \\ &= \sum_{k=0}^{N-n} \frac{(-1)^k}{n!k!} \frac{N!}{(N-n-k)!} \left[\xi \left(1 - e^{-\gamma_a T}\right)\right]^{n+k} \\ &= \binom{N}{N-n} \left[\xi \left(1 - e^{-\gamma_a T}\right)\right]^n \left[1 - \xi \left(1 - e^{-\gamma_a T}\right)\right]^{N-n}. \end{aligned} \tag{4.106}$$

This probability distribution is a *binomial distribution* and corresponds to the probability of accepting n out of N independent events with probability $\mathcal{T}(T) = \xi \left(1 - e^{-\gamma_a T}\right)$, that we call the one-photon detection probability. In other words, the photon-counting process in the SE regime can be understood from a classical point of view where each event, accepting or rejecting a photon, is independent from the others but whose detection probability follows the rules of quantum mechanics.

4.5.1 FILTERED EMISSION

In the presence of a non-ideal and time-limited detector, whose best efficiency is reached at $\omega = \omega_1$ and has got a characteristic range of detection around it (also known as filter frequency width Γ), the total number of photons collected by the detector differs from the blind (non frequency-resolved) detection. The probability of detecting all the photons will not reach 100% (assuming perfect efficiency) even if the integration time T goes to infinity. To take into account this detrimental effect, we model the detector as a Lorentzian filter (with half-width Γ and centred at ω_1). For a Lorentzian filter $F_{\mathrm{L}}(t)$ (1.64) and the operator $a(t)$ associated with the cavity, we have the filtered operator (1.60)

$$\begin{aligned} \varsigma(t) &= \left(\int_{-\infty}^{\infty} F_{\mathrm{L}}(t - t_1) \theta(t_1) e^{-(\gamma_a/2 + i\omega_a)t_1} \, dt_1 \right) a(0) \\ &= \Xi(t) a(0), \end{aligned} \tag{4.107}$$

where $\Xi(t)$ codifies the frequency-resolved time evolution. After integrating, it yields

$$\Xi(t) = \Gamma \frac{e^{-(\gamma_a/2+i\,\omega_a)t} - e^{-(\Gamma/2+i\,\omega_1)t}}{\Gamma_- + 2i\Delta}\,\theta(t)\,, \tag{4.108}$$

where $\Delta \equiv \omega_1 - \omega_a$ is the detuning between the cavity and the filter and where $\Gamma_\pm \equiv \Gamma \pm \gamma_a$. The time-integrated intensity operator from $(0, T]$ is

$$\begin{aligned}\Omega(T;\Gamma,\Delta) &= \xi\,\gamma_a \int_0^T \varsigma^\dagger\varsigma(t)\,dt = \left(\xi\,\gamma_a \int_0^T \left[\Xi(t)\right]^* \Xi(t)\,dt\right) a^\dagger a \\ &= \xi\,\Gamma\,\mathcal{A}(T)\,a^\dagger a\,,\end{aligned} \tag{4.109}$$

and the function $\mathcal{A}(T)$ is defined as

$$\begin{aligned}\mathcal{A}(T) = &\frac{\Gamma_+}{\Gamma_+^2 + 4\Delta^2} - \frac{\Gamma\,e^{-\gamma_a T} + \gamma_a\,e^{-\Gamma T}}{\Gamma_-^2 + 4\Delta^2} + \\ &\frac{4\Gamma\gamma_a e^{-\Gamma_+ T}\left[\Gamma_+\cos(\Delta T) - 2\Delta\sin(\Delta T)\right]}{\left(\Gamma_-^2 + 4\Delta^2\right)\left(\Gamma_+^2 + 4\Delta^2\right)}\,,\end{aligned} \tag{4.110}$$

and when integration time $T \to \infty$, it gives

$$\mathcal{A}(T\to\infty) = \frac{\Gamma_+}{\Gamma_+^2 + 4\Delta^2}\,. \tag{4.111}$$

If the detection does not start at $t = 0$ but at a later time $t > 0$, the previous function is modified to:

$$\begin{aligned}\mathcal{A}(T,t) = &\frac{\Gamma e^{-\gamma_a t} + \gamma_a e^{-\Gamma t}}{\Gamma_-^2 + 4\Delta^2} - \frac{\Gamma\,e^{-\gamma_a(t+T)} + \gamma_a\,e^{-\Gamma(t+T)}}{\Gamma_-^2 + 4\Delta^2} \\ &+ \frac{4\Gamma\gamma_a e^{-\Gamma_+(t+T)}\left[\Gamma_+\cos(\Delta(t+T)) - 2\Delta\sin(\Delta(t+T))\right]}{\left(\Gamma_-^2 + 4\Delta^2\right)\left(\Gamma_+^2 + 4\Delta^2\right)} \\ &- \frac{4\Gamma\gamma_a e^{-\Gamma_+ T}\left[\Gamma_+\cos(\Delta T) - 2\Delta\sin(\Delta T)\right]}{\left(\Gamma_-^2 + 4\Delta^2\right)\left(\Gamma_+^2 + 4\Delta^2\right)}\,.\end{aligned} \tag{4.112}$$

The probability of detecting n photons from the N-photon SE in the time window of length T is:

$$\begin{aligned}p(n;T) = &\frac{1}{n!}\sum_{k=0}^{N-n}\frac{(-1)^k}{k!}\langle{:}\,(a^\dagger a)^{n+k}\,{:}\rangle\,(\xi\,\Gamma\,\mathcal{A}(T))^{n+k} = \\ &\frac{1}{n!}\sum_{k=0}^{N-n}\frac{(-1)^k}{k!}\frac{N!}{(N-n-k)!}\,(\xi\,\Gamma\,\mathcal{A}(T))^{n+k} = \\ &\binom{N}{N-n}\,(\xi\,\Gamma\,\mathcal{A}(T))^n\,(1-\xi\,\Gamma\,\mathcal{A}(T))^{N-n}\,.\end{aligned} \tag{4.113}$$

As said before, the filtered emission loses some photons that are left undetected. The one-photon detection probability is, in this case, $\mathcal{T}(T) = \xi\Gamma\mathcal{A}(T)$ and does not reach 1 even if $T \to \infty$. However, due to energy conservation, the rest of the emission must go elsewhere. This is reflected in the field decomposition $a(t) = \varsigma(t) + \bar{\varsigma}(t)$. Having fixed the filter response $F(t)$, it is easy to see that $\bar{\varsigma}(t)$ should be in this case

$$\begin{aligned}\bar{\varsigma}(t) &= \int_{-\infty}^{\infty} (\delta(t-t_1) - F(t-t_1))\, a(t_1)\, dt_1 \\ &= \left(\int_{-\infty}^{\infty} (\delta(t-t_1) - F(t-t_1))\, \theta(t) e^{-(\gamma_a/2 + i\omega_a)t_1}\, dt_1\right) a(0) \\ &= \Xi_{1-F}(t) a(0)\,. \end{aligned} \tag{4.114}$$

In these last steps, we are considering the case of SE and we include the time evolution of $\bar{\varsigma}$ in $\Xi_{1-F}(t)$. Now, we could proceed exactly the same as we did before. However, it is useful to derive the next result via an alternative way. If we look again the definition of $\Xi_{1-F}(t)$, the (complementary) filter response is being convoluted with the SE unfiltered evolution. If we take the Fourier transform of $\Xi_{1-F}(t)$, due to the Convolution Theorem, we get the product of the Fourier transforms

$$\check{\Xi}_{1-F}(\omega) = [1 - \check{F}(\omega)]\, \frac{1}{\gamma_a/2 - i(\omega - \omega_a)}\,. \tag{4.115}$$

Similarly, the time evolution of $\varsigma(t)$ on the Fourier space looks the same just by changing $1 - \check{F} \to \check{F}$. We can reverse the transformation

$$\begin{aligned}\Xi_F(t) &= \frac{1}{2\pi}\int_{-\infty}^{\infty} \check{\Xi}_F(\omega) e^{-i\omega t}\, dt \\ &= \frac{1}{2\pi}\int_{-\infty}^{\infty} \frac{\check{F}(\omega)}{\gamma_a/2 - i(\omega - \omega_a)} e^{-i\omega t}\, dt\,. \end{aligned} \tag{4.116}$$

From this, the time-integrated intensity operator for $T \to \infty$ is

$$\begin{aligned}\Omega_F &= \xi\gamma_a a^\dagger a \int_0^{\infty} (\Xi_F(t))^* \Xi_F(t)\, dt \\ &= \frac{\xi\gamma_a a^\dagger a}{(2\pi)^2}\int_0^{\infty}\int_{-\infty}^{\infty}\int_{-\infty}^{\infty} (\check{\Xi}_F(\omega'))^* \check{\Xi}_F(\omega) e^{-i(\omega-\omega')t}\, d\omega d\omega' dt\,. \end{aligned} \tag{4.117}$$

If we make the reasonable assumption that the filter response F is causal, i.e., only exist for $t > 0$, then $\Xi_F(t)$ will only be non-zero for

$t > 0$ and we can extend the integration limit of t to $-\infty$. Exchanging the order of the integrals and integrating on t leads to

$$\begin{aligned}\Omega_F &= \xi\gamma_a a^\dagger a \frac{1}{2\pi}\int_{-\infty}^{\infty}\int_{-\infty}^{\infty}(\breve{\Xi}_F(\omega'))^*\breve{\Xi}_F(\omega)\delta(\omega-\omega')\,d\omega' d\omega \\ &= \xi\gamma_a a^\dagger a \frac{1}{2\pi}\int_{-\infty}^{\infty}(\breve{\Xi}_F(\omega))^*\breve{\Xi}_F(\omega)\,d\omega\,, \end{aligned} \tag{4.118}$$

where we have used $\int_{-\infty}^{\infty} e^{-i(\omega-\omega')}dt = 2\pi\,\delta(\omega-\omega')$. Substituting the expression for $\breve{\Xi}_F(\omega)$

$$\begin{aligned}\Omega_F &= \xi\gamma_a a^\dagger a\left(\frac{1}{2\pi}\int_{-\infty}^{\infty}\frac{|\breve{F}(\omega)|^2}{(\gamma_a/2)^2+(\omega-\omega_a)^2}\,d\omega\right) \\ &= \xi\gamma_a I_F\; a^\dagger a\,, \end{aligned} \tag{4.119}$$

where the integral

$$\boxed{I_F = \frac{1}{2\pi}\int_{-\infty}^{\infty}\frac{|\breve{F}(\omega)|^2}{(\gamma_a/2)^2+(\omega-\omega_a)^2}\,d\omega} \tag{4.120}$$

This provides the general form of the one-photon detection probability $\mathcal{T}_F$ for an arbitrary filter F.

allows us to obtain the one-photon detection probability as $\mathcal{T}_F = \xi\gamma_a I_F$. Inserting this expression into the photon-counting formula

$$\begin{aligned}p_F(n;T\to\infty) &= \frac{1}{n!}\sum_{k=0}^{N-n}\frac{(-1)^k}{k!}\frac{N!}{(N-n-k)!}\left(\mathcal{T}_F\right)^{n+k} \\ &= \binom{N}{N-n}\left(\mathcal{T}_F\right)^n\left(1-\mathcal{T}_F\right)^{N-n}\,. \end{aligned} \tag{4.121}$$

With this general result, we are able to compute the probability distribution for a wide variety of filters. In particular, we are interested in concatenated filters. We consider the possibility of redirecting the fraction of the undetected emission (that the first detector did not collect) to a second detector and, then, repeat the same process up to n filters. In terms of operators, the second-order filter $\varsigma^{(2)}(t)$ is constructed filtering the complementary field $\bar{\varsigma}(t)$

$$\varsigma^{(2)}(t) = \int_{-\infty}^{\infty} F(t-t_1)\bar{\varsigma}(t_1)\,dt_1\,, \tag{4.122}$$

and, after inserting Eq. (4.114),

$$\varsigma^{(2)}(t) = \left(\int_{-\infty}^{\infty} F(t-t_1)\Xi_{1-F}(t_1)\,dt_1\right)a(0) = \Xi_F^{(2)}(t)a(0)\,. \tag{4.123}$$

Expressing the time evolution $\Xi_F^{(2)}(t)$ in the Fourier space, we have

$$\breve{\Xi}_F^{(2)}(\omega) = \breve{F}(\omega)\,\breve{\Xi}_{1-F}(\omega) = \frac{\breve{F}(\omega)\left(1-\breve{F}(\omega)\right)}{\gamma_a/2-i(\omega-\omega_a)} = \frac{\breve{F}^{(2)}(\omega)}{\gamma_a/2-i(\omega-\omega_a)}\,,$$

(4.124)

where $\check{F}^{(2)}(\omega) = \check{F}(\omega)(1 - \check{F}(\omega))$ is the effective second-order filter response. If we repeat this process of filtering the k-order complementary emission up to n times, it is straightforward to show that the n-th order effective response is $\check{F}^{(n)}(\omega) = \check{F}(\omega)[1 - \check{F}(\omega)]^{n-1}$. If we introduce this result into I_F, in Eq. (4.119), we get the integral

$$I_F^{(n)} = \frac{1}{2\pi} \int_{-\infty}^{\infty} \frac{|\check{F}(\omega)|^2 |1 - \check{F}(\omega)|^{2(n-1)}}{(\gamma_a/2)^2 + (\omega - \omega_a)^2} \, d\omega \,. \tag{4.125}$$

If we choose a Lorentzian filter, so that $\check{F}_{\mathrm{L}}(\omega) = \Gamma/2 \; [\Gamma/2 - i(\omega - \omega_1)]^{-1}$, now $I_F^{(n)}$ takes the form

$$I_{\mathrm{L}}^{(n)} = \frac{1}{2\pi} \int_{-\infty}^{\infty} \frac{(\Gamma/2)^2 (\omega - \omega_1)^{2(n-1)}}{[(\gamma_a/2)^2 + (\omega - \omega_a)^2][(\Gamma/2)^2 + (\omega - \omega_1)^2]^n} \, d\omega \,. \tag{4.126}$$

In order to solve this integral for any $n \geq 1$, we should write it in a more suitable way,

$$I_{\mathrm{L}}^{(n)} = (\Gamma/2)^2 \frac{1}{2\pi} \int_{-\infty}^{\infty} \frac{(\omega - \omega_1)^{2(n-1)}}{(\omega - z_a)(\omega - z_a^*)(\omega - z_1)^n (\omega - z_1^*)^n} \, d\omega \,, \tag{4.127}$$

where $z_a \equiv \omega_a - i\,\gamma_a/2$ and $z_1 \equiv \omega_1 - i\,\Gamma/2$. In this form, the integral is equivalent to the contour integral (choosing the half-circle on the upper complex plane as the contour C):

$$I_{\mathrm{L}}^{(n)} = (\Gamma/2)^2 \frac{1}{2\pi} \oint_C \frac{(z - \omega_1)^{2(n-1)}}{(z - z_a)(z - z_a^*)(z - z_1)^n (z - z_1^*)^n} \, dz \,. \tag{4.128}$$

Using Cauchy's integral formula [75], we find

$$I_{\mathrm{L}}^{(n)} = i(\Gamma/2)^2 \left(g_1(z_a^*) + \frac{1}{(n-1)!} \frac{d^{n-1}}{dz^{n-1}} g_a(z_1^*) \right) \,, \tag{4.129}$$

with

$$g_1(z) = \frac{(z - \omega_1)^{2(n-1)}}{(z - z_a)(z - z_1)^n (z - z_1^*)^n} \,, \tag{4.130}$$

and

$$g_a(z) = \frac{(z - \omega_1)^{2(n-1)}}{(z - z_a)(z - z_a^*)(z - z_1)^n} \,. \tag{4.131}$$

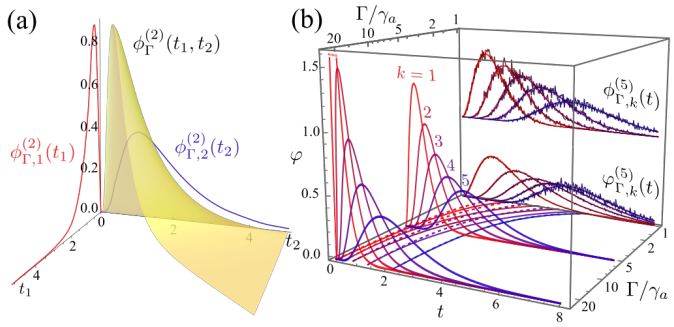

Figure 4.5: In (a), the full representation of the 2-photon joint distribution $\phi^{(2)}(t_1,t_2)$ together with the marginal distributions, $\phi^{(2)}_1(t_1)$ and $\phi^{(2)}_2(t_2)$, in the projected spaces. In (b), the $N=5$ marginal non- and conditional distributions, $\phi^{(5)}_k(t)$ and $\varphi^{(5)}_k(t)$, for several filter widths. For $\Gamma/\gamma_a=1$, the analytics are superimposed with the numerical simulations. On the bottom the mean times for each photon as a function of Γ is displayed (solid for φ and dashed for ϕ).

As an application of this formula, we show the time-integrated intensity operator $\Omega^{(n)}=\xi\gamma_a I^{(n)}a^\dagger a$ for a few cases

$$n=1\ :\ \Omega^{(1)}=\xi\,\Gamma\frac{F_{11}}{F_{11}^2+4\Delta^2}(a^\dagger a)\,, \tag{4.132a}$$

$$n=2\ :\ \Omega^{(2)}=\frac{\xi\,\Gamma}{2}\frac{\gamma_a F_{11}^2+4\Delta^2F_{21}}{(F_{11}^2+4\Delta^2)^2}(a^\dagger a)\,, \tag{4.132b}$$

$$n=3\ :\ \Omega^{(3)}=\frac{\xi\,\Gamma}{8}\left[\gamma_a F_{11}^3F_{13}+24\gamma_a\Delta^2F_{11}F_{21}+16\Delta^4F_{83}\right]\left[F_{11}^2+4\Delta^2\right]^{-3}(a^\dagger a)\,, \tag{4.132c}$$

where $F_{jk}\equiv j\Gamma+k\gamma_a$ and, of course, the photon-counting probability for the m-order filter is

$$p^{(m)}_{\rm L}(n;T\to\infty)=\binom{N}{N-n}\left(\xi\gamma_a\,I^{(m)}_{\rm L}\right)^n\left(1-\xi\gamma_a\,I^{(m)}_{\rm L}\right)^{N-n}\,. \tag{4.133}$$

If the filter-emitter detuning is zero ($\Delta=0$), the efficiency is perfect ($\xi=1$) and if we take the first-order Lorentzian filter, the probability distribution simplifies to

$$P(n,N)\equiv p_{\rm L}(n,T\to\infty)=\binom{N}{N-n}\frac{\gamma_a^{N-n}\Gamma^n}{F_{11}^N}\,. \tag{4.134}$$

By inspecting this last expression, we can already see that the probability of detecting all the photons, N out of N, is not one (unless $\Gamma\to\infty$). The chances of accepting each photon is $\Gamma/(\Gamma+\gamma_a)$

rather than unity, which clearly explains the origin of the distribution $P(n)$. We can delve into the temporal structure of the SE photon emission, that is, how the arrival times of each photon t_k (with $N \geq k > 0$) are distributed. The probability of the k-th photon of being detected at time t_k is measured through the joint probability distribution $\phi^{(N)}(\{t_k\})$. This distribution is linked to the photon counting distribution $p(t_1, \ldots, t_N)$, the probability of detecting the k photon up to t_k, as $p(\{t_k\}) = \int_0^{t_1} \ldots \int_0^{t_N} \phi^{(N)}(\{\tau_k\}) d\vec{\tau}$. Using the fundamental theorem of calculus, we can obtain the inverse relation, i.e., $\phi^{(N)}(t_1, \ldots, t_N) = \frac{\partial^N}{\partial t_1 \ldots \partial t_N} p(t_1, \ldots, t_N)$. The function can be expressed in terms of the one-photon detection probability $\mathcal{T}$, which is then, $p(t_1, \ldots, t_N) = N! \mathcal{T}(t_1) \prod_{k=1}^{N-1} (\mathcal{T}(t_{k+1}) - \mathcal{T}(t_k))$. With this, we are able to compute $\phi^{(N)}$ for the filtered emission:

This provides the joint probability distribution for the spontaneous emission of N photons, from which one can derive all statistical quantities of interest, as illustrated through, e.g., Eq. (4.138).

$$\phi_\Gamma^{(N)}(\{t_k\}) = N! \gamma_a^N \left(\frac{\Gamma}{F_{1\bar{1}}} \right)^{2N} \prod_{i=1}^{N} (e^{-\Gamma t_i/2} - e^{-\gamma_a t_i/2})^2 \mathbb{I}_{[t_{i-1}, t_{i+1}]}(t_i), \tag{4.135}$$

where $\mathbb{I}_T(t)$ is the indicator function which is one if $t \in T$ and zero everywhere else. The marginal distribution for the k-th photon, that describes the emission of a single photon, is found by integrating over all the times $t_{p \neq k}$ and yields

$$\phi_{\Gamma,k}^{(N)} = -(\Gamma / F_{1\bar{1}})^{2N} \gamma_a^N k \binom{N}{k} g(t_k)^{N-k} (g(0) - g(t_k))^{k-1} g'(t_k), \tag{4.136}$$

where $g(t) = \gamma_a^{-1} e^{-\gamma_a t} + \Gamma^{-1} e^{-\Gamma t} - 4 F_{11}^{-1} e^{-F_{11} t/2}$ and its derivative is $g'(t) = -(e^{-\Gamma t/2} - e^{-\gamma_a t/2})$. The mean arrival time and other higher-order moments are simply computed as $\langle (t_k^{(N)})^n \rangle = \int_0^\infty t_k^n \phi_k^{(N)}(t_k) dt_k$. This distribution, however, is only valid if all the photons are ultimately detected, that is, it describes the temporal structure of the N-photon emission. Then, we shall define the conditional k-th photon probability $\varphi_k^{(N)}(t)$, valid for any size of the final photon bundle (whether all the photons are detected or not). The expression is written in terms of the probabilities $P(k, N)$ and the marginal distributions $\phi_{\Gamma,k}^{(n)}$ (where $n \leq N$). Using the law of total probability, we find

$$\varphi_k^{(N)}(t_k) = \sum_{n=k}^{N} \frac{P(n, N)}{P(n, n)} \phi_{\Gamma,k}^{(n)}(t_k), \tag{4.137}$$

where the normalisation of the conditional distribution is not one but $\mathcal{N}(k, N) \equiv \sum_{n=k}^{N} P(n, N) = \Gamma^k \gamma_a^{N-k} / F_{11}^N \binom{N}{k} {}_2F_1(1, k - N, k + 1, -\Gamma/\gamma_a)$.

In the same way, we have defined the moments of t_k for the full or unbroken bundle emission, we can compute their counterparts for the conditional distribution, taking into account the broken bundles too. In Figure 4.5 is shown the full distribution for $N = 2$ (the only case that can be represented in 3D) together with its marginal distributions and the marginal distributions, $\phi_k^{(n)}$ and $\varphi_k^{(n)}$, for the 5-photon bundle. Besides the theoretical curves, the distributions are numerically obtained from frequency-resolved Monte Carlo simulations of the SE. The expressions for the mean time are enough complicated so we only include first-order properties here. Prior to writing down the equation, we have to define the summation $\sum_{\{k_i\}} \equiv \sum_{k_1+k_2+k_3=N-k} \sum_{k_1+\ldots+k_9=k-1} \sum_{k_{10}+k_{11}=2}$ over the 11 indices. Then,

$$\langle t_k^{(N)} \rangle = 2N! \left(\frac{\gamma_a \Gamma F_{11}}{F_{1\bar{1}}^2} \right)^N \sum_{\{k_i\}} \prod_{j=1}^{11} \frac{1}{k_j!} \times \frac{(-1)^{k_3+k_6+k_7+k_8+k_{11}}}{\gamma_a^{\Sigma_1} \Gamma^{\Sigma_2} (F_{11}/4)^{\Sigma_3} \left[\gamma_a \Sigma_4 + \Gamma \Sigma_5 + F_{11}/2(k_3+k_9)\right]^2}, \tag{4.138}$$

where $\Sigma_1 \equiv k_1 + k_4 + k_7$, $\Sigma_2 \equiv k_2 + k_5 + k_8$, $\Sigma_3 \equiv k_3 + k_6 + k_9$, $\Sigma_4 \equiv k_1 + k_7 + k_{11}/2$ and $\Sigma_5 \equiv k_2 + k_8 + k_{10}/2$. In the unfiltered limit ($\Gamma \to \infty$), we recover $\langle t_k^{(N)} \rangle \to (H_N - H_{N-k})/\gamma_a$, where H_N is the N-th Harmonic number (assuming $H_0 = 0$). Within the same limit, the (time) size of the bundle, that is, the time elapsed between the arrival of the first and last photon is $\langle \tau \rangle_N = \langle t_N^{(N)} \rangle - \langle t_1^{(N)} \rangle = H_{N-1}/\gamma_a$ (already reported in Refs. [6, 76]). Furthermore, the mean delay of the k-th photon tends to $\langle t_k^{(N)} \rangle - \langle t_{k-1}^{(N)} \rangle \to 1/(k\gamma_a)$ (that also has been measured in Refs. [77, 78]). On the other hand, for very narrow filters ($\Gamma \to 0$), the bundle structure is dominated by the filter dynamics so that $\langle t_k^{(N)} \rangle \to (H_N - H_{N-k})/\Gamma$ and therefore the bundle size goes to $\langle \tau \rangle_N \to H_{N-1}/\Gamma$.

Sticking to 2-photon bundle, we obtain the WTD from the joint distribution $\phi_\Gamma^{(2)}(t_1, t_2)$. The delay time of the second is $\tau = t_2 - t_1$ or, inverting the relation, $t_2 = t_1 + \tau$. Then, the distribution reads $w(\tau) = \int_0^\infty \phi_\Gamma^{(2)}(t_1, t_1 + \tau) dt_1$ and, after substituting, we get

$$\boxed{w(\tau) = \frac{\Gamma \gamma_a F_{11}}{F_{1\bar{1}}^2 F_{31} F_{13}} \left(\Gamma F_{31} e^{-\gamma_a \tau} + \gamma_a F_{13} e^{-\Gamma \tau} - 8\Gamma \gamma_a e^{-F_{11}\tau/2} \right).} \tag{4.139}$$

The waiting time distribution for the SE of 2 photons is the most exotic case study of our list and serves as an interesting reference point for multiphoton emission.

This quantity is especially interesting because it allows direct comparison of 2-photon emission in SE, which we have thoroughly analysed,

with more complex systems with multiphoton emission such as the *bundler* [6], a source of N-photon bundles (actually with $N = 2$), realised as a 2LS coupled to a cavity (Jaynes–Cummings) and the toy-model of Continuous Wave Spontaneous Emission (CWSE) (see [Z3]), in which the stream of photons is generated by randomly triggered 2-photon SE bundles that emulates the CW uncorrelated emission of bundles, including the broken ones induced by the spectral filtering. We gather information about filtered emission of the former performing a Monte Carlo simulation [27]. In Fig. 4.6, we show the waiting time distribution and the bundle purity π_2, i.e., the percentage of pristine or unbroken bundles, of both CWSE model and the actual bundler. The main features of the emission qualitatively agrees if the purity π_2 is equal for both CW models (thus we do not display both curves with the same purity for the sake of clarity). However, the CWSE model fails to reproduce the exact bundler purity curve as a function of the filter width Γ. The bundler emission has actually a greater number of unbroken bundles for each filter width than the CWSE case. This could be due to a dynamical effect between each N-Fock state collapse that slows down the emission but, nevertheless, prevents the photon bundle from breaking.

Other typical cases of multiphoton emission is the thermal state. We have discussed the thermal emission of an incoherently-driven cavity in Section 4.3 and obtained the multiphoton correlators $g^{(n)}(\vec{\tau})$. We complement the description computing the waiting time distribution. Using (1.57) applied to (4.74a) and inverting the Laplace transform, we find

This waiting time distribution for the thermal state completes our list of analytical results for the most important and fundamental types of photon emission.

$$w_{\rm th}(\tau) = \frac{2\gamma_a P_a}{Q_a(\gamma_a - P_a)} \exp\left[-\frac{\gamma_a^2 + P_a^2}{2(\gamma_a - P_a)}\right] \left[Q_a \cosh\left(\frac{Q_a \tau}{2(\gamma_a - P_a)}\right) - 2P_a\gamma_a \sinh\left(\frac{Q_a \tau}{2(\gamma_a - P_a)}\right)\right], \tag{4.140}$$

where $Q_a = \sqrt{(\gamma_a - P_a)^4 + 4P_a^2\gamma_a^2}$. This distribution behaves similar by to the rest of the WTDs in the unfiltered limit but differs qualitatively under filtering. For instance, the average mean time $\langle \tau_\Gamma \rangle_{\rm th}$ is also completely different (see Appendix A.10). Inspecting the limit $\Gamma \to \infty$, we obtain $\langle \tau_\infty \rangle_{\rm th} = (\gamma_a - P_a)/(P_a\gamma_a)$, which is bounded between 0 and 1 (in units of γ_a^{-1}), whereas the SE emission is quantised. The effective state of the filtered thermal emission is not thermal any more (the resulting dynamics is different). Only in the limit of narrow filters, in which any kind of emission is effectively thermalised, we recover the thermal state, although the effective temperature is different from $\theta = P_a/\gamma_a$, as we will see. In fact, we find

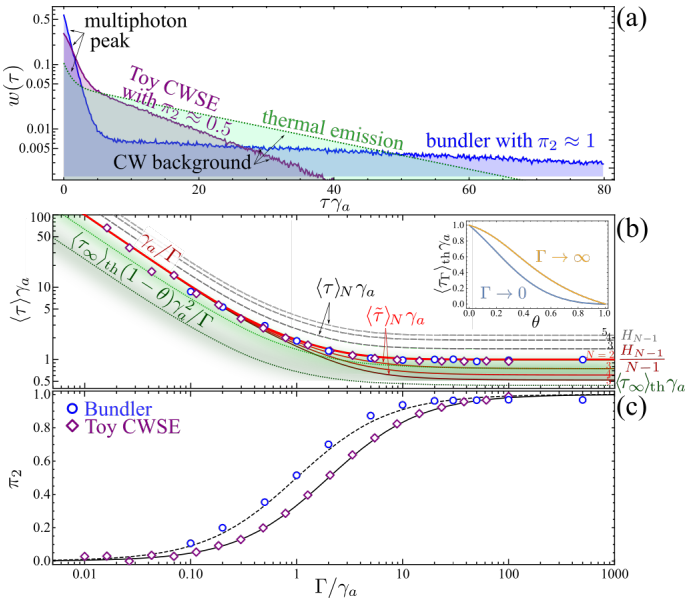

This figure shows that the dynamical emission of photon bundles differs qualitatively from the SE of a photon Fock state. This suggests that important dynamical aspects intervene in the general problem of multiphoton emission.

Figure 4.6: Dynamical description of the multiphoton emission. The waiting time distribution for the CWSE toy-model (in purple), the actual bundler (in blue) and the thermal state (in green) showed in (a). In all the cases, the distributions display a multiphoton peak on top of the background CW emission tail. With same purity π_2, bundler and toy-model curves would perfectly overlap. In (b), mean time of the multiphoton peak as a function of the filter width Γ for the pure multiphoton emission $\langle\tilde{\tau}\rangle_N$ (N from 2 to 5). Both the bundler (blue dots) and the toy-model (purple diamonds) agrees with this description. The thermal emission, however, always conserves contributions of all orders and hence $\langle\tau_\Gamma\rangle_{\rm th}$ is not quantised. In the narrow and wide filter limit, the filtered thermal mean time is shown in the inset as function of the reduced temperature $\theta = P_a/\gamma_a$. In (c), the two-photon purity for the SE (dashed and solid lines, where the decay rates are $\gamma/2$ and γ, respectively), the toy-model (diamonds) and the bundler (circles). The latter exhibits greater purity and fits the dashed line (with decay rate $\gamma_a/2$).

that $\gamma_a\langle\tau_0\rangle_{\rm th} = \langle\tau_\infty\rangle_{\rm th}(1-\theta)/\Gamma$. In contrast, when the multiphoton emission is filtered, a family of fragmented bundles of several sizes is produced. This is reflected in the WTD shape, which is decomposed in the multiphoton peak (closer to zero) and the background (CW) emission (from different bundles) that survives for longer times.

The multiphoton peak contribution can be detached from the whole WTD and has a characteristic mean time

$$\langle\tilde{\tau}\rangle_N = \sum_{k=2}^{N} \frac{(\langle t_k^{(N)}\rangle - \langle t_1^{(N)}\rangle)}{k-1} P(k,N) \Big/ \sum_{k=2}^{N} P(k,N)\,, \tag{4.141}$$

taking into account broken bundles of different sizes, and behaves differently from the filtered thermal emission, that keeps multiphoton

events of all the orders (for finite filter widths and unfiltered cases). The narrow filter, however, leads to thermalisation no matter the origin of the state. The thermal field, in particular, displays an interesting feature. For $\Gamma \to 0$, the emission stays thermal but, at the same time, is monochromatic. The effective temperature of the state is $\theta_\Gamma = P_a\gamma_a/[P_a^2 + (\gamma_a + \Gamma)(\gamma_a - P_a)]$, which is greater than θ if $\Gamma < P_a$. This effect is induced by the filter dynamics that have a much longer time scale and clump the photons together.

Another important aspect we would like to investigate is how photon detection, that ultimately depends on the one-photon kernel $\mathcal{T}_\Gamma$, is affected by the shape of the filter and not only its width (which we have discussed above). We already have concluded that N-photon bundle could break when filtering it. So the question turns out to be which kind of filter is less detrimental, which one rejects, on average, less photons. A possible way to resolve this issue is to use the rejected light and redirect it towards a second filter. Then, we would expect a larger fraction of accepted photons. Repeating the process (depicted in Fig 4.7) n times should enlarge the one-photon detection probability even more, given that we are increasing the chances of a rejected photon to be eventually accepted. For an infinite chain of filters ($n \to \infty$), we are confident that every photon eventually arrive.

We define the joint or total probability distribution $p_{\text{tot}}(n; T \to \infty)$, that is, the probability distribution if we take into account the n detectors. To find this, we need to know the total intensity Ω_{tot} to generate the correct distribution. Since each detector records its signal independently (this statement does not imply that the signals are independent), the total intensity is just the sum of the intensities, i.e., $\Omega_{\text{tot}} = \sum_{k=1}^{n} \Omega_k$ (where Ω_k is the intensity of the k-th detector). For the case of interest, this yields $\Omega_{\text{tot}} = \xi\gamma_a(\sum_{k=1}^{n} I_F^{(k)})(a^\dagger a)$, which effectively looks like a single filter. We may solve each integral $I_F^{(k)}$ separately and then gather all the contributions or make the following sum

$$\begin{aligned}\sum_{k=1}^{n} I_F^{(k)} &= \sum_{k=1}^{n} \frac{1}{2\pi}\int_{-\infty}^{\infty} \frac{|\check{F}(\omega)|^2|1-\check{F}(\omega)|^{2(k-1)}}{(\gamma_a/2)^2 + (\omega-\omega_a)^2}\, d\omega \\ &= \frac{1}{2\pi}\int_{-\infty}^{\infty} \frac{|\check{F}(\omega)|^2\left(\sum_{k=1}^{n}|1-\check{F}(\omega)|^{2(k-1)}\right)}{(\gamma_a/2)^2 + (\omega-\omega_a)^2}\, d\omega\,, \end{aligned} \tag{4.142}$$

where the sum in the integrand is a geometric sum and can be rewritten as

$$S_F^{(n)}(\omega) = \sum_{k=1}^{n} |1-\check{F}(\omega)|^{2(k-1)} = \frac{1-|1-\check{F}(\omega)|^{2n}}{1-|1-\check{F}(\omega)|^2}\,, \tag{4.143}$$

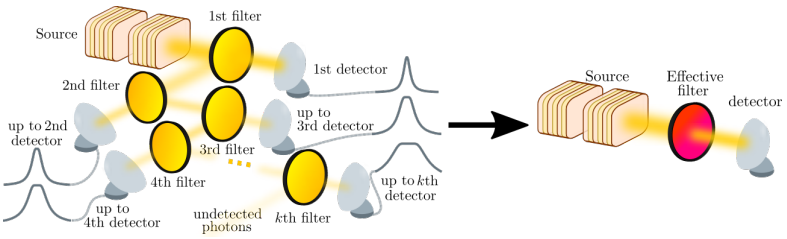

Figure 4.7: Possible filter setup to build the composite filter $S^{(n)}$. The light in sent to an interference (Lorentzian) filter and the transmitted light is subsequently detected. The rejected (reflected) fraction is directed to a second filter and collected by a detector. The procedure is repeated up to n filters. Eventually, considering the collective action of the n detectors is effectively identical to a single filter with spectral response $S^{(n)}$.

and then we turn the sum of integrals into a single integral

$$J_F^{(n)} = \sum_{k=1}^{n} I_F^{(k)} = \frac{1}{2\pi}\int_{-\infty}^{\infty} \frac{|\check{F}(\omega)|^2 S_F^{(n)}(\omega)}{(\gamma_a/2)^2 + (\omega-\omega_a)^2}\, d\omega\,. \tag{4.144}$$

Again, if we select the Lorentzian case, the sum of filters $S_F^{(n)}(\omega)$ is then

$$S_F^{(n)}(\omega) = \frac{1 - \left[\frac{(\omega-\omega_1)^2}{(\Gamma/2)^2+(\omega-\omega_1)^2}\right]^n}{1 - \frac{(\omega-\omega_1)^2}{(\Gamma/2)^2+(\omega-\omega_1)^2}}, \tag{4.145}$$

and the effective filter within the integrand $J_F^{(n)}$ reads

$$|\check{F}_{\mathrm{L}}^{(n)}(\omega)|^2 = |\check{F}_L(\omega)|^2 S_F^{(n)}(\omega) = 1 - \left(\frac{(\omega-\omega_1)^2}{(\Gamma/2)^2 + (\omega-\omega_1)^2}\right)^n, \tag{4.146}$$

and if we take the limit $n \to \infty$, we find

$$S_F^{(\infty)}(\omega) = \frac{1}{1 - \frac{(\omega-\omega_1)^2}{(\Gamma/2)^2+(\omega-\omega_1)^2}} = \frac{(\Gamma/2)^2 + (\omega-\omega_1)^2}{(\Gamma/2)^2} = \frac{1}{|\check{F}_{\mathrm{L}}|^2}, \tag{4.147}$$

so that $|\check{F}_{\mathrm{L}}^{(\infty)}(\omega)|^2 = S_F^{(\infty)}(\omega)|\check{F}_{\mathrm{L}}(\omega)|^2 = 1$. This means that an infinite series of filters with fixed width Γ leads to a white spectrum and thus each photon will be detected. The composite filter becomes flatter around its top as the order n increases. The FWHM turns out to be $\Gamma_n = \Gamma(2^{1/n}-1)^{-1/2}$, that grows like $\Gamma\sqrt{2n/\log(2)}$. Knowing that, we can build up a filter that retains this shape but has FWHM equal

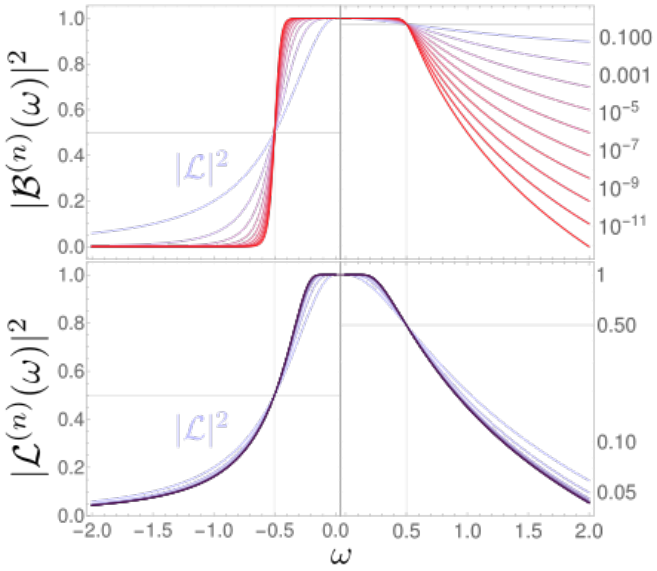

Figure 4.8: Butterworth filter ($\mathcal{B}^{(n)}$) shape for different orders compared to the Lorentzian ($\mathcal{L}^{(1)}$) shown in the upper plot. The left-hand side of the plot is in linear scale, whereas the right-hand side is in log scale. The lower plot displays the composite filters ($\mathcal{L}^{(n)}$) with the same FWHM, equal to Γ.

to Γ. It is achieved by substituting the filter width $\Gamma \to \Gamma\sqrt{2^{1/n}-1}$. Interestingly, an infinite chain of filters having this width will converge to the following filter

$$|\check{F}_{\mathrm{L}}^{(\infty)}(\omega)|^2 = 1 - 2^{-(\Gamma/2)^2/(\omega-\omega_1)^2}\,. \tag{4.148}$$

which is non-analytic at its maximum.

Other types of filters that we can include in this comparison are the Butterworth filters (see Fig. 4.8),

$$|\check{F}_{\mathrm{BW}}^{(n)}|^2 = \frac{(\Gamma/2)^{2n}}{(\Gamma/2)^{2n} + (\omega-\omega_1)^{2n}}\,, \tag{4.149}$$

which, in the case $\omega_1 = \omega_a$, the one-photon kernel integral I_F yields

$$I_{\mathrm{BW}}^{(n)} = \frac{1}{1+(-\beta^2)^n}\left(1 - \frac{\beta}{n}\sum_{p=0}^{n-1}\frac{(-\beta^2)^{n-1-p}}{\sin[\frac{\pi}{2n}(2p+1)]}\,,\right) \tag{4.150}$$

where $\beta \equiv \gamma_a/\Gamma$. Another possible filter is the square filter

$$|\check{F}_{\mathrm{Sq}}^{(n)}|^2 = \theta(\omega-\omega_1+\Gamma/2)\theta(\Gamma/2-\omega+\omega_1)\,, \tag{4.151}$$

that is not zero around when $\Gamma/2 < \omega - \omega_1 < -\Gamma/2$. Assuming that $\omega_1 = \omega_a$, the integral has the following expression

$$I_{\mathrm{Sq}} = \frac{2}{\pi}\arctan(\Gamma/\gamma_a)\,. \tag{4.152}$$

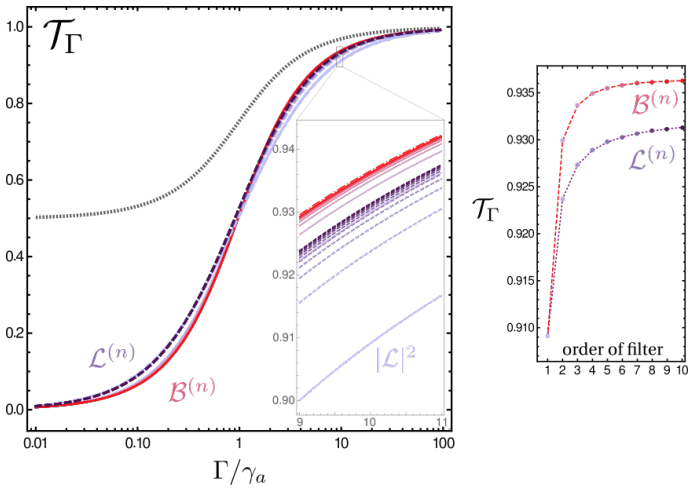

No filtering scheme is perfect and improvements from the family of filters widely available are fairly modest. This makes the simplest Lorentzian type of filter of great use for qualitative studies.

Figure 4.9: One-photon detection probability for different kinds of filters as a function of the filter width. Lorentzian and composite filters ($\mathcal{L}^{(n)}$) are shown in blue while the Butterworth filters ($\mathcal{B}^{(n)}$) have different shades of red. The artificial squared filter that optimises the one-photon detection probability, obtained from Eq. (4.153), corresponds to the black dotted line. In the right hand side there is a comparison of the two families of filters with fixed width $\Gamma = 10\gamma_a$ for increasing order. For flatter filters, the photon collection improves and eventually saturates to the square filter (Butterworth) and the non-analytical filter (composite).

Lastly, we consider the optimum filter that fulfil the FWHM criterion. It is trivial to see that this filter consists of two parts: around ω_1, in a frequency window with width Γ, a square top with value 1 and, outside this region, the filter has value 1/2. In such a case, the single-photon detection probability is

$$I_{\text{Opt}} = \frac{1}{2} + \frac{1}{\pi}\arctan(\Gamma/\gamma_a)\,. \tag{4.153}$$

Despite of how unrealistic this filter is, it provides an upper bound for the one-photon detection probability for a fixed FWHM, shown in Fig. 4.9 as the black dotted line and grows from 0.5 to 1. The composite filters keep more signal than the Butterworth ones for widths less than the natural linewidth of the cavity because of the fat tails (it decays like ω^{-2}), which have greater overlap (better for higher order n). However, for $\Gamma > \gamma_a$ we have the opposite situation. The flatter top of the Butterworth filters within the region $|\omega - \omega_a| < \Gamma$ increases the chances of accepting the photons. For increasing order, all the filters are flatter around the maximum, which increases the chances of detecting the photon. However, both the Butterworth and the composite filter rapidly converge to the square filter (4.151) and the non-analytical filter (4.148), respectively. The probability is never

equal to one although they reach values closer to one, so the filters maintain, in the end, the bundle structure mostly untouched.

With such results, the next step, which is beyond scope of this Thesis, would be to apply these filters to the actual bundle emission. In Ref. [79] is shown that the spectral filtering seems to increase the bundle purity rather than destroying the bundle integrity. The bundler is system under excitation and beside the N-photon bundle, other kinds of transitions are taking place and contaminate the emission. Filtering around the desired transition should eliminate or, at least, reduce the appearance of these unwanted photons. However, what we find in this work is that narrow filters, below the linewidth of the emitter, have a noticeable detrimental effect on the bundle. Then, it has to exist an optimum filter width Γ that, on one hand, keeps the secondary or non-bundling emission away and, on the other hand, is wide enough to retain the bundle structure. As well, the type of filter could play an important role. Flatter filters, like high-order Butterworth filters, seem to have better overlapping (in the region where $\Gamma > \gamma_a$) than Lorentzian filters. So the prospects of designing a reliable source of N-photon bundles could be aimed to follow these ideas.

5

SPATIAL CORRELATIONS IN LIGHT-MATTER SYSTEMS

In general, continuous variable systems, i.e., when position or momentum are spread all over a dense set (it could be finite or infinite) present difficulties to be faithfully described. Some frequency cut-off is needed or the wave-function has to be discretised. However, sometimes solving the whole many-particle problem is not mandatory. For instance, to know the mean number of particles and how they are distributed in space or in momentum (this is usually called the particle density $\rho^{(1)}(x)$), only a particular set of correlators is required. If we want to compute, e.g., the mean distance between particles, which involve two body measurements, then finding two point correlations suffices.

In the second quantisation formalism, the family of n-particle density distributions is written in terms of the field operator

$$\Psi^\dagger(x) = \sum_m \phi_m^*(x) a_m^\dagger \,, \tag{5.1}$$

where $\phi_m(x)$ is the one-particle wavefunction corresponding to the m-th state $|m\rangle$ and $a_m^\dagger$ is the creation operator of this state (we have not set the statistics of the particles as yet). The functions $\phi_m(x)$ have to comprise a complete set of orthonormal functions, so that, $\langle m|m'\rangle = \int \phi_m^*(x)\phi_{m'}(x)dx = \delta_{m,m'}$, where $\delta_{m,m'}$ is the Kronecker delta function. Here, x may stand for the position coordinates in any dimension and the domain, the region of integration, can be either finite or infinite. For continuous sets of *quantum numbers*, the sum over the states and the Kronecker delta are substituted by an integral and the Dirac delta, respectively.

The physical meaning of the operator in Eq. (5.1) is easy to understand when applied on the vacuum state $|0\rangle$ and projected in the position basis:

$$\begin{aligned} \langle x|\, \Psi^\dagger(x')\, |0\rangle &= \sum_m \langle x|\, \phi_m^*(x') a_m^\dagger\, |0\rangle = \sum_m \phi_m^*(x')\, \langle x|m\rangle \\ &= \sum_m \langle x|m\rangle \langle m|x'\rangle = \langle x| \left(\sum_m |m\rangle \langle m| \right) |x'\rangle \,. \end{aligned} \tag{5.2}$$

Since $|m\rangle$ is part of a complete set of states, we can make use of the identity $\mathbf{1} = \sum_p |p\rangle \langle p|$ to finally get

$$\langle x| \Psi^\dagger(x') |0\rangle = \langle x|x'\rangle = \delta(x - x') \,. \tag{5.3}$$

That is, the field operator creates or locates a particle at the position $x = x'$. For the moment, we have not included times, namely t and t', in this description and incorporating them requires some extra steps. We would like that $\Psi^\dagger(x', t')$ places a particle at space-time coordinates (x', t'). In the Schrödinger picture, for instance, replacing $\phi_p^*(x')$ by $\phi_p^*(x', t')$ (and $|p\rangle$ by $|p(t)\rangle$ as well) will work if $t > t'$ but not the other way around since the creation of this particle must not affect the past. Later on, we will complete the explanations and define the field operator properly.

For the moment, timeless (or same time $t = t'$) field operators are enough to describe particle density operators and, after them, their density functions. We present here the 1-particle density operator

$$\hat{n}^{(1)}(x) = \Psi^\dagger(x)\Psi(x) \,. \tag{5.4}$$

In order to find its position representation, we first need to know if $\hat{n}^{(1)}(x)$ conserves the total number of particles. If so, $\hat{n}^{(1)}(x)$ has a very simple expression for each N-particle subspace $\mathcal{H}_N$. This is the case since the commutator $[\hat{N}, \hat{n}^{(1)}(x)] = 0$, where $\hat{N} = \sum_i a_i^\dagger a_i$ is the number operator. When it is applied on the N-particle Hilbert space

$$\langle \mathbf{x}| \hat{n}^{(1)} |\mathbf{x}\rangle = n^{(1)}(x) = \sum_{i=1}^{N} \delta(x - x_i) \,, \tag{5.5}$$

which has exactly the same expression as the classical case. From this definition (5.5), we can derive the expression of the particle density for a general many-body quantum state ρ (not necessarily a pure quantum state $|\psi\rangle$). Let us start with a pure state. For a general state, we can split it into a sum of states with the same quantum number for the operator $\hat{N}$ [80]

$$|\psi\rangle = \sum_{n=0}^{\infty} c^{(n)} |\psi_n\rangle \,, \tag{5.6}$$

such that $\sum_{n=0}^{\infty} |c^{(n)}|^2 = 1$ and each *subspace* only contains states with n particles. For instance, $|\psi_0\rangle = |0\rangle$ and $|\psi_1\rangle = \sum_p c_p^{(n)} a_p^\dagger |0\rangle = |\psi_1\rangle = \sum_p c_p^{(n)} |1_p\rangle$. For the n-particle state

$$|\psi_n\rangle = \sum_{\vec{p}_n} c_{\vec{p}_n}^{(n)} |\vec{p}_n\rangle \,, \tag{5.7}$$

where $\vec{p}_n$ is a n-vector with the quantum numbers that occupies each particle. If the system allows two or more particles to be in the same quantum state, this number will appear repeated as many times as needed in the quantum state vector $\vec{p}$. The sum over the squared modulus of the coefficients $c_{\vec{p}}^{(n)}$ must return $|c^{(n)}|^2$, naturally. This implies that the global coefficient $c^{(n)}$ is defined by its constituents up to a global phase which has to be chosen as an independent parameter.

We can define an extended family of states through the density matrix formalism. Besides these pure states, namely $\rho = |\psi\rangle \langle\psi|$, *mixed states* are also possible:

$$\rho = \sum_{m,n=0}^{\infty} \rho_{m,n} |n\rangle \langle m| \ , \tag{5.8}$$

where $|n\rangle$ ($\langle m|$) represents the quantum states with n particles (m particles in the adjoint space) and the elements $\rho_{m,n}$ is an abbreviated way of representing the matrix coefficients. Expanding this further,

$$\rho = \sum_{m,n=0}^{\infty} \chi(\vec{p}_n, \vec{q}_m) \ |\vec{p}_n\rangle \langle \vec{q}_m| \ , \tag{5.9}$$

where the coefficients $\chi(\vec{p}_n, \vec{q}_m)$ are the matrix elements. Therefore, the probability of each state is given by the diagonal elements $\chi(\vec{p}_n, \vec{p}_n)$. With this, we are able to calculate n-particle density matrices [81]. For one particle, the diagonal part of the matrix is

$$\rho^{(1)}(x) = \langle \hat{n}^{(1)}(x) \rangle = \int d\mathbf{x} \, \langle \mathbf{x}| \, \rho \, \hat{n}^{(1)}(x) \, |\mathbf{x}\rangle \ . \tag{5.10}$$

In the same manner, the 2 particle diagonal density matrix is

$$\rho^{(2)}(x, x') = \langle : \hat{n}^{(1)}(x) \hat{n}^{(1)}(x') : \rangle = \int d\mathbf{x} \, \langle \mathbf{x}| \, \rho \, (: \hat{n}^{(1)}(x) \hat{n}^{(1)}(x') :) \, |\mathbf{x}\rangle \ . \tag{5.11}$$

In term of the field operators,

$$\rho^{(1)}(x) = \sum_{p,q} \mathrm{tr}\Big\{ \rho a_p^\dagger a_q \Big\} \phi_p^*(x) \phi_q(x) = \sum_{p,q} \langle a_p^\dagger a_q \rangle \, \langle x|q\rangle \, \langle p|x\rangle \ , \tag{5.12}$$

and

$$\begin{aligned} \rho^{(2)}(x, x') = & \sum_{p,p',q,q'} \mathrm{tr}\Big\{ \rho a_p^\dagger a_{p'}^\dagger a_{q'} a_q \Big\} \phi_p^*(x) \phi_{p'}^*(x') \phi_{q'}(x') \phi_q(x) = \\ & \sum_{p,p',q,q'} \langle a_p^\dagger a_{p'}^\dagger a_{q'} a_q \rangle \, \langle x|q\rangle \, \langle x'|q'\rangle \, \langle p'|x'\rangle \, \langle p|x\rangle \ , \end{aligned} \tag{5.13}$$

and so on.

Since Eq. (5.13) is written in term of one-particle wavefunctions, the overall reduced density matrix has the same symmetry than particles. For fermions, $\langle a_p^\dagger a_{p'}^\dagger a_q a_{q'}\rangle = -\langle a_p^\dagger a_{p'}^\dagger a_{q'} a_q\rangle$ and the same change of sign for interchanging p and p'. Then, fixing an order for the indices, the summation over (p,p') and (p',p) ((q',q) and (q,q') too) will give $\langle a_p^\dagger a_{p'}^\dagger a_{q'} a_q\rangle(\phi_p^*(x)\phi_{p'}^*(x') - \phi_{p'}^*(x)\phi_p^*(x'))(\phi_q(x)\phi_{q'}(x') - \phi_{q'}(x)\phi_q(x'))$. Now, the wavefunction is explicitly antisymmetric. The same idea applies for bosons, changing the minus sign for a plus one. In addition, when $p = p'$ (or $q = q'$), the fermionic correlators give zero while the bosonic ones get magnified by a factor $\sqrt{2}$.

The integration of $\rho^{(1)}(x)$ and $\rho^{(2)}(x,x')$ over the space x and x' leads, as expected, to $\langle\hat{N}\rangle$ and $\langle{:}\,\hat{N}^2\,{:}\rangle$, respectively. Therefore, they do not represent a probability distribution per se. However, normalising the reduced density matrices by the factor $\langle{:}\,\hat{N}^n\,{:}\rangle$ achieves this. Any one and two-body properties can be computed from these normalised reduced density matrices. For instance,

$$\langle f_1(\hat{x})\rangle = \frac{\mathrm{tr}\left\{\hat{\rho}^{(1)} f_1(\hat{x})\right\}}{\mathrm{tr}\left\{\hat{\rho}^{(1)}\right\}} = \frac{\int \rho^{(1)}(x) f_1(x) dx}{\langle\hat{N}\rangle}\,, \tag{5.14}$$

or, for two-body quantities,

$$\langle f_2(\hat{x},\hat{x}')\rangle = \frac{\mathrm{tr}\left\{\hat{\rho}^{(2)} f_2(\hat{x},\hat{x}')\right\}}{\mathrm{tr}\left\{\hat{\rho}^{(2)}\right\}} = \frac{\int \rho^{(2)}(x,x') f_2(x,x') dx dx'}{\langle{:}\,\hat{N}^2\,{:}\rangle}\,. \tag{5.15}$$

We will consider some general kind of states for fermions, bosons and classically indistinguishable particles. First, finite combinations of Fock states, e.g., $n-k$ particles in the state 0 and k in the state 1 (where labels 0 and 1 do not necessarily correspond to the ground and first excited states, respectively). After that, for bosons, we study Gaussian states with contribution from all number of particles such as coherent and thermal states. We will focus on the mean squared distance between two particles, that is, $\langle(x-x')^2\rangle$ in some particular systems like the 1D harmonic oscillator or the infinite square well. We also assume that particles do not interact with each other.

5.1 FOCK STATES WITH FIXED n

Hereafter, we denote fermion operators as c_p and $c_p^\dagger$. They fulfil the anticommutation rules

$$\{c_p, c_q^\dagger\} = \delta_{p,q} \quad \text{and} \quad \{c_p, c_q\} = 0\,. \tag{5.16}$$

Likewise, bosonic operators are indicated as a_p and $a_p^\dagger$ and follow the commutation rules

$$[a_p, a_q^\dagger] = \delta_{p,q} \quad \text{and} \quad [a_p, a_q] = 0\,. \tag{5.17}$$

Restricting the description to two different states that, without loss of generality, we label as 0 and 1, we can define the next possible states

$$|\phi_{\mathrm{F}}\rangle = c_1^\dagger c_0^\dagger\,|0\rangle = |1\,,1\rangle_{\mathrm{F}}\,, \tag{5.18}$$

and

$$|\phi_{\mathrm{B}}\rangle = \frac{1}{\sqrt{(n-k)!\,k!}} a_1^{\dagger k} a_0^{\dagger (n-k)}\,|0\rangle = |n-k\,,k\rangle_{\mathrm{B}}\,. \tag{5.19}$$

The fermionic case only admits one possible configuration because only one particle can occupy each state. Then, with two states we have two particles at most. The bosons, on the contrary, can share the same quantum number, so that with n particles, k on them can be in the second state. The corresponding correlators are, for the fermionic state,

$$\langle c_p^\dagger c_q\rangle_{\mathrm{F}} = \delta_{p,0}\delta_{q,0} + \delta_{p,1}\delta_{q,1}\,, \tag{5.20}$$

and

$$\langle c_p^\dagger c_{p'}^\dagger c_{q'} c_q\rangle_{\mathrm{F}} = \left(\delta_{p,1}\delta_{p',0} - \delta_{p,0}\delta_{p',1}\right)\left(\delta_{q,1}\delta_{q',0} - \delta_{q,0}\delta_{q',1}\right)\,. \tag{5.21}$$

Then, substituting these in Eqs. (5.12) and (5.13), we find the 1-particle and 2-particle reduced density matrix associated to $|\phi_{\mathrm{F}}\rangle$ as

$$\boxed{\rho_{\mathrm{F}}^{(1)}(x) = |\phi_0(x)|^2 + |\phi_1(x)|^2\,,} \tag{5.22}$$

These provide the density matrices, here for the Fermion case, from which one can derive spatial correlations of multi-particle observables. This is to be compared with the expressions for $\rho_{B,C}$ below.

and

$$\boxed{\rho_{\mathrm{F}}^{(2)}(x,x') = |\phi_0(x)\phi_1(x') - \phi_1(x)\phi_0(x')|^2 = 2|\phi_{01}^{(-)}(x,x')|^2\,,} \tag{5.23}$$

where $\phi_{01}^{(-)}(x,x') = (\phi_0(x)\phi_1(x') - \phi_1(x)\phi_0(x'))/\sqrt{2}$ is the antisymmetrised wavefunction with one particle in each state.

On the other hand, the bosonic counterparts give

$$\langle a_p^\dagger a_q\rangle_{\mathrm{B}} = (n-k)\delta_{p,0}\delta_{q,0} + k\delta_{p,1}\delta_{q,1}\,, \tag{5.24}$$

and

$$\begin{aligned}\langle a_p^\dagger a_{p'}^\dagger a_{q'} a_q\rangle_{\mathrm{B}} = {}& k(k-1)\delta_{p,0}\delta_{p',0}\delta_{q',0}\delta_{q,0} + \\ & (n-k)k\left(\delta_{p,1}\delta_{p',0} + \delta_{p,0}\delta_{p',1}\right)\left(\delta_{q,1}\delta_{q',0} + \delta_{q,0}\delta_{q',1}\right) + \\ & (n-k)(n-k-1)\delta_{p,1}\delta_{p',1}\delta_{q',1}\delta_{q,1}\,.\end{aligned} \tag{5.25}$$

Hence, inserting these results in (5.12) and (5.13), we find

$$\rho_{\mathrm{B}}^{(1)}(x) = (n-k)|\phi_0(x)|^2 + k\,|\phi_1(x)|^2\,, \tag{5.26}$$

$$\begin{aligned}\rho_{\mathrm{B}}^{(2)}(x,x') = &(n-k)(n-k-1)|\phi_0(x)\phi_0(x')|^2+\\ &(n-k)k\,|\phi_0(x)\phi_1(x')+\phi_1(x)\phi_0(x')|^2+\\ &k(k-1)|\phi_0(x)\phi_0(x')|^2\\ =&(n-k)(n-k-1)|\phi_{00}^{(+)}(x,x')|^2+\\ &2(n-k)k\,|\phi_{01}^{(+)}(x,x')|^2+\\ &k(k-1)|\phi_{11}^{(+)}(x,x')|^2\,,\end{aligned} \tag{5.27}$$

where $\phi_{pq}^{(+)}(x,x')$ are the symmetrised wavefunctions with two particles (with quantum numbers p and q). Hence the reduced density matrix is written in term of the 2-particle states as

$$\begin{aligned}\hat{\rho}_{\mathrm{B}}^{(2)} = \;&(n-k)(n-k-1)\,|2\,,0\rangle_{\mathrm{B}}\,\langle 2\,,0|_{\mathrm{B}}+\\ &2(n-k)k\,|1\,,1\rangle_{\mathrm{B}}\,\langle 1\,,1|_{\mathrm{B}}+\,k(k-1)\,|0\,,2\rangle_{\mathrm{B}}\,\langle 0\,,2|_{\mathrm{B}}\,.\end{aligned} \tag{5.28}$$

Then, the effective 2-particle state is a mixed state containing the three possible states, i.e., $|2\,,0\rangle_{\mathrm{B}}$ (two particles in the first state), $|0\,,2\rangle_{\mathrm{B}}$ (two particles in the second state) and $|1\,,1\rangle_{\mathrm{B}}$ (one particle in each state). The weights are the number of combinations to obtain those states, accounting for the two possible orders (due to the two spaces coordinates x and x'). For instance, if $n=4$ and $k=2$, there are 2 ways to get two particles in the state 0. The fermionic case, however, consists of only the single possible combination $|1\,,1\rangle_{\mathrm{F}}$.

So far we have not considered the third possibility mentioned before, the classically indistinguishable case. The particles is this situation do not obey any particular statistics so that, from the quantum-mechanical point of view, these are distinguishable. However, when measuring we are not able to tell apart which particle is being detected. Therefore, classically speaking, they are indistinguishable.

Such state with $n-k$ particles in the state 0 and k in the second one is $\phi^{(\mathrm{C})}(x_1,\ldots,x_n) = \prod_{p=1}^{n-k}\phi_0(x_p)\prod_{p=n-k+1}^{n}\phi_1(x_q)$, i.e., the product of single-particle wavefunctions. Applying the density operator $\hat{n}^{(1)}(x)$ to the density matrix $\rho_{\mathrm{C}}(\vec{x}) = |\phi^{(\mathrm{C})}(x_1,\ldots,x_n)|^2$ yields

$$\begin{aligned}\rho_{\mathrm{C}}^{(1)}(x) = \int \rho_{\mathrm{C}}(\vec{x})\Big(\sum_{p=1}^{n}\delta(x-x_p)\Big)dx_1\ldots dx_n =\\ (n-k)|\phi_0(x)|^2 + k|\phi_1(x)|^2\,.\end{aligned} \tag{5.29}$$

The one-particle density matrix is therefore the same as the bosonic case (5.26) and, if $n = 2$ and $k = 1$, both are identical to the fermionic one (5.22). Therefore, it is not possible to resolve the statistics from single-body measurements.

For two-body correlations, we need to find out the two-particle reduced density matrix for the distinguishable case. The two-particle density operator is $\hat{n}^{(2)}(x, x') =: \hat{n}^{(1)}(x)\hat{n}^{(1)}(x') :$ which in the position basis is

$$n^{(2)}(x, x') = \sum_{p=1}^{n} \sum_{q \neq p}^{n} \delta(x - x_p)\delta(x' - x_q)\,. \tag{5.30}$$

Counting how many ways we have to obtain the reduced states ($|0\,0\rangle$, $|1\,1\rangle$, $|1\,0\rangle$ and $|0\,1\rangle$), we obtain the same coefficients as (5.27). The 2-particle reduced density matrix is then

$$\begin{aligned}\rho_{\mathrm{C}}^{(2)}(x, x') &= \int \rho_{\mathrm{C}}(\vec{x}) \Big(\sum_{p=1}^{n} \sum_{q \neq p}^{n} \delta(x - x_p)\delta(x' - x_q) \Big) dx_1 \ldots dx_n \\ &= (n-k)(n-k-1)|\phi_0(x)\phi_0(x')|^2 + \\ &\quad (n-k)k\left(|\phi_0(x)\phi_1(x')|^2 + |\phi_1(x)\phi_0(x')|^2\right) + \\ &\quad k(k-1)|\phi_1(x)\phi_1(x')|^2\,. \end{aligned} \tag{5.31}$$

The main difference here is in the state with different quantum numbers, since $|0\,1\rangle$ and $|1\,0\rangle$ do not have any exchanging (anti)symmetry and thus they are different states. However, the overall state is indeed symmetric under the exchange $x \leftrightarrow x'$. We have found that the particle density $\rho^{(1)}(x)$, having the same configuration, is identical for all the ensembles (fermions, bosons and classical indistinguishable). The 2-particle density matrices are a mixture of the all possible two-particle states.

5.1.1 INFINITE SQUARE WELL

We have not specified neither the system nor its eigenstates as yet. Let us begin with the infinite square well of length L. The set of eigenfunctions are

$$\phi_n(x) = \sqrt{\frac{2}{L}} \sin\left(n\pi \frac{x}{L}\right), \tag{5.32}$$

for $0 < x < L$ and zero elsewhere. The quantum numbers n are all the positive integers. We choose 0 and 1 states to be $n = 1$ and $n = 2$ for simplicity. Then, the mean square distance is computed as

$$\langle (x - x')^2 \rangle_{\mathrm{S}} = \frac{\int \rho_{\mathrm{S}}^{(2)} (x - x')^2 \, dx dx'}{\int \rho_{\mathrm{S}}^{(2)} \, dx dx'}\,, \tag{5.33}$$

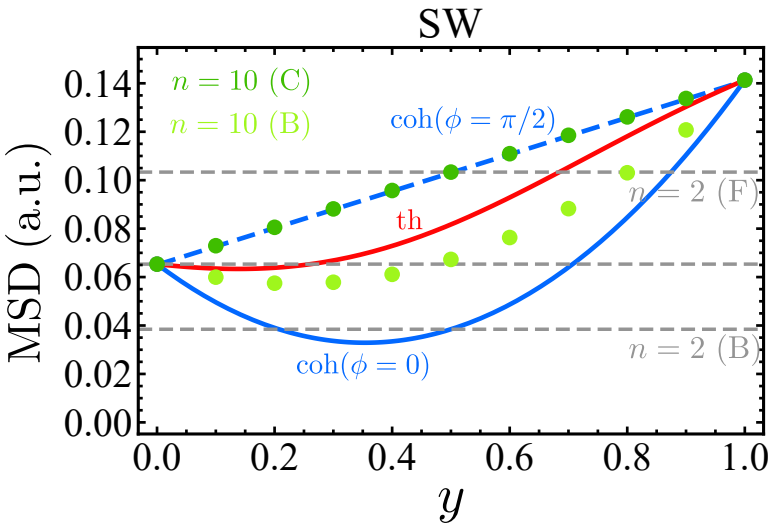

Figure 5.1: Mean squared distance $\langle (x - x')^2 \rangle$ as a function of the mixing parameter y for a Fock state of $n = 10$ particles, displayed as green points, and Gaussian multi-particle states (coherent in blue and thermal in red). The phase of the coherent state is chosen to minimise ($\theta = 0$, solid line) and maximise ($\theta = \pi/2$, dashed line) the MSD for any value of y.

where S indicates the statistics of the ensemble (fermions, bosons or none of both). With only two different states, the total number of particles is not the same for the three cases since the fermions cannot have more than two due to the Pauli exclusion principle. A way to compare them on equal footing is to fix $n = 2$ and $k = 1$ and take these results as a reference for the remaining cases. Choosing $n = 2$ and $k = 1$, the mean squared distance (MSD) in units of L^2 is

$$\langle (x - x')^2 \rangle_{\mathrm{F}} = \frac{1}{6} - \frac{5}{8\pi^2} + \frac{512}{81\pi^4}, \tag{5.34a}$$

$$\langle (x - x')^2 \rangle_{\mathrm{B}} = \frac{1}{6} - \frac{5}{8\pi^2} - \frac{512}{81\pi^4}, \tag{5.34b}$$

$$\langle (x - x')^2 \rangle_{\mathrm{D}} = \frac{1}{6} - \frac{5}{8\pi^2}. \tag{5.34c}$$

Even from this simple result, we can clearly see the effect of statistics on the correlations. This is a well-known behaviour in atomic and molecular Physics. Depending on the spin coordinates, the spatial wavefunction is either symmetric or antisymmetric. The electronic repulsion is greater when orbital overlapping is big or, in other words, when the mean distance between electrons is small. This is translated into an excess of Coulomb electrostatic energy which is usually identified in some tight-binding models, like the Hubbard model, as the U terms in the Hamiltonian.

The bosonic and classically indistinguishable cases can be extended to include more particles of both species:

$$\langle (x-x')^2 \rangle_{\mathrm{B}} = \frac{1}{6} - \frac{1}{\pi^2} + \frac{3k}{4\pi^2 n} - \frac{1024(n-k)k}{81\pi^4 n(n-1)}\,, \tag{5.35a}$$

$$\langle (x-x')^2 \rangle_{\mathrm{C}} = \frac{1}{6} - \frac{1}{\pi^2} + \frac{3k}{4\pi^2 n}\,. \tag{5.35b}$$

There is an obvious difference between the two ensembles. While $\langle (x-x')^2 \rangle_{\mathrm{D}}$ grows linearly with k, meaning that the minimum of MSD is always at $k = 0$, when all the particles are in the ground state, $\langle (x-x')^2 \rangle_{\mathrm{D}}$ has a region $0 < k \leq \lfloor k_0 \rfloor$ (where $k_0 = \frac{243\pi^2}{4096} + (1 - \frac{243\pi^2}{4096})n$) with its MSD below that minimum. The global minimum is around $k_0/2$, so it could be either $k = \lfloor k_0/2 \rfloor$ or $k = \lfloor k_0/2 \rfloor + 1$. The minimum MSD depends on the number of particle n and reaches its lowest value when $n = 2$ (as shown in Fig. 5.1) and increases as n enlarges.

In the limit of an infinite number of particles ($n \to \infty$), we can define the continuous variable $y \equiv k/n$ and equations (5.35) reduce to

$$\langle (x-x')^2 \rangle_{\mathrm{B}} = \frac{1}{6} - \frac{1}{\pi^2} + \frac{3y}{4\pi^2} - \frac{1024(1-y)y}{81\pi^4}\,, \tag{5.36a}$$

$$\langle (x-x')^2 \rangle_{\mathrm{D}} = \frac{1}{6} - \frac{1}{\pi^2} + \frac{3y}{4\pi^2}\,, \tag{5.36b}$$

which reveal the linear and parabolic behaviour of the MSD. Even in this limit, it is possible to find a minimum below the value at $y = k = 0$. Deriving with respect to y and solving the equation for the extrema, we find $y_{\min} = k_0/2$ and

$$\langle (x-x')^2 \rangle_{\mathrm{B}}(n \to \infty, k_0/2) = \frac{30581}{196608} - \frac{256}{81\pi^4} - \frac{5}{8\pi^2}\,. \tag{5.37}$$

5.1.2 1-D HARMONIC POTENTIAL

Another relevant example which brings analytical results is the one-dimensional harmonic potential, with parameter $m\,\omega$. The eigenfunctions are

$$\phi_n(x) = \frac{1}{\sqrt{2^n n!}} \left(\frac{m\omega}{\pi\hbar}\right)^{1/4} e^{-\frac{m\omega x^2}{2\hbar}} H_n\left(\sqrt{\frac{m\omega}{\pi\hbar}}\,x\right)\,, \tag{5.38}$$

where $H_n(u)$ are the Hermite polynomials and n are natural numbers including 0. We choose again the ground and the first excited states, i.e., $n = 0, 1$. In this system, the position x is not bounded and can

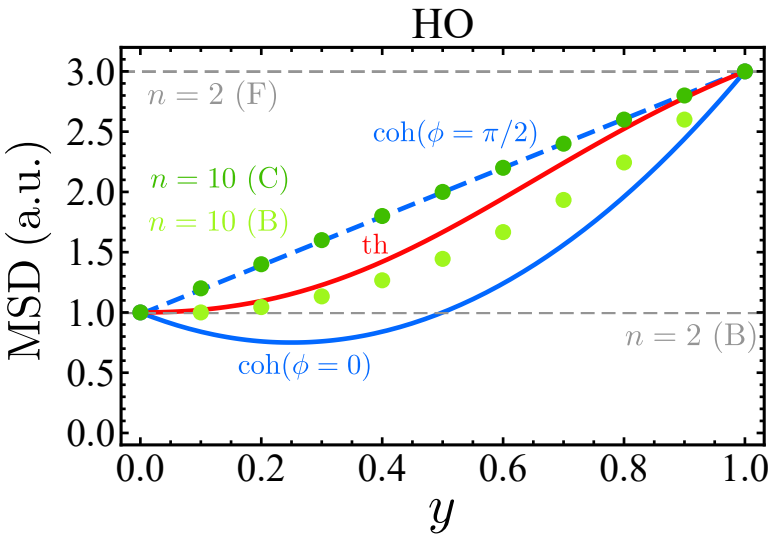

Figure 5.2: Mean squared distance $\langle (x - x')^2 \rangle$ as a function of the mixing parameter y for $n = 10$ Fock states, displayed as green points, and Gaussian multi-particle states (coherent in blue and thermal in red). The phase of the coherent state is chosen to minimise ($\theta = 0$, solid line) and maximise ($\theta = \pi/2$, dashed line) the MSD for any value of y.

take any value $x \in \mathbb{R}$. The characteristic length of the oscillator is $x_0 = \sqrt{\frac{\hbar}{m\omega}}$ and we thus write the MSD in units of x_0^2. We start calculating the case $n = 2$ and $k = 1$ for fermions, bosons and classically indistinguishable particles:

$$\langle (x - x')^2 \rangle_{\mathrm{F}} = 3\,, \tag{5.39a}$$
$$\langle (x - x')^2 \rangle_{\mathrm{B}} = 1\,, \tag{5.39b}$$
$$\langle (x - x')^2 \rangle_{\mathrm{C}} = 2\,. \tag{5.39c}$$

Again, the MSD is bigger for fermion and smaller for bosons compared to the distinguishable case, which is in the middle. The extension to more particles is straightforward:

$$\langle (x - x')^2 \rangle_{\mathrm{B}} = 1 + \frac{2k(k-1)}{n(n-1)}\,, \tag{5.40a}$$
$$\langle (x - x')^2 \rangle_{\mathrm{D}} = 1 + \frac{2k}{n}\,, \tag{5.40b}$$

From these equations we find that the distance is always greater for the classically indistinguishable case unless $k = 0$ or $k = n$ given that when all the particles are in the same state, the collective wavefunctions are identical. There are two minima for $\langle (x - x')^2 \rangle_{\mathrm{B}}$, one at $k = 0$ and a second one at $k = 1$. Both return the same result $\langle (x - x')^2 \rangle_{\mathrm{B}} = 1$. For greater values of k, unlike the previous case, the

distance grows monotonically. In the limit $n \to \infty$, we can define the coordinate $y \equiv k/n$, which goes from 0 to 1 and approximate (5.40) as $1 + 2y$ and $1 + 2y^2$, respectively.

5.2 GAUSSIAN STATES

So far, we have only dealt with quantum states with the number of particles N well-defined. With a few extra steps, we can extend these results to other kind of states, especially the Gaussian coherent and thermal states. The multi-mode version of them are easy to obtain due to the factorisation properties that they enjoy. The displacement operator is defined as

$$D(\vec{\alpha}) = \exp\left(\sum_k \alpha_k a_k^\dagger - \alpha_k^* a_k\right). \tag{5.41}$$

where $\alpha_k = |\alpha_k| e^{i\phi_k}$ are complex numbers. Having the commutation rules (5.17) and making use of the Baker-Campbell-Hausdorff lemma, we can factor out the single-mode displacement operators

$$D(\vec{\alpha}) = \prod_k e^{\alpha_k a_k^\dagger - \alpha_k^* a_k} = \prod_k D_k(\alpha_k)\,, \tag{5.42}$$

Moreover, we can exchange the order of the displacement operators, since each one do commute with the rest. The similarity transformations work identically. For f a function of the operators a_i and $a_i^\dagger$, that is, $f = f(a_1, a_1^\dagger \ldots, a_n, a_n^\dagger)$, transforms as

$$D^\dagger(\vec{\alpha}) f(a_1, a_1^\dagger \ldots, a_n, a_n^\dagger) D(\vec{\alpha}) = f(a_1{+}\alpha_1, a_1^\dagger{+}\alpha_1^* \ldots, a_n{+}\alpha_n, a_n^\dagger{+}\alpha_n^*)\,. \tag{5.43}$$

The multi-mode coherent state is defined as

$$|\vec{\alpha}\rangle = D(\vec{\alpha})\,|0\rangle\,. \tag{5.44}$$

Then, the one-body correlations are

$$\begin{aligned}\langle a_p^\dagger a_q\rangle = \; & \langle\vec{\alpha}|\, a_p^\dagger a_q\,|\vec{\alpha}\rangle = \langle 0|\, D^\dagger(\vec{\alpha}) a_p^\dagger a_q D(\vec{\alpha})\,|0\rangle \\ & \langle 0|\,(a_p^\dagger + \alpha_p^*)(a_q + \alpha_q)\,|0\rangle = \alpha_p^* \alpha_q\,.\end{aligned} \tag{5.45}$$

From the first to the second line, we used the property in Eq. (5.43). In the same manner, we get the two-body correlations as

$$\langle a_p^\dagger a_{p'}^\dagger a_{q'} a_q\rangle = \alpha_p^* \alpha_{p'}^* \alpha_{q'} \alpha_q\,. \tag{5.46}$$

The reduced density matrices are

$$\begin{aligned}\rho^{(1)}(x) &= \sum_p \sum_q \alpha_p^* \alpha_q \, \phi_p^*(x) \phi_q(x) \\ &= \Big(\sum_p \alpha_p^* \phi_p^*(x) \Big) \Big(\sum_q \alpha_q \phi_q(x) \Big) = \Big| \sum_q \alpha_q \phi_q(x) \Big|^2 . \end{aligned} \tag{5.47}$$

This result shows that a coherent state remains a pure state (up to a normalisation constant) which is a linear combination of the one-particle eigenfunctions. Moreover, this behaviour is inherited for the two-body reduced density matrix too.

$$\begin{aligned}\rho^{(2)}(x,x') &= \sum_p \sum_{p'} \sum_{q'} \sum_q \alpha_p^* \alpha_{p'}^* \alpha_{q'}' \alpha_q \, \phi_p^*(x) \phi_{p'}^*(x) \phi_{q'}(x') \phi_q(x) \\ &= \Big| \sum_q \alpha_q \phi_q(x) \Big|^2 \Big| \sum_{q'} \alpha_{q'} \phi_{q'}(x') \Big|^2 = \rho^{(1)}(x) \rho^{(1)}(x') . \end{aligned} \tag{5.48}$$

As a general statement, the n-particle reduced density matrix is a product of one-particle matrices with all the chosen coordinates $x^{(i)}$.

Another popular Gaussian state is the thermal state

$$\rho_{\text{th}} = \frac{\exp\big(-\sum_k \beta_k a_k^\dagger a_k\big)}{Z} = \prod_k \frac{e^{-\beta_k a_k^\dagger a_k}}{Z_k} = \prod_k \rho_{\text{th},k} , \tag{5.49}$$

where β_k are the reduced temperatures and $Z_k = \operatorname{tr}\Big(e^{-\beta_k a_k^\dagger a_k}\Big)$. The mean population of each state is $\bar{n}_k = (e^{\beta_k} - 1)^{-1}$, which is the Bose-Einstein distribution. Inversely, we can write the exponential weights as $e^{-\beta_k} = \bar{n}_k / (\bar{n}_k + 1)$ and, therefore, the density matrix as

$$\rho_{\text{th}} = \prod_k \frac{1}{\bar{n}_k + 1} \sum_{n_k=0}^{\infty} \Big(\frac{\bar{n}_k}{\bar{n}_k + 1} \Big)^{n_k} |n_k\rangle \langle n_k| , \tag{5.50}$$

Given the structure of this state, only the correlators with diagonal operators do not vanish:

$$\langle a_p^\dagger a_q \rangle = \delta_{p,q} \, \bar{n}_p , \tag{5.51a}$$

$$\langle a_p^\dagger a_{p'}^\dagger a_{q'} a_q \rangle = \big(\delta_{p,q} \delta_{p,q} + \delta_{p,q'} \delta_{p',q} \big) \bar{n}_p \bar{n}_{p'} . \tag{5.51b}$$

Then, substituting these in Eq. (5.12),

$$\rho^{(1)}(x) = \sum_p \bar{n}_p |\phi_p(x)|^2 , \tag{5.52}$$

and, in Eq. (5.13),

$$\rho^{(2)}(x,x') = \sum_{p,p'} \bar{n}_p \bar{n}_{p'} \big(|\phi_p(x)|^2 |\phi_p(x')|^2 + \phi_p^*(x) \phi_p(x') \phi_{p'}^*(x') \phi_{p'}(x) \big) ,$$

(5.53)

The most noticeable difference between the coherent and thermal cases is the behaviour of $\rho^{(1)}(x)$. While the coherent state consists of the sum of amplitudes, that is, the coherent superposition of eigenfunctions, the thermal state cancels out the crossed terms and involves the incoherent sum of the squared amplitudes. Additionally, the second term in (5.53) is the bosonic counterpart of the exchange term in electronic systems. The thermal state keeps some correlations at the two-body level.

Then, we can compute the MSD for these states. First, we take $\alpha_{p>1} = 0$ and $\bar{n}_{p>1} = 0$. We also need to fix the mean number of particles $\bar{N}$. Integrating $\rho^{(1)}(x)$ all over the domain, we get $\bar{N} = |\alpha_0|^2 + |\alpha_1|^2$ for the coherent state and $\bar{N} = \bar{n}_0 + \bar{n}_1$ for the thermal states. Parametrising the coherent coefficients as $\alpha_0 = \sqrt{n(1-y)}$ and $\alpha_1 = e^{i\theta}\sqrt{ny}$, where $0 \leq y \leq 1$ and n is a positive integer, the mean population is always n. Likewise, for the thermal state, $\bar{n}_0 = n(1-y)$ and $\bar{n}_1 = ny$. This allows us to compare directly the results with the Fock states. For the infinite square well

$$\langle (x-x')^2 \rangle_{\text{coh}} = \frac{1}{6} - \frac{1}{\pi^2} - \frac{8192\cos^2(\theta) - 243\pi^2}{324\pi^4} y + \frac{2048\cos^2(\theta)}{81\pi^4} y^2 , \tag{5.54}$$

$$\langle (x-x')^2 \rangle_{\text{th}} = \frac{1}{6} - \frac{1}{\pi^2} - \frac{1053\pi^2 - 4096}{648\pi^4} + \frac{486\pi^2 y - 243\pi^2 - 4096}{648\pi^4(y^2 - y + 1)} , \tag{5.55}$$

This shows how two particles correlate in space when they originate from different quantum states, in different potentials. This is to be compared to the Fock case (Eqs. (5.34) & (5.39)). Such results could be experimentally implemented by near-field imaging of polaritons.

while, for the quantum harmonic oscillator,

$$\langle (x-x')^2 \rangle_{\text{coh}} = 1 + 2y^2 + 2\cos(2\theta) y(y-1) , \tag{5.56}$$

$$\langle (x-x')^2 \rangle_{\text{th}} = 1 + \frac{2y^2}{y^2 - y + 1} . \tag{5.57}$$

The phase difference θ plays an important role. The interference between the particles in each state affects the overall spatial configuration and it can modulated by the fraction y and the phase, in the same manner that two wave are admixed. The optimum phase that minimises the MSD for all the values of the mixing parameter y is $\theta = 0$ (or $\phi = \pi$), that is shown in Fig. 5.2, while the orthogonal phase $\phi = \pi/2$ maximises the MSD and, in fact, coincides with the classically indistinguishable when $y = k/n$. The values of the phase ϕ between o and $\phi/2$ produce intermediate results between these two curves.

5.3 UNCONFINED PARTICLES IN FREE SPACE

Having in mind these ideas and their corresponding results, we could try to generalise them to continuum energy spectra, as it is the case of particles in free space. We assume that the particle can be anywhere without restrains, i.e., its coordinate x can take any real value. Otherwise, if there is a confinement like the infinite square well, the reasoning would be similar, changing the integrals by discrete sums.

Any state is built up from elements of the chosen basis as a superposition or linear combination of them. The number of different of bases is infinite, so the number of ways we can represent a particular state is countless. In free space, there are two paradigmatic cases to start with: the position and momentum bases. An element from the first one places a particle at a fixed position x_0, $\langle x|x_0\rangle = \varphi_{x_0}(x) = \delta(x - x_0)$. The momentum basis, conversely, describes particles with a defined momentum k_0. Represented in this space, which is the Fourier space, this state is $\langle k|k_0\rangle = \breve{\varphi}_{k_0}(k) = \delta(k - k_0)$. Both representations are linked by the defined momentum state written in the position basis $\langle x|k_0\rangle = \varphi_{k_0}(x) = e^{ik_0x}$, which is a plane wave. Any state in the position basis $\phi(x)$ has its corresponding image in the momentum basis via the Fourier transform:

$$\breve{\phi}(k) = \int_{-\infty}^{\infty} \phi(x) e^{-ikx} dx\,, \tag{5.58}$$

or, inversely,

$$\phi(x) = \frac{1}{2\pi} \int_{-\infty}^{\infty} \breve{\phi}(k) e^{ikx} dk\,. \tag{5.59}$$

Then, any state $|\phi\rangle$ can be written in terms of plane waves

$$|\phi\rangle = \frac{1}{2\pi} \int_{-\infty}^{\infty} \breve{\phi}(k)\, |k\rangle\, dk\,. \tag{5.60}$$

In the language of second quantisation, the boson operators that create and annihilate particles with defined momentum k are $a_k^\dagger$ and a_k, respectively. The commutation relations are $[a_k, a_q] = 0$ and $[a_k, a_q^\dagger] = (2\pi)\delta(k - q)$ (in d dimensions, the normalisation factor would be $(2\pi)^d$). For fermions, the operators $c_k^\dagger$ and c_k have to fulfil the anticommutation rules $\{c_k, c_q\} = 0$ and $\{c_k, c_q^\dagger\} = (2\pi)\delta(k - q)$. In terms of the second quantisation operators, we have $|k\rangle = a_k^\dagger |0\rangle$ or $|k\rangle = c_k^\dagger |0\rangle$. Then, we can define a generalised operator that creates a particle in the state $|\phi\rangle$ as

$$A^\dagger(\phi) = \frac{1}{2\pi} \int_{-\infty}^{\infty} \breve{\phi}(k) a_k^\dagger\, dk\,, \tag{5.61}$$

such that $|\phi\rangle = A^\dagger(\phi)\,|0\rangle$. For fermions, the operator $C^\dagger(\phi)$ has exactly the same shape replacing $a_k^\dagger$ by $c_k^\dagger$.

Having two arbitrary states, namely ϕ and ψ, we ask if the order when applying this operator to the vacuum affects the resulting state. The commutation relations of $A(\phi)$ and $A^\dagger(\psi)$ are, remembering that the commutation is linear in its two entries,

$$[A(\phi), A(\psi)] = \frac{1}{(2\pi)^2}\int_{-\infty}^{\infty}\int_{-\infty}^{\infty}\check{\phi}^*(k)\check{\psi}^*(q)[a_k, a_q]\,dkdq = 0\,, \quad (5.62)$$

given that $[a_k, a_q] = 0$. The missing rule is

$$[A(\phi), A^\dagger(\psi)] = \frac{1}{(2\pi)^2}\int_{-\infty}^{\infty}\int_{-\infty}^{\infty}\check{\phi}^*(k)\check{\psi}(q)[a_k, a_q^\dagger]\,dkdq = \frac{1}{2\pi}\int_{-\infty}^{\infty}\int_{-\infty}^{\infty}\check{\phi}^*(k)\check{\psi}(k)\,dk = \langle\phi|\psi\rangle = S(\phi,\psi)\,, \quad (5.63)$$

where $S(\phi,\psi) = S^*(\psi,\phi)$ is the overlap between the wavefunctions. When $\phi = \psi$, then $S(\phi,\phi) = 1$ because of the normalisation. In other case, the modulus of overlap is less than one due to the Cauchy-Schwarz inequality.

The multiparticle generalised coherent state is $D_\phi(\alpha)\,|0\rangle$, where the exponential map is now $D_\phi = e^{\alpha A^\dagger(\psi) - \alpha^* A(\psi)}$. The description of the creation operator as a sum of plane waves allows to write the displacement operator D_ϕ as $D_\phi = \exp\left\{\int \frac{dk}{2\pi}\alpha_k a^\dagger{}_k - \alpha_k^* a_k\right\}$, where $\alpha_k = \alpha\,\check{\phi}(k)$, that is, it is a (continuous) superposition of displacement operators, so the rules (5.43) still apply and the state is a limiting case of (5.44) where α_k are not only an infinite set of parameters but a continuous one. The summation turns into a integral over the k-space. The reduced density matrices are then

$$\rho^{(1)}(x) = \left|\int_{-\infty}^{\infty}\frac{dk}{2\pi}\alpha_k e^{ikx}\right|^2 = \left|\alpha\int_{-\infty}^{\infty}\frac{dk}{2\pi}\check{\phi}(k)e^{ikx}\right|^2 = |\alpha|^2|\phi(x)|^2\,, \quad (5.64)$$

and

$$\rho^{(2)}(x,x') = \rho^{(1)}(x)\rho^{(1)}(x')\,. \quad (5.65)$$

The main result is that a coherent state of a specific state ϕ keeps the same expression as the canonical n-particle description (up to a constant $|\alpha|$, which is the population). Such a result may be seen as obvious but it justifies the one-particle description. A coherent state can be generated by a short laser pulse with a given profile $\phi(x)$, the consequent evolution is provided by the Schrödinger equation or by the dissipative Gross-Pitaevskii equation.

5.4 TIME AND SPATIAL CORRELATIONS

In this Section, we study a dynamical situation. The spatial correlations, such as the density profile $\rho^{(1)}$, evolve with time. The problem we solve can describe, for instance, a polariton wavepacket propagating in one dimension steered towards a defect (fixed at $x = 0$ for the sake of simplicity). The simplest way to represent this scattering process with a single defect is a Dirac delta potential, that also have analytical expressions which, in turn, simplify all the computations.

In absence of dissipation or self-interaction, the wavefunction evolves following the Schrödinger equation

$$i\partial_t \psi(x,t) = \left(-\frac{1}{2m}\partial_{xx}^2 + V_0\delta(x)\right)\psi(x,t)\,. \tag{5.66}$$

The simplest solution, which can be consulted in Quantum Mechanics textbooks [30, 82], is a combination of plane waves with the same energy $\frac{k^2}{2m}$. An incident wave (coming from the left hand side) reaches the defect and scatters back and forward. For our purpose, we use the time-independent Schrödinger equation (we substitute $i\hbar\partial_t \to E$) and split the space in two regions, before and after the barrier (region I for $x < 0$ and region II for $x > 0$). Solving the equation gives the following well-known solution

$$\psi(x) = \begin{cases} Ae^{ikx} + Be^{-ikx}, & x < 0 \\ Ce^{ikx}, & x > 0 \end{cases}, \tag{5.67}$$

where we have discarded the backward solution in the region II because we assume that there are no incoming waves from the right-hand side. Now, we need the matching conditions at $x = 0$. The wavefunction should be continuous everywhere. This leads to $\psi(0^-) = \psi(0^+)$ or, after substituting the wavefunction, $A + B = C$. The second condition requires to take into account the delta potential. Integrating around $x = 0$, for instance, taking the region $(-\epsilon, +\epsilon)$ (with $\epsilon \to 0^+$), leads to

$$\psi'(0^+) - \psi'(0^-) = 2\beta_0\psi(0) \;\Rightarrow\; A - B = \left(1 - i\frac{2\beta_0}{k}\right)C\,, \tag{5.68}$$

where $\beta_0 = \frac{mV_0}{\hbar^2}$. We can express the reflected and transmitted waves coefficients in terms of the incoming one, i.e., $B/A = r$ and $C/A = t$. Finally, the two conditions allow us to obtain the coefficients

$$r(k) = \frac{i\beta_0}{k - i\beta_0}, \qquad t(k) = \frac{k}{k - i\beta_0}. \tag{5.69}$$

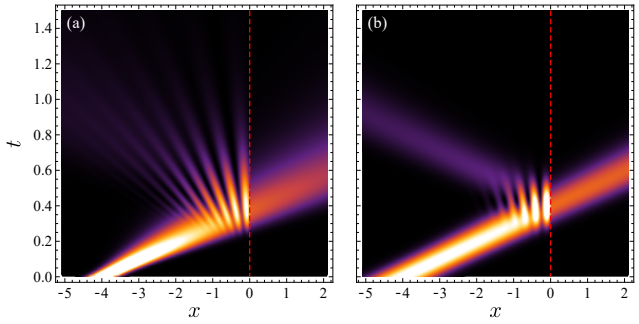

Figure 5.3: Time evolution of the Gaussian wave packet scattered by the Delta potential (marked as a dashed red line) for two different initial widths σ_0. Brighter regions indicate higher probability of detecting the particle. For narrow widths, the distribution of momenta is wide and the packet spreads faster so after the scattering the interference pattern (between the incoming and scattered fractions) is visible along a wide region comparable to x_0. The transmitted fraction travels towards infinity without interacting. For wider widths, the packet retains its shape for much longer times, even after the interaction with the potential. The interference effect lasts only in the intermediate region where the incoming and scattered waves overlap.

The whole solution can then be written as

$$\psi(x) = \theta(-x)\left(e^{ikx} + r(k)e^{-ikx}\right) + \theta(x)t(k)e^{ikx}\,. \tag{5.70}$$

From this simple solution for a standing plane wave, any other configuration can be computed at all times as a superposition of well-defined k states. We choose as an initial condition a Gaussian wavepacket, centred at $x_0 < 0$, with mean momentum $k_0 > 0$ and space uncertainty σ_0:

$$\psi(x,0) = \frac{1}{(\pi\sigma_0^2)^{1/4}} \exp\left[ik(x+x_0) - \frac{(x+x0)^2}{4\sigma_0^2}\right]. \tag{5.71}$$

In the previous equation we have made explicit the sign of x_0, i.e., $x_0 \to -x_0$. The evolution of the wavepacket is given by the sum of two terms:

$$\psi\,(x,t) = \psi_0\,(x,t) + \psi_I\,(x,t)\,. \tag{5.72}$$

The first term is the free evolution of the initial packet that reads

$$\psi_0\,(x,t) = \left(\frac{\sigma_0^2}{2\pi\alpha(t)}\right)^{1/4} \exp\left\{-\frac{(x+x_0)^2}{4\alpha(t)} + \frac{i\sigma_0^2}{\alpha(t)}\left[k_0(x+x_0) - \omega_0 t\right]\right\}, \tag{5.73}$$

where we have defined the following parameters

$$\alpha(t) = \sigma_0^2 + \frac{i\hbar t}{2m}, \qquad \omega_0 = \frac{\hbar k_0^2}{2m}. \tag{5.74}$$

The remaining term is, then, the back- and forward-scattered wave due to the potential. The computation of this one is not straightforward and was already tackled in Ref. [83], so we will omit the details and present the solution

$$\psi_I(x,t) = A(x,t)\Big\{ \int_{-\infty}^{\infty} \frac{e^{-u^2} du}{u + z(x,t)} - 2\pi i \theta[-\operatorname{Im} z(x,t)] e^{-z(x,t)^2} \Big\}, \tag{5.75}$$

where $\theta(x)$ is the Heaviside function and we have used the following auxiliary functions

$$A(x,t) = -i\beta_0 \sqrt{\frac{\alpha(t)}{\pi}} \psi_0(|x|,t), \tag{5.76a}$$

$$z(x,t) = (\alpha(t))^{1/2} (\kappa(x,t) + i\beta_0), \tag{5.76b}$$

$$\kappa(x,t) = \frac{k_0 \sigma_0^2}{\alpha(t)} + i \frac{|x| + x_0}{2\alpha(t)}. \tag{5.76c}$$

The probability of detection is proportional to the probability distribution $|\psi(x,t)|^2$. We observe in the time evolution (see Fig. 5.3) how the initial wave packet impinges the Delta potential and scatters some fraction to the right (backwards) and some other to the left (forwards). For intermediate times, we find a characteristic fringe pattern due to the interference between the incoming and reflected (scattered) waves. The region of visibility of those fringes (their periodicity depends on the mean momenta k_0) changes with the width of the packet σ_0: the narrower the packet, the faster the spreading. The potential strength V_0 determines the reflected and transmitted fractions. In Fig. 5.3, we show the evolution of the wavefunction for narrow and wide initial widths σ_0. The interference pattern is more visible when the wave packet is spread. In some way, we can understand these two contributions (incoming and scattered waves) as the past and future of the particle, that is, before and after the scattering. A beautiful example of this (self-)interference in a more complex situation was actually measured by Suárez-Forero *et al.* [84], where the evolution of a single-polariton wave that travels (in 2D) towards a cylindrical defect displays an interference pattern composed of the incoming plane wave and the scattered radial *s*-wave. The resulting image resembles the hydrodynamic flow of a fluid surrounding an obstacle.

However, as we have discussed and characterised all throughout the text, the observations may be critically affected by the temporal and spatial resolutions of the detectors. The first issue is ubiquitous along this Thesis in the form of spectral response and we already know how to approach this problem. Up to now, only time resolution limitations have been taken into account but we could expect that spatial resolution limitations can be modelled in a similar way. The most general spatially- and spectrally-resolved operator or, in our case, wave-function has to be a convolution of the bare system operator (wavefunction) with the detection kernel $\mathcal{K}(y,\tau;x,t)$. Our first simplification is to assume that $\mathcal{K}$ is homogeneous both in space and time, so that it does only depend on the differences $x-y$ and $t-\tau$. The filtered version of the wavefunction is

$$\psi_{\mathcal{K}}(x,t) = \int_{-\infty}^{\infty}\int_{-\infty}^{\infty} \mathcal{K}(x-y,t-\tau)\psi(y,\tau)d\tau dy\,, \tag{5.77}$$

where we fix that $\psi(x,t<0)=0$, that is, the wavefunction is created at $t=0$. If the time resolution is limited but the spatial one is not, we can settle on, for instance, the Lorentzian kernel $\mathcal{K}_{\mathrm{L}}(y,\tau)=\delta(y)\,\frac{\Gamma}{2}\theta(\tau)e^{-(\Gamma/2+\omega_1)\tau}$. The previous double integral turns into

$$\psi_{\mathrm{L}}(x,t) = \int_0^t \frac{\Gamma}{2}e^{-(\Gamma/2+\omega_1)(t-\tau)}\,\psi(x,\tau)d\tau\,. \tag{5.78}$$

Then, we can compute the convolved wavefunction forthwith or make use of the equivalent sensor equation, that we obtain by deriving $\psi_{\mathrm{L}}(x,t)$ with respect to time,

$$\partial_t\psi_{\mathrm{L}}(x,t) = -\big(\Gamma/2+i\omega_1\big)\psi_{\mathrm{L}}(x,t)+\frac{\Gamma}{2}\psi(x,t)\,, \tag{5.79}$$

with the initial condition $\psi_{\mathrm{L}}(x,0)=0$ which assures that the solution is exactly the integral (5.78). In order to optimise the interference effect in the detector, we chose $\omega_1=\omega_0$, the energy corresponding to the incident mean momentum k_0 or, if we want to retain the shape of the wave packet, then we shall fix $\omega_1=0$. Even if the spatial resolution is assumed to be perfect, selecting some frequencies over others undoubtedly changes the contribution from different k wave vectors, given that $\omega(k)=k^2/(2m)$ or, inversely, $k=\pm\sqrt{2m\omega}$. For wide filters ($\Gamma\gg 1$), as expected, the filtered wavefunction resembles the unfiltered case. As the filter width shrinks, the wavefunction starts to blur at short times, before the scattering takes place, and fringes appear right after. The visibility, compared to the unfiltered case, is much greater and the orientation of the pattern is not slanted but

This shows how detection settles the wave-particle duality of a propagating single polariton: long integration times manifest a compelling interference phenomenon. While it is always resolved even at small integration times—as it would be from the naked Schrödinger equation in absence of space resolution—fringes only occur in a small are of spacetime and the dynamics is overall that of a propagating wavepacket.

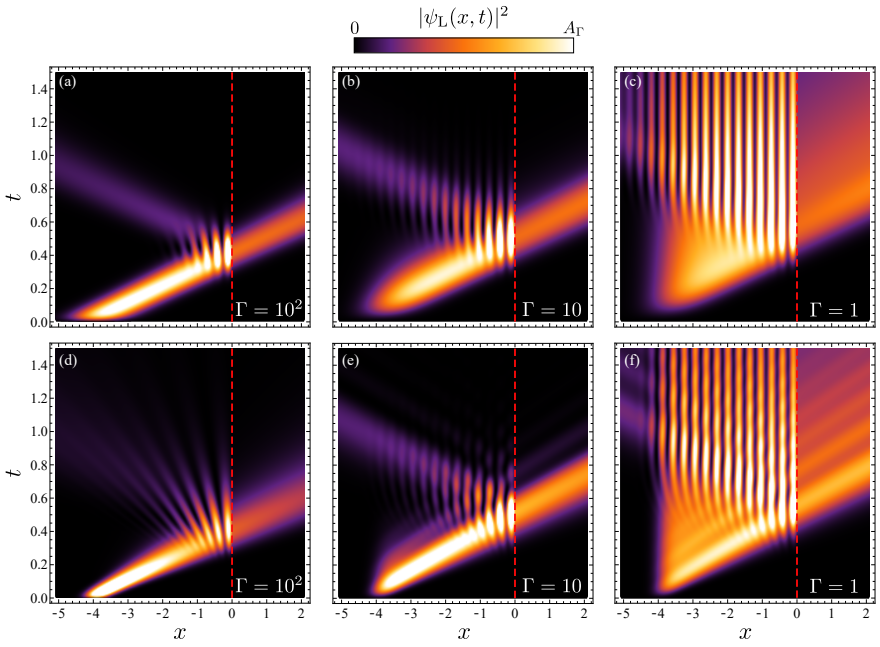

Figure 5.4: Time-filtered evolution of the wave packets in the case $\omega_1 = \omega_0$. In the first row the parameters corresponds to the wide case of Fig. 5.3 (with $\sigma_0 = 0.5$) and the bottom row to the narrow packet of the same figure (with $\sigma_0 = 0.2$). The filter's width is chosen to maximize the visibility of the interference fringes. In both cases, the filtering induces the appearance of a standing wave before the defect. The normalisation, namely A_Γ, changes for different widths Γ and we have chosen the most suitable to compare all the cases. Fixed parameters: $\beta_0 = 10$, $k_0 = 10$ and $x_0 = 4$.

vertical. In Fig. 5.4, for the intermediate case (second column), not only does the wave packet seem to be wider but interferences stay, more or less, in the same spot and have a better definition for the wide packet. We can also differentiate a dim echo of the incident and transmitted waves packet in the lower plot that appears as a series of beatings resembling the unfiltered propagation of the packet at longer times. In the narrowest case (right column), the region between $-x_0$ and o contains an undefined cloud that turns into a standing wave after the time when the center of the packet reaches its minimum distance with the Delta potential. The extent of the echoes is larger and they stand as secondary oblique pattern in the narrow packet case. The overall effect is the loss of time order since we cannot distinguish *past* (incident wave) and *future* (scattered wave). If we fix $\omega_1 = 0$, see Fig. 5.5, we do not find the vertical standing wave pattern but some of the original features are enhanced. For instance, the angled lines fringes in Fig. 5.3(a) have a greater relative intensity. The transmitted packet spreads in time but does not display beatings (that we called echoes). If the time scale of the filter ($\tau \propto 1/\Gamma$) is much

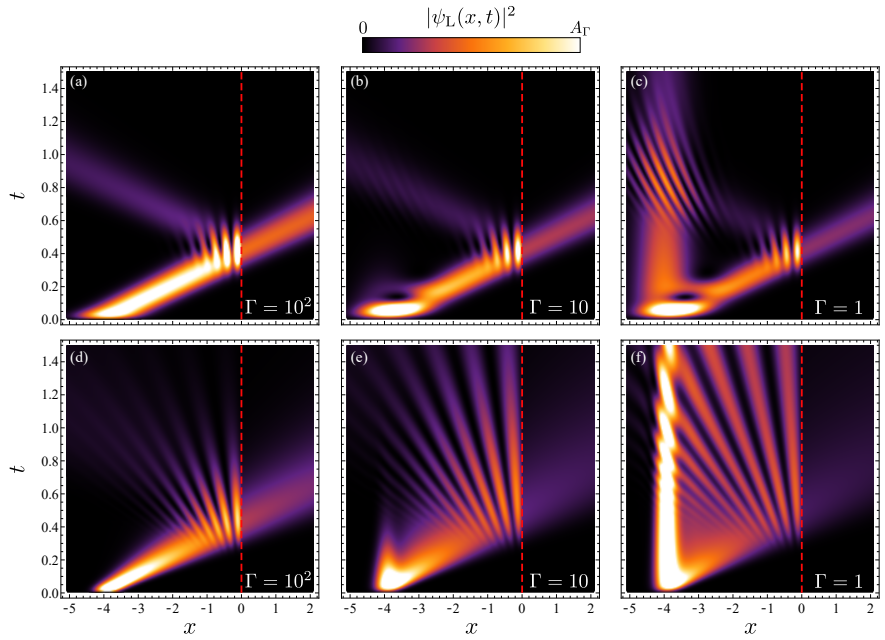

Figure 5.5: Time-filtered evolution of the wave packets in the case $\omega_1 = 0$. In the first row the parameters corresponds to the wide filter case of Fig. 5.3 and the bottom row to the narrow packet of the same figure. The filter maximum is $\omega_1 = 0$, which retain low k features such as the envelope of the packet.

longer than the characteristic time of the packet (corresponding to the right column), there is a static contribution that comes from the initial state. When the outcoming wave reaches the initial position again, a second interference process occurs. In the upper row, there is a noticeable dark spot. The origin seems to be an interference too. Through the control of the filtering process, we can make the system interfere with itself and hence we modify its effective dynamics and, in principle, we can engineer new patterns without convoluted non-linear processes and, ultimately, change the spatial and time correlations of the observed particle. The main drawback of this procedure is that it is only valid for non-stationary signals. Moreover, we are implicitly assuming that the system is not undergoing any incoherent process and that self-interaction and subsequent many-body correlations are completely negligible. We can also make a CW version, in which case we need to add dissipation and a driving source to obtain the stationary solution.

5.4.1 SPATIAL DISSIPATIVE MODEL

The previous theory applies when we know the exact initial conditions for the incoming packet. We make some modifications in the

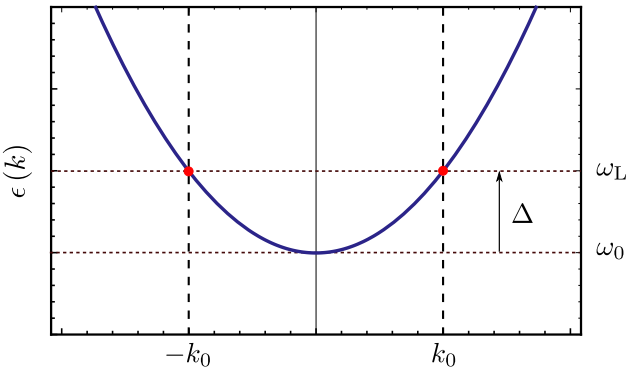

Figure 5.6: Parabolic dispersion of the polariton. The frequency of the laser has to match $\omega_L = \epsilon(k_0)$ so that the system is driven in branch. Notice that the laser excites two different points in-branch (marked by the red points): $\pm k_0$.

Schrödinger equation to include dissipation and external excitation. The lossy version of the equation reads [85]

$$i\partial_t \psi(x,t) = \left[\omega_0 - \frac{\hbar}{2m}\partial_{xx}^2 + V_o\delta(x) - i\frac{\gamma}{2}\right]\psi(x,t) + i\mathcal{E}(x,t)\ , \quad (5.80)$$

where ω_0 is the energy of the polariton at $k = 0$, γ is the polariton decay rate and $\mathcal{E}(x,t)$ represents the driving term (e.g., the laser beam). Assuming that the source is in CW regime and monochromatic, we can write it as $\mathcal{E}(x,t) = \mathcal{E}(x)e^{-i\omega_L t}$ (ω_L is the frequency of the laser). For the sake of simplicity, we remove the explicit temporal dependence of the driving term by transforming the wavefunction $\psi(x,t) \to \psi(x,t)\, e^{-i\omega_L t}$ (rotating frame transformation). Plugging this into Eq. (5.80) leads to

$$i\partial_t \psi(x,t) = \left[\Delta - \frac{\hbar}{2m}\partial_{xx}^2 + V_o\delta(x) - i\frac{\gamma}{2}\right]\psi(x,t) + i\mathcal{E}(x)\ , \quad (5.81)$$

with, here, $\Delta = \omega_0 - \omega_L$ the detuning between the zero-k polariton energy and the laser.

We are interested in the steady-state solution of the system. This regime is reached when $t \to \infty$ or, in other words, $\partial_t\psi(x,t) = 0$. To make a distinction between the time-dependent and steady-state solutions, we name the latter $\phi(x)$. After that change, the equation to solve is

$$\left[-\frac{\hbar}{2m}\frac{d^2}{dx^2} + V_o\delta(x) + \Delta - i\frac{\gamma}{2}\right]\phi(x) = -i\mathcal{E}(x)\ . \quad (5.82)$$

From this equation, we can calculate the Fourier transform, which after substituting is just

$$\check{\phi}(k) = -\frac{V_0\phi(0)}{\frac{\hbar k^2}{2m} + \Delta - i\frac{\gamma}{2}} - \frac{i\check{\mathcal{E}}(k)}{\frac{\hbar k^2}{2m} + \Delta - i\frac{\gamma}{2}} = -V_0\phi(0)\check{\phi}_0(k) + \check{\phi}_1(k)\,. \tag{5.83}$$

Equation (5.83) is implicit since it does depend on the value of the solution at $x = 0$. Nevertheless, after inverting the Fourier transform, we find that it is possible to write it down explicitly. The first term $\check{\phi}_0$ represents the scattered contribution due to the potential while the second one $\check{\phi}_1$ is the steady solution for the particular beam $\mathcal{E}(x)$ exciting the system in absence of potential. The inversion of the scattering term gives us

$$\phi_0(x) = \sqrt{\frac{2\pi i m/\hbar}{\gamma + 2i\Delta}}\exp\left(-\sqrt{\frac{\gamma + 2i\Delta}{i\hbar/m}}|x|\right). \tag{5.84}$$

The remaining one can be expressed, in accordance with the Convolution Theorem, as

$$\phi_1(x) = \int_{-\infty}^{\infty}\mathcal{E}(x-y)\phi_0(y)dy. \tag{5.85}$$

Thus, the solution in real space is:

$$\phi(x) = -V_0\phi(0)\phi_0(x) + \phi_1(x)\,. \tag{5.86}$$

Fixing $x = 0$ in the previous equation let us solve $\phi(0)$, giving as a result:

$$\beta_0 \equiv -V_0\phi(0) = -\frac{V_0\phi_1(0)}{1 + V_0\phi_0(0)}\,, \tag{5.87}$$

which is completely determined by the two already known contributions to the whole solution. So both representations of the solution (space and momentum) are complete now:

$$\phi(x) = \beta_0\phi_0(x) + \phi_1(x)\,, \tag{5.88a}$$
$$\check{\phi}(k) = \beta_0\check{\phi}_0(k) + \check{\phi}_1(k)\,. \tag{5.88b}$$

Of course, the solution is not always analytical, depending on the shape of the beam (given by the function $\mathcal{E}(x)$). In the case of a Gaussian beam, centred at $x = -x_0 < 0$, with width σ_0, carrying mean momentum k_0 and intensity $|\mathcal{E}_0|^2$:

$$\mathcal{E}(x) = -i\frac{\mathcal{E}_0}{\left(\pi\sigma_0^2\right)^{1/4}}\exp\left[ik_0(x + x_0) - \frac{(x + x_0)^2}{2\sigma_0^2}\right], \tag{5.89}$$

there is a solution, but it is quite bulky so we do not show it here. To excite in-branch, we need that the laser frequency and the energy of the polariton at $k = k_0$ match (as shown in Fig. 5.6). Then, the relation must be $\Delta = \omega_0 - \omega_L = -\frac{\hbar k_0^2}{2m}$. Since the steady-state is not

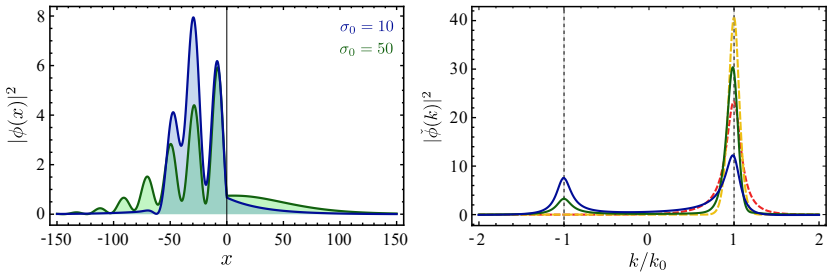

Figure 5.7: Example showing the solution given by Eq. (5.88a) for the case of a Gaussian beam. The left figure shows the space representation of the solution for two different values of σ_0 (the rest of the parameters are fixed). In the right hand side figure, the absolute value of the Fourier transform of the two cases shown above are represented (solid lines) together with their counterparts without any interaction (dashed lines, red for the first case and yellow for the second one). Parameters: $\hbar = 1$, $m = 0.48, k_0 = 0.15$, $V_0 = 10$, $\gamma = 0.01$, $\mathcal{E}_0 = 1$ and $x_0 = 50$.

changing in time, we cannot study the time resolution. Our detector only collects light from a single point x, that would correspond to $\phi(x)$ and therefore the probability of collecting photons from that point is proportional to the squared modulus $|\phi(x)|^2$. Figure 5.7 shows, as the time-dependent case did, an interference pattern. However, this time it is not transient but forms a standing pattern when the system reaches equilibrium. In k-space, the effect of interference is well understood. The positive and negative momenta are superimposed and, as a result, the fringe pattern is displayed. In absence of the delta potential, there is no scattered wave and we do not find such a characteristic shape. We find that the visibility and effective range of the fringes improve as the ratio of the waves travelling to the left (positive k) and the one moving back (negative k) goes to one. For a perfect standing wave, we would need infinitely narrow peaks at $k = \pm k_0$.

The fringes shown in the previous figure 5.7 are not homogeneously distributed and their profile is not constant, so we cannot apply the classical formula to calculate the contrast [86]: $\mathcal{C} = (I_{max} - I_{min})/(I_{max} + I_{min})$ (these quantities being the maximum and minimum values of the intensity). Instead of that, we compute the upper and lower envelopes, $I_{max}(x)$ and $I_{min}(x)$, which enclose the interference pattern and define the contrast as a function of both,

which is essentially the same expression as the usual contrast but changing along space, that is,

$$\mathcal{C} = \frac{I_{max}(x) - I_{min}(x)}{I_{max}(x) + I_{min}(x)}\,. \tag{5.90}$$

After this, we can compute the averaged contrast $\langle \mathcal{C} \rangle$:

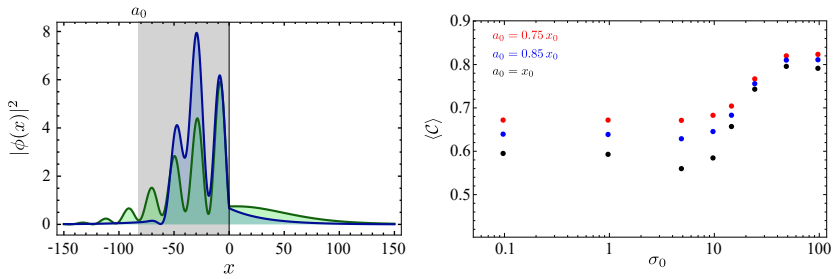

Figure 5.8: Left: the shadowed region indicates the range of integration (black line of the right panel) for the mean contrast (beam width: $\sigma_0 = 10, 50$, blue and green, respectively). Right: Mean contrast for several beam widths. The range of integration also changes the resulting contrast but the dependence in σ_0 is similar for all the selected cases. As a general trend, the contrast grows as the beam widens. This corresponds to a smaller spread in k-space. Only the case $a_0 = x_0$ displays a small for intermediate widths, possibly because the region of integration covers not only the interference pattern. Parameters: $\hbar = 1$, $m = 0.48, k_0 = 0.15$, $V_0 = 10$, $\gamma = 0.01$, $\mathcal{E}_0 = 1$ and $x_0 = 100$.

$$\langle \mathcal{C} \rangle = \frac{1}{a_0} \int_{-a_0}^{0} \mathcal{C}(x) dx\,, \tag{5.91}$$

where the mean value is taken over a finite interval $(-a_0, 0)$, so that we only consider the region where the interference is effectively taking place. It is not exact but we can study how contrast is affected by the choice of a_0. The optimum range appears to be around the center of the laser spot but there is no perfect method to determine it given that the spreading of the interference pattern may not depend only on the effective width of the beam, i.e., σ_0 but also on the potential effective strength β and the mean transferred momentum k_0. In Figure 5.8, we compute the contrast $\langle \mathcal{C} \rangle$ and found that, even though it varies with the choice of a_0, the three cases (red, blue and black) do agree qualitatively. The visibility of the fringes improves when the laser beam covers a range of space between $-0.75x_0$ and the Delta potential barrier. Unlike the transient situation considered previously, the time-resolution is not a problem since the system is in a steady-state, where photon gains and losses completely compensate each other. The pattern changes with the external parameters of the laser and can

modulate the fringes to a certain degree. The main limitation is the effective scattering strength β, which depends on the effective mass m and the potential constant V_0, that eventually saturates the solution and then the maximum contrast.

6

CONCLUSIONS

We have addressed in detail the quantum nature of light, tackling in the first place its quantum state description and its connection to the observables such as the n-photon coherence functions $g^{(n)}$, which are the heart of Quantum Optics and provide information about the statistical properties of the photons. Then, the dynamical aspects of the emission were included in the picture, for instance, the luminescence spectrum, the time-dependent Glauber correlators or the Waiting Time distribution. The latter seems to have been overlooked for decades and, in fact, provides very useful information. We identified in such distributions at short times the multiphoton peak and found a qualitative and quantitative agreement between the N-photon SE and the actual bundler.

We have presented an analysis of the epitome of the single-photon generation: the 2-level system. Making particular emphasis in the incoherently and coherently driven (resonance fluorescence) cases. With the perturbation method we are able to obtain analytical expressions of the frequency-resolved correlators for several types of filters. For Resonance Fluorescence, these results were confirmed experimentally by two independent groups [73] and [Z2], which reinforces the validity of the theory. Furthermore, an analysis of the possible sources of error when measuring, such as the noise and time jitter of the detectors, were discussed. After providing general expressions for both the time jitter and noise contamination, the loss of antibunching can be quantified. In addition to the 2LS, we described an alternative scheme of on-demand single-photon source based on semiconductor Quantum Dots that combines two techniques: two-photon cascade and resonant excitation. Through the use of two laser pulses, separated by a fixed time delay, the system yields single photons with near-unity purity and high indistinguishability (experimentally up to 86%).

With the perturbation tools, we demonstrated how to solve photon correlations in the low pumping regime both analytically and numerically. For instance, we could address many-body problems such as the Dicke model without the necessity of using complicated methods such as the scattering matrix [65] and provide analytical expression valid for any number N of emitters. The Dicke model exhibits interesting properties, depending on the system parameters such as

the frequency of the laser or the cavity-emitter coupling strength, the photon statistics modulate from bunching to antibunching, so it could be a good candidate for both single-photon and multiphoton sources. We could also solve a similar problem, the Jaynes-Cummings model, this time under incoherent driving. With this approach, we could reproduce and extend the low-driving linear behaviour of the light-matter system [70, 71]. Then, we can conclude that the range of applicability of the perturbation theory is wide. Other cases of interest can be, for instance, higher order corrections of the correlators, needed when the strength of the pumping increases and the first order is not a good approximation any more.

We derived analytical expressions for the photon-counting formula for CW systems and then for SE. In the process, we have derived a procedure to compute multi-time correlations of arbitrarily large m order, successively applying the Quantum Regression Theorem. We highlighted the factorisation property of the 2LS, that allows to write the m-photon correlation functions $G^{(m)}(t_1, \ldots, t_m)$ as the product of 2-photon Glauber correlators of successive times. Although all the orders of the correlation functions are required to obtain the complete counting distribution, we found out that they are dominated by the few-photon correlations. In particular, the long term behaviour of the variance-mean ratio Σ^2/μ depends on the time-integrated $G^{(2)}$. We compared the 2LS and the cavity, which show very different results, the first is always Sub-Poissonian ($\Sigma^2/\mu < 1$) while the second can be either Poissonian ($\Sigma^2/\mu = 1$) or Super-Poissonian ($\Sigma^2/\mu > 1$). The counting distribution of the SE of N photons turns to be a binomial distribution. This means that each photon is detected independently of the rest with the same probability, the single-photon detection probability $\mathcal{T}$. Even if the emission undergoes any type of filtering, this result is still true. The single-photon detection is less efficient given that the photon can be eventually rejected. The kind of filter and its overlapping with the spectral shape of the emission determines, in average, the fraction of photons that is ultimately detected. Therefore, when the circumstances require spectral filtering, we will be able to choose the optimum filter that maximises the photon collection. As a consequence of filtering, the N-photon bundle may arrive partially broken. Then, we could derive the probability distribution of the arrival time of the k-th photon (out of N), excluding or not the broken bundles, and compute the average size of the bundle (how long it takes to emit the last photon) or the mean arrival time of each photon. Theses results obtained from a simple case such the free decay of a emitter, i.e., SE agree with the bundler, described by the Jaynes-Cummings model (cavity + 2LS) under CW excitation. Thus, it let us

better comprehend the underlying mechanism that drives the bundler, a very promising source of quantum multiphoton states.

Lastly, we studied the effect of statistics on the observables in continuous variable systems. The spatial correlations change depending on the particle symmetry (fermion, bosons or classically indistinguishable). We focus on the one- and two-particle reduced density matrices, $\rho^{(1)}$ and $\rho^{(2)}$, that we use to compute the particle density or the average distance between pairs of particle for different kinds of states, for instance, Fock states (with defined number of particles) or the Gaussian coherent and thermal states. The two confined systems under study reveal that while fermions repel each other, exhibiting then a greater mean interparticle distance, bosonic particles do the opposite and have a smaller average distance, both compared to the classical indistinguishable case, that lays in the middle of these two. Then, we turn to investigate the scattering of a particle by a delta potential, the simplest 1D system that includes this kind of interaction. We discuss the effect of interference between the past and future of the wavepacket, i.e., the incoming and backscattered contribution of the wavefunction. Through spectral filtering, using the sensor method adapted to include space coordinates, we are able to modify the detected spatial distribution of the packet. For instance, a standing wave pattern appears if the filter width is small enough. Finally, we investigated this pattern formation in steady-state situation including both excitation and losses. The visibility of the fringes increases when the spatial spreading of the beam profile is large and the contributions from the positive and negative momenta have ratio close to one.

Overall, this thesis brought together various themes of study related to the correlations between multiple quantum systems (states, particles, etc.), deriving on several occasions results of a surprising fundamental character, with an emphasis on the possibility to obtain exact, analytical and closed-form expressions. The cases highlighted in the text have been chosen chiefly for their illustrative character and/or special importance, and several related considerations have been published in the literature instead (see the list of publications on page *vii*); in contrast, other results are to be found exclusively in the current text. Regardless of these specific cases, the concepts and formalism developed here are of general importance and constitute the substance of this text (several key ideas and results have been highlighted in the margins for illustration). This description of such correlations and of its emitters should become increasingly relevant with the emergence of multiphoton physics.

A

APPENDICES

A.1 BRIEF REMINDER OF QUANTUM OPTICS

We associate to a single-mode EM field the boson operators a and $a^\dagger$, which has identical shape to the harmonic oscillator ones. The natural basis are the Fock or number states $|n\rangle$ with $n \geq 0$, being the natural numbers. This basis is orthonormal, that is, $\langle n|m\rangle = \delta_{n,m}$. In the second quantisation context, the interpretation of $|n\rangle$ is different from that for harmonic oscillator. Rather than one particle in the n-th state, $|n\rangle$ represents a state with n particles in the same mode, in this case, n photons in a single mode. They are Fock or number states and can be generated from the vacuum $|0\rangle$ as $|n\rangle = \frac{a^{\dagger n}}{\sqrt{n!}}$.

For the moment, only states with a well-define number of photons have been defined. However, the family of quantum states of light are much larger than that. Number states are belong to the canonical basis which allows to build any quantum state $|\psi\rangle = \sum_n c_n |n\rangle$ with the coefficients $c_n \in \mathbb{C}$. The normalisation of the state imposes a restraint $\sum_n |c_n|^2 = 1$ over the set of coefficients. The interpretation that Born gave to the coefficient c_n or more precisely its squared modulus is as the probability of finding the n-th state $P_n = |c_n|^2$. The necessity of normalising is then naturally explained is the context of probability theory (the total probability is always one). Any state defined as a superposition of the elements of any basis is called a *pure state*.

An alternative and more general way to describe the quantum states is the density operator ρ. Using this formalism, any pure state has the form of an dyad operator $|\psi\rangle\langle\psi|$. Expanding ρ in the Fock basis, we get

$$\rho = \sum_{m,n} c_n^* c_m |m\rangle\langle n| \ . \tag{A.1}$$

More generally, we could have any state

$$\rho = \sum_{m,n} \rho_{n,m} |m\rangle\langle n| \tag{A.2}$$

where the density matrix elements $\rho_{n,m}$ have to satisfy $\mathrm{tr}(\rho) = \sum_n \rho_{n,n} = 1$ and $0 \leq |\rho_{n,m}| \leq 1$, where $\mathrm{tr}()$ denotes the matrix trace. It is clear that the meaning of the diagonal elements $\rho_{n,n}$ is the same as

$P_n = |c_n|^2$. With this description, the set of quantum states that span the Hilbert space grows considerably and is complete. Excluding the pure states that fulfil $\rho_{n,m} = c_n^* c_m$, any other is classified as a mixed state and the transformation from ket to density matrix cannot be reverted. Therefore, the mixed states are not linear combinations of the basis states any more but statistical ensembles of states. An extreme example are the thermal states $\rho = (1-\theta)\sum_n \theta^n |n\rangle \langle n|$, with $0 < \theta < 1$, which are completely diagonal. A simple test to distinguish the kind of family of ρ is to compute the purity $\mathrm{tr}(\rho^2)$. This quantity, for infinite dimensional Hilbert spaces, is bounded between zero and one and it only reaches one if ρ is a pure state. It is a measure of how close to a pure state the current state is [87]. For instance, the thermal states have purity $\mathrm{tr}(\rho^2) = (1-\theta)/(1+\theta)$, that goes from 1 to 0 as the parameter θ grows.

The observables associated to quantum states is what is actually measured in an experiment and not the matrix elements themselves. From these measurements, only if the set of quantities is large enough, we could infer or reconstruct the state. In Quantum Optics, these observables are quantities derived from the statistical properties of light, which are nowadays described in terms of the *Glauber correlators* (also known as the nth-order quantum coherence functions):

$$g^{(n)} \equiv \langle a^{\dagger n} a^n \rangle / \langle a^\dagger a \rangle^n \,. \tag{A.3}$$

The Glauber correlators are normalised functions obtained from the ratio of the observables:

$$G^{(n)} \equiv \langle a^{\dagger n} a^n \rangle \,. \tag{A.4}$$

The first-order Glauber correlator $g^{(1)}$ is always equal to unity. Instead, we will use the mean population (average number of quanta)

$$n_0 \equiv G^{(1)} = \langle a^\dagger a \rangle \,. \tag{A.5}$$

Then, this set of observables provides an essentially comprehensive description of the quantum states of an harmonic oscillator, through its n-particle fluctuation properties.

For instance, $G^{(1)}(\tau) \equiv \langle a^\dagger(0) a(\tau) \rangle$ becomes an important correlator given that its Fourier transform is related to the luminescence spectrum (frequency distribution of the photons emitted). In the context of photon-number distributions, $g^{(n)}$ provide information about the fluctuations concerning n particles. Among them, the most widely used is $g^{(2)}$. Written as $(\langle N^2 \rangle - \langle N \rangle)/\langle N \rangle^2$ (where $N = a^\dagger a$ is the photon-number operator), we straightforwardly see that it is related to the variance of the photon-number distribution. For Poisson distributions, $\mathrm{Var}(n_0) = n_0$ and, as a result, $g^{(2)} = 1$. The photons are

emitted following a Poisson process, this is, each of them is emitted independently. As it was established by Glauber, the modern definition of coherence is described by means of $g^{(n)}$. An idealised monochromatic laser would have a quantum state corresponding to the coherent state [88] theorised by Sudarshan [89] and Glauber [1]. For values $g^{(2)} < 1$, the fluctuations are Sub-Poissonian and they are characteristic of genuine non-classical quantum states of light, such as the Fock states [90]. They do not have classical analogue due to the Cauchy-Schwarz inequality that forbids any classical field to have $g^{(2)}$ less than unity. By contrast, chaotic light such as the black-body radiation has greater variance than the Poisson distribution, with $g^{(2)} = 2$. The underlying quantum state is the thermal density matrix [1].

A.2 EXACT EXPRESSIONS FOR THE MARGINAL DISTRIBUTIONS OF 3-PARTICLE HILBERT SPACE

We list some of the exact and closed-form (but bulky) expressions for quantities discussed or plotted in the main text. They are obtained from the methods explained therein.

These are the auxiliary functions introduced to define the boundaries for the population in the Hilbert space $\mathcal{H}_3$ (f_0 is used in f_1):

$$f_0(g^{(2)},g^{(3)}) = \left[6(g^{(2)})^3(g^{(3)})^2 - 3(g^{(2)})^2(g^{(3)})^2 - 18g^{(2)}(g^{(3)})^3 + 9(g^{(3)})^4 + 8(g^{(3)})^3\right]^{1/2}, \tag{A.6}$$

$$f_1(g^{(2)},g^{(3)}) = -\frac{\sqrt[3]{-(g^{(2)})^3 + f_0(g^{(2)},g^{(3)}) + 3g^{(2)}g^{(3)} - 3(g^{(3)})^2}}{g^{(3)}} + \frac{18g^{(3)} - 9(g^{(2)})^2}{9g^{(3)}\sqrt[3]{-(g^{(2)})^3 + f_0(g^{(2)},g^{(3)}) + 3g^{(2)}g^{(3)} - 3(g^{(3)})^2}} + \frac{g^{(2)}}{g^{(3)}}, \tag{A.7}$$

$$f_2(g^{(3)}) = \mathrm{Re}\left(\frac{\sqrt[3]{-8748(g^{(3)})^2 - 4860g^{(3)} + 8748\left(g^{(3)} - \frac{2}{9}\right)^{3/2}\sqrt{g^{(3)}} + 54}}{18\sqrt[3]{2}} - \frac{-324g^{(3)} - 9}{9 \times 2^{2/3}\sqrt[3]{-8748(g^{(3)})^2 - 4860g^{(3)} + 8748\left(g^{(3)} - \frac{2}{9}\right)^{3/2}\sqrt{g^{(3)}} + 54}}\right) + \frac{1}{6}. \tag{A.8}$$

These are reduced probability distribution in $\mathcal{H}_3$:

$$\mathcal{P}_g(n_0, g^{(2)}) = \begin{cases} 3n_0^2 - 3n_0^3 + \frac{3}{2}g^{(2)}n_0^4 & \text{if } g^{(2)} < \frac{3}{n_0} - \frac{3}{n_0^2}g^{(2)} \leq \frac{1}{n_0}\,, \\ 3n_0^2 - 2n_0^3 + \frac{g^{(2)}n_0^4}{2} & \text{if } g^{(2)} < \frac{3}{n_0} - \frac{3}{n_0^2} \text{ and } g^{(2)} > \frac{1}{n_0}\,, \\ \frac{g^{(2)}n_0^4}{2} & \text{if } g^{(2)} \geq \frac{3}{n_0} - \frac{3}{n_0^2} \text{ and } g^{(2)} < \frac{1}{n_0}\,, \\ n_0^3 - \frac{g^{(2)}n_0^4}{2} & \text{if } g^{(2)} \geq \frac{3}{n_0} - \frac{3}{n_0^2} \text{ and } g^{(2)} \geq \frac{1}{n_0}\,, \end{cases} \tag{A.9}$$

$$\mathcal{P}_g(n_0, g^{(3)}) = \frac{n_0^5}{2} \times \begin{cases} \frac{2}{n_0^2} - \frac{1}{n_0} + \frac{n_0 g^{(3)}}{6} & \text{if } g^{(3)} < \frac{6-6n_0}{n_0^3-3n_0}\,, \\ -\frac{g^{(3)}}{n_0} + \frac{1}{n_0} + \frac{n_0 g^{(3)}}{2} & \text{if } g^{(3)} \geq \frac{6-6n_0}{n_0^3-3n_0} \text{ and } n_0 \geq \sqrt{3}\,, \\ \frac{2}{n_0^2} - \frac{1}{n_0} + \frac{n_0 g^{(3)}}{6} & \text{if } g^{(3)} \geq \frac{6-6n_0}{n_0^3-3n_0} \text{ and } n_0 < \sqrt{3}\,. \end{cases} \tag{A.10}$$

$$\mathcal{P}_g(g^{(2)}) = (g^{(2)})^{-4} \begin{cases} \frac{1}{60}\Big(2g^{(2)}\big[\,(-12A_1 + 16A_2 + 75)\,g^{(2)} + \\ 63A_1 - 56A_2 - 190\big] - \\ 81A_1 + 48A_2 + 195\Big) & \text{if } 0 \leq g^{(2)} \leq \frac{1}{2}\,, \\ \frac{1}{60}\Big(2g^{(2)}\big[\,-3\,(4A_1 - 16A_3 + 75)\,g^{(2)} + \\ 63A_1 - 224A_3 + 370\big] - \\ 81A_1 + 256A_3 - 271\Big) & \text{if } \frac{1}{2} < g^{(2)} \leq \frac{2}{3}\,, \\ \frac{1}{10}\left[2A_1(21 - 4g^{(2)})g^{(2)} - 27A_1 + 5\right] & \text{if } \frac{2}{3} < g^{(2)} \leq \frac{3}{4}\,, \\ \frac{1}{2} & \text{if } g^{(2)} > \frac{3}{4}\,. \end{cases} \tag{A.11}$$

where $A_1 = \sqrt{9 - 12g^{(2)}}$, $A_2 = \sqrt{1 - 2g^{(2)}}$ and $A_3 = \sqrt{4 - 6g^{(2)}}$.

A.3 UPPER BOUNDARIES FOR THE N-PARTICLE HILBERT SPACE

Proposition A.3.1. *Given some $\mathcal{H}_N$, for every pair $G^{(k-1)}$ and $G^{(k)}$ with $k \leq N$, the inequality $(N-k+1)!G^{(k-1)} \geq (N-k)!G^{(k)}$ is satisfied. Subsequently, it holds that $0!G^{(N)} \leq 1!G^{(N-1)} \leq \cdots \leq (N-3)!G^{(3)} \leq (N-2)!G^{(2)}$.*

Since these observables can be expressed as:

$$G^{(k-1)} = \sum_{n=k-1}^{N} \frac{n!}{(n-k+1)!} P_n \,, \tag{A.12a}$$

$$G^{(k)} = \sum_{n=k}^{N} \frac{n!}{(n-k)!} P_n \,, \tag{A.12b}$$

it follows that:

$$\begin{aligned} G^{(k-1)} - \frac{(N-k)!}{(N-k+1)!} G^{(k)} = (k-1)! P_{k-1} + \\ \sum_{n=k}^{N} \left(\frac{1}{(n-k+1)!} - \frac{(N-k)!}{(N-k+1)!(n-k)!)} \right) n! P_n \,. \end{aligned} \tag{A.13}$$

The term between parentheses in the summation is always greater than 0 and is equal to zero only if $n = N$. Therefore, the right side of the last equation is greater than 0 as well:

$$G^{(k-1)} - \frac{(N-k)!}{(N-k+1)!} G^{(k)} \geq 0 \,, \tag{A.14}$$

i.e., $(N-k+1)! G^{(k-1)} \geq (N-k)! G^{(k)}$.

Proposition A.3.2. *In every Hilbert space $\mathcal{H}_N$, $g^{(2)}$ admits an upper boundary, that is given by $\frac{N-1}{n_0}$.*

From the definition for $n_0 = \sum_{n=0}^{N} n P_n$ and $G^{(2)} = \sum_{n=0}^{N} n(n-1) P_n$ in $\mathcal{H}_N$, we find, multiplying n_0 by $N-1$:

$$\sum_{n=0}^{N} n(N-1) P_n = (N-1) P_1 + \cdots + N(N-1) P_N \,. \tag{A.15}$$

Subtracting $G^{(2)}$ from expression (A.15) leads to $\sum_{n=0}^{N} n(N-n) P_n$. This is always greater than 0 and only equal if every term of the summation is null since all of them are positive (remembering that $1 \geq P_n \geq 0$). Therefore:

$$(N-1) n_0 \geq G^{(2)} \,, \tag{A.16}$$

or, since $G^{(2)} = n_0^2 g^{(2)}$:

$$g^{(2)} \leq \frac{N-1}{n_0} \,. \tag{A.17}$$

Finally, $g^{(2)}$ can reach its upper boundary only if every P_n vanishes excepting P_0 and P_N, i.e., when the corresponding state is a "Coin state", cf. Eq. ((1.20)). Assuming both propositions, we can infer that:

$$G^{(k)} \leq \frac{(N-2)!}{(N-k)!} G^{(2)} \,. \tag{A.18}$$

Furthermore, as $G^{(k)}$ can be written as $n_0^k g^{(k)}$ and from Eq. ((A.17)), we obtain:

$$g^{(k)} \leq \frac{(N-2)!}{(N-k)!}\frac{g^{(2)}}{n_0^{k-2}} \leq \frac{(N-1)!}{(N-k)!}\frac{1}{n_0^{k-1}}\,. \tag{A.19}$$

A.4 EQUIVALENCE BETWEEN CORRELATOR EQUATIONS AND INTEGRALS

A.4.1 CORRELATOR EQUATIONS

We prove now the equivalence between the equations of motions for the filtered correlators and the direct expressions of the filtered field. The n sensors dynamics, with associated operators ς_j, centre frequencies ω_i and widths Γ, relays on the Hamiltonian:

$$H = H_a + \sum_{j=1}^{n} \omega_j \varsigma_j^\dagger \varsigma_j + \epsilon\left(\varsigma_j^\dagger a + a^\dagger \varsigma_j\right) = H_0 + \epsilon \sum_{j=1}^{n}\left(\varsigma_j^\dagger a + a^\dagger \varsigma_j\right) \tag{A.20}$$

where H_a corresponds to the unfiltered dynamics, a is any annihilation operator associated to the unperturbed system and the coupling constant ϵ must be infinitely small ($\epsilon \to 0$). The dissipative dynamics are governed by the master equation:

$$\partial_t \rho = -i\,[H,\rho] + \sum_d \frac{\gamma_d}{2}\mathcal{L}_d\rho + \frac{\Gamma}{2}\sum_{j=1}^{n}\mathcal{L}_{\varsigma_j}\rho\,, \tag{A.21}$$

where d are operators which act on the unperturbed Hilbert space and $\mathcal{L}_d\rho = 2d\rho d^\dagger - d^\dagger d\rho - \rho d^\dagger d$ is the Lindbladian operator.

From the master equation, we can obtain equations of motion for the correlators $\langle\vec{c}\rangle$, as described in the main text: $\partial_t\langle\vec{c}\,(t)\rangle = M\langle\vec{c}\,(t)\rangle$. In particular, the unperturbed set $\langle\vec{c}_0\rangle$ follows $\partial_t\langle\vec{c}_0(t)\rangle = M_{0,0}\langle\vec{c}_0(t)\rangle$ (here $\vec{c}_0$ includes the unity as the first element). Continuing the procedure, we get the subsequent set $\langle\vec{c}_1\rangle$ which consists of the collections $\langle\varsigma_j^\dagger\vec{c}_0\rangle$ and $\langle\vec{c}_0\varsigma_j\rangle$. From the regression matrix elements shown in A.7, we see that any element of the set $\langle\vec{c}_1\rangle$, also represented by $\{m,n,1,0\}$ (and $\{m,n,0,1\}$), is connected to $\{m+1,n,0,0\}$ (and $\{m,n+1,0,0\}$), to itself and other elements $\{m',n',1,0\}$. Knowing that, it is easier to visualize that $M_{1,0}$ links $\langle\vec{c}_0\varsigma_j\rangle$ to $\langle\vec{c}_0 a\rangle$ (and $\langle\varsigma_j^\dagger\vec{c}_0\rangle$ to $\langle a^\dagger\vec{c}_0\rangle$) while $M_{1,1}$ returns $M_{0,0}$ plus the sensor *free* contribution $-(\Gamma/2 \pm i\,\omega_j)\,I$. Of

course, both $\langle \vec{c}_0 a \rangle$ and $\langle a^\dagger \vec{c}_0 \rangle$ are contained in $\langle \vec{c}_0 \rangle$ by definition. We explicitly show the equations right below

$$\partial_t \langle \vec{c}_0 \varsigma_j \rangle = \left[M_{0,0} - \left(\Gamma/2 + i\,\omega_j \right) I \right] \langle \vec{c}_0 \varsigma_j \rangle - i\epsilon \langle \vec{c}_0 a \rangle \,, \tag{A.22a}$$

$$\partial_t \langle \varsigma_j^\dagger \vec{c}_0 \rangle = \left[M_{0,0} - \left(\Gamma/2 - i\,\omega_j \right) I \right] \langle \varsigma_j^\dagger \vec{c}_0 \rangle + i\epsilon \langle a^\dagger \vec{c}_0 \rangle \,. \tag{A.22b}$$

For brevity, we did and will omit the time dependency of all variables. These equations can be rewritten using matrix notation as shown in the main text.

The next set of equations are:

$$\begin{aligned} \partial_t \langle \vec{c}_0 \varsigma_j \varsigma_k \rangle = {} & \left[M_{0,0} - \left(\Gamma + i(\omega_k + \omega_j) \right) I \right] \langle \vec{c}_0 \varsigma_j \varsigma_k \rangle - \\ & i\epsilon \left(\langle \vec{c}_0 a \varsigma_j \rangle + \langle \vec{c}_0 a \varsigma_k \rangle \right) \,, \end{aligned} \tag{A.23a}$$

$$\begin{aligned} \partial_t \langle \varsigma_j^\dagger \vec{c}_0 \varsigma_k \rangle = {} & \left[M_{0,0} - \left(\Gamma + i(\omega_k - \omega_j) \right) I \right] \langle \varsigma_j^\dagger \vec{c}_0 \varsigma_k \rangle - \\ & i\epsilon \left(\langle \varsigma_j^\dagger \vec{c}_0 a \rangle - \langle a^\dagger \vec{c}_0 \varsigma_k \rangle \right) \,, \end{aligned} \tag{A.23b}$$

$$\begin{aligned} \partial_t \langle \varsigma_j^\dagger \varsigma_k^\dagger \vec{c}_0 \rangle = {} & \left[M_{0,0} - \left(\Gamma - i(\omega_k + \omega_j) \right) I \right] \langle \varsigma_j^\dagger \varsigma_k^\dagger \vec{c}_0 \rangle + \\ & i\epsilon \left(\langle \varsigma_j^\dagger a^\dagger \vec{c}_0 \rangle + \langle \varsigma_k^\dagger a^\dagger \vec{c}_0 \rangle \right) \,, \end{aligned} \tag{A.23c}$$

Or, using the matrix notation introduced in the main text,

$$\partial_t \begin{pmatrix} \langle \varsigma_j^\dagger \varsigma_k^\dagger \vec{c}_0 \rangle \\ \langle \varsigma_j^\dagger \vec{c}_0 \varsigma_k \rangle \\ \langle \vec{c}_0 \varsigma_j \varsigma_k \rangle \end{pmatrix} = M_{2,2} \begin{pmatrix} \langle \varsigma_j^\dagger \varsigma_k^\dagger \vec{c}_0 \rangle \\ \langle \varsigma_j^\dagger \vec{c}_0 \varsigma_k \rangle \\ \langle \vec{c}_0 \varsigma_j \varsigma_k \rangle \end{pmatrix} + M_{2,1}^{(j)} \begin{pmatrix} \langle \varsigma_j^\dagger \vec{c}_0 \rangle \\ \langle \vec{c}_0 \varsigma_j \rangle \end{pmatrix} + M_{2,1}^{(k)} \begin{pmatrix} \langle \varsigma_k^\dagger \vec{c}_0 \rangle \\ \langle \vec{c}_0 \varsigma_k \rangle \end{pmatrix} \,, \tag{A.24}$$

where

$$M_{2,2} = \begin{pmatrix} M_{0,0} - (z_j^* + z_k^*) I & 0 & 0 \\ 0 & M_{0,0} - (z_j^* + z_k) I & 0 \\ 0 & 0 & M_{0,0} - (z_j + z_k) I \end{pmatrix} \,, \tag{A.25}$$

and

$$M_{2,1}^{(j)} = \begin{pmatrix} i\epsilon \mathrm{T}_+ & 0 \\ -i\epsilon \mathrm{T}_- & 0 \\ 0 & -i\epsilon \mathrm{T}_- \end{pmatrix} \quad \text{and} \quad M_{2,1}^{(k)} = \begin{pmatrix} i\epsilon \mathrm{T}_+ & 0 \\ 0 & i\epsilon \mathrm{T}_+ \\ 0 & -i\epsilon \mathrm{T}_- \end{pmatrix} \,. \tag{A.26}$$

The steady-state solution is found using Eq. (3.5), leading to

$$\langle \varsigma_j^\dagger \varsigma_k^\dagger \vec{c}_0 \rangle_{ss} = \left[M_{0,0} - (z_j^* + z_k^*) I \right]^{-1} \left(- i\epsilon \, \mathrm{T}_+ \langle \varsigma_j^\dagger \vec{c}_0 \rangle_{ss} + (j \leftrightarrow k) \right), \tag{A.27}$$

$$\langle \varsigma_j^\dagger \vec{c}_0 \varsigma_k \rangle_{ss} = \left[M_{0,0} - (z_j^* + z_k) I \right]^{-1} \left(i\epsilon \, \mathrm{T}_- \langle \varsigma_j^\dagger \vec{c}_0 \rangle_{ss} - i\epsilon \, \mathrm{T}_+ \langle \vec{c}_0 \varsigma_k \rangle_{ss} \right), \tag{A.28}$$

$$\langle \vec{c}_0 \varsigma_j \varsigma_k \rangle_{ss} = \left[M_{0,0} - (z_j + z_k) I \right]^{-1} \left(i\epsilon \, \mathrm{T}_- \langle \vec{c}_0 \varsigma_j \rangle_{ss} + (j \leftrightarrow k) \right), \tag{A.29}$$

where $(j \leftrightarrow k)$ indicates that the previous expression is taken with indices j and k exchanged. Note that choosing $k = j$ and keeping only the first element of the vector equation (A.23b) leads to the equation for $n_j \equiv \langle \varsigma_j^\dagger \varsigma_j \rangle$, this is, the j-th sensor population (proportional to the 1-photon spectrum $s_\Gamma^{(1)}(\omega_j)$).

$$\langle \varsigma_j^\dagger \varsigma_j \rangle = \left\{ \left[M_{0,0} - (z_j^* + z_j) I \right]^{-1} \left(i\epsilon \, \mathrm{T}_- \langle \varsigma_j^\dagger \vec{c}_0 \rangle_{ss} - i\epsilon \, \mathrm{T}_+ \langle \vec{c}_0 \varsigma_j \rangle_{ss} \right) \right\}_1 \tag{A.30}$$

$$= \left[\left(M_{0,0} - \Gamma I \right)^{-1} \mathrm{Re} \left\{ 2i\epsilon \, \mathrm{T}_- \langle \varsigma_j^\dagger \vec{c}_0 \rangle_{ss} \right\} \right]_1, \tag{A.31}$$

here the terms in round brackets are conjugate each other.

Then, moving up to the third order,

$$\partial_t \langle \varsigma_j^\dagger \varsigma_k^\dagger \vec{c}_0 \varsigma_j \rangle = \left[M_{0,0} - \left(\frac{3}{2}\Gamma - i\omega_k \right) I \right] \langle \varsigma_j^\dagger \varsigma_k^\dagger \vec{c}_0 \varsigma_j \rangle + i\epsilon \left(\langle \varsigma_j^\dagger a^\dagger \vec{c}_0 \varsigma_j \rangle + \langle \varsigma_k^\dagger a^\dagger \vec{c}_0 \varsigma_j \rangle - \langle \varsigma_j^\dagger \varsigma_k^\dagger \vec{c}_0 a \rangle \right), \tag{A.32a}$$

$$\partial_t \langle \varsigma_j^\dagger \vec{c}_0 \varsigma_k \varsigma_j \rangle = \left[M_{0,0} - \left(\frac{3}{2}\Gamma + i\omega_k \right) I \right] \langle \varsigma_j^\dagger \vec{c}_0 \varsigma_k \varsigma_j \rangle + i\epsilon \left(\langle a^\dagger \vec{c}_0 \varsigma_k \varsigma_j \rangle - \langle \varsigma_j^\dagger \vec{c}_0 a \varsigma_j \rangle - \langle \varsigma_j^\dagger \vec{c}_0 a \varsigma_k \rangle \right), \tag{A.32b}$$

These ones, written in matrix form, are

$$\partial_t \begin{pmatrix} \langle \varsigma_j^\dagger \varsigma_k^\dagger \vec{c}_0 \varsigma_j \rangle \\ \langle \varsigma_j^\dagger \vec{c}_0 \varsigma_j \varsigma_k \rangle \end{pmatrix} = M_{3,3} \begin{pmatrix} \langle \varsigma_j^\dagger \varsigma_k^\dagger \vec{c}_0 \varsigma_j \rangle \\ \langle \varsigma_j^\dagger \vec{c}_0 \varsigma_j \varsigma_k \rangle \end{pmatrix} + M_{3,2}^{(j)} \begin{pmatrix} 0 \\ \langle \varsigma_j^\dagger \vec{c}_0 \varsigma_j \rangle \\ 0 \end{pmatrix} + M_{3,2}^{(k)} \begin{pmatrix} \langle \varsigma_k^\dagger \varsigma_j^\dagger \vec{c}_0 \rangle \\ \langle \varsigma_k^\dagger \vec{c}_0 \varsigma_j \rangle \\ \langle \vec{c}_0 \varsigma_k \varsigma_j \rangle \end{pmatrix}, \tag{A.33}$$

where

$$M_{3,3} = \begin{pmatrix} M_{0,0} - (z_j + z_j^* + z_k^*) I & 0 \\ 0 & M_{0,0} - (z_j + z_k + z_j^*) I \end{pmatrix} \tag{A.34}$$

and

$$M_{3,2}^{(j)} = \begin{pmatrix} 0 & i\epsilon \mathrm{T}_+ & 0 \\ 0 & -i\epsilon \mathrm{T}_- & 0 \end{pmatrix} \quad \text{and} \quad M_{3,2}^{(k)} = \begin{pmatrix} -i\epsilon \mathrm{T}_- & i\epsilon \mathrm{T}_+ & 0 \\ 0 & i\epsilon \mathrm{T}_+ & -i\epsilon \mathrm{T}_- \end{pmatrix}. \tag{A.35}$$

which have the solution

$$\begin{aligned} \langle \varsigma_j^\dagger \varsigma_k^\dagger \vec{c}_0 \varsigma_j \rangle_{ss} = & \Big[M_{0,0} - \Big(\frac{3\Gamma}{2} - i\omega_k \Big) \Big]^{-1} \big(i\epsilon \mathrm{T}_- \langle \varsigma_j^\dagger \varsigma_k^\dagger \vec{c}_0 \rangle_{ss} - \\ & i\epsilon \mathrm{T}_+ \langle \varsigma_j^\dagger \vec{c}_0 \varsigma_j \rangle_{ss} - i\epsilon \mathrm{T}_+ \langle \varsigma_k^\dagger \vec{c}_0 \varsigma_j \rangle_{ss} \big) , \end{aligned} \tag{A.36}$$

$$\begin{aligned} \langle \varsigma_j^\dagger \vec{c}_0 \varsigma_j \varsigma_k \rangle_{ss} = & \Big[M_{0,0} - \Big(\frac{3\Gamma}{2} + i\omega_k \Big) \Big]^{-1} \big(i\epsilon \mathrm{T}_- \langle \varsigma_j^\dagger \vec{c}_0 \varsigma_j \rangle_{ss} + \\ & i\epsilon \mathrm{T}_- \langle \varsigma_j^\dagger \vec{c}_0 \varsigma_k \rangle_{ss} - i\epsilon \mathrm{T}_+ \langle \vec{c}_0 \varsigma_j \varsigma_k \rangle_{ss} \big) , \end{aligned} \tag{A.37}$$

And, finally, we reach the fourth order set of equations. However, we only display the first component (corresponding to $(\vec{c}_0)_1 = 1$) which yields

$$\begin{aligned} \partial_t \langle \varsigma_j^\dagger \varsigma_k^\dagger \varsigma_k \varsigma_j \rangle = & -2\Gamma \langle \varsigma_j^\dagger \varsigma_k^\dagger \varsigma_k \varsigma_j \rangle + i\epsilon \big(\langle \varsigma_j^\dagger a^\dagger \varsigma_k \varsigma_j \rangle + \langle \varsigma_k^\dagger a^\dagger \varsigma_k \varsigma_j \rangle - \\ & \langle \varsigma_j^\dagger \varsigma_k^\dagger a \varsigma_j \rangle - \langle \varsigma_j^\dagger \varsigma_k^\dagger a \varsigma_k \rangle \big) \\ = & -2\Gamma \langle \varsigma_j^\dagger \varsigma_k^\dagger \varsigma_k \varsigma_j \rangle + 2\,\mathrm{Re}\Big\{ i\epsilon \langle \varsigma_j^\dagger a^\dagger \varsigma_k \varsigma_j \rangle \Big\} + (j \leftrightarrow k) , \end{aligned} \tag{A.38}$$

Its steady-state solution, using the matrix notation, is

$$\langle \varsigma_j^\dagger \varsigma_k^\dagger \varsigma_k \varsigma_j \rangle_{ss} = \frac{1}{\Gamma} \Big[\mathrm{Re}\Big\{ i\epsilon\, \mathrm{T}_+ \langle \varsigma_j^\dagger \vec{c}_0 \varsigma_k \varsigma_j \rangle_{ss} \Big\} + (j \leftrightarrow k) \Big]_1 , \tag{A.39}$$

The correlator $G_\Gamma^{(2)}(\omega_i, \omega_k) \equiv \langle \varsigma_j^\dagger \varsigma_k^\dagger \varsigma_k \varsigma_j \rangle$ is proportional to the 2-photon spectrum $s_\Gamma^{(2)}(\omega_j, \omega_k)$. These equations do completely determinate evolution of $G_\Gamma^{(2)}(\omega_i, \omega_k)$.

In the same way, the 2-time correlations $\vec{v}_{A,B}(t,\tau) = \langle A(t)\vec{c}(t+\tau)B(t) \rangle$ can be calculated through the equation $\partial_\tau \vec{v}_{A,B}(t,\tau) = M\,\vec{v}_{A,B}(t,\tau)$ ($A(t)$ and $B(t)$ are properly normal ordered) and identically solved using the stratified equations shown above just by making the substitution $\vec{c}(t) \to A(t)\vec{c}(t+\tau)B(t)$. For instance, in order to

compute $G_{\Gamma}^{(2)}\left(\omega_j,\omega_k;t,t+\tau\right) \equiv \langle \mathcal{T}[\varsigma_j^{\dagger}(t)(\varsigma_k^{\dagger}\varsigma_k)(t+\tau)\varsigma_j(t)]\rangle$ (where $\mathcal{T}$ denotes time ordering), we need the sequence of equations

$$\partial_\tau\langle A(t)(\vec{c}_0)(t+\tau)B(t)\rangle = M_{0,0}\langle A(t)(\vec{c}_0)(t+\tau)B(t)\rangle\,, \tag{A.40a}$$

$$\partial_\tau\langle A(t)(\vec{c}_0\varsigma_k)(t+\tau)B(t)\rangle = [M_{0,0} - (\Gamma/2 + i\,\omega_k)\,I]\,\langle A(t)(\vec{c}_0\varsigma_k)(t+\tau)B(t)\rangle - i\epsilon\langle A(t)(\vec{c}_0 a)(t+\tau)B(t)\rangle\,, \tag{A.40b}$$

$$\partial_\tau\langle A(t)(\varsigma_k^{\dagger}\vec{c}_0)(t+\tau)B(t)\rangle = [M_{0,0} - (\Gamma/2 - i\,\omega_k)\,I]\,\langle A(t)(\varsigma_k^{\dagger}\vec{c}_0)(t+\tau)B(t)\rangle + i\epsilon\langle A(t)(a^{\dagger}\vec{c}_0)(t+\tau)B(t)\rangle\,, \tag{A.40c}$$

$$\partial_\tau\langle A(t)(\varsigma_k^{\dagger}\varsigma_k)(t+\tau)B(t)\rangle = -\Gamma\,\langle A(t)(\varsigma_k^{\dagger}\varsigma_k)(t+\tau)B(t)\rangle + i\epsilon\big(\langle A(t)(a^{\dagger}\varsigma_k)(t+\tau)B(t)\rangle - \langle A(t)(\varsigma_k^{\dagger}a)(t+\tau)B(t)\rangle\big)\,, \tag{A.40d}$$

where A and B would be replaced by $\varsigma_j^{\dagger}$ and ς_j, respectively. To solve the system, we assume that the system is in the steady-state, so $t \to \infty$ and the correlators will only depend on τ.

$$\partial_\tau\langle\varsigma_j^{\dagger}(\vec{c}_0)(\tau)\,\varsigma_j\rangle = M_{0,0}\langle\varsigma_j^{\dagger}(\vec{c}_0)(\tau)\,\varsigma_j\rangle\,, \tag{A.41a}$$

$$\partial_\tau\langle\varsigma_j^{\dagger}(\vec{c}_0\varsigma_k)(\tau)\,\varsigma_j\rangle = [M_{0,0} - z_k I]\,\langle\varsigma_j^{\dagger}(\vec{c}_0\varsigma_k)(\tau)\,\varsigma_j\rangle - i\epsilon\mathrm{T}_-\langle\varsigma_j^{\dagger}(\vec{c}_0)(\tau)\,\varsigma_j\rangle\,, \tag{A.41b}$$

$$\partial_\tau\langle\varsigma_j^{\dagger}(\varsigma_k^{\dagger}\varsigma_k)(\tau)\,\varsigma_j\rangle = -\,\Gamma\,\langle\varsigma_j^{\dagger}(\varsigma_k^{\dagger}\varsigma_k)(\tau)\,\varsigma_j\rangle + \mathrm{Re}\left[2i\epsilon\mathrm{T}_+\langle\varsigma_j^{\dagger}(\vec{c}_0\varsigma_k)(\tau)\,\varsigma_j\rangle\right]_1\,, \tag{A.41c}$$

As explained in the text, we do the following change $\langle\varsigma_j^{\dagger}\,\vec{c}(\tau)\,\varsigma_j\rangle \to \Delta\langle\varsigma_j^{\dagger}\,\vec{c}(\tau)\,\varsigma_j\rangle = \langle\varsigma_j^{\dagger}\,\vec{c}(\tau)\,\varsigma_j\rangle - \langle\varsigma_j^{\dagger}\varsigma_j\rangle_{ss}\langle\vec{c}\rangle_{ss}$ to simplify further calculations. This step is not strictly necessary and can be absorbed in the eigenvector and their inverse matrices. For instance, where this change is made the off-diagonal blocks of $M_{0,0}$ disappear. Then, it turns into

$$M_{0,0} = \begin{pmatrix} 0 & 0 \\ 0 & M'_{0,0} \end{pmatrix} = \begin{pmatrix} 1 & 0 \\ 0 & E' \end{pmatrix}\begin{pmatrix} 0 & 0 \\ 0 & D' \end{pmatrix}\begin{pmatrix} 1 & 0 \\ 0 & E'^{-1} \end{pmatrix} = E\,D\,E^{-1}\,, \tag{A.42}$$

where the matrix eigenvalue decomposition is shown in the second term, the diagonal matrix $D = \mathrm{diag}(\lambda^{(0)}) = \mathrm{diag}(0, d_1, ..., d_m)$ has a total amount of $m+1$ eigenvalues. This decomposition is also valid for $M_{0,0} - aI$, the eigenvector remain untouched while the eigenvalues get rigidly displaced, i.e., $D_a = D - aI = \mathrm{diag}(\lambda^{(0)} - a)$. Following this, the solution of A.41 are:

$$\Delta\langle\varsigma_j^{\dagger}(\vec{c}_0)(\tau)\,\varsigma_j\rangle = \sum_{p=1}^{m+1}\vec{l}_p^{(0)}e^{\lambda_p^{(0)}\tau}\,, \tag{A.43}$$

where the vector elements are $\ell_{ip}^{(0)} = (E)_{ip}\sum_q (E^{-1})_{pq}(\Delta\langle\varsigma_j^\dagger \vec{c}_0\,\varsigma_j\rangle_{ss})_q$.

$$\Delta\langle\varsigma_j^\dagger(\vec{c}_0\varsigma_k)(\tau)\,\varsigma_j\rangle = \sum_{p=1}^{2(m+1)} \vec{\ell}_p^{(1)} e^{\lambda_p^{(1)}\tau}\,, \tag{A.44}$$

where $\lambda^{(1)}$ includes $\lambda^{(0)}$ and, subsequently, $\lambda^{(0)} - z_k$ and $\ell_{ip}^{(1)}$ follows Eq. (3.31). Developing the last expression

$$\begin{aligned}\Delta(\langle\varsigma_j^\dagger(\vec{c}_0\varsigma_k)(\tau)\,\varsigma_j\rangle)_i = &\sum_{q=1}^{m+1}\left(-\sum_p R_{ipq}^{(1)}\right) e^{\lambda_q^{(0)}\tau} + \\ &\sum_{p=1}^{m+1}\left(L_{ip}^{(1)} + \sum_q R_{ipq}^{(1)}\right) e^{(\lambda_p^{(0)}-z_k)\tau}\,,\end{aligned} \tag{A.45}$$

being $L_{ip}^{(1)} = (E)_{ip}\sum_q (E^{-1})_{pq}(\Delta\langle\varsigma_j^\dagger\vec{c}_0\varsigma_k\,\varsigma_j\rangle_{ss})_q$ and, reminding that $Q_1 = -i\epsilon E^{-1}\mathrm{T}_-$ in this case,

$$\begin{aligned}R_{ipq}^{(1)} &= -i\epsilon\,(E)_{ip}\sum_{q'}(E^{-1}\mathrm{T}_-)_{pq'}L_{q'q}^{(0)}\frac{1}{\lambda_p^{(0)} - z_k - \lambda_q^{(0)}} = \\ &-i\epsilon\sum_{q',k,l}\frac{(E)_{ip}(E^{-1})_{pk}(\mathrm{T}_-)_{kq'}(E)_{q'q}(E^{-1})_{ql}}{\lambda_p^{(0)} - \lambda_q^{(0)} - z_k}(\Delta\langle\varsigma_j^\dagger\vec{c}_0\,\varsigma_j\rangle_{ss})_l\,,\end{aligned} \tag{A.46}$$

And, applying this to Eq. (A.41c),

$$\begin{aligned}\Delta\langle\varsigma_j^\dagger(\varsigma_k^\dagger\varsigma_k)(\tau)\,\varsigma_j\rangle = &\left[\Delta\langle\varsigma_j^\dagger\varsigma_k^\dagger\varsigma_k\varsigma_j\rangle_{ss} + 2\,\mathrm{Re}\left\{\sum_{q=1}^{2(m+1)} R_q^{(2)}\right\}\right] e^{-\Gamma\tau} + \\ &2\,\mathrm{Re}\left\{-\sum_{q=1}^{2(m+1)} R_q^{(2)} e^{\lambda_p^{(1)}\tau}\right\},\end{aligned} \tag{A.47}$$

where

$$R_q^{(2)} = -i\epsilon\sum_i(\mathrm{T}_+)_{1i}\frac{\ell_{iq}^{(1)}}{\Gamma + \lambda_q^{(1)}}\,. \tag{A.48}$$

Rearranging (A.47) to show the equivalence with the expression shown in the Supplemental Material of [55],

$$\begin{aligned}
&\Delta\langle\varsigma_j^\dagger(\varsigma_k^\dagger\varsigma_k)(\tau)\,\varsigma_j\rangle = \Delta\langle\varsigma_j^\dagger\varsigma_k^\dagger\varsigma_k\varsigma_j\rangle_{ss}\; e^{-\Gamma\tau} + \\
&2\,\mathrm{Re}\left\{-\sum_{q=1}^{2(m+1)} R_q^{(2)}(e^{\lambda_q^{(1)}\tau} - e^{-\Gamma\tau})\right\} \\
&= \Delta\langle\varsigma_j^\dagger\varsigma_k^\dagger\varsigma_k\varsigma_j\rangle_{ss}\; e^{-\Gamma\tau} + \\
&2\,\mathrm{Re}\left\{i\epsilon\sum_i(\mathrm{T}_+)_{1i}\sum_{q=1}^{m+1}\frac{-\sum_p R_{ipq}^{(1)}}{\Gamma+\lambda_q^{(0)}}(e^{\lambda_q^{(0)}\tau} - e^{-\Gamma\tau})\right\} + \\
&\qquad 2\,\mathrm{Re}\left\{i\epsilon\sum_k(\mathrm{T}_+)_{1i}\sum_{p=1}^{m+1}\frac{L_{ip}^{(1)} + \sum_q R_{ipq}^{(1)}}{\Gamma+\lambda_p^{(0)} - z_k}[e^{(\lambda_p^{(0)}-z_k)\tau} - e^{-\Gamma\tau}]\right\},
\end{aligned} \tag{A.49}$$

Now, isolating the term proportional to $L_{ip}^{(1)}$ inside the real part and substituting $z_k = \Gamma/2 + i\omega_k$

$$\begin{aligned}
&i\epsilon\sum_{i,p,q}(\mathrm{T}_+)_{1i}\; e^{-\Gamma\tau}(E)_{ip}\frac{e^{(\lambda_p^{(0)}+\Gamma/2-i\omega_k)\tau}-1}{\lambda_p^{(0)}+\Gamma/2-i\omega_k}(E^{-1})_{pq}(\Delta\langle\varsigma_j^\dagger\vec{c}_0\varsigma_k\,\varsigma_j\rangle_{ss})_q = \\
&\left(i\epsilon\mathrm{T}_+\; e^{-\Gamma\tau}E\frac{e^{(D-i\omega_k+\Gamma/2)\tau}-1}{D-i\omega_k+\Gamma/2}E^{-1}\Delta\langle\varsigma_j^\dagger\vec{c}_0\varsigma_k\,\varsigma_j\rangle_{ss}\right)_1 = \\
&(i\epsilon\,\mathrm{T}_+\,\mathcal{F}(\tau)\,\Delta\langle\varsigma_j^\dagger\vec{c}_0\varsigma_k\,\varsigma_j\rangle_{ss})_1\,,
\end{aligned} \tag{A.50}$$

where we have gather all matrix products and identified the factor form

$$\mathcal{F}(\tau) = e^{-\Gamma\tau}\frac{e^{[M_{0,0}+(-i\omega_k+\Gamma/2)I]\tau} - I}{M_{0,0}+(-i\omega_k+\Gamma/2)I}\,, \tag{A.51}$$

In the same, adding the terms proportional to $R_{ipq}^{(1)}$

$$\begin{aligned}
&i\epsilon\sum_{i,p,q}(\mathrm{T}_+)_{1i}\; e^{-\Gamma\tau}R_{ipq}^{(1)}\left(\frac{e^{(\lambda_p^{(0)}+\Gamma/2-i\omega_k)\tau}-1}{\lambda_p^{(0)}+\Gamma/2-i\omega_k} - \frac{e^{(\lambda_q^{(0)}+\Gamma)\tau}-1}{\lambda_q^{(0)}+\Gamma}\right) = \\
&\epsilon^2\sum_{i,p,q,q',k,l}(\mathrm{T}_+)_{1i}\left[e^{-\Gamma\tau}\frac{(E)_{ip}(E^{-1})_{pk}(\mathrm{T}_-)_{kq'}(E)_{q'q}(E^{-1})_{ql}}{\lambda_p^{(0)}-\lambda_q^{(0)}-i\omega_k-\Gamma/2}\right. \\
&\left.\left(\frac{e^{(\lambda_p^{(0)}-i\omega_k+\Gamma/2)\tau}-1}{\lambda_p^{(0)}-i\omega_k+\Gamma/2} - \frac{e^{(\lambda_q^{(0)}+\Gamma)\tau}-1}{\lambda_q^{(0)}+\Gamma}\right)\right](\Delta\langle\varsigma_j^\dagger\vec{c}_0\,\varsigma_j\rangle_{ss})_l = \\
&\left(\epsilon^2\,\mathrm{T}_+\,\mathcal{Z}(\tau)\;\Delta\langle\varsigma_j^\dagger\vec{c}_0\,\varsigma_j\rangle_{ss}\right)_1\,,
\end{aligned} \tag{A.52}$$

where we have substituted (A.46) and the elements of the matrix $\mathcal{Z}(\tau)$ are

$$\mathcal{Z}_{i,j}(\tau) = e^{-\Gamma\tau} \sum_{p,q,k,l} \frac{(E)_{ip}(E^{-1})_{pk}(\mathrm{T}_-)_{kl}(E)_{lq}(E^{-1})_{qj}}{\lambda_p^{(0)} - \lambda_q^{(0)} - \Gamma/2 - i\omega_k} \times \left(\frac{e^{(\lambda_p^{(0)} - i\omega_k + \Gamma/2)\tau} - 1}{\lambda_p^{(0)} - i\omega_k + \Gamma/2} - \frac{e^{(\lambda_q^{(0)} + \Gamma)\tau} - 1}{\lambda_q^{(0)} + \Gamma} \right), \tag{A.53}$$

Finally, inserting these results in Eq. (A.49), we obtain

$$\begin{aligned} \Delta\langle \varsigma_j^\dagger (\varsigma_k^\dagger \varsigma_k)(\tau)\, \varsigma_j \rangle = {} & \Delta\langle \varsigma_j^\dagger \varsigma_k^\dagger \varsigma_k \varsigma_j \rangle_{ss}\, e^{-\Gamma\tau} + \\ & 2\,\mathrm{Re}\Big\{ i\epsilon\, \mathrm{T}_+\, \mathcal{F}(\tau)\, \Delta\langle \varsigma_j^\dagger \vec{c}_0 \varsigma_k\, \varsigma_j \rangle_{ss} \Big\}_1 + \\ & 2\,\mathrm{Re}\Big\{ \epsilon^2\, \mathrm{T}_+\, \mathcal{Z}(\tau)\, \Delta\langle \varsigma_j^\dagger \vec{c}_0\, \varsigma_j \rangle_{ss} \Big\}_1 . \end{aligned} \tag{A.54}$$

Aside the change $\Delta\langle \varsigma_j^\dagger\, \vec{c}(\tau)\, \varsigma_j \rangle = \langle \varsigma_j^\dagger\, \vec{c}(\tau)\, \varsigma_j \rangle - \langle \varsigma_j^\dagger \varsigma_j \rangle_{ss} \langle \vec{c} \rangle_{ss}$, this expression is formally equivalent to Eq. (47) from Supplemental [55].

A.4.2 INTEGRALS

On the other hand, the filtered operator can be described as the following integral:

$$\varsigma_j(\omega_j, \Gamma; t) = \xi \frac{\Gamma}{2} \int_{-\infty}^{\infty} \theta(t - t') e^{-z_j(t-t')} a(t') dt' , \tag{A.55}$$

where $z_j \equiv \Gamma/2 + i\,\omega_j$, $\theta(x)$ is the Heaviside step function and ξ is a complex constant that would be properly chosen to match both approaches. Henceforth, we omit the filter frequencies and widths for brevity.

Following Eq. (A.55), $G_\Gamma^{(2)}\left(\omega_j, \omega_k; t, t+\tau\right)$ (for $\tau > 0$) can written as:

$$\begin{aligned} & \langle \varsigma_j^\dagger(t) (\varsigma_k^\dagger \varsigma_k)(t+\tau) \varsigma_j(t) \rangle = |\xi|^4 \left(\frac{\Gamma}{2}\right)^4 \int_{-\infty}^{\infty}\int_{-\infty}^{\infty}\int_{-\infty}^{\infty}\int_{-\infty}^{\infty} d\vec{t} \\ & \theta(t - t_1)\theta(t + \tau - t_2)\theta(t + \tau - t_3)\theta(t - t_4) \\ & \times e^{-z_j^*(t-t_1)} e^{-z_k^*(t+\tau-t_2)} e^{-z_k(t+\tau-t_3)} e^{-z_j(t-t_4)} \times \\ & \qquad \langle \mathcal{T}[a^\dagger(t_1) a^\dagger(t_2) a(t_3) a(t_4)] \rangle . \end{aligned} \tag{A.56}$$

Now, we derive last expression with respect to τ using Leibniz integral rule, which allows to differentiate under the integral sign, and we also use the fact $\partial_x \theta(x-y) = \delta(x-y)$:

$$\begin{aligned}
&\frac{d}{d\tau}\langle \varsigma_j^\dagger(t)(\varsigma_k^\dagger\varsigma_k)(t+\tau)\varsigma_j(t)\rangle = |\xi|^4\left(\frac{\Gamma}{2}\right)^4 \int_{-\infty}^{\infty}\int_{-\infty}^{\infty}\int_{-\infty}^{\infty}\int_{-\infty}^{\infty} d\vec{t}\\
&\frac{\partial}{\partial\tau}\big[\theta(t-t_1)\theta(t+\tau-t_2)\theta(t+\tau-t_3)\theta(t-t_4)\\
&\times e^{-z_j^*(t-t_1)}e^{-z_k^*(t+\tau-t_2)}e^{-z_k(t+\tau-t_3)}e^{-z_j(t-t_4)}\times\\
&\langle \mathcal{T}[a^\dagger(t_1)a^\dagger(t_2)a(t_3)a(t_4)]\rangle\big] =\\
&|\xi|^4\left(\frac{\Gamma}{2}\right)^4 \int_{-\infty}^{\infty}\int_{-\infty}^{\infty}\int_{-\infty}^{\infty}\int_{-\infty}^{\infty} d\vec{t}\,\big[\delta(t+\tau-t_2)\theta(t+\tau-t_3)+\\
&\theta(t+\tau-t_2)\delta(t+\tau-t_3) - (z_k^*+z_k)\theta(t+\tau-t_2)\theta(t+\tau-t_3)\big]\\
&\times\theta(t-t_1)\theta(t-t_4)e^{-z_j^*(t-t_1)}e^{-z_k^*(t+\tau-t_2)}e^{-z_k(t+\tau-t_3)}e^{-z_j(t-t_4)}\times\\
&\qquad\qquad \langle \mathcal{T}[a^\dagger(t_1)a^\dagger(t_2)a(t_3)a(t_4)]\rangle\,, \quad \text{(A.57)}
\end{aligned}$$

which, after some simplification and rearrangement, yields

$$\begin{aligned}
\frac{d}{d\tau}\langle \varsigma_j^\dagger(t)(\varsigma_k^\dagger\varsigma_k)(t+\tau)\varsigma_j(t)\rangle =& -(z_k^*+z_k)\langle \varsigma_j^\dagger(t)(\varsigma_k^\dagger\varsigma_k)(t+\tau)\varsigma_j(t)\rangle +\\
&\xi^*\frac{\Gamma}{2}\langle \varsigma_j^\dagger(t)(a^\dagger\varsigma_k)(t+\tau)\varsigma_j(t)\rangle + \xi\frac{\Gamma}{2}\langle \varsigma_j^\dagger(t)(\varsigma_k^\dagger a)(t+\tau)\varsigma_j(t)\rangle\,, \quad \text{(A.58)}
\end{aligned}$$

Last two terms are easily obtained by straight application of Dirac delta properties and Eq. (A.55). We define the next quantities:

$$\begin{aligned}
&\langle \varsigma_j^\dagger(t)(\vec{c}_0\varsigma_k)(t+\tau)\varsigma_j(t)\rangle = \xi|\xi|^2\left(\frac{\Gamma}{2}\right)^3 \int_{-\infty}^{\infty}\int_{-\infty}^{\infty}\int_{-\infty}^{\infty} d\vec{t}\\
&\theta(t-t_1)\theta(t+\tau-t_2)\theta(t-t_3)e^{-z_j^*(t-t_1)}e^{-z_k(t+\tau-t_2)}e^{-z_j(t-t_3)}\\
&\qquad\qquad \times\langle \mathcal{T}[a^\dagger(t_1)\vec{c}_0(t+\tau)a(t_2)a(t_3)]\rangle\,, \quad \text{(A.59)}
\end{aligned}$$

and

$$\begin{aligned}
&\langle \varsigma_j^\dagger(t)(\varsigma_k^\dagger\vec{c}_0)(t+\tau)\varsigma_j(t)\rangle = \xi^*|\xi|^2\left(\frac{\Gamma}{2}\right)^3 \int_{-\infty}^{\infty}\int_{-\infty}^{\infty}\int_{-\infty}^{\infty} d\vec{t}\\
&\theta(t-t_1)\theta(t+\tau-t_2)\theta(t-t_3)e^{-z_j^*(t-t_1)}e^{-z_k^*(t+\tau-t_2)}e^{-z_j(t-t_3)}\\
&\qquad\qquad \times\langle \mathcal{T}[a^\dagger(t_1)a^\dagger(t_2)\vec{c}_0(t+\tau)a(t_3)]\rangle\,. \quad \text{(A.60)}
\end{aligned}$$

Differentiating with respect to τ both (A.59) and (A.60) and remembering that Eq. (A.40a) is valid for higher multi-time cases immediately leads to:

$$\frac{d}{d\tau}\langle\varsigma_j^\dagger(t)(\vec{c}_0\varsigma_k)(t+\tau)\varsigma_j(t)\rangle = (M_{0,0} - z_k\, I)\,\langle\varsigma_j^\dagger(t)(\vec{c}_0\varsigma_k)(t+\tau)\varsigma_j(t)\rangle + \xi\frac{\Gamma}{2}\langle\varsigma_j^\dagger(t)(\vec{c}_0 a)(t+\tau)\varsigma_j(t)\rangle \quad \text{(A.61)}$$

$$\frac{d}{d\tau}\langle\varsigma_j^\dagger(t)(\varsigma_k^\dagger\vec{c}_0)(t+\tau)\varsigma_j(t)\rangle = (M_{0,0} - z_k^*\, I)\,\langle\varsigma_j^\dagger(t)(\varsigma_k^\dagger\vec{c}_0)(t+\tau)\varsigma_j(t)\rangle + \xi^*\frac{\Gamma}{2}\langle\varsigma_j^\dagger(t)(a^\dagger\vec{c}_0)(t+\tau)\varsigma_j(t)\rangle \quad \text{(A.62)}$$

Ultimately, we find that, by straight differentiation, $\langle\varsigma_j^\dagger(t)\vec{c}_0(t+\tau)\varsigma_j(t)\rangle$ fulfils the differential equation.

$$\frac{d}{d\tau}\langle\varsigma_j^\dagger(t)\vec{c}_0(t+\tau)\varsigma_j(t)\rangle = M_{0,0}\langle\varsigma_j^\dagger(t)\vec{c}_0(t+\tau)\varsigma_j(t)\rangle\,. \quad \text{(A.63)}$$

Reminding that $z_k = \Gamma/2 + i\,\omega_k$ and choosing $\xi = -2i\epsilon/\Gamma$ let us compare (A.58)-(A.63) to Eqs. (A.40) and we determine that both will lead to the same solution. This enables to claim that both methods are equivalent. In the same manner, single time dynamics are derived from the integral expression of the correlators, albeit we omit explicit calculations for conciseness of the proof.

A.5 GENERAL MOLLOW SPLITTING IN RESONANCE FLUORESCENCE AND GENERAL EXPRESSIONS OF SPECTRUM AND $g^{(2)}$ COEFFICIENTS

The eigenvalue decomposition of the regression matrix M for the detuned case has the following eigenvalues $-z_i/2$, where z_i $(i = 1, 2, 3)$ are the roots of the cubic polynomial

$$z^3 + 4\gamma_\sigma z^2 + \left[5\gamma_\sigma^2 + 4(4\Omega_\sigma^2 + \Delta_\sigma^2)\right]z + 2\gamma_\sigma(\gamma_\sigma^2 + 4\Delta_\sigma^2 + 8\Omega_\sigma^2)\,, \quad \text{(A.64)}$$

Since the coefficients of the polynomial are real, the zeros thereof have to be either all real or one real and the remaining two complex conjugate of each other. The quantity that tells the two possibilities apart is the discriminant

$$\zeta = \frac{\gamma_\sigma^4\Delta_\sigma^2}{16} + (\Delta_\sigma^2 + 4\Omega^2)^3 + \frac{\gamma_\sigma^2}{2}(\Delta_\sigma^4 - 10\Delta_\sigma^2\Omega_\sigma^2 - 2\Omega_\sigma^4)\,. \quad \text{(A.65)}$$

If $\zeta > 0$, then we are in the second situation. One solution, namely z_1, is real so that $\omega_1 = -\operatorname{Im}\{z_1\}/2 = 0$ and the corresponding peak is always at the center. The other two, z_2 and z_3, are mutual complex conjugate ($z_3 = z_2^*$) and therefore the position of one peak is always the specular image of the other, this is, $\omega_2 = -\omega_3 = -\operatorname{Im}\{z_2\}/2$. These two, when $\Delta_\sigma = 0$, contribute to the sidepeaks of the Mollow triplet shape of the resonance fluorescence spectrum. The condition $\zeta > 0$ simplifies to $64\Omega_\sigma^2 - \gamma_\sigma^2 > 0$ when the detuning is exactly zero. Similarly, for weak driving ($\Omega_\sigma \ll \gamma_\sigma$), the inequality is approximated as $\gamma_\sigma^2\Delta_\sigma^2 - 16\Omega_\sigma^4 > 0$. The splitting of the sidepeaks or satellites is twice $\Omega_+ = \omega_2$ which, for arbitrary detuning, reads

$$\begin{aligned}\Omega_+ = \Big\{ & 48\Omega_\sigma^2 + 12\Delta_\sigma^2 - \gamma_\sigma^2 + \big[36\gamma_\sigma^4(5\Delta_\sigma^2 - 4\Omega_\sigma^2) - \\ & 1728\sqrt{3\zeta}\gamma_\sigma(\Delta_\sigma^2 - 2\Omega_\sigma^2) + \\ & 432\gamma_\sigma^2(-32\Delta_\sigma^2\Omega_\sigma^2 + 5\Delta_\sigma^4 + 8\Omega_\sigma^4) - 48\sqrt{3\zeta}\gamma_\sigma^3 + \gamma_\sigma^6 + \\ & 1728(\Delta_\sigma^2 + 4\Omega_\sigma^2)^3\big]^{1/3}\Big\} \Big/ \Big\{ 4\sqrt{3}\big[\gamma_\sigma^6 + 36\gamma_\sigma^4(5\Delta_\sigma^2 - 4\Omega_\sigma^2) - \\ & 48\sqrt{3\zeta}\gamma_\sigma^3 + 432\gamma_\sigma^2(5\Delta_\sigma^4 - 32\Delta_\sigma^2\Omega_\sigma^2 + 8\Omega_\sigma^4) - \\ & 1728\sqrt{3\zeta}\gamma_\sigma(\Delta_\sigma^2 - 2\Omega_\sigma^2) + 1728(\Delta_\sigma^2 + 4\Omega_\sigma^2)^3\big]^{1/6}\Big\} \end{aligned} \tag{A.66}$$

This lengthy expression collapses to $\Omega_+ = \sqrt{4\Omega_\sigma^2 - \gamma_\sigma^2/16}$ if the excitation is resonant ($\Delta_\sigma = 0$). Whether Ω_σ or Δ_σ are much greater than γ_σ, the splitting can be approximated as $\Omega_+ \approx \sqrt{\Delta_\sigma^2 + 4\Omega_\sigma^2}$, this is twice the effective Rabi splitting induced by the laser predicted by the Hamiltonian dynamics. For the detuned case, the coefficients l_p and l_p for $g^{(2)}(\tau)$ and the luminescence spectrum, respectively, are

$$\begin{aligned} l_p = & \frac{\langle\sigma^\dagger\sigma\rangle}{\prod_{k\neq p}(z_p - z_k)}\big[(z_p + \gamma_\sigma - 2i\,\Delta_\sigma)(Z - z_p + \gamma_\sigma - 2i\,\Delta_\sigma) + \\ & \frac{(\gamma_\sigma + 2i\Delta_\sigma)\mathcal{Z}}{8\Omega_\sigma^2}\big]\,, \end{aligned} \tag{A.67}$$

and

$$\begin{aligned} \mathit{l}_p = & \langle\sigma^\dagger\sigma\rangle\frac{(z_p + 2\gamma_\sigma)(z_p + \gamma_\sigma - 2i\Delta_\sigma) + 8\Omega_\sigma^2}{8\Omega_\sigma^2(\gamma_\sigma^2 + 4\Delta_\sigma^2 + 8\Omega_\sigma^2)} \\ & \prod_{k\neq p}\Big[\gamma_\sigma^2 + 4\Delta_\sigma^2 + 8\Omega_\sigma^2 + z_k(\gamma_\sigma + 2i\Delta_\sigma)\Big]/(z_p - z_k)\,, \end{aligned} \tag{A.68}$$

where $Z = z_1 + z_2 + z_3$ and $\mathcal{Z} = \prod_k(z_k + \gamma_\sigma - 2i\Delta_\sigma)$.

A.6 DICKE MODEL SECOND MANIFOLD COUPLED EQUATIONS

We give here the second set of equations coupling each correlator with other same subsets elements and fed by the previous first order ones:

$$\frac{d}{dt}\langle a^2\rangle = -2i\Omega_a\langle a\rangle - (\gamma_a + 2i\Delta_a)\langle a^2\rangle - 2igN\langle a\Sigma\rangle\,, \tag{A.69a}$$

$$\frac{d}{dt}\langle a^\dagger a\rangle = i\Omega_a\left(\langle a\rangle - \langle a^\dagger\rangle\right) - \gamma_a\langle a^\dagger a\rangle + igN\left(\langle\Sigma^\dagger a\rangle - \langle a^\dagger\Sigma\rangle\right), \tag{A.69b}$$

$$\frac{d}{dt}\langle a^\dagger\Sigma\rangle = i\Omega_a\langle\Sigma\rangle - \left[\frac{\gamma_a+\gamma_\sigma}{2} - i\left(\Delta_a - \Delta_\sigma\right)\right]\langle a^\dagger\Sigma\rangle + ig\left(N\langle\Sigma^\dagger\Sigma\rangle - \langle a^\dagger a\rangle\right), \tag{A.69c}$$

$$\frac{d}{dt}\langle a^\dagger\Sigma^\dagger\rangle = i\Omega_a\langle\Sigma^\dagger\rangle - \left[\frac{\gamma_a+\gamma_\sigma}{2} - i\left(\Delta_a + \Delta_\sigma\right)\right]\langle a^\dagger\Sigma^\dagger\rangle + ig\left(\langle a^{\dagger 2}\rangle + (N-1)\langle\Sigma^{\dagger 2}\rangle\right), \tag{A.69d}$$

$$\frac{d}{dt}\langle\Sigma^\dagger\Sigma\rangle = -\gamma_\sigma\langle\Sigma^\dagger\Sigma\rangle + ig\left(\langle a^\dagger\Sigma\rangle - \langle\Sigma a^\dagger\rangle\right), \tag{A.69e}$$

$$\frac{d}{dt}\langle\Sigma^{\dagger 2}\rangle = -\left(\gamma_\sigma - 2i\Delta_\sigma\right)\langle\Sigma^{\dagger 2}\rangle + 2ig\langle a^\dagger\Sigma^\dagger\rangle\,, \tag{A.69f}$$

and the rest of the equations are obtained by taking the conjugate of the previous ones. The equation that correspond to the third order correlators are

$$\frac{d}{dt}\langle a^\dagger a^2\rangle = i\Omega_a\left(\langle a^2\rangle - 2\langle a^\dagger a\rangle\right) - \left(\frac{3\gamma_a}{2} + i\Delta_a\right)\langle a^\dagger a^2\rangle + igN\left(\langle\Sigma^\dagger a^2\rangle - 2\langle a^\dagger a\Sigma\rangle\right), \tag{A.70a}$$

$$\frac{d}{dt}\langle a^\dagger a\Sigma\rangle = i\Omega_a\left(\langle a\Sigma\rangle - \langle a^\dagger\Sigma\rangle\right) - \left(\frac{2\gamma_a+\gamma_\sigma}{2} + i\Delta_\sigma\right)\langle a^\dagger a\Sigma\rangle + ig\left[N\left(\langle\Sigma^\dagger\Sigma a\rangle - \langle a^\dagger\Sigma^2\rangle\right) - \langle a^\dagger a^2\rangle\right], \tag{A.70b}$$

$$\frac{d}{dt}\langle\Sigma^\dagger a^2\rangle = -2i\Omega_a\langle\Sigma^\dagger a\rangle - \left(\frac{2\gamma_a+\gamma_\sigma}{2} + i\left(2\Delta_a - \Delta_\sigma\right)\right)\langle\Sigma^\dagger a^2\rangle - ig\left(N\langle\Sigma^\dagger\Sigma a\rangle + \langle a^\dagger a^2\rangle\right), \tag{A.70c}$$

$$\frac{d}{dt}\langle\Sigma^\dagger\Sigma a\rangle = -i\Omega_a\langle\Sigma^\dagger\Sigma\rangle - \left(\frac{\gamma_a+2\gamma_\sigma}{2}+i\Delta_a\right)\langle\Sigma^\dagger\Sigma a\rangle + ig\left(-N\langle\Sigma^\dagger\Sigma^2\rangle + \langle a^\dagger a\Sigma - \langle\Sigma^\dagger a^2\rangle\rangle\right), \tag{A.70d}$$

$$\frac{d}{dt}\langle\Sigma^\dagger\Sigma^2\rangle = -\left(\frac{3\gamma_\sigma}{2}+i\Delta_\sigma\right)\langle\Sigma^\dagger a^2\rangle + ig\left(\langle a^\dagger\Sigma^2\rangle - 2\langle\Sigma^\dagger\Sigma a\rangle\right), \tag{A.70e}$$

$$\frac{d}{dt}\langle a^\dagger\Sigma^2\rangle = i\Omega_a\langle\Sigma^2\rangle - \left(\frac{\gamma_a+2\gamma_\sigma}{2}-i\left(\Delta_a-2\Delta_\sigma\right)\right)\langle a^\dagger\Sigma^2\rangle + ig\left(N\langle\Sigma^\dagger\Sigma^2\rangle - 2\langle a^\dagger a\Sigma\rangle\right), \tag{A.70f}$$

and the rest of the equations can be computed in the same way.

A.7 REGRESSION MATRIX ELEMENTS FOR THE INCOHERENT JAYNES–CUMMINGS MODEL

The regression matrix elements $\mathcal{M}^{m,n,\mu,\nu}_{m',n',\mu',\nu'}$, in the case of a coupled cavity-2LS, are given by:

$$\mathcal{M}^{m,n,\mu,\nu}_{m,n,\mu,\nu} = -\frac{\Gamma_a}{2}(m+n) - \frac{\Gamma_\sigma}{2}(\mu+\nu) + i(m-n)\Delta_a + i(\mu-\nu)\Delta_\sigma \tag{A.71a}$$

$$\mathcal{M}^{m,n,\mu,\nu}_{m,n,1-\mu,\nu} = i\Omega_\sigma[\mu+2\nu(1-\mu)], \tag{A.71b}$$

$$\mathcal{M}^{m,n,\mu,\nu}_{m,n,\mu,1-\nu} = -i\Omega_\sigma[\nu+2\mu(1-\nu)], \tag{A.71c}$$

$$\mathcal{M}^{m,n,\mu,\nu}_{m-1,n,\mu,\nu} = i\Omega_a m, \qquad \mathcal{M}^{m,n,\mu,\nu}_{m,n-1,\mu,\nu} = -i\Omega_a n, \tag{A.71d}$$

$$\mathcal{M}^{m,n,\mu,\nu}_{m-1,n-1,\mu,\nu} = P_a\, mn, \qquad \mathcal{M}^{m,n,\mu,\nu}_{m,n,1-\mu,1-\nu} = P_\sigma\,\mu\nu, \tag{A.71e}$$

$$\mathcal{M}^{m,n,\mu,\nu}_{m,n-1,\mu,1-\nu} = -ig(1-\nu)n, \qquad \mathcal{M}^{m,n,\mu,\nu}_{m-1,n,1-\mu,\nu} = ig(1-\mu)m, \tag{A.71f}$$

$$\mathcal{M}^{m,n,\mu,\nu}_{m,n+1,\mu,1-\nu} = -ig\nu, \qquad \mathcal{M}^{m,n,\mu,\nu}_{m+1,n,1-\mu,\nu} = ig\mu, \tag{A.71g}$$

$$\mathcal{M}^{m,n,\mu,\nu}_{m,n+1,1-\mu,\nu} = 2i\nu g(1-\mu), \qquad \mathcal{M}^{m,n,\mu,\nu}_{m+1,n,\mu,1-\nu} = -2i\mu g(1-\nu), \tag{A.71h}$$

and zero everywhere else. We introduce the notation for the effective linewidth $\Gamma_a = \gamma_a - P_a$ and $\Gamma_\sigma = \gamma_\sigma + P_\sigma$. Here, $m, n \geq 0$ are indeces associated to bosons (cavity mode) and $\mu, \nu = 0, 1$ are bound to 2LSs (emitters). In the main text, we discuss first the case of filtered resonance fluorescence, which corresponds to having one 2LS coupled to two detectors/cavity modes s_i (taking $g \to 0$, $\Omega_{s_i} = P_i = 0$ here).

On the other hand, we solve the N-emitters Jaynes–Cummings model (also known as Dicke model) with a single cavity weakly driven by a coherent source, which corresponds to setting $\Omega_{\sigma_i} = P_i = 0$ and $\Omega_a \to 0$ here. Other combinations are considered latter, for instance, JC model with incoherent pumping.

These matrix elements applied for each pair of emitter or cavity indeces, i.e., μ_i, ν_i or m, n, respectively. Any connection between two different emitters or cavities is not allowed in these examples, hence there are not any extra matrix element to be referred.

A.8 INCOHERENT JC CORRELATORS

Second-order Glauber correlator for Cavity-driven JC

$$\begin{aligned} g_a^{(2)} = &\Big\{2\Gamma_1^2(4g^2+\Gamma_a\Gamma_\sigma)\big[48g^4\Gamma_1\Gamma_3+\Gamma_\sigma\Gamma_1(\Gamma_1^2+4\Delta^2)(\Gamma_3^2+4\Delta^2)+ \\ &4g^2(\Gamma_1^2\Gamma_3^2+4\Delta^2[\Gamma_a^2+10\Gamma_a\Gamma_\sigma]+5\Gamma_\sigma^2)\big]\Big\}\Big/ \\ &\Big\{\big[\Gamma_3^2(4g^2+\Gamma_a\Gamma_1)+4\Gamma_a\Gamma_1\Delta^2\big]\big[4g^2\Gamma_1+\Gamma_\sigma(\Gamma_1^2+4\Delta^2)\big]^2\Big\}, \end{aligned} \tag{A.72}$$

where we remember that $\Gamma_k \equiv k\,\Gamma_a + \Gamma_\sigma$ as defined in the main text.

The spectrum coefficients for $P_a = 0$ are

$$n_a^{-1}L_{1,2}^{(a)} = \frac{\Gamma_1\big[4R_r^2+R_i(4R_i\pm\Gamma_1)\big]\pm 2R_r\Delta\Gamma_-}{8\Gamma_1(R_r^2+R_i^2)}, \tag{A.73a}$$

$$n_a^{-1}K_{1,2}^{(a)} = \pm\frac{R_r\Gamma_1^2-2R_i\Delta\Gamma_-}{8\Gamma_1(R_r^2+R_i^2)}, \tag{A.73b}$$

$$\begin{aligned} n_\sigma^{-1}L_{1,2}^{(\sigma)} = &\big\{8g^2\Gamma_1\big[R_i(4R_i\pm\Gamma_-)+2R_r(2R_r\pm\Delta)\big]+ \\ &\Gamma_a\big[\pm 16R_i^3\Gamma_1\pm R_i\Gamma_1(16R_r^2+\Gamma_-\Gamma_3+4\Delta^2)+ \\ &2R_r(4R_r\Gamma_1^2\pm\Delta[16R_r^2+\Gamma_+^2+4\Gamma_\sigma^2]+16R_r\Delta^2\pm 4\Delta^3)+ \\ &8R_i^2(\Gamma_1^2+4\Delta[\Delta\pm R_r])\big]\big\}\Big/ \\ &\big[16(R_r^2+R_i^2)(4g^2\Gamma_1+\Gamma_a[\Gamma_1^2+4\Delta^2])\big], \end{aligned} \tag{A.73c}$$

$$\begin{aligned} n_\sigma^{-1}K_{1,2}^{(\sigma)} = &\pm\big\{8g^2\Gamma_1(R_r\Gamma_- - 2R_i\Delta)+\Gamma_a\big[-16R_i^2R_r\Gamma_1+32R_r^3\Delta- \\ &2R_i\Delta(-16R_r^2+\Gamma_1^2+4\Gamma_\sigma^2+4\Delta^2)+ \\ &R_r\Gamma_1(-16R_r^2+\Gamma_-\Gamma_3+4\Delta^2)\big]\big\}\Big/ \\ &\big[16(R_r^2+R_i^2)(4g^2\Gamma_1+\Gamma_2[\Gamma_1^2+4\Delta^4])\big], \end{aligned} \tag{A.73d}$$

and, for $P_\sigma = 0$, are

$$n_a^{-1}L_{1,2}^{(a)} = \{4g^2[\Gamma_1(4R_r^2 + R_i[4R_i \mp \Gamma_1]) \mp 2R_r\Delta(\Gamma_a + 3\Gamma_\sigma)] + \Gamma_\sigma(\Gamma_1^2 + 4\Delta^2)[R_i(4R_i \mp \Gamma_-) + R_r(2R_r \mp \Delta)]\} \Big/ [8(R_r^2 + R_i^2)(4g^2\Gamma_1 + \Gamma_\sigma[\Gamma_1^2 + 4\Delta^2])], \quad \text{(A.74a)}$$

$$n_a^{-1}K_{1,2}^{(a)} = \mp\{4g^2[R_r\Gamma_1^2 - R_i\Delta(\Gamma_a + 3\Gamma_\sigma)] + \Gamma_\sigma(\Gamma_1^2 + 4\Delta^2)(R_r\Gamma_- - 2R_i\Delta)\} \Big/ \{8(R_r^2 + R_i^2)(4g^2\Gamma_1 + \Gamma_\sigma[\Gamma_1^2 + 4\Delta^2])\}, \quad \text{(A.74b)}$$

$$n_\sigma^{-1}L_{1,2}^{(\sigma)} = \{8g^2\Gamma_1[R_i(4R_i \pm \Gamma_-) + R_r(2R_r \pm \Delta)] \pm \Gamma_\sigma[\Gamma_1 R_i(\Gamma_-^2 - 16R_r^2 - 16R_i^2) + 2R_r\Delta(\Gamma_-[\Gamma_a + 3\Gamma_\sigma] - 16R_r^2 - 16R_i^2) + 4R_i\Delta^2(\Gamma_a - 3\Gamma_\sigma) + 8R_r\Delta^3]\} \Big/ [64g^2\Gamma_1(R_r^2 + R_i^2)], \quad \text{(A.74c)}$$

$$n_\sigma^{-1}K_{1,2}^{(\sigma)} = \pm\{8g^2\Gamma_1(R_r\Gamma_- - 2R_i\Delta) + \Gamma_\sigma[R_r\Gamma_1(16R_r^2 + 16R_i + \Gamma_-^2) - 2R_i\Delta(16R_r^2 + 16R_i + \Gamma_1[\Gamma_a + 3\Gamma_\sigma]) + 4R_r\Delta^2(\Gamma_a - 3\Gamma_\sigma) - 8R\Delta^3]\} \Big/ [64g^2\Gamma_1(R_r^2 + R_i^2)]. \quad \text{(A.74d)}$$

Coefficients of $g^{(2)}$ for the resonant case $\Delta = 0$ and $P_\sigma = 0$:

$$l_{1,2}^{(a)} = -\Big\{2048g^8[\Gamma_1\Gamma_3\Gamma_-\Gamma_\sigma \pm \sqrt{2}iR^{(+)}(9\Gamma_a^3 + 37\Gamma_a^2\Gamma_\sigma + 51\Gamma_a\Gamma_\sigma^2 + 15\Gamma_\sigma^3)] + \Gamma_1^4\Gamma_3^2\Gamma_a\Gamma_\sigma^2(\pm i2\sqrt{2}R^{(+)} + \Gamma_-)(\Gamma_\sigma^2 - \chi) + 4g^2\Gamma_1^2\Gamma_3^2\Gamma_\sigma[\Gamma_1\Gamma_-(2\Gamma_a^3 + \Gamma_a^2\Gamma_\sigma - 4\Gamma_a\Gamma_\sigma^2 + \Gamma_\sigma^3 - \Gamma_2\chi) \pm 2i\sqrt{2}R^{(+)}(2\Gamma_a^4 + 5\Gamma_a^3\Gamma_\sigma + 9\Gamma_a^2\Gamma_\sigma^2 - \Gamma_a\Gamma_\sigma^3 + \Gamma_\sigma^4 - \chi[2\Gamma_a^2 + 5\Gamma_a\Gamma_\sigma + \Gamma_\sigma^2])] + 64g^6[\Gamma_1\Gamma_3\Gamma_-(3\Gamma_a^3 + 19\Gamma_a^2\Gamma_\sigma + 29\Gamma_a\Gamma_\sigma^2 + 5\Gamma_\sigma^3 - 3\Gamma_a\chi - 5\Gamma_\sigma\chi) \pm 2i\sqrt{2}R^{(+)}(45\Gamma_a^5 + 227\Gamma_a^4\Gamma_\sigma + 538\Gamma_a^3\Gamma_\sigma^2 + 526\Gamma_a^2\Gamma_\sigma^3 + 137\Gamma_a\Gamma_\sigma^4 - \Gamma_\sigma^5 - \chi[9\Gamma_a^3 + 37\Gamma_a^2\Gamma_\sigma + 51\Gamma_a\Gamma_\sigma^2 + 15\Gamma_\sigma^3])] + 16g^4\Gamma_1[\Gamma_1\Gamma_3\Gamma_-(3\Gamma_a^4 + 13\Gamma_a^3\Gamma_\sigma + 13\Gamma_a^2\Gamma_\sigma^2 - 9\Gamma_a\Gamma_\sigma^3 - 4\Gamma_\sigma^4 - \Gamma_a\chi[3\Gamma_a + 7\Gamma_\sigma]) \pm 2i\sqrt{2}R^{(+)}(9\Gamma_a^6 + 105\Gamma_a^5\Gamma_\sigma + \Gamma_a^4[336\Gamma_\sigma^2 - 9\chi] - 2\Gamma_\sigma^4[\Gamma_\sigma^2 + \chi] + 17\Gamma_a^3[26\Gamma_\sigma^3 - 3\Gamma_\sigma\chi] + \Gamma_a^2[137\Gamma_\sigma^4 - 89\Gamma_\sigma^2\chi] - 3\Gamma_a[\Gamma_\sigma^5 + 11\Gamma_\sigma^3\chi])]\Big\} \times [4\Gamma_1\Gamma_3^2\Gamma_-\chi(4g^2 + \Gamma_1\Gamma_a)(4g^2 + \Gamma_1\Gamma_\sigma)^2]^{-1}, \quad \text{(A.75a)}$$

$$
\begin{aligned}
l_{3,4}^{(a)} =& \Big\{ 2048 g^8 \big[\Gamma_1\Gamma_3\Gamma_-\Gamma_\sigma \pm i\sqrt{2}\mathrm{R}^{(-)}(9\Gamma_a^3 + 37\Gamma_a^2\Gamma_\sigma + \\
& 51\Gamma_a\Gamma_\sigma^2 + 15\Gamma_\sigma^3)\big] + \Gamma_1^4\Gamma_3^2\Gamma_a\Gamma_\sigma^2(\pm i2\sqrt{2}\mathrm{R}^{(-)} + \Gamma_-)(\Gamma_\sigma^2 - \chi) \\
& + 4g^2\Gamma_1^2\Gamma_3^2\Gamma_\sigma\big[\Gamma_1\Gamma_-(2\Gamma_a^3 + \Gamma_a^2\Gamma_\sigma - 4\Gamma_a\Gamma_\sigma^2 + \Gamma_\sigma^3 + \Gamma_2\chi) \pm \\
& i2\sqrt{2}\mathrm{R}^{(-)}(2\Gamma_a^4 + 5\Gamma_a^3\Gamma_\sigma + 9\Gamma_a^2\Gamma_\sigma^2 - \Gamma_a\Gamma_\sigma^3 + \Gamma_\sigma^4 + \\
& \chi[2\Gamma_a^2 + 5\Gamma_a\Gamma_\sigma + \Gamma_\sigma^2])\big] + 64g^6\big[\Gamma_1\Gamma_3\Gamma_-(3\Gamma_a^3 + \\
& 19\Gamma_a^2\Gamma_\sigma + 29\Gamma_a\Gamma_\sigma^2 + 5\Gamma_\sigma^3 + 3\Gamma_a\chi + 5\Gamma_\sigma\chi) \pm \\
& i\,2\sqrt{2}\mathrm{R}^{(-)}(45\Gamma_a^5 + 227\Gamma_a^4\Gamma_\sigma + 538\Gamma_a^3\Gamma_\sigma^2 + 526\Gamma_a^2\Gamma_\sigma^3 + \\
& 137\Gamma_a\Gamma_\sigma^4 - \Gamma_\sigma^5 + \chi[9\Gamma_a^3 + 37\Gamma_a^2\Gamma_\sigma + 51\Gamma_a\Gamma_\sigma^2 + 15\Gamma_\sigma^3])\big] + \\
& 16g^4\Gamma_1\big[\Gamma_1\Gamma_3\Gamma_-(3\Gamma_a^4 + 13\Gamma_a^3\Gamma_\sigma + 13\Gamma_a^2\Gamma_\sigma^2 - 9\Gamma_a\Gamma_\sigma^3 - \\
& 4\Gamma_\sigma^4 + \Gamma_a\chi[3\Gamma_a + 7\Gamma_\sigma]) \pm i\,2\sqrt{2}\mathrm{R}^{(-)}(9\Gamma_a^6 + 105\Gamma_a^5\Gamma_\sigma + \\
& \Gamma_a^4[336\Gamma_\sigma^2 + 9\chi] - 2\Gamma_\sigma^4[\Gamma_\sigma^2 - \chi] + 17\Gamma_a^3[26\Gamma_\sigma^3 + 3\Gamma_\sigma\chi] + \\
& \Gamma_a^2[137\Gamma_\sigma^4 + 89\Gamma_\sigma^2\chi] - 3\Gamma_a[\Gamma_\sigma^5 - 11\Gamma_\sigma^3\chi])\big]\Big\} \\
& \times \big[4\Gamma_1\Gamma_3^2\Gamma_-\chi(4g^2 + \Gamma_1\Gamma_a)(4g^2 + \Gamma_1\Gamma_\sigma)^2\big]^{-1}, \qquad \text{(A.75b)}
\end{aligned}
$$

$$
\begin{aligned}
l_{1,2}^{(\sigma)} =& \big[1024g^4\mathrm{R}^{(+)}\Gamma_1\Gamma_3\Gamma_-\chi(4g^2 + \Gamma_1\Gamma_a)\big]^{-1} \times \\
& \big\{4096g^8\Gamma_-\big[\Gamma_a\Gamma_\sigma(16\mathrm{R}^{(+)} \pm i\,3\sqrt{2}\Gamma_\sigma) \pm \sqrt{2}i(\Gamma_\sigma^3 - \Gamma_a^2\Gamma_3)\big] \mp \\
& \sqrt{2}i\Gamma_1^2\Gamma_3\Gamma_a\Gamma_\sigma^2(8\mathrm{R}^{(+)2} + \Gamma_-^2)(\Gamma_-^2 - \chi)^2 + \\
& 256g^6\big[\pm\, i\,32\sqrt{2}\Gamma_a\Gamma_\sigma\mathrm{R}^{(+)2}(\Gamma_-^2 - \chi) \mp \\
& \sqrt{2}i\Gamma_1\Gamma_-^2(9\Gamma_a^3 + 31\Gamma_a^2\Gamma_\sigma - \Gamma_a\Gamma_\sigma^2 - 7\Gamma_\sigma^3 + 3\Gamma_1\chi) + \\
& 4\mathrm{R}^{(+)}\Gamma_-(3\Gamma_a^4 - 2\Gamma_a^3\Gamma_\sigma - 38\Gamma_a\Gamma_\sigma^3 - 11\Gamma_\sigma^4 - \Gamma_1\Gamma_3\chi)\big] + \\
& 32g^4\big[\pm 16\sqrt{2}i\Gamma_\sigma\mathrm{R}^{(+)2}(\Gamma_-^2 - \chi)(\Gamma_a^3 - \Gamma_a^2\Gamma_\sigma - 9\Gamma_a\Gamma_\sigma^2 - 3\Gamma_\sigma^3 - \Gamma_a\chi) + \\
& 4\Gamma_3\Gamma_-\mathrm{R}^{(+)}(2\Gamma_a^5 + \Gamma_a^4\Gamma_\sigma - 10\Gamma_a^2\Gamma_\sigma^3 - 26\Gamma_a\Gamma_\sigma^4 + \Gamma_\sigma^5 - \\
& 2\Gamma_1^2\Gamma_a\chi - \Gamma_\sigma\chi^2) \mp i\sqrt{2}\Gamma_1\Gamma_-^2(-6\Gamma_a^5 + 11\Gamma_a^4\Gamma_\sigma + 38\Gamma_a^3\Gamma_\sigma^2 - \\
& 20\Gamma_a^2\Gamma_\sigma^3 - 24\Gamma_a\Gamma_\sigma^4 + \Gamma_\sigma^5 + 2\Gamma_1\chi[3\Gamma_a^2 + 9\Gamma_a\Gamma_\sigma - \Gamma_\sigma^2] + \Gamma_\sigma\chi^2)\big] + \\
& 4g^2\Gamma_1\Gamma_\sigma(\Gamma_\sigma^2 - \chi)\big[\pm\sqrt{2}i\Gamma_1\Gamma_-^2(6\Gamma_a^3 + 15\Gamma_a^2\Gamma_\sigma - 4\Gamma_a\Gamma_\sigma^2 - \Gamma_\sigma^3 + \Gamma_6\chi) + \\
& 8\mathrm{R}^{(+)}(\Gamma_3\Gamma_a\Gamma_-[\Gamma_-^2 + \chi] \mp i\sqrt{2}\mathrm{R}^{(+)}\Gamma_\sigma[-7\Gamma_a^3 + 23\Gamma_a^2\Gamma_\sigma + \\
& 15\Gamma_a\Gamma_\sigma^2 + \Gamma_\sigma^3 - \chi\Gamma_5])\big]\big\}, \qquad \text{(A.76a)}
\end{aligned}
$$

$$
\begin{aligned}
l_{3,4}^{(\sigma)} =& \left[1024g^4\mathrm{R}^{(-)}\Gamma_1\Gamma_3\Gamma_-\chi(4g^2+\Gamma_1\Gamma_a)\right]^{-1}\times \\
& \left\{4096g^8\Gamma_-\left[\Gamma_a\Gamma_\sigma(16\mathrm{R}^{(-)}\pm i\,3\sqrt{2}\Gamma_\sigma)\pm\sqrt{2}i(\Gamma_\sigma^3-\Gamma_a^2\Gamma_3)\right]\mp\right. \\
& \sqrt{2}i\Gamma_1^2\Gamma_3\Gamma_a\Gamma_\sigma^2(8\mathrm{R}^{(-)2}+\Gamma_-^2)(\Gamma_-^2-\chi)^2+ \\
& 256g^6\left[\pm 32\sqrt{2}i\Gamma_a\Gamma_\sigma\mathrm{R}^{(-)2}(\Gamma_-^2-\chi)\mp\sqrt{2}i\Gamma_1\Gamma_-^2(9\Gamma_a^3+31\Gamma_a^2\Gamma_\sigma-\right. \\
& \Gamma_a\Gamma_\sigma^2-7\Gamma_\sigma^3+3\Gamma_1\chi)+4\mathrm{R}^{(-)}\Gamma_-(3\Gamma_a^4-2\Gamma_a^3\Gamma_\sigma-38\Gamma_a\Gamma_\sigma^3- \\
& \left.11\Gamma_\sigma^4-\Gamma_1\Gamma_3\chi)\right]+32g^4\left[\pm i\,16\sqrt{2}\Gamma_\sigma\mathrm{R}^{(-)2}(\Gamma_-^2-\chi)\right. \\
& (\Gamma_a^3-\Gamma_a^2\Gamma_\sigma-9\Gamma_a\Gamma_\sigma^2-3\Gamma_\sigma^3-\Gamma_a\chi)+4\Gamma_3\Gamma_-\mathrm{R}^{(-)}(2\Gamma_a^5+ \\
& \Gamma_a^4\Gamma_\sigma-10\Gamma_a^2\Gamma_\sigma^3-26\Gamma_a\Gamma_\sigma^4+\Gamma_\sigma^5-2\Gamma_1^2\Gamma_a\chi-\Gamma_\sigma\chi^2)\mp \\
& i\sqrt{2}\Gamma_1\Gamma_-^2(-6\Gamma_a^5+11\Gamma_a^4\Gamma_\sigma+38\Gamma_a^3\Gamma_\sigma^2-20\Gamma_a^2\Gamma_\sigma^3- \\
& 24\Gamma_a\Gamma_\sigma^4+\Gamma_\sigma^5+2\Gamma_1\chi[3\Gamma_a^2+9\Gamma_a\Gamma_\sigma-\Gamma_\sigma^2]+\Gamma_\sigma\chi^2)\big]+ \\
& 4g^2\Gamma_1\Gamma_\sigma(\Gamma_\sigma^2-\chi)\left[\pm i\sqrt{2}\Gamma_1\Gamma_-^2(6\Gamma_a^3+15\Gamma_a^2\Gamma_\sigma-4\Gamma_a\Gamma_\sigma^2-\right. \\
& \Gamma_\sigma^3+\Gamma_6\chi)8\mathrm{R}^{(-)}(\Gamma_3\Gamma_a\Gamma_-[\Gamma_-^2+\chi]\mp i\sqrt{2}\mathrm{R}^{(-)}\Gamma_\sigma\times \\
& \left.\left.[-7\Gamma_a^3+23\Gamma_a^2\Gamma_\sigma+15\Gamma_a\Gamma_\sigma^2+\Gamma_\sigma^3-\chi\Gamma_5])\right]\right\}, \qquad \text{(A.76b)}
\end{aligned}
$$

where $\chi \equiv \sqrt{\chi_+\chi_-}$.

For $\Delta = 0$ and $P_a = 0$:

$$
\begin{aligned}
l_{1,2}^{(a)} =& \left\{128g^4\left[\Gamma_1\Gamma_3\Gamma_a\Gamma_-\mp i\sqrt{2}\mathrm{R}^{(+)}(11\Gamma_a^3+3\Gamma_a^2\Gamma_\sigma+\Gamma_a\Gamma_\sigma^2+\Gamma_\sigma^3)\right]+\right. \\
& 4g^2\left[\Gamma_1\Gamma_3\Gamma_-(9\Gamma_a^3+17\Gamma_a^2\Gamma_\sigma-\Gamma_a\Gamma_\sigma^2-\Gamma_\sigma^3-\chi\Gamma_-)\mp\right. \\
& i2\sqrt{2}\mathrm{R}^{(+)}(31\Gamma_a^5+53\Gamma_a^4\Gamma_\sigma-26\Gamma_a^3\Gamma_\sigma^2-6\Gamma_a^2\Gamma_\sigma^3+ \\
& 11\Gamma_a\Gamma_\sigma^4+\Gamma_\sigma^5-\chi[11\Gamma_a^3+3\Gamma_a^2\Gamma_\sigma+\Gamma_a\Gamma_\sigma^2+\Gamma_\sigma^3])\big]+ \\
& \Gamma_1\Gamma_a\left[\Gamma_1\Gamma_a\Gamma_-(3\Gamma_a^3+13\Gamma_a^2\Gamma_\sigma+\Gamma_a\Gamma_\sigma^2-\Gamma_\sigma^3-\chi[3\Gamma_a-\Gamma_\sigma])\mp\right. \\
& i2\sqrt{2}\mathrm{R}^{(+)}(9\Gamma_a^5+37\Gamma_a^4\Gamma_\sigma-30\Gamma_a^3\Gamma_\sigma^2-22\Gamma_a^2\Gamma_\sigma^3+5\Gamma_a\Gamma_\sigma^4+ \\
& \left.\Gamma_\sigma^5-\chi[9\Gamma_a^3-\Gamma_a^2\Gamma_\sigma-\Gamma_a\Gamma_\sigma^2+\Gamma_\sigma^3])\right]\Big\}\times \\
& \left[4\Gamma_1\Gamma_3^2\Gamma_-\chi(4g^2+\Gamma_1\Gamma_a)\right]^{-1}, \qquad \text{(A.77a)} \\
l_{3,4}^{(a)} =& \left\{128g^4\left[-\Gamma_1\Gamma_3\Gamma_a\Gamma_-\pm\sqrt{2}i\mathrm{R}^{(-)}(11\Gamma_a^3+3\Gamma_a^2\Gamma_\sigma+\Gamma_a\Gamma_\sigma^2+\Gamma_\sigma^3)\right]+\right. \\
& \Gamma_1\Gamma_a\left[\Gamma_1\Gamma_3\Gamma_-(-3\Gamma_a^3-13\Gamma_a^2\Gamma_\sigma-\Gamma_a\Gamma_\sigma^2+\Gamma_\sigma^3-\chi[3\Gamma_a-\Gamma_\sigma])\pm\right. \\
& 2\sqrt{2}i\mathrm{R}^{(-)}(9\Gamma_a^5+37\Gamma_a^4\Gamma_\sigma-30\Gamma_a^3\Gamma_\sigma^2-22\Gamma_a^2\Gamma_\sigma^3+ \\
& 5\Gamma_a\Gamma_\sigma^4+\Gamma_\sigma^5+\chi[9\Gamma_a^3-\Gamma_a^2\Gamma_\sigma-\Gamma_a\Gamma_\sigma^2+\Gamma_\sigma^3])\big]+ \\
& 4g^2\left[\Gamma_1\Gamma_3\Gamma_-(-9\Gamma_a^3-17\Gamma_a^2\Gamma_\sigma+\Gamma_a\Gamma_\sigma^2+\Gamma_\sigma^3-\chi\Gamma_-)\pm\right. \\
& 2i\sqrt{2}\mathrm{R}^{(-)}(31\Gamma_a^5+53\Gamma_a^4\Gamma_\sigma-26\Gamma_a^3\Gamma_\sigma^2-6\Gamma_a^2\Gamma_\sigma^3+ \\
& 11\Gamma_a\Gamma_\sigma^4+\Gamma_\sigma^5+\chi[11\Gamma_a^3+3\Gamma_a^2\Gamma_\sigma+\Gamma_a\Gamma_\sigma^2+\Gamma_\sigma^3])\big]\Big\}\times \\
& \left[4\Gamma_1\Gamma_3^2\Gamma_-\chi(4g^2+\Gamma_1\Gamma_a)\right]^{-1}, \qquad \text{(A.77b)}
\end{aligned}
$$

$$
\begin{aligned}
l_{1,2}^{(\sigma)} =& \{-4096g^8\Gamma_-\left[\pm R^{(+)}\Gamma_a^2+\sqrt{2}i\Gamma_1\Gamma_3\Gamma_-\right]+\Gamma_1^2\Gamma_3\Gamma_-[\Gamma_-^2-\chi]\\
&\left[-8i\sqrt{2}(R^{(+)})^2(\Gamma_a\Gamma_-+7\Gamma_-\Gamma_\sigma-\chi)\pm\right.\\
&8R^{(+)}\Gamma_-(\Gamma_a^2+6\Gamma_a\Gamma_\sigma+\Gamma_\sigma^2-\chi)+i\sqrt{2}\Gamma_-^2([\Gamma_a+3\Gamma_\sigma]^2-\chi)\left.\right]+\\
&256g^6\left[32\sqrt{2}i\Gamma_a^2(R^{(+)})^2(\chi-\Gamma_-^2)-i\sqrt{2}\Gamma_1\Gamma_-^2(23\Gamma_a^2+57\Gamma_a^2\Gamma_\sigma+\right.\\
&17\Gamma_a\Gamma_\sigma^2-\Gamma_\sigma^3+\Gamma_1\chi)\mp R^{(+)}\Gamma_-(33\Gamma_a^4+66\Gamma_a^3\Gamma_\sigma-8\Gamma_a^2\Gamma_\sigma^2-\\
&10\Gamma_a\Gamma_\sigma^3-\Gamma_\sigma^4+\Gamma_1\Gamma_3\chi)\left.\right]+32g^4\Gamma_a\left[-i\sqrt{2}\Gamma_1\Gamma_-^2(17\Gamma_a^4+146\Gamma_a^3\Gamma_\sigma+\right.\\
&192\Gamma_a^2\Gamma_\sigma^2+38\Gamma_a\Gamma_\sigma^3-9\Gamma_\sigma^4+8\Gamma_1\Gamma_a\chi+10\Gamma_1\Gamma_\sigma\chi-\chi^2)\pm\\
&R^{(+)}\Gamma_3\Gamma_-(-3\Gamma_a^4-44\Gamma_a^3\Gamma_\sigma-26\Gamma_a^2\Gamma_\sigma^2+36\Gamma_a\Gamma_\sigma^3+\\
&5\Gamma_\sigma^4-6\Gamma_1^2\chi+\chi^2)+16\sqrt{2}i(R^{(+)})^2(\Gamma_-^2-\chi)\times\\
&(-10\Gamma_a^3-14\Gamma_a^2\Gamma_\sigma+2\Gamma_a\Gamma_\sigma^2+2\Gamma_\sigma^3+\Gamma_a\chi)\left.\right]+4g^2\Gamma_1\Gamma_a^2\times\\
&\left[8\sqrt{2}i(R^{(+)})^2(\Gamma_-^2-\chi)(-21\Gamma_a^3-47\Gamma_a^2\Gamma_\sigma+21\Gamma_a\Gamma_\sigma^2+15\Gamma_\sigma^3+\right.\\
&\Gamma_9\chi)\pm16R^{(+)}\Gamma_3\Gamma_-(2\Gamma_a^4-4\Gamma_a^3\Gamma_\sigma-12\Gamma_a^2\Gamma_\sigma^2+12\Gamma_a\Gamma_\sigma^3+\Gamma_\sigma^4-\\
&3\Gamma_1^2\chi+\chi^2)+i\sqrt{2}\Gamma_1\Gamma_-^2(3\Gamma_a^4-48\Gamma_a^3\Gamma_\sigma+[23\Gamma_\sigma^2-2\chi]\times\\
&[\Gamma_\sigma^2-\chi]-6\Gamma_a^2[35\Gamma_\sigma^2+\chi]-24\Gamma_a[\Gamma_\sigma^3+2\Gamma_\sigma\chi])\left.\right]\}\times\\
&\left[64R^{(+)}\Gamma_1\Gamma_3\Gamma_-\chi(4g^2+\Gamma_1\Gamma_a)^3\right]^{-1}, \qquad \text{(A.78a)}\\
l_{3,4}^{(\sigma)} =& \quad l_{1,2}^{(\sigma)} \quad (R^{(+)}\to R^{(-)},\chi\to-\chi). \qquad \text{(A.78b)}
\end{aligned}
$$

A.9 EXACT EXPRESSION OF $g^{(2)}(\tau)$ FOR FILTERED RESONANCE FLUORESCENCE

If both the filter and 2LS are at resonance ($\Delta_\sigma = \Delta_1 = 0$), then the exact exponents are

$$\lambda_{1,2} = (3\gamma_\sigma \pm 4\gamma_M)/4, \quad \lambda_3 = \Gamma/2, \quad \lambda_4 = \gamma_{11}/2, \qquad \text{(A.79)}$$

$$\lambda_{5,6} = (\gamma_{23} \pm 4\gamma_M)/4, \quad \lambda_7 = \Gamma, \qquad \text{(A.80)}$$

and the coefficients are

$$
\begin{aligned}
l_1 =& 512\Gamma^2\gamma_{11}\Omega_\sigma^2(\gamma_{11}\gamma_{12}+16\Omega_\sigma^2)\{\Gamma\gamma_{1\bar{2}}\gamma_{1\bar{1}}(4\gamma_M+\gamma_\sigma)+\\
&8\Omega_\sigma^2[14\Gamma^2+2\gamma_\sigma(4\gamma_M+\gamma_\sigma)-\Gamma(28\gamma_M+17\gamma_\sigma)]-512\Omega_\sigma^4\}\\
&\{\gamma_{11}\gamma_{12}\gamma_{21}[\Gamma(4\gamma_M-3\gamma_\sigma)+2\gamma_\sigma(4\gamma_M-\gamma_\sigma)]+\\
&8\Omega_\sigma^2[8\Gamma^3+32\Gamma\gamma_\sigma^2-2\gamma_\sigma^2(4\gamma_M-7\gamma_\sigma)+\Gamma^2(4\gamma_M+25\gamma_\sigma)]+\\
&256\Gamma\Omega_\sigma^4\}/[4\gamma_M(4\gamma_M-\Gamma)(4\gamma_M-\gamma_\sigma)(4\gamma_M+\gamma_\sigma)^2\\
&(4\gamma_M+\gamma_\sigma-2\Gamma)(4\gamma_M+3\gamma_\sigma-4\Gamma)(4\gamma_M+3\gamma_\sigma-2\Gamma)\\
&(\gamma_{11}\gamma_{21}+8\Omega_\sigma^2)(\gamma_{11}^2\gamma_{12}+8\Gamma\Omega_\sigma^2)^2], \qquad \text{(A.81)}
\end{aligned}
$$

$$l_2 = l_1 \text{ (with } \gamma_M \leftrightarrow -\gamma_M), \tag{A.82}$$

$$\begin{aligned} l_3 = {} & 2\Gamma\gamma_\sigma\gamma_{11}[\gamma_{1\bar{2}}\gamma_{11}^3\gamma_{21}^2\gamma_{12}^2 + 8\gamma_{11}^2\gamma_{12}\Omega_\sigma^2(17\Gamma^3 + 12\Gamma^2\gamma_\sigma + \\ & 6\Gamma\gamma_\sigma^2 + 4\gamma_\sigma^3) + 256\gamma_{11}^2\Omega_\sigma^2(5\Gamma^2 + 6\Gamma\gamma_\sigma + 4\gamma_\sigma^2) + \\ & 2048\Gamma^2\Omega_\sigma^6]/[\gamma_{12}(\gamma_{11}\gamma_{21} + 8\Omega_\sigma^2)(\gamma_{1\bar{2}}\gamma_{1\bar{1}} + 16\Omega_\sigma^2) \\ & (\gamma_{11}^2\gamma_{12} + 8\Gamma\Omega_\sigma^2)^2], \end{aligned} \tag{A.83}$$

$$\begin{aligned} l_4 = {} & 4\Gamma^3[(\gamma_\sigma^2 + 8\Omega_\sigma^2)(\gamma_{11}\gamma_{12} + 16\Omega_\sigma^2)(\gamma_{11}^2\gamma_{12}^2\gamma_{31} + 48\Gamma\gamma_{11}^2\Omega_\sigma^2 - \\ & 256\gamma_\sigma\Omega_\sigma^4)]/[\gamma_{1\bar{1}}\gamma_{31}(16\gamma_M^2 - \gamma_{2\bar{1}}^2)(\gamma_{11}\gamma_{21} + 8\Omega_\sigma^2) \\ & (\gamma_{11}^2\gamma_{12} + 8\Gamma\Omega_\sigma^2)^2], \end{aligned} \tag{A.84}$$

$$\begin{aligned} l_5 = {} & -2048\Gamma^2\gamma_{11}\Omega_\sigma^4\{\gamma_{11}^2\gamma_{12}^2\gamma_{21}\gamma_{31}\gamma_{32}[2\Gamma^2(4\gamma_M - 3\gamma_\sigma) - \\ & \Gamma\gamma_\sigma(4\gamma_M + 3\gamma_\sigma) - 2\gamma_\sigma^2(4\gamma_M - \gamma_\sigma)] + 8\gamma_{11}\gamma_{12}\Omega_\sigma^2 \\ & [-108\Gamma^6 + \Gamma^5(860\gamma_M - 1203\gamma_\sigma) + 3\Gamma^4\gamma_\sigma(956\gamma_M - 1081\gamma_\sigma) + \\ & \Gamma^3\gamma_\sigma^2(4204\gamma_M - 3947\gamma_\sigma) + \Gamma^2\gamma_\sigma^3(3212\gamma_M - 2465\gamma_\sigma) + \\ & 10\Gamma\gamma_\sigma^4(124\gamma_M - 77\gamma_\sigma) + 48\gamma_\sigma^5(4\gamma_M - 2\gamma_\sigma)] + 128\Omega_\sigma^4[6\Gamma^6 + \\ & \Gamma^5(524\gamma_M - 227\gamma_\sigma) + \Gamma^4\gamma_\sigma(2184\gamma_M - 776\gamma_\sigma) + \\ & \Gamma^3\gamma_\sigma^2(3556\gamma_M - 933\gamma_\sigma) + \Gamma^2\gamma_\sigma^3(2896\gamma_M - 488\gamma_\sigma) + \\ & \Gamma\gamma_\sigma^4(1184\gamma_M - 96\gamma_\sigma) + 192\gamma_M\gamma_\sigma^5] + 2048\Omega_\sigma^6[74\Gamma^4 + \\ & 2\Gamma^3(24\gamma_M + 109\gamma_\sigma) + 5\Gamma^2\gamma_\sigma(12\gamma_M + 61\gamma_\sigma) + \\ & 2\Gamma\gamma_\sigma^2(-4\gamma_M + 103\gamma_\sigma) - 4\gamma_\sigma^2(4\gamma_M - 13\gamma_\sigma)] + \\ & 131072\Gamma\gamma_{21}\Omega_\sigma^8\}/[4\gamma_{21}\gamma_M(4\gamma_M + \Gamma)(4\gamma_M - \gamma_\sigma) \\ & (4\gamma_M + \gamma_\sigma)^2(4\gamma_M - \gamma_{2\bar{3}})(\gamma_{11}\gamma_{21} + 8\Omega_\sigma^2) \\ & (\gamma_{11}^2\gamma_{12} + 8\Gamma\Omega_\sigma)^2(\gamma_{31}\gamma_{31} + 16\Omega_\sigma^2)], \end{aligned}$$

$$l_6 = l_5 \text{ (with } \gamma_M \leftrightarrow -\gamma_M), \tag{A.85}$$

$$\begin{aligned} l_7 = {} & \{32\Gamma^2\gamma_{11}(\gamma_\sigma^2 + 8\Omega_\sigma^2)[(\gamma_{11}\gamma_{12} + 16\Omega_\sigma^2)(\gamma_{11}\gamma_{12}\gamma_{21}^2\gamma_{31}^2\gamma_{32} \\ & \gamma_{1\bar{1}}\gamma_{1\bar{2}}\gamma_{2\bar{1}}) + 8\gamma_{31}\Omega_\sigma^2(142\Gamma^7 + 239\Gamma^6\gamma_\sigma - 241\Gamma^5\gamma_\sigma^2 - \\ & 677\Gamma^4\gamma_\sigma^3 + 77\Gamma^3\gamma_\sigma^4 + 832\Gamma^2\gamma_\sigma^5 + 580\Gamma\gamma_\sigma^6 + 128\gamma_\sigma^7) + \\ & 64\Omega_\sigma^4(219\Gamma^6 + 386\Gamma^5\gamma_\sigma + 565\Gamma^4\gamma_\sigma^2 + 344\Gamma^3\gamma_\sigma^3 - \\ & 98\Gamma^2\gamma_\sigma^4 - 208\Gamma\gamma_\sigma^5 - 56\gamma_\sigma^6) + 1024\Omega_\sigma^6(15\Gamma^4 - \\ & 11\Gamma^3\gamma_\sigma - 4\Gamma^2\gamma_\sigma^2 - 16\Gamma\gamma_\sigma^3 - 8\gamma_\sigma^4) - 16384\Omega_\sigma^8\gamma_\sigma\gamma_{21}]\}/ \\ & [\gamma_{21}\gamma_{31}\gamma_{1\bar{1}}(16\gamma_M^2 - \gamma_{2\bar{3}}^2)(16\gamma_M^2 - \gamma_{4\bar{3}}^2)(\gamma_{11}\gamma_{21} + 8\Omega_\sigma^2) \\ & (\gamma_{11}\gamma_{12} + 8\Omega_\sigma^2)(\gamma_{31}\gamma_{32} + 16\Omega_\sigma^2)], \end{aligned} \tag{A.86}$$

A.10 FILTERED THERMAL EMISSION

The filtered emission of a thermal cavity is governed by the master equation

$$\dot{\rho} = -i\omega_a[a^\dagger a + \varsigma^\dagger\varsigma, \rho] - i\epsilon[a^\dagger\varsigma + \varsigma^\dagger a, \rho] + \frac{\gamma_a}{2}\mathcal{L}_a\rho + \frac{P_a}{2}\mathcal{L}_{a^\dagger}\rho + \frac{\Gamma}{2}\mathcal{L}_\varsigma\rho\,, \tag{A.87}$$

which, in the steady-state, leads to effective population

$$n_{\Gamma,\mathrm{th}} = \Gamma^2/(4\epsilon^2)\langle\varsigma^\dagger\varsigma\rangle = \frac{\Gamma P_a}{(\gamma_a - P_a)(\Gamma + \gamma_a - P_a)}\,, \tag{A.88}$$

while the 2-photon autocorrelation at zero delay is

$$g^{(2)}_{\Gamma,\mathrm{th}}(0) = 2\,, \tag{A.89}$$

and for non-zero delay is

$$\begin{aligned} g^{(2)}_{\Gamma,\mathrm{th}}(\tau) = 1 &+ \frac{\Gamma^2}{(\Gamma - \gamma_a + P_a)^2}\, e^{-(\gamma_a - P_a)\tau} - \\ &\frac{2\Gamma(\gamma_a - P_a)}{(\Gamma - \gamma_a + P_a)^2}\, e^{-(\Gamma + \gamma_a - P_a)\tau/2} + \frac{(\gamma_a - P_a)^2}{(\Gamma - \gamma_a + P_a)^2}\, e^{-\Gamma_a\tau}\,, \end{aligned} \tag{A.90}$$

The corresponding waiting time distribution $w_{\Gamma,\mathrm{th}}(\tau)$ cannot be directly compute inverting (1.57) because of the complexity of $g^{(2)}_{\Gamma,\mathrm{th}}(\tau)$. However, the very Laplace transform $\tilde{w}_{\Gamma,\mathrm{th}}(s)$ is closely related to the moment generating function. Indeed, the moments of the distribution $w_{\Gamma,\mathrm{th}}(\tau)$ are $\langle\tau^n_\Gamma\rangle_{\mathrm{th}} = (-1)^n \frac{d^n\tilde{w}(s)}{ds^n}\big|_{s=0}$. Computing the first derivative of $\tilde{w}_{\Gamma,\mathrm{th}}(s)$ leads to the filtered thermal mean time

$$\langle\tau_\Gamma\rangle_{\mathrm{th}} = \frac{(\gamma_a - P_a)(\Gamma + \gamma_a - P_a)}{\Gamma\gamma_a P_a}\,. \tag{A.91}$$

Taking both the wide and narrow filter limits leads to

$$\langle\tau_\infty\rangle_{\mathrm{th}} = \frac{\gamma_a - P_a}{\gamma_a P_a}\,, \tag{A.92}$$

$$\langle\tau_0\rangle_{\mathrm{th}} = \frac{(\gamma_a - P_a)^2}{\Gamma\gamma_a P_a} = \langle\tau_\infty\rangle_{\mathrm{th}}\frac{\gamma_a - P_a}{\Gamma}\,. \tag{A.93}$$

To compute the variance of τ, $(\Delta\tau_\Gamma)^2_{\mathrm{th}} = \langle\tau^2_\Gamma\rangle_{\mathrm{th}} - \langle\tau_\Gamma\rangle^2_{\mathrm{th}}$, we need the second-order moment $\langle\tau^2_\Gamma\rangle_{\mathrm{th}} = \frac{d^2\tilde{w}(s)}{ds^2}\big|_{s=0}$ and thus the second derivative of $\tilde{w}(s)$ and, after all, we find that

$$(\Delta\tau_\Gamma)^2_{\mathrm{th}} = \frac{P_a^4 - 2P_a^3 F_{11} + P_a^2(\Gamma^2 + 2P_a^2) - 2P_a\gamma_a^3 + \gamma_a^2 F_{11}^2}{P_a^2\Gamma^2\gamma_a^2}\,, \tag{A.94}$$

which, in the same limits as before, leads to

$$(\Delta\tau_\infty)^2_{\text{th}} = \frac{\gamma_a^2 + P_a^2}{\gamma_a^2 P_a^2}\,, \tag{A.95}$$

$$(\Delta\tau_0)^2_{\text{th}} = \frac{(\gamma_a - P_a)^2\gamma_a^2 + P_a^2}{\Gamma^2\gamma_a^2 P_a^2} = (\Delta\tau_\infty)^2_{\text{th}} \left(\frac{\gamma_a - P_a}{\Gamma}\right)^2 . \tag{A.96}$$

The bare time variance can be written in terms of the population $n_{\infty,\text{th}}$ and the mean $\langle\tau_\infty\rangle_{\text{th}}$ as

$$(\Delta\tau_\infty)^2_{\text{th}} = (\langle\tau_\infty\rangle_{\text{th}})^2\left[1 + 2n_{\infty,\text{th}}(1 + n_{\infty,\text{th}})\right] . \tag{A.97}$$

REFERENCES

[1] R. J. Glauber. "Photon Correlations." In: *Phys. Rev. Lett.* 10 (1963), p. 84. DOI: 10.1103/PhysRevLett.10.84.

[2] R. J. Glauber. "The Quantum Theory of Optical Coherence." In: *Phys. Rev.* 130 (1963), p. 2529. DOI: 10.1103/PhysRev.130.2529.

[3] D. T. Pegg and S. M. Barnett. "Unitary Phase Operator in Quantum Mechanics." In: *Europhys. Lett.* 6 (1988), p. 483. DOI: 10.1209/0295-5075/6/6/002.

[4] J. C. López Carreño, C. Sánchez Muñoz, D. Sanvitto, E. del Valle, and F. P. Laussy. "Exciting Polaritons with Quantum Light." In: *Phys. Rev. Lett.* 115 (2015), p. 196402. DOI: 10.1103/PhysRevLett.115.196402.

[5] J. C. López Carreño and F. P. Laussy. "Excitation with quantum light. I. Exciting a harmonic oscillator." In: *Phys. Rev. A* 94 (2016), p. 063825. DOI: 10.1103/PhysRevA.94.063825.

[6] C. Sánchez Muñoz, E. del Valle, A. González Tudela, K. Müller, S. Lichtmannecker, M. Kaniber, C. Tejedor, J.J. Finley, and F.P. Laussy. "Emitters of N-photon bundles." In: *Nature Photon.* 8 (2014), p. 550. DOI: 10.1038/nphoton.2014.114.

[7] R. J. Glauber. "Coherent and Incoherent States of the Radiation Field." In: *Phys. Rev.* 131 (1963), p. 2766. DOI: 10.1103/PhysRev.131.2766.

[8] L. Susskind and J. Glogower. "Quantum mechanical phase and time operator." In: *Physics* 1 (1964), p. 49. DOI: 10.1103/PhysicsPhysiqueFizika.1.49.

[9] J. H. Shapiro and S. R. Shepard. "Quantum phase measurement: A system-theory perspective." In: *Phys. Rev. A* 43 (1991), p. 3795. DOI: 10.1103/physreva.43.3795.

[10] S. M. Barnett and P. M. Radmore. *Methods in Theoretical Quantum Optics*. Oxford University Press, 1997. ISBN: 9780198563624.

[11] T. C. H. Liew, Y. G. Rubo, A. S. Sheremet, S. De Liberato, I. A. Shelykh, F. P. Laussy, and A. V. Kavokin. "Quantum statistics of bosonic cascades." In: *New J. Phys.* 18 (2016), p. 023041. DOI: 10.1088/1367-2630/18/2/023041.

[12] M. A. Nielsen and I. L. Chuang. *Quantum computation and quantum information*. Cambridge University Press, 2000. ISBN: 9781107002173.

[13] P. Michler, A. Kiraz, C. Becher, W. V. Schoenfeld, P. M. Petroff, Lidong Zhang, E. Hu, and A. Ĭmamoḡlu. "A Quantum Dot Single-Photon Turnstile Device." In: *Science* 290 (2000), p. 2282. DOI: 10.1126/science.290.5500.2282.

[14] S. Dong, T. Huang an Y. Liu, J. Wang, Liantuan Xiao G. Zhang, and S. Jia. "Fast recognition of single molecules based on single-event photon statistics." In: *Phys. Rev. A* 76 (2007), p. 063820. DOI: 10.1103/PhysRevA.76.063820.

[15] V. B. Verma, M. J. Stevens, K. L. Silverman, N. L. Dias, A. Garg, J. J. Coleman, and R. P. Mirin. "Photon antibunching from a single lithographically defined InGaAs/GaAs quantum dot." In: *Opt. Express* 19 (2011), p. 4182. DOI: 10.1364/OE.19.004182.

[16] G. Di Martino, Y. Sonnefraud, S. Kéna-Cohen, M. Tame, Ş. K. Özdemir, M. S. Kim, and S. A. Maier. "Quantum Statistics of Surface Plasmon Polaritons in Metallic Stripe Waveguides." In: *Nano Lett.* 12 (2012), p. 2504. DOI: 10.1021/nl300671w.

[17] M. E. Reimer, G. Bulgarini, N. Akopian, M. Hocevar, M. Bouwes Bavinck, M. A. Verheijen, E. P.A.M. Bakkers, L. P. Kouwenhoven, and V. Zwiller. "Bright single-photon sources in bottom-up tailored nanowires." In: *Nature Comm.* 3 (2012), p. 737. DOI: 10.1038/ncomms1746.

[18] M. Leifgen, T. Schröder, F. Gädeke1, R. Riemann, V. Métillon, E. Neu, C. Hepp, C. Arend, C. Becher, and K. Lauritsen. "Evaluation of nitrogen- and silicon-vacancy defect centres as single photon sources in quantum key distribution." In: *New J. Phys.* 16 (2014), p. 023021. DOI: 10.1088/1367-2630/16/2/023021.

[19] P. Grünwald. "Effective second-order correlation function and single-photon detection." In: *New J. Phys.* 21 (2019), p. 093003. DOI: 10.1088/1367-2630/ab3ae0.

[20] J. C. López Carreño, E. Zubizarreta Casalengua, E. del Valle, and F. P. Laussy. "Criterion for Single Photon Sources." In: *arXiv:1610.06126* (2016). DOI: 10.48550/arXiv.1610.06126.

[21] G. W. Gardiner and P. Zoller. *Quantum Noise*. 2nd. Springer-Verlag, Berlin, 2000. ISBN: 9783540665717.

[22] M.S. Kim, P.L. Knight, and K. Wodkiewicz. "Correlations between successively emitted photons in resonance fluorescence." In: *Opt. Commun.* 62.6 (1987), pp. 385–388. DOI: 10.1016/0030-4018(87)90005-8.

[23] J.H. Eberly and K. Wódkiewicz. "The time-dependent physical spectrum of light." In: *J. Opt. Soc. Am.* 67 (1977), p. 1252. DOI: 10.1364/JOSA.67.001252.

[24] L. Knöll, G. Weber, and T. Schafer. "Theory of time-resolved correlation spectroscopy and its application to resonance fluorescence radiation." In: *J. Phys. B.: At. Mol. Phys.* 17 (1984), p. 4861. DOI: 10.1088/0022-3700/17/24/020.

[25] L. Knöll and G. Weber. "Theory of *n*-fold time-resolved correlation spectroscopy and its application to resonance fluorescence radiation." In: *J. Phys. B.: At. Mol. Phys.* 19 (1986), p. 2817. DOI: 10.1088/0022-3700/19/18/012.

[26] J. C. López Carreño, E. Zubizarreta Casalengua, B. Silva, E. del Valle, and F. P. Laussy. "Loss of Antibunching." In: *Phys. Rev. A* 105.023724 (2022). DOI: 10.1103/PhysRevA.105.023724.

[27] J. C. López Carreño, E. del Valle, and F. P. Laussy. "Frequency-resolved Monte Carlo." In: *Sci. Rep.* 8 (2018), p. 6975. DOI: 10.1038/s41598-018-24975-y.

[28] Klaus Mølmer, Yvan Castin, and Jean Dalibard. "Monte Carlo wave-function method in quantum optics." In: *J. Opt. Soc. Am. B* 10.3 (1993), pp. 524–538. DOI: 10.1364/JOSAB.10.000524.

[29] H. Goldstein. *Classical Mechanics*. Addison-Wesley, 2002. ISBN: 9780201657029.

[30] D. J. Griffiths. *Introduction to Quantum Mechanics*. Prentice Hall International, 1994. ISBN: 9780131855137.

[31] C. C. Gerry and P. L. Knight. *Introductory Quantum Optics*. Cambridge University Press, 2005. ISBN: 9780521527354.

[32] E.T. Jaynes and F.W. Cummings. "Comparison of quantum and semiclassical radiation theories with application to the beam maser." In: *ProcIEEE* 51.1 (1963), pp. 89–109. DOI: 10.1109/PROC.1963.1664.

[33] A. G. Redfield. "The Theory of Relaxation Processes." In: *Adv. Magn. Opt. Reson.* 1 (1965), pp. 1–32. DOI: 10.1016/B978-1-4832-3114-3.50007-6.

[34] E. B. Davies. *Quantum theory of open systems*. Academic Press, 1976. ISBN: 9780122061509.

[35] H.-P. Breuer and F. Petruccione. *The Theory of Open Quantum Systems*. Oxford University Press, 2007. ISBN: 9780199213900.

[36] H. J. Carmichael. *Statistical methods in quantum optics 1*. 2nd ed. Springer Science & Business Media, 2002. ISBN: 9783662038758.

[37] G. Lindblad. "On the generators of quantum dynamical semigroups." In: *Commun. Math. Phys* 48 (1976), p. 119. DOI: 10.1007/BF01608499.

[38] H. Carmichael. "An open systems approach to Quantum Optics." In: Springer, 1993. Chap. 1 Master Equations and Sources I, pp. 6–21. ISBN: 9783540566342.

[39] C. W. Gardiner and P. Zoller. "Quantum Noise." In: Third. Springer, 2004. Chap. 3 Quantum Langevin Equations, pp. 42–89. ISBN: 9783540665717.

[40] M. Lax. "Formal Theory of Quantum Fluctuations from a Driven State." In: *Phys. Rev.* 129 (1963), p. 2342. DOI: 10.1103/PhysRev.129.2342.

[41] M. Lax. "Quantum Noise. X. Density-Matrix Treatment of Field and Population-Difference Fluctuations." In: *Phys. Rev.* 157 (1967), p. 213. DOI: 10.1103/PhysRev.157.213.

[42] E. del Valle, F. P. Laussy, and C. Tejedor. "Luminescence spectra of quantum dots in microcavities. II. Fermions." In: *Phys. Rev. B* 79 (2009), p. 235326. DOI: 10.1103/PhysRevB.79.235326.

[43] B. R. Mollow. "Power Spectrum of Light Scattered by Two-Level Systems." In: *Phys. Rev.* 188 (1969), p. 1969. DOI: 10.1103/PhysRev.188.1969.

[44] W. Heitler. *The Quantum Theory of Radiation*. Oxford University Press, 1944.

[45] J. C. López Carreño, E. Zubizarreta Casalengua, E. del Valle, and F. P. Laussy. "Joint subnatural-linewidth and single-photon emission from resonance fluorescence." In: *Quantum Science and Technology* 3 (2018), p. 045001. DOI: 10.1088/2058-9565/aacfbe.

[46] J. C. López Carreño, E. Zubizarreta Casalengua, F. P. Laussy, and E. del Valle. "Impact of detuning and dephasing on a laser-corrected subnatural-linewidth single-photon source." In: *J. Phys. B.: At. Mol. Phys.* 52 (2019), p. 035504. DOI: 10.1088/1361-6455/aaf68d.

[47] L. Hanschke, L. Schweickert, J. C. López Carreño, E. Schöll, K. D. Zeuner, T. Lettner, E. Zubizarreta Casalengua, M. Reindl, S. F. Covre da Silva, R. Trotta, et al. "The Origin of Antibunching in Resonance Fluorescence." In: *Phys. Rev. Lett.* 125.170402 (2020). DOI: 10.1103/PhysRevLett.125.170402.

[48] E. Wigner. "On the Quantum Correction For Thermodynamic Equilibrium." In: *Phys. Rev.* 40.749 (1932). DOI: 10.1103/PhysRev.40.749.

[49] H. J. Groenewold. "On the principles of elementary quantum mechanics." In: *Physica* 12.7 (1946), pp. 405–460. DOI: 10.1016/S0031-8914(46)80059-4.

[50] J. E. Moyal. "Quantum mechanics as a statistical theory." In: *Math. Proc. Cambridge Philos. Soc.* 45.1 (1949), pp. 99–124. DOI: 10.1017/S0305004100000487.

[51] M.-A. Lemonde, N. Didier, and A. A. Clerk. "Antibunching and unconventional photon blockade with Gaussian squeezed states." In: *Phys. Rev. A* 90 (6 2014), p. 063824. DOI: 10.1103/PhysRevA.90.063824.

[52] M. Walschaers. "Non-Gaussian Quantum States and Where to Find Them." In: *PRX Quantum* 2 (3 2021), p. 030204. DOI: 10.1103/PRXQuantum.2.030204.

[53] C. N. Cohen-Tannoudji and S. Reynaud. "Dressed-atom description of resonance fluorescence and absorption spectra of a multi-level atom in an intense laser beam." In: *J. Phys. B.: At. Mol. Phys.* 10 (1977), p. 345. DOI: 10.1088/0022-3700/10/3/005.

[54] J. C. López Carreño, E. del Valle, and F. P. Laussy. "Photon Correlations from the Mollow Triplet." In: *Laser Photon. Rev.* 11 (2017), p. 201700090. DOI: 10.1002/lpor.201700090.

[55] E. del Valle, A. González-Tudela, F. P. Laussy, C. Tejedor, and M. J. Hartmann. "Theory of Frequency-Filtered and Time-Resolved *N*-Photon Correlations." In: *Phys. Rev. Lett.* 109 (2012), p. 183601. DOI: 10.1103/PhysRevLett.109.183601.

[56] J. C. López Carreño, C. Sánchez Muñoz, E. del Valle, and F. P. Laussy. "Excitation with quantum light. II. Exciting a two-level system." In: *Phys. Rev. A* 94 (2016), p. 063826. DOI: 10.1103/PhysRevA.94.063826.

[57] M. Bayer, G. Ortner, O. Stern, A. Kuther, A. A. Gorbunov, A. Forchel, P. Hawrylak, S. Fafard, K. Hinzer, T. L. Reinecke, et al. "Fine structure of neutral and charged excitons in self-assembled In(Ga)As/(Al)GaAs quantum dots." In: *Phys. Rev. B* 65 (19 2002), p. 195315. DOI: 10.1103/PhysRevB.65.195315.

[58] C. Santori, D. Fattal, J. Vukovick, G. S. Solomon, and Y. Yamamoto. "Indistinguishable photons from a single-photon device." In: *Nature* 419 (2002), p. 594. DOI: 10.1038/nature01086.

[59] K. A. Fischer, K. Müller, K. G. Lagoudakis, and J. Vučković. "Dynamical modeling of pulsed two-photon interference." In: *New J. Phys.* 18.11 (2016), p. 113053. DOI: 10.1088/1367-2630/18/11/113053.

[60] Y.-M. He, Y. He, Y.-J. Wei, D. Wu, M. Atatüre, C. Schneider, S. Höfling, M. Kamp, C.-Y. Lu, and J.-W. Pan. "On-demand semiconductor single-photon source with near-unity indistinguishability." In: *Nat. Nanotechnol.* 8.3 (2013), pp. 213–217. DOI: 10.1038/nnano.2012.262.

[61] A. Ridolfo, E. del Valle, and M. J. Hartmann. "Photon correlations from ultrastrong optical nonlinearities." In: *Phys. Rev. A* 88 (2013), p. 063812. DOI: 10.1103/PhysRevA.88.063812.

[62] D. I. H. Holdaway, V. Notararigo, and A. Olaya-Castro. "Perturbation approach for computing frequency- and time-resolved photon correlation functions." In: *Phys. Rev. A* 98 (2018), p. 063828. DOI: 10.1103/PhysRevA.98.063828.

[63] K. Hepp and E. H. Lieb. "On the superradiant phase transition for molecules in a quantized radiation field: the dicke maser model." In: *Ann. Physics* 76.2 (1973), pp. 360–404. DOI: 10.1016/0003-4916(73)90039-0.

[64] R. H. Dicke. "Coherence in Spontaneous Radiation Processes." In: *Phys. Rev.* 93.1 (1954), pp. 99–110. DOI: 10.1103/PhysRev.93.99.

[65] R. Trivedi, M. Radulaski, K. A. Fischer, S. Fan, and J. Vučković. "Photon Blockade in Weakly Driven Cavity Quantum Electrodynamics Systems with Many Emitters." In: *Phys. Rev. Lett.* 122 (2019), p. 243602. DOI: 10.1103/PhysRevLett.122.243602.

[66] M. Bamba, A. İmamoğlu, I. Carusotto, and C. Ciuti. "Origin of strong photon antibunching in weakly nonlinear photonic molecules." In: *Phys. Rev. A* 83 (2 2011), p. 021802. DOI: 10.1103/PhysRevA.83.021802.

[67] T. C. H. Liew and V. Savona. "Single Photons from Coupled Quantum Modes." In: *Phys. Rev. Lett.* 104 (18 2010), p. 183601. DOI: 10.1103/PhysRevLett.104.183601.

[68] A. Delteil, T. Fink, A. Schade, S. Höfling, C Schneider, and A İmamoğlu. "Towards polariton blockade of confined exciton–polaritons." In: *Nat. Mater.* 18.3 (2019), pp. 219–222. DOI: 10.1038/s41563-019-0282-y.

[69] G. Muñoz-Matutano, A. Wood, M. Johnsson, X. Vidal, B. Q. Baragiola, A. Reinhard, A. Lemaître, J. Bloch, A. Amo, G. Nogues, et al. "Emergence of quantum correlations from interacting fibre-cavity polaritons." In: *Nat. Mater.* 18.3 (2019), pp. 213–218. DOI: 10.1038/s41563-019-0281-z.

[70] E. del Valle and F. P. Laussy. "Regimes of strong light-matter coupling under incoherent excitation." In: *Phys. Rev. A* 84 (2011), p. 043816. DOI: 10.1103/PhysRevA.84.043816.

[71] P. Gartner. "Two-level laser: Analytical results and the laser transition." In: *Phys. Rev. A* 84.5 (2011), p. 053804. DOI: 10.1103/PhysRevA.84.053804.

[72] I. V. Panyukov, V. Yu. Shishkov, and E. S. Andrianov. "Second-Order Autocorrelation Function of Spectrally Filtered Light From an Incoherently Pumped Two-Level System." In: *Annalen der Physik* 534.2 (2022), p. 2100286. DOI: 10.1002/andp.202100286.

[73] C. L. Phillips, A. J. Brash, D. P. S. McCutcheon, J. Iles-Smith, E. Clarke, B. Royall, M. S. Skolnick, A. M. Fox, and A. Nazir. "Photon Statistics of Filtered Resonance Fluorescence." In: *Phys. Rev. Lett.* 125.4 (2020), p. 043603. DOI: 10.1103/PhysRevLett.125.043603.

[74] L. Mandel and E. Wolf. *Optical Coherence and Quantum Optics*. Cambridge University Press, 2014. ISBN: 9781299820852.

[75] L. Ahlfors. *Complex Analysis*. 3rd. McGraw-Hill Education, 1979. ISBN: 9780070006577.

[76] M. Cosacchi, A. Mielnik-Pyszczorski, T. Seidelmann, M. Cygorek, A. Vagov, D. E. Reiter, and V. M. Axt. "N-photon bundle statistics on different solid-state platforms." In: *Phys. Rev. B* 106 (2022), p. 115304. DOI: 10.1103/PhysRevB.106.115304.

[77] H. Wang, M. Hofheinz, M. Ansmann, R. C. Bialczak, E. Lucero, M. Neeley, A. D. O'Connell, D. Sank, J. Wenner, A. N. Cleland, et al. "Measurement of the Decay of Fock States in a Superconducting Quantum Circuit." In: *Phys. Rev. Lett.* 101 (24 2008), p. 240401. DOI: 10.1103/PhysRevLett.101.240401.

[78] M. Brune, J. Bernu, C. Guerlin, S. Deléglise, C. Sayrin, S. Gleyzes, S. Kuhr, I. Dotsenko, J. M. Raimond, and S. Haroche. "Process Tomography of Field Damping and Measurement of Fock State Lifetimes by Quantum Nondemolition Photon Counting in a Cavity." In: *Phys. Rev. Lett.* 101 (2008), p. 240402. DOI: 10.1103/PhysRevLett.101.240402.

[79] C. Sánchez Muñoz, F. P. Laussy, E. del Valle, C. Tejedor, and A. González-Tudela. "Filtering multiphoton emission from state-of-the-art cavity quantum electrodynamics." In: *Optica* 5.1 (2018), pp. 14–26. DOI: 10.1364/OPTICA.5.000014.

[80] A. L. Fetter and J. D. Walecka. *Quantum theory of many-particle systems*. Dover, 2003. ISBN: 9780486428277.

[81] A.J. Coleman and V.I. Yukalov. *Reduced Density Matrices: Coulson's Challenge*. Springer Berlin Heidelberg, 2000. ISBN: 9783540671480.

[82] C. Cohen-Tannoudji, B. Diu, and F. Laloe. *Quantum Mechanics: Volume 1*. Wiley, 2019. ISBN: 9783527345533.

[83] F. Sun. "The Scattering and Shrinking of a Gaussian Wave Packet by Delta Function Potentials." MA thesis. Massachusetts Institute of Technology, 2012.

[84] Daniel Gustavo Suárez-Forero, Vincenzo Ardizzone, Saimon Filipe Covre da Silva, Marcus Reindl, Antonio Fieramosca, Laura Polimeno, Milena De Giorgi, Lorenzo Dominici, Loren N. Pfeiffer, Giuseppe Gigli, et al. "Quantum hydrodynamics of a single particle." In: *Light: Science & Applications* 9.1 (2020), p. 85. DOI: 10.1038/s41377-020-0324-x.

[85] A. Kavokin, J. J. Baumberg, G. Malpuech, and F. P. Laussy. *Microcavities*. 2nd ed. Oxford University Press, 2017. ISBN: 9780191085864.

[86] E. Hecht. *Optics*. Pearson Education, 2016. ISBN: 9781292096933.

[87] G. Jaeger. *Quantum Information: An Overview*. Springer New York, 2006. ISBN: 9780387357256.

[88] W.-M. Zhang, D. H. Feng, and R. Gilmore. "Coherent states: Theory and some applications." In: *Rev. Mod. Phys.* 62 (1990), p. 867. DOI: 10.1103/RevModPhys.62.867.

[89] E. C. G. Sudarshan. "Equivalence of Semiclassical and Quantum Mechanical Descriptions of Statistical Light Beams." In: *Phys. Rev. Lett.* 10 (1963), p. 277. DOI: 10.1103/PhysRevLett.10.277.

[90] A. I. Lvovsky, H. Hansen, T. Aichele, O. Benson, J. Mlynek, and S. Schiller. "Quantum State Reconstruction of the Single-Photon Fock State." In: *Phys. Rev. Lett.* 87 (2001), p. 050402. DOI: 10.1103/PhysRevLett.87.050402.

A little spark, a little patience.

It fills all Space, and what It fills, It is. What It thinks, that It utters; and what It utters, that It hears; and It itself is Thinker, Utterer, Hearer, Thought, Word, Audition; it is the One, and yet the All in All. Ah, the happiness, ah, the happiness of Being!

— A. Square, Flatland: A Romance of Many Dimensions